UNIVERSITA' POLITECNICA DELLE MARCHE

DIPARTIMENTO DI SCIENZE CLINICHE E MOLECOLARI

DOTTORATO DI RICERCA IN "HUMAN HEALTH"

Ciclo XXXIII

Coordinatore Dottorato: Prof. Carlo Catassi

LINE1 METHYLATION AND EXPRESSION CHANGES ASSOCIATED TO REPLICATIVE SENESCENCE OF HUMAN ENDOTHELIAL CELLS AND DERMAL FIBROBLASTS

Settore Scientifico Disciplinare: *PATOLOGIA GENERALE E CLINICA*

Settore Concorsuale: *06/A2*

Candidato:

Dott.ˢˢᵃ Silvia Latini   *Firma del candidato*

Università Politecnica Marche   _____

Docente Tutor:

Prof.ˢˢᵃ Fabiola Olivieri   *Firma del Tutor*

Università Politecnica Marche   _____

Co-Tutor:

Prof. Maurizio Cardelli   *Firma del Co-Tutor*

I.N.R.C.A. - Ancona   _____

Data esame Finale_____

Index

Summary

Aging is characterized by a morpho-functional adaptation, variably affecting major physiological systems. One of the main challenge of aging research is to explain how cellular mechanisms can affect the complex phenomena observed at organismal level. In this framework, the understanding of the epigenetic mechanisms involved in the acquisition of the senescent phenotype, could help to underpinn the key features of aging process.

We firstly analysed genome-wide DNA methylation of young and senescent human endothelial cells (HUVECs), hightlighting increased levels of demethylated sequences in senescent cells. The most significantly demethylated single CpG sites were then mapped on the reference genome and annotated for their localization inside trasposable elements (TEs) sequences. The most demethylated sequences within TEs in senescent cells belong to the LINE subfamilies L1M, L1P ed L1HS. Among these, L1PA2 was identified as the only L1 potentially active.

To verify if L1 demethylation could be associated also with the retrotrascription of Alu sequences, that usually depend on the enzyme ORF2 encoded by L1 for their reverse transcription and retrotransposition, we analysed L1PA2 and ORF2 (both belonging to L1 family) and Alu (belonging to SINE family) DNA sequencies in young andsenescent cells. This analysis was performed on HUVECs and dermal human fibroblasts (NHDF). RNA expression of Alu and ORF2 sequences was significantly increased in both senescent HUVEC and NHDF, whereas L1PA2 RNA was not significantly modulated in senescent cells.

Since an increase in DNA TEs copies in the nucleus could indicate an increase of the integrated sequences, while the same in the cytoplasm should indicate an increase in the retrotranscription process, which proceeds through a cDNA intermediate, we analysed also the cellular localization of the L1PA2, ORF2 and Alu DNA sequencies.

ORF2 and Alu DNA copy numbers were significantly increased in cytoplasm of senescet HUVECs and NHDF, in association with decreasing trends in the nucleus.

To verify if the increased burden of ORF2 and Alu DNA in cytosol of senescent cells could activate the cytoplasmic sensors inducing antiviral response characterized by increased type 1 INF genes expression, we analysed the INF-1β esxpression levels in young and senescent cells. As predicted, senescent NHDF showed increased INF-1β expression. Surprisingly, in senescent HUVECs INF-1β expression was not significantly modulated.

Our results suggest that specific TEs sequences can significantly increase in senescent cells, expecially in cytoplasm, where they could be sensed by a number of nucleic acid sensors, including those able to detect viral infections.

We observed that senescent endothelial cells seems to be more "tolerant" than fibroblasts to endogenous misplaced nucleic acids, since INF-1β expression levels was not significantly increased in senescent HUVECs.

Overall our results could help to identify molecular mechanisms modulating the susceptibility of senescent cells to viral infections.

1. Introduction

Aging is characterized by a morpho-functional adaptation, variably affecting major physiological systems, depending on a complex interaction between genetic, environmental and stochastic factors (Fülöp et al. 2016; 2018).

Population aging is a demographic phenomenon which involves the rise in the median age of people living in a county, as a result of decreasing birth and death rates, and increasing life expectancy. The increase in life expectancy has been accompanied by an increase in the percentage of old subjects affected by age-related chronic diseases, ARDs, including cardiovascular diseases, type 2 diabetes, neurodegenerative diseases and cancers. The increasing incidence of these diseases gives rise to the growing interest of research for the molecular and cellular mechanisms underly the aging process.

One of the main risk factors for ARDs is the chronic-systemic, non-infectious inflammation that increases during aging, named "inflammaging (Franceschi et all., 2000). Despiste the extensive studies in the last 20 years, many aspects are still unclear. Inflammaging is characterized by increased circulating levels of the main proinflammatory cytokines, such as IL-1, IL-6, TNF-α and chemokines.

These molecules are considered also circulating biomarkers for the most common ARDs (Meduri and Yates 2004).

1.1 Basic aspects of aging

Aging is characterized by a general functional decline associated with increased accumulation of damaged molecules at cellular level (López-Otín et al. 2013).

Based on this basic concept, numerous criticisms have arisen regarding the sources of the associated age damage, as well as the compensatory responses of the different tissues and the possible interventions to delay aging aoutcomes.
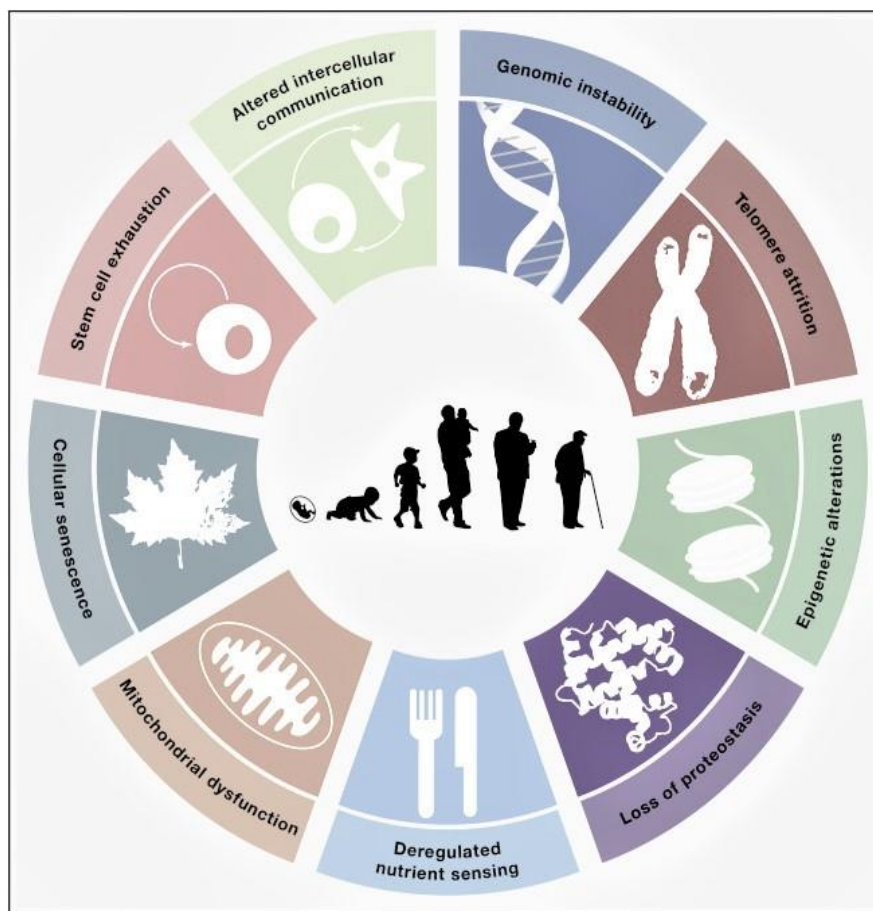
Figure 1. The nine hallmarks of aging: genomic instability, telomere shortening, epigenetic alterations, loss of proteostasis, deregulation of nutrient-sensitive pathways, mitochondrial dysfunction, cellular senescence, stem cell exhaustion, impaired intercellular communication (López-Otín et al. 2013)

These studies have identified and categorized the cellular and molecular elements that characterize the senescent phenotype. In Figure 1 are depicted the nine well characterized hallmarks of aging: genomic instability, telomere shortening, epigenetic alterations, loss of proteostasis, deregulation of nutrient-sensitive pathways,

mitochondrial dysfunction, cellular senescence, stem cell exhaustion and impaired intercellular communication .

1.2 Genomic instability

A common denominator of aging is the accumulation of DNA damage. Eukaryotic cells accrue DNA damage as a result of physical, chemical and biological exogenous agents, endogenous stress, errors in replication, hydrolytic reactions, increased production of reactive oxygen species (ROS).

The resulting DNA damage is manifold and includes point mutations, translocations, loss or gain of chromosomes, telomere shortening, alteration of gene sequences due to the integration of viruses or transposons. (Guo et al. 2018)(Wu and Burgess 2004). In order to reduce genome damages, organisms have evolved a set of DNA shelter mechanisms (Tan and Lan 2016), including a system for maintaining the appropriate length and function of telomeres; other types of aging-related damages such as aneuploidia and changes in the number of genes copies have also been observed.

All the aforementioned alterations are able to modify genes and influence essential transcriptional pathways and, if not eliminated by apoptosis mechanism, can lead to serious alterations in tissue homeostasis. This becomes particularly important when genomic damage comes to alter the functionality of stem cells, compromising their role in tissue renewal.

Mutations and deletions in mtDNA can be frequent, so that mtDNA is considered one of the main targets of associated age somatic mutations (Quan et al. 2020) (Jang et al. 2018). The frequent damage to mitochondrial DNA is due to the oxidative microenvironment present in the mitochondria, the lack of histones (which play a

protective role against DNA alterations), the limited effectiveness of shelter mechanisms compared to those present in genomic DNA.

The first evidence of the link between mtDNA damage and ARDs derives from the identification of multi-organ disorders, phenotypically similar to aging but caused by mitochondrial mutations (Liu et al. 2019).

Defects in nuclear foils can also cause genomic instability, as foils participate in genome integrity maintenance by providing support for anchoring chromatin and protein complexes that regulate genomic stability.

Alterations of nuclear foil and the production of an aberrant isoform of prelamine A, called progerin, have also been found in normal human aging. (Worman and Michaelis 2018) An increase in progerin has been detected in human fibroblasts with telomere dysfunction.

The relevance of the link between premature aging and alterations of nuclear foil is supported by the delayed onset of progeroid symptoms with the decrease in prelamine A or progerin levels.

1.3 Telomere shortening

Telomeres are regions located at the ends of the chromosomes, made of repetitions of TTAGGG nucleotide sequences, whose function is to protect the important genetic informations contained in the DNA of the inner chromosomal portions. Telomeres attrition occurs during replication process, due to the inability of DNA polymerase to fully replicate the terminal portions of DNA, a function that is instead proper to a specific polymerase known as telomerase ("Telomeres and Aging - Telomere Shortening - T.A. Sciences").

Most mammalian somatic cells do not express this enzyme, showing progressive telomere shortening, whereas stemm cells and cancerous cells are characterized by telomerase expression. Therefore, telomere depletion explains the limited proliferational capacity of some *in vitro*-grown cell lines, phenomeno knowns as replicative senescence or Hayflick limit.

Telomeres can be considered as DNA breaks invisible to shelter mechanisms, since associated with proteins constituting the Shelterin complex. Whitout the Shelterin complex, telomeres could be repaired as DNA breaks, leading to the fusion of chromosomes.

Multiple epidemiological studies have found a significant association between telomere shortening, aging and the onset of morbidity and mortality (Gorenjak et al. 2018). A reduced length of the leukocytic telomere (LTL) has been identified as an independent risk factor for functional decline in European elderly populations (Rojas et al. 2018).

In mammals, the aging process is accompanied by telomere shortening and telomere's pathological dysfunctions that accelerate aging, while experimental stimulation of telomerase could be able to delay aging.

1.4 Epigenetic alterations

Numerous epigenetic alterations affect cells and tissues during aging. Epigenic changes involve alterations in the DNA methylation pattern, post transcriptional changes of histones, remodeling of chromatin and modulation of non coding RNA.

Some characteristic epigenetic alterations associated with age are the increased acetylation of H4K16 histone, the trimethylation of H4K20 or H3K4, the demethylation of H3K9 and the trimethylation of H3K27.

The multienzimatic systems that ensure the formation and maintenance of the correct epigenetic pattern are DNA methyltransferase, histone deacetylase, methylase, demethylase and protein complexes involved in the remodeling of chromatin.

Epigenetic regulation acts on gene expression at different levels; from direct DNA changes to histonic tails, to the modulation of transcription and translation of messenger RNAs (mRNAs).

Since epigenetic processes play a key regulatory role in aging and ARDs and specific epigenome-modulating enzymes are involved in such processes, the pharmacological targeting of epigenetic enzymes holds promise in anti-aging therapy (Zhao et al. 2019).

Chromatin has dynamic and stochastic properties, being continuously remodeled, redistribute and "breathe"; however the stochastic unpredictable alterations of chromatin structure could, over time, contribute to the breakage of nuclear, cellular and tissue function, and consequently contribute to ageing process and ARDs development.

In mammals, there is an age-associated decline in total methylation of genomic DNA (Marioni et al. 2019)(Min et al. 2019); that being mainly associated with repetitive DNA sequences, probably occurs predominantly in constitutive heterochromatine domains.

Since DNA methylation promotes the formation of transcribed silent heterochromatin (Kane and Sinclair 2019), this change will facilitate the loss of eterochromatin structure of these regions.

However, although genomic methylation levels decrease with age in mammals, in other specific sites there is a tendency to increase DNA methylation (Jones, Goodman, and Kobor 2015).

This occurs in CpG islands, some of which are located in gene-promotive regions. CpG islands are CG-rich sequences typically unmethylated, that can be metilated.

In eukaryotic cells, the phenomenon of cellular senescence is associated with epigenetic alteration of chromatin regions containing transposable elements (TEs) and others repetitive elements, thus promotin the transcriptional activation of transposable elements (Pal and Tyler 2016).

This transcriptional activation of TEs (and specifically of EREs in mammals) could potentially expose the cells to an increased risk of mutation and genomic instability, due to the transposition activity.

Recent studies showed as 353 CpG sites with a similar age-related variation of hypermethylation or hypomethylation in different tissues can be selected as part of the "epigenetic clock" (Horvath 2013).

Intriguingly, the age estimated by the methylation-clock differs by less than 3.6 years from the chronological age in healthy subjects.

Other recent studies demonstrated that a precise estimation of age can be made analysing DNA methylation profiles in blood, and that using a minimal set of 3CpG sites is also possible to estimates the age (Eipel et al. 2016); (Hannum et al. 2013).

While the methylation level, observed at single CpG sites, can show either an increase or a decrease during aging respect to younger ages, the average of CpG methylation in the genome (global genome methylation) exhibits a general tendency to decrease in aged cells or tissues; indeed, global DNA methylation, measured by biochemical methods in *in vitro* cultured fibroblasts, decreases in senescent cells (PA Jones et al. 1983).

The methylation of repetitive elements, TEs included, is considered largely responsible of the average CpG methylation in human genome and therefore sometimes it is used as a surrogate marker of global genome methylation (A. S. Yang et al. 2004).

This assumption is justified by the observation that, in the mammalian genome, most of the CpG sites are contained in repetitive element.

Interestingly, the age-related loss of methylation appeared weaker in centenarians, suggesting that there are inheritable genetic traits predisposing for longevity and delayed epigenetic changes of the global TEs and Alu methylation (Puca et al. 2018).

1.5 Loss of proteostasis

Aging and age associated diseases are linked to an altered proteostasis or protein homeostasis; all cells are equipped with a series of control mechanisms, in order to preserve the stability and functionality of their pool of proteins.

Proteostasis involves mechanisms that stabilize the correct folding of proteins, including the "heat shock proteins" and other mechanisms that promote proteasomes or lysosomes degradation of unfolded or damaged proteins.

Recently, MOAG-4/SERF has been identified as a class of evolutionarily conserved proteins that positively regulates protein aggregate formation (Yoshimura et al. 2017).

The mechanisms described above act together in a coordinated way, reclaiming the correct folding of polypeptides, or completely degrading and removing proteins with incorrect folding; preventing the accumulation of damaged components and ensuring the continuous renewal of intercellular proteins.

Many studies have shown changes in proteostasis associated with aging.

Moreover, alteration in proteolysis processes resulting in the accumulation of peptides aggregates, proteins not folded or incorrectly folded, was associated to the development os some associated age pathologies such as Alzheimer's and Parkinson's.

To further support the link between aging and the reduction of proteostasis, it should be remembered that two main proteolytic systems involved in protein quality control, such as ubiquitin-proteasome and lysosomal autophagy systems, decrease with age. (A. S. Yang et al. 2004).

1.6 Nutrient-sensitive Pathway deregulation

The somatotropic axis in mammals includes growth hormone (GH), produced by adenoipophysis (anterior part of the pituitary gland) and its second mediator, the insulin-like growth factor (IGF-1). IGF-1 is produced by different cell types, mainly hepatocytes, in response to growth hormone.

The IGF-1 signaling pathway is the same of insulin, hence the designation "Insulin and IGF-1 Signaling Pathway" (IIS).

IIS is a mechanism that has been most preserved in the course of evolution; it targets the FOXO family transcription factors and mTOR complexes. (Barzilai et al. 2012).

Polymorphisms or genetic mutations that reduce the functionality of GH receptors, IGF-1, insulin, or intracellar effectors such as AKT, mTOR, and FOXO, are related to an increased life expectancy (Maiese 2016).

Consistently with the deregulation of nutrient-sensitive pathways, caloric restriction increases the life and health span of all eukaryotic organisms studied (Cruzen and Colman 2009)(Fontana, Partridge, and Longo 2010).

In addition to the previously described IIS pathway, that participates in glucose detection, there are three additional "nutrient detection" systems, such as mTOR that detects the concentration of amino acids, AMPK that recognizes low energy conditions from AMP levels and Sirtuins that notice low energy conditions with a high concentration of NAD+ (Houtkooper et al. 2010).

1.7 Mitochondrial dysfunction

As the age of the organism and cells increases: the effectiveness of the respiratory chain tends to decrease, therefore the loss of electrons increases and ATP production is consequently reduced.(Green, Galluzzi, and Kroemer 2011).

The relationship between mitondrial dysfunction and aging was extensively investigated, but some aspects remain unclear.

There is a theory called "mitochondrial free radical theory" that proposes an increase in ROS production due to mitochondrial dysfunction during aging; the ROS produced can cause further damage and general deterioration of mitochondria and other cellular structures and organelles (Harman, 1972).

As the body's age, ROS also increases stimulating the anti-ROS endogenous defense in order to maintain homeostasis and survival; this happens up to a certain "threshold value", beyond which ROS change their effects aggravating the age-associated damage (Hekimi, Lapointe, and Wen 2011).

Mitochondrial dysfunction could contribute to aging independently of ROS, this becuase the inflammatory responses interfere with the apoptosis signaling system.

An increased mitochondrial permeability that favors the activation of the inflammasome is associated to inflammatory processes (Green, Galluzzi, and Kroemer 2011).

Other mechanisms able of causing bionenergetic defects are the accumulation of mutations and deletions in mtDNA, oxidation of mitochondrial proteins, destabilization of the macromolecular organization of the respiratory chain, changes in the lipid composition of mitochondrial membranes, defective mitophagy (mitophagy is a form of organello-specific macroautophagy (Wang and Klionsky 2011).

Therefore, the combination of increasing damage and reduced mitochondrial turnover contigues and accelerates the aging process in mammals (Guillozet et al. 1993).

It remains to be clarified whether increasing the mitochondrial function during aging could increase life expectancy.

1.8 Stem cell exhaustion

Aging is characterized by a decrease in the regenerative capacity of all tissues, including the hematopoietic compartment. A decreased number and proportion of specific phenotypes of innate and adaptive immune cells, occurs during aging, process called immuno-senescence, increasing the susceptibility to infections and cancers (Shaw et al. 2010).

Although limited proliferation of stem cells is harmful to the long-term maintenance of the organism, excessive proliferation can have similarly harmful effects, accelerating the depletion of the niches of progenitor cells and leading to premature aging. (Rera et al. 2011).

1.9 Altered intercellular comunication

Aging process involves changes and alterations of intercellular comunication process involving endocrine, neuroendocrine and neuronal signals. Among neurohormonal

signaling, the renin-angiotensin signaling, adrenergic and insulin IGF1, tend to be downregulated with aging. Parallely, the inflammatory processes increase during aging in association with a decline of the immunosurveillance against pathogens and malignant cells (Laplante and Sabatini 2012).

The aging associated proinflammatory status was named as "Inflammaging" and it is considered the main risk factors for the development of ARDs (Franceschi et al., 2000; Fulop et al., 2018; Barzilai et al., 2012).

The main triggers of this process are the increase amount of tissue damages, the failures of immune system to clear dysfunctional host cells and pathogens, a defective autophagy response, and the accumulation of senescent cells with a characteristic proinflammatory phenotype, named senescent-associated proinflammatory phenotype (SASP) (Salminen and Kaarniranta 2012).

These alterations determine an enhanced activation of the inflammasome NLRP3 and an enhanced activation of the transcription factor NF-Kb, leading in turn to an increased production of IL-1β, IL-6 and TNF alpha. SASP is characterized by the same proinflammatory lanscape, thus spreading senescence and activation of inflammation to surrounding tissues and to systemic level.

Inflammatory cytokines, together with other inflammation associated molecules, act like a sort of contagious aging and are responsible of the "bystander effect", where senescent cells induce senescence in their nearby cells through gap-junction contacts and processes involving ROS (Nelson et al. 2012).

When it was demonstrated that exstracellular vesicles (EVs) can be actively released from living cells not only locally but also systemically, it was hypothesized that EVs could explain, almost in part, how cellular phenomena can affect aging at the systemic level (Olivieri et al. 2015).

1.10 Cellular senescence

Cellular senescence occurs *in vitro* and *in vivo* as a response to excessive extracellular or intracellular stress. The senescence program locks the cells into a cell-cycle arrest, preventing the spread of damages to the next cell generation and precludes potential malignant transformation (Campisi and D'Adda Di Fagagna 2007). This phenomenon was initially observed and described by Hayflick in human fibroblasts following serial cultured passages (Hayflick and Moorhead 1961).

Senescent cells have been shown to accumulate over the life span of rodents, non human primates, and humans. These cells are found primarily in renewable tissues and in tissues that experience prolonged inflammation.

A plethora of stresses can promote cellular senescence, including telomeric dysfunction (telomere uncapping) resulting from repeated cell division (termed replicative senescence), mitochondrial deterioration, oxidative stress, severe or irreparable DNA damage and chromatin disruption (genotoxic stress), and the expression of certain oncogenes (oncogene-induced senescence) (Collado, Blasco, and Serrano 2007). The excessive mitogenic signaling is in fact a strong source of stress, beyond DNA damage, associated with senescence; more than 50 oncogenic or mitogenic alterations capable of inducing senescence have been detected (Negrini et al, 2010).

Senescent cells are characterized by specific biomarkers, such as DNA damage, increased enzymatic activity, *i.e.* β-galactosidase activity (SABG) (Childs, Bussian, and Baker 2019), increased expression of p16INK/Rb and p19ARF/p53. P16INK levels correlate with the chronological age of almost all tissues, in animal models and humans. Through a meta analysis of 300 genomes it has been found that INK4a/ARF

is the gene locus most linked to a wide spectrum of ARDs, including cardiovascular diseases, diabetes, glaucoma, Alzheimer's (Jeck et al, 2012).

Since the number of senescent cells increases with age, senescence is assumed to contribute to aging.

However, senescence can play also prolongevity functions, such as preventing the expansion of damaged and potentially oncogenic cells, promoting their elimination by the immune system. In aged organisms, this replacement system becomes inefficient, or the regenerative capacity of progenitor cells may run out, resulting in an accumulation of senescent cells that in turn worsen cellular damage and contribute to aging. Senescent cells accumulation that occurs with aging, is due to the increased production of senescent cells and/or a decrease in their clearance, probably associated to above mentioned immunosenescence.

Recent studies have shown that senescent cells are characterized by significant alterations in their secretoma, which is particularly enriched in proinfiamatory cytokines and metalloprotease, named as secretory phenotype associated with aging or SASP, which contributes to the spreading of senescence (Rodier and Campisi 2011) (Olivieri et al., 2015) (Figure 2)
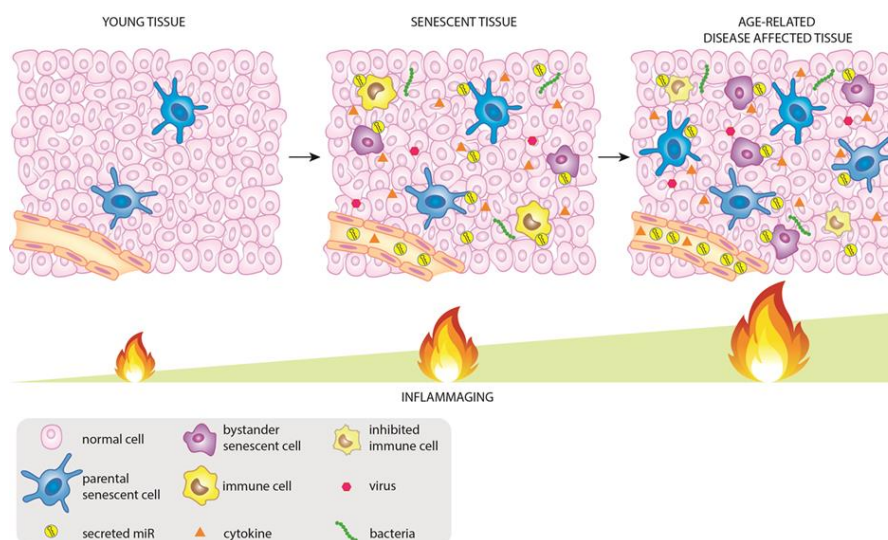
1.11 SASP

SASP, the senescence-associated secretory phenotype, is considered as a peculiar case of DNA damage response (DDR). The senescent cell is a non proliferating but potentially persisting metabolically active cell that acquire the SASP (Fig 3).
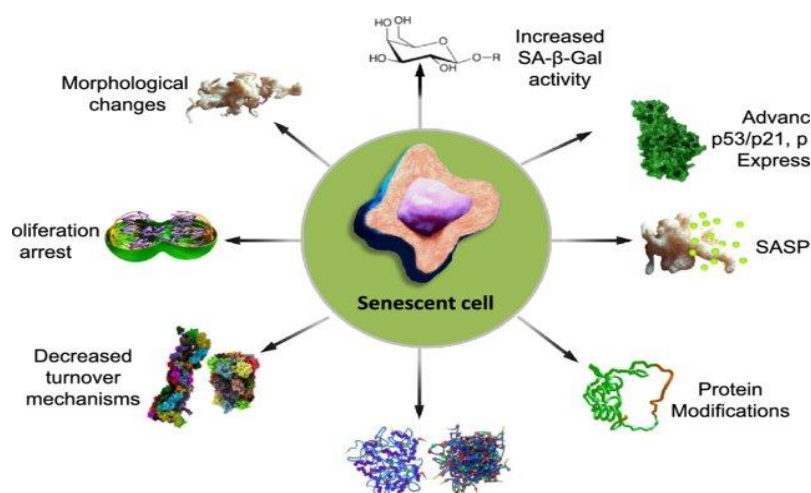
Figure 3. The key features of senescent cells, including the acquisition of SASP (Höhn et al., 2017)

A large-scale characterization of the SASP was recently provided, using antibody arrays to quantitatively measure factors secreted by human fibroblasts and epithelial cells, showing as senescence cells secrete high levels of immunomodulatory cytokines, extracellular matrix modulators, growth factors and proteases (Partridge, Fuentealba, and Kennedy 2020). IL-6, TNF alpha and IL-8 are the most conserved and robust features of SASP.

Recent evidence confirmed that senescent cells can release also vesicles (EVs), including exosomes and ectosomes, with very heterogeneous content, whose composition depends from the senescence inducers and from the specific cell-type.

The small vescicles released from senescent cells contain multiple cellular components such as proteins, lipids, nucleic acids that can act on sorrounding tissues or remote organs as potential SASP factors, but also non coding RNA, such as microRNAs and the telomeric repeat containing RNA (TERRA) (Z. Wang & Lieberman, 2016; Mensà et al., 2020).

The inhibition of small EVs secretion results in the accumulation of nuclear DNA fragments in the cytoplasm and DNA damage both in young and senescent fibroblast, suggesting that EVs release is important for excretion of harmful DNA fragments, mantaining homeostasis and preventing the accumulation of DNA damage. During aging decreases the expression of lamin B1, leading to the weakening of nuclear envelope structure and increased release outside the nucleus of chromatin fragments. (Loo et al. 2020).

Increasing evidences showed tha senescent cells release more small EVs compared to young cells. Increased EVs secretion was observed not only in normal human senescent cells but also in cancer cells (Lehmann et al., 2008).

1.12 Cellular models of senescence

Endothelial cells

The link between aging and vascular function has been well expressed in the axiom that "a man is only as old as his arteries" (Brew and McArthur 2020).

In this framework, longevity can be considered as a vascular issue (Thijssen, Carter, and Green 2016) and the occurrence of endothelial cell senescence in the vasculature is gaining increasing recognition. Endothelial dysfunction characterizes a number of age-related cardiovascular and cerebrovascular diseases suggesting the clinical

relevance to better elucidate mechanisms underlying endothelial aging (Ungvari et al., 2018).

The two main components of the vasculature, the vascular endothelium and the media arterial wall undergo several structural and functional changes during aging (Izzo et al., 2018). The age-related alterations of endothelial cells lead to increased aortic stiffness develop at a variable rate during aging (Bruno et al., 2020).

The endothelial dysfunction represents the first step of vascular alterations and the onset of endothelial dysfunction depends on the quality of vascular tissue which the individual has inherited (genetic predisposition), and on the amount of wear and tear to whom they have been subjected (environmental factors) (reviewed in (Kovacic et al., 2011a) and (Kovacic et al., 2011b).

The increasing effort to understand the biological mechanisms driving the age-related changes in endothelial cells suggested that also the increased burden of senescent vascular cells could play a crucial role in promoting endothelial dysfunction (Katsuumi et al., 2018).

The presence of cells displaying markers of senescence was demonstrated in advanced atherosclerotic plaques (Gorenne et al., 2006; Minamino et al., 2002), but whether senescent cells accumulate as a result of the plaque formation or themselves promote atherosclerosis is still unclear (Wang and Bennett, 2012). Senescent cells are endowed of a proatherogenic phenotype (Childs et al., 2016), and a proinflammatory atherosclerotic milieu able to induce the acquisition of senescence markers in vascular smooth muscle cells (Kunieda et al., 2006) and endothelial cells (Riahi et al., 2015).

Similarly, senescent vascular cells have been invoked in the pathogenesis of heart failure (Gogiraju et al., 2015) and systemic metabolic dysfunction associated with obesity (Yokoyama et al., 2014). Senescent endothelial cells are characterized by the

acquisition of the SASP, reduced replicative ability, telomere attrition (Wilson et al., 2008), and metabolic alterations (Sabbatinelli et al., 2019).

Interestingly, increasing observations in animal models and in humans indicate that genomic instability, characterized by DNA damage accumulation, characteristics associated with cellular senescence, can contribute to endothelial dysfunction.

Human umbilical vein endothelial cells (HUVECs) are among one of the most popular models used for disentangle the molecular mechanisms promoting endothelial cells senescence *in vitro* (Fig. 4).

The replicative senescence of HUVEC cells is a complicated physiological process closely associated with significantly impaired energy metabolism and blocked protein synthesis.
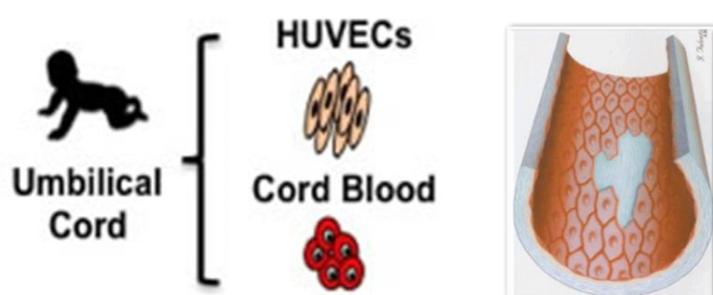
Figure 4. Human umbilical vein endothelial cells (HUVECs)

Normal Human dermal fibroblasts

Fibroblasts, like HUVECs, were extensively investigated in studies on cellular senescence. Normal human dermal fibroblasts (NHDF) were investigated for researches about skin aging and irradiation effects.

Fibroblasts senescence proceeds through an early DNA damage response phase, followed by SASP response; a third later phase was identified and characterized (De Cecco et al. 2019). Senescent fibrablasts can be identifyed by the most common analysed senescence biomarkers.

However, increasing evidence suggest that senescent fibroblasts are characterized by significant increased expression of specific TE subfamily, *i.e.* long interspersed nuclear elements (LINE 1). It was therefore hypothesized that TEs can play an important role in mediating the effects of the environment on the genome, and can contribute to inflammation, as well as to promote ARDs development (Cardelli and Marchegiani 2013).

1.13 Transposable elements

Transposable elements (TEs; also known as 'jumping genes') are discrete pieces of DNA that can move within (and sometimes between) genomes; changes of their positions can generate or reverse mutations, thereby altering the cellular genotype.

TEs were discovered in 1940 by Barbara McClintock, approximately half a century before scientists began to understand how TEs interact with their genomic environment. Crucially was the completion of the first human genome sequence revealed that nearly half of our genome is derived from TEs, (Fig. 5).
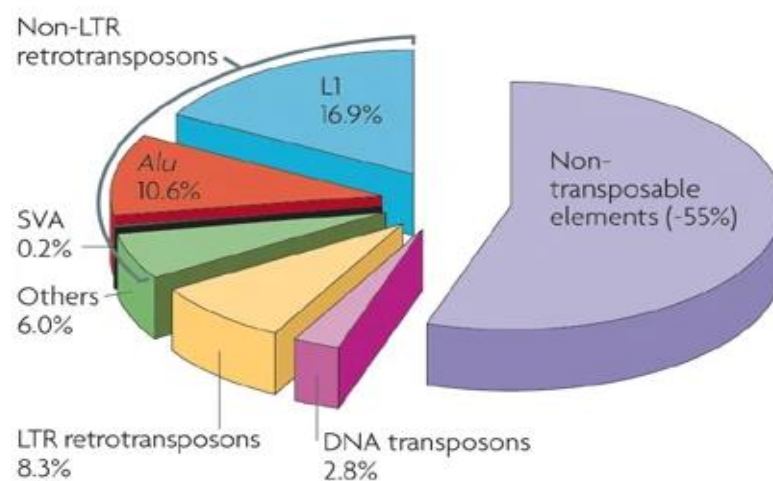
Figure 5. The transposable elments in human genome

Transposable elements can be grouped in two major classes:

➢ **Class 1. Retrotraspososns.** Retrotrasposons are RNA seqeuences that need of retrotrascription for their insertion in the human genome. Retrotrasposons are further classified in two groups: <u>LTR</u> and <u>non-LTR</u> (LTR stands for Long Terminal repeat) (Lagisquet et al., 2021);

➢ **Class 2. DNA transposons**. DNA sequences that can move and insert themselves into a new genomic site (Pace and Feschotte 2007).

Each TE subclass can be further divided into subgroups (or superfamilies) that are typically found across a wide range of organisms, but share a common genetic organization and a monophyletic origin.

In a most detailed level of classification, TE are grouped into families or subfamilies, which can be defined as a closely related group of elements that can be traced as descendants of a single ancestral unit.

This ancestral copy can be inferred as a consensus sequence, which is representative of the entire (sub)family. Thus, every TE sequence in a genome can be affiliated to a (sub)family, superfamily, subclass, and class (Fig. 6A).
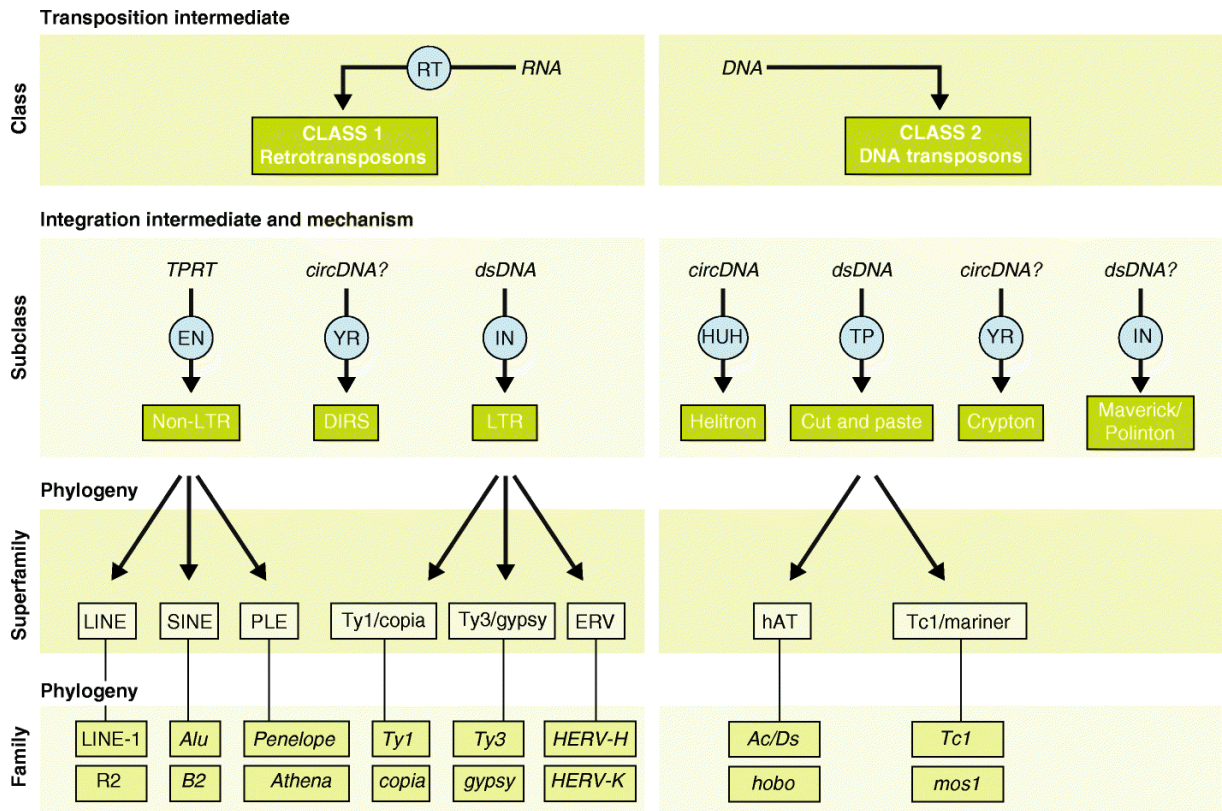
Figure 6A. Classification of eukaryotic transposable elements (Bourque et al., 2018). TE classes, subclasses, superfamilies, and families. Blue circles represent TE-encoded enzymes. circDNA: circular DNA intermediate, DIRS: Dictyostelium repetitive sequence, dsDNA: linear double-stranded DNA intermediate, EN: endonuclease, IN: integrase, PLEs: Penelope-like elements, HUH: Rep/Helicase protein with HUH endonuclease activity, RT: reverse transcriptase, TP: transposase, TPRT: target primed reverse transcription, YR: tyrosine recombinase
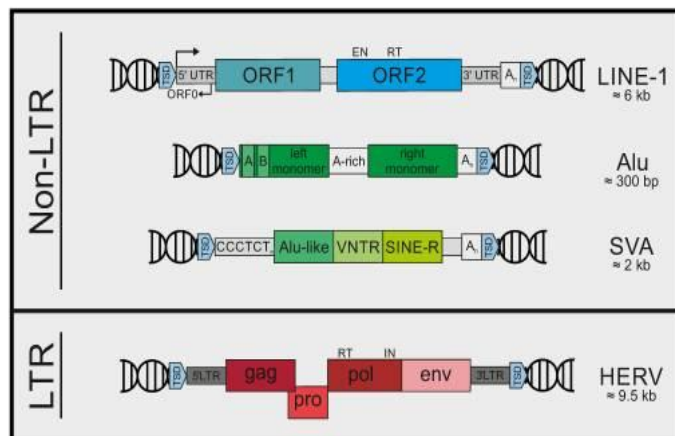
Figure 6B. LTR and NON-LTR TEs (Lagisquet et al., 2021)

Human LTR and NON-LTR will be described in detail (Fig. 6B)

Class 1 retrotrasposons: Human LTR-retrotransposons

Human LTR elements are called HERVs (Human Endogenous Retro Viruses). LTR constitute about 8% of the genome and were inserted in the genome about 25 Million years ago (Mya).

LTR of HERVs help in regulating the expression of nearby genes; it is proposed that some of these endogenous retroviruses may have been integrated into regulatory regions of the genome, contributing to its evolution (Khodosevich, Lebedev, and Sverdlov 2002). (Fig. 7)

On the other hand it is possible that regulatory sequences found in retroviral LTRs could alter or inactivate the expression of nearby genes; cannot be excluded that some HERV insertions benefit to the host, by reverting harmful mutations.
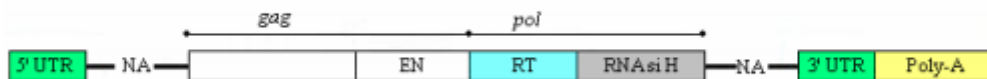
Figure 7. Structure of LTR-retroransposon

Class 1 retrotrasposons: human *non-LTR retrotransposons*

Approximately 45% of the human genome can currently be recognized as being derived from TEs. Non-LTR retrotransposons lack of the long terminal repeats and can be grouped in LINEs (long interspersed nuclear elements) and SINEs (short interspersed nuclear elements). SINE VNTR Alu (SVA) elements are the exception between the two, as they are shorter than LINEs but longer than SINE. SVA is a composite retrotransposon currently active in humans and present in about 2700 copies in the human genome reference sequence (Deininger and Batzer 1999)(Chen et al. 2005).

Although DNA transposons are currently not mobile in the human genome, they were active during early primate evolution until~37 Myr ago.

Long Interspersed Nuclear Elements (LINE)

Long interspersed element-1 sequences (LINE-1s or L1s) constitute a~17% of the human nuclear DNA, as a result of their continued mobilization activity over the past 150 Myr (Brouha et al. 2003).

The canonical, full-length L1 element is a~6 kb long and consists of a 5′ UTR containing an internal RNA polymerase II (RNAPII) promoter, two open reading frames (ORF1 and ORF2) and a 3′ UTR containing a polyadenylation signal ending with an oligo(dA)-rich tail of variable length (Fig. 8). ORF1 encodes an RNA-binding protein and ORF2 encodes a protein with endonuclease and reverse-transcriptase activities.

Figure 8. Structure of non-LTR-retrotransposon (L1 family)

This molecular machinery allows the retrotransposition process known as target-primed reverse transcription (TPRT) to occur, making L1 elements the only autonomous TEs in the human genome.

The transposition of these elements was observed in some genetic diseases, like neurofibromatosi and some cancer types.

L1 retroelements in mammalian genomes can be traced back over 100 million years (Fig. 9) (Burton et al. 1986);(Furano 2000); (Lander et al, 2001). Most of L1 copies are either fossils of previously active or truncated L1 elements.
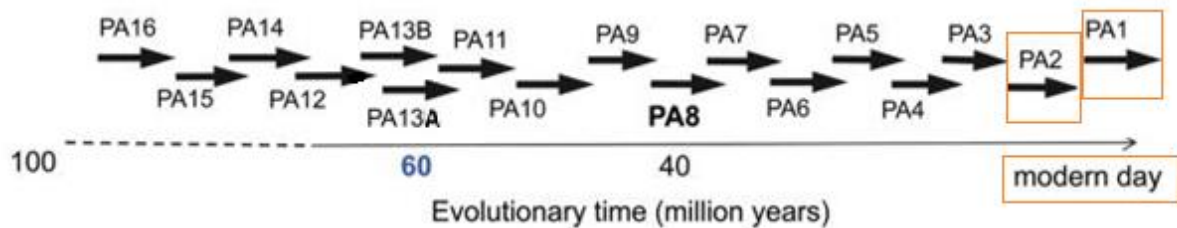
Figure 9. Divergency among L1 families sequences in the human genome during evolutionary time (Khan, Smit, and Boissinot 2006)

An estimated 80–100 full-length retrotransposition competent L1s (all belonging to the modern L1 family L1Hs, L1PA1 and L1PA2) are present in a typical diploid human genome, and a small number, termed "hot L1s" exhibit high retrotransposition efficiencies in cultured human cells (Brouha et al. 2003).

Short interspersed nuclear elements (SINE)

Short interspersed nuclear elements (SINEs) are non-autonomous, non-coding TEs that are about 100 to 700 base pairs in length. SINE sequences are widely distributed in eukaryotic genomes and have crucial roles in genome organization, genome evolution and gene expression modulation. SINE sequences have been implicated as being involved in cell survival during physiological stresses including heat shock, DNA damage, irradiation, oxidative stress, low temperature, exposure to toxic agents, and infection by pathogens.

SINE sequences are referred to as non-autonomous retrotransposons because they usually depend on enzymes encoded by long nuclear interspersed element (LINE) sequences for reverse transcription and retrotransposition.

SINE sequences are transcribed by RNA polymerase III (pol III). Subsequently RNA pol III-SINE transcripts are reverse transcribed by reverse transcriptase (RT) and re-integrated by endonuclease (EN) into various sites in the genome.

Some SINE sequences, which possess an intact RNA pol III promoter, are functionally active but the majority are not actively transcribed. Large numbers of SINE sequences in eukaryotes are derived from tRNAs while others are derived from 5S rRNAs or 7SL RNAs (Kramerov et al., 2011).

Alu elements

Alu elements belong to SINE and are characteristic of primates. Alu elements represent one of the most successful of all mobile elements, having a copy number exceedind 1 million copies in the human genome, thus contributing to almost 11% of the human genome. These elements were colled "Alu" since they are sensible to the restriction enzyme AluI. The typical full-length of an Alu element is ~300 bp long and has a dimeric structure made by the fusion of two monomers derived from the 7SL RNA gene (a component of the signal recognition particle) (Fig. 10).

The monomers are separated by an A-rich linker region, the 5′ region contains an internal RNA polymerase III (RNAPIII) promoter (A and B boxes).

Figure 10. Structure of Alu element, belonging to the family of SINE elements

B box is essential for the transcription of Alu, while the A box seems important to define the transcription starting site of the element (TSS), located at 10-12 nucleotides upstream of the sequence itself.

The element ends at 3' with a poly-A and with a region with variable length and variable sequence called 3'Trailer.

Alu elements do not possess RNAPIII termination signals, and Alu transcripts extend into the downstream flanking sequence until a terminator (typically a run of four or more consecutive thymines) is found. (Fig. 11)
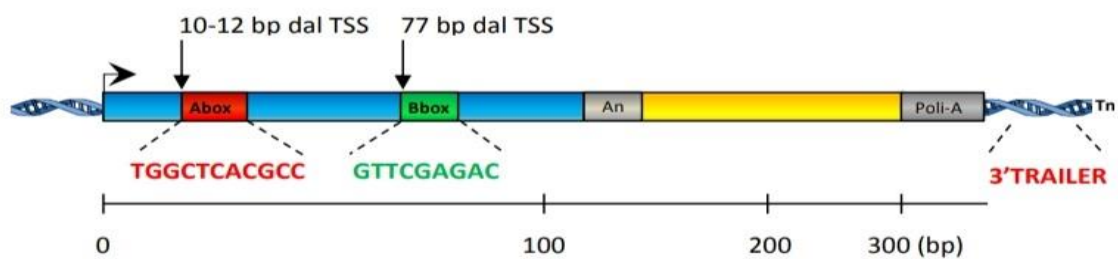
Figure 11. Alu element: localization of the transcription starting sites

Alu elements have no coding capacity and are therefore non-autonomous TEs. Instead, they make use of the retrotransposition molecular machinery encoded by L1 elements, which is the reason why Alu elements are sometimes referred to as 'paresite sequences'. Also Alu elements can influence DNA architecture: they can induce non allelic homologue ricombination, favouring deletions or duplications of large chromosomal regions (Srikanta et al. 2009).

Alu have an important role even postranscriptionally, in fact they can act on the alternative splicing process, determining different proteins production; Alu can also stop or regulate miRNAs expression (Gu et al. 2009).

Non-LTR Retrospansposons activity

The shift of a retrotransposon from one part of the genome to another is called transposition; in particular the transposistion of retrotransposons follows the pattern of replicative transposition. According to this model, common to some transposon types and insertion sequences, when the TE moves to a new positon in the genome there is always a copy in its original position.

The replicative transposition is possible thanks to the ORF2 domain, which consists of a first part codifying for an endonuclease (EN) and a second part codifying for a retrotranscriptase (RT).

The ORF1 protein also may play a role in the transposition, but this function is still the subject of study and debate.

During retrotransposition, encoded proteins are transferred on the mature mRNA of the LINE forming with this an intermediate ribonucleoproteic (RNP) complex.

The RNP complex moves to a target site on a host chromosome; at this point is activated the endonuclease that cuts the DNA of the guest. The preferential cutting sites are at 5'-TTTT/AA-3' sequences, in fact the presence of many T allows the DNA to match with the RNA poly-A tail. (Fig. 12)

The Retrotranscripase (RT) can now act backwards transcribing the mRNA into DNA using the primer sequences generated by the 3' cut; this reaction is called "target-primed-reverse transcription"(TPRT). (Luan et al. 1993);(Cost et al. 2002).
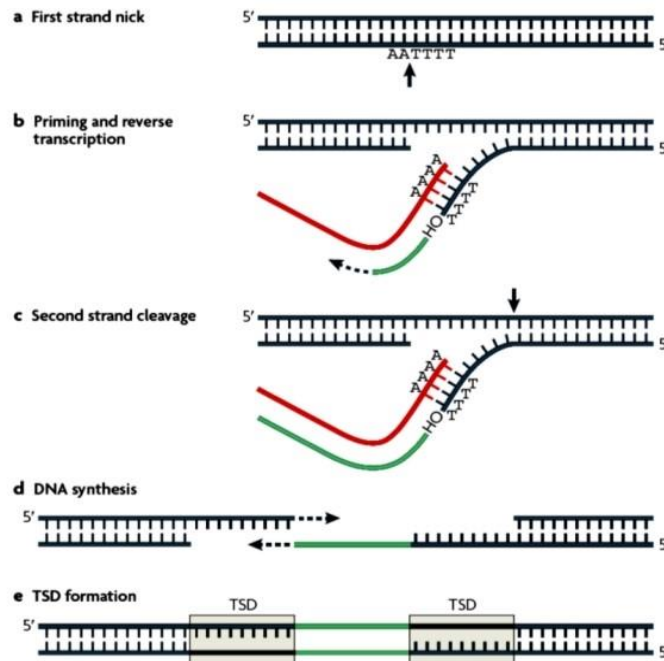
Figure 12. Target-primed-reverse transcription (TPRT) mechanism.

TPRT and the integration in the genome of the newly formed DNA sequence, is followed by the RNAse activity that eliminates the mold of mRNA.

Characteristic elements of the integration process are the 3' poly-A, 5' truncations and short target site duplications (TSD, Target Site Duplications) of 2-20 bp, flanking the new copy element.

This mechanism allows transposons to greatly and rapidly increase their copies number within the genome, thereby furthering the size of the genome itself.

Like other types of transposable elements, retrotransposons can induce mutations by randomly inserting themselves into functional genes, altering them or, in some cases, preventing their expression.

However, experimental evidences show that the transposition and the maintenance of retrotransposon copies within the host genome, is regulated by genes present both on the backtransposons themselves and in the host genome. These genes would

cooperate in preventing transposition from having deleterious effects on both the rear and host.

Anyway, understanding how these mechanisms operate and how they may have co-evolved in order to ensure the mutual survival of rear-transposons and guests is an open and developing field of research.

Transposition is mutagenic and organisms have evolved mechanisms to repress the activity of their TEs. TEs can be silenced via different epigenetic mechanisms such as histone modifications and DNA methylation. The loss of effective silencing of TEs can lead to their activation, which in turn can lead to mutagenic and gene regulatory consequences, as well as induction of the interferon defense pathway.

Transposition in somatic cells is very low but recent evidence suggest that it may be derepressed in some cases, such as cancer development and during normal ageing. In advance age and age associated diseases, the expression culminates in active transposition, being an important contributor to the progressive dysfunction of aging cells.

Genome integrity is mantained by multiple pathways involving the DNA damage response machinery and chromatin remodeling complexes. These pathways that are normally highly efficient, begin to lose their effectiveness with age contributing to destabilization of the genome. Multiple environmental endogenous sources of DNA damage have been already documented; one potentially important mechanism impacting genome stability is the activation of endogenous transposable elements (TEs), resulting in mutagenesis, DNA damage and genome rearrangements. (Burns and Boeke 2012).

As mentioned in the previous paragraph, SINE elements are unable to transpose autonomously, in fact for their retrotransposition they exploit the LINE elements, this is made possible by the presence of similar sequences at the 3' ends of LINE and SINE.

Experimental evidence has shown that ORF1p may not be essential in the backtransposition process, however it seems to improve its efficiency. The ORF2p protein, on the other hand, is necessary and mediats the integration of Alu through the TPRT mechanism. The process begins with the binding of Alu transcribed with two Signal Recognition Particle (SRP) proteins, and with the Poli-A Binding Protein (PABP); that help Alu RNA to associate with ribosome, at this level it can interact with LINE ORF2p during translation. The complex Alu RNA and ORF2p is transported in the nucleus, where the endonucleasic activity of ORF2 makes a cut at regions A-rich. The cut generates two ends, one of which is rich in T, enabling the interacton with Aluthrough linking with the poli-A tail. The cut generates a 3' OH end that acts as a trigger fot the retrotranscription mediated by the ORF2 activity.

1.14 General considerations on TEs transpositions

The genome may be viewed as an ecosystem inhabited by diverse communities of TEs, which seek to propagate and multiply through sophisticated interactions with each other and with other components of the cell.

A shematic summarization of how TEs can impact on genomes in direct and indirect ways in eukaryotic cells is depicted in Fig. 13 (Bourque et al., 2018).

As potent insertional mutagens, TEs can have both positive and negative effects on host fitness. However, the majority of TE copies in any given species, especially those present in humans genome, have probably reached fixation through genetic drift and are now largely neutral to their host. As for any other organism, the 'reference' human

genome sequence does not represent a comprehensive inventory of TEs in humans (Sudmant et al., 2015). Thousands of 'non-reference', unfixed TE insertions have been catalogued through whole genome sequencing and other targeted approaches. On average, two human haploid genomes differ by approximately a thousand TE insertions, primarily from the L1 or Alu families.
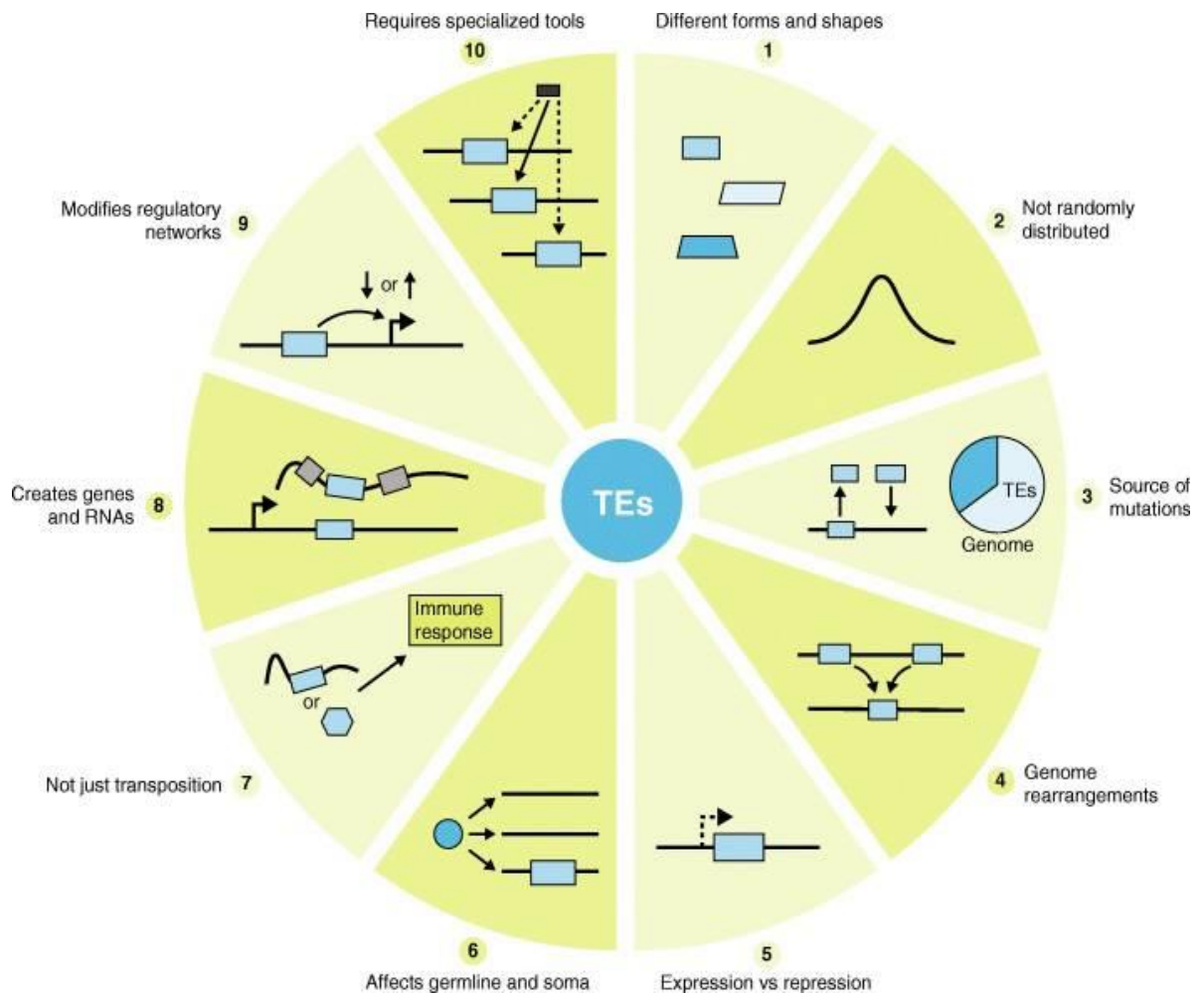
Figure 13. Examples of how TEs can impact genomes in direct and indirect ways (Bourque et al., 2018). Blue boxes represent TEs, gray boxes represent canonical exons, and the black box represents a sequencing read. Right-angled arrows represent gene or TE promoters.

1.15 Retrotranspotion of TEs in aging and cellular senescence

Transposition in somatic cells is very low, but some evidence suggested that it may be derepressed in normal aging and in some ARDs, expecially in tumors. Disruption of tumor suppressor genes (by insertional mutagenesis) and inappropriate activation of positive effectors (by epigenetic dysregulation) are obvious mechanisms that could promote tumorigenesis. However, the extent to which activation of retrotransposition contributes to the total human cancer burden is currently actively debated.

Regarding aging, several families of TEs can be transcribed in aged tissues of animal models, and in advanced age their expression appeared to be associated with active transposition (De Cecco et al., 2013; Cardelli et al., 2018). Studies of diverse species have revealed that chromatin undergoes extensive rearrangements during aging and in senescent cells can be observed a decreased heterochromatinization of normally silenced regions of the genome (Sedivy et al., 2013). These changes can lead to the expression of TEs, culminating in their transposition.

A transcriptional derepression of LINE1 elements was described in senescent human fibroblasts, after cessation of proliferation (Sedivy et al., 2013). Target primed reverse transcription (TPRT) appears to be the primary mechanism by which novel genomic L1 insertions are generated, but there are considerable evidences that cytosolic reverse transcription of L1, without integration, can also occur. Studies on mice deficient for the DNA exonuclease TREX1 revealed the development of inflammatory myocarditis, cardiomyopathies and circulatory failure.

This inflammation was caused by the abundant accumulation of cytosolic DNA mainly represented by L1 and Alu single-stranded DNA (ssDNA), which can triggers an cGAS/STING/IRF3 dependent innate immune response (Fig. 14).
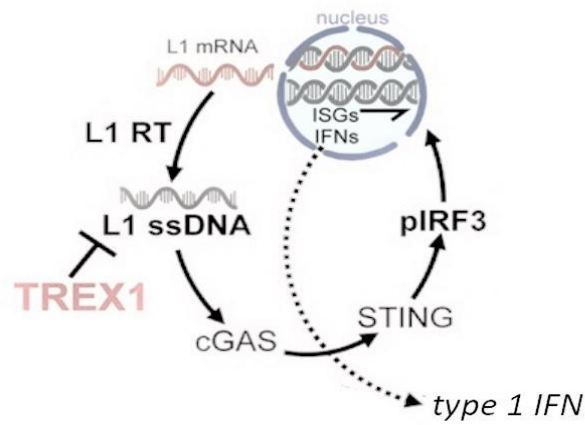
Figure 14. Cytosolic L1 ssDNA: TREX1 degradation

1.16 Accumulation of cytosolic LINE 1 DNA in senescent cells

Two possible mechanisms for the cytosolic accumulation of L1 DNA have been proposed: in the first one the L1 RNA and proteins exist at high levels in the cytosol, thus, reverse transcription occurs without a standard DNA template resulting in elevated cytosolic ssDNA elements, cDNA sequencies (Stetson et al. 2008) (Fig. 15).
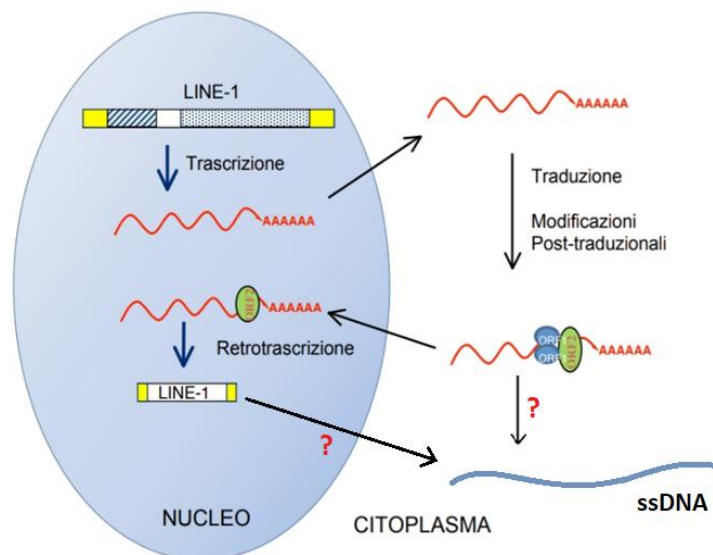
Figure 15. Retrotrasposition of LINE-1 elements

In the second proposed mechanism, the L1 RNA and proteins move into the nucleus, as typically happens for retrotransposition. Then, as L1 begins to reverse transcribe using chromosomal DNA as its template, the resultant ssDNA does not integrate, but instead is cleaved from the chromosomal DNA and exits from the nucleus into the cytosol through a currently unrecognized process. (Thomas et al. 2017).

LINE1-encoded proteins and L1 RNA cytoplasmic foci are often associated with stress granules.

In vitro senescent cells are characterized by low expression of RNAseH2C and high RNAseH2C locus methylation; this molecular setup seems to facilitate the cytosolic nucleic acids accumulation, thus activating the cytosolic sensors (Mensà et al. 2019).

1.17 Cytosilic pathways sensing misplaced nucleic acids

Cytosolic DNAs and RNAs sequencies derived from TEs can be sensed by pattern recognition receptors (PRRs) stimulating the induction of the so-called antiviral response, characterized by increased expression and release of IFNs and of other cytokines genes. A number of cytosolic sensor can detect cytosolic DNA and RNA sequencies (Fig. 16A).

The nucleic acids sensing TLRs 3, 7 and 9 are most prominently expressed in endosomes of phagocytic immune cells, such as monocytes, macrophages, and dendritic cells (DCs), and have been implicated in LINE-1 and Alu sensing.

The well-described group of RIG-I-like receptors (RLRs) sense the presence of dsRNA structures in the cytoplasm and include the retinoic acid-inducible gene I (RIG-I/DDX58 the melanoma differentiation-associated gene 5 (MDA5/IFIH1) and the laboratory of genetics and physiology 2 (LGP2/DHX58). RIG-I recognizes short dsRNA, MDA5

recognizes long dsRNA and LGP2 sequesters dsRNA and thereby functions as a negative regulator.

A number of different candidates for sensing DNA have been proposed over the years. While some of them might only serve as DNA sensors under certain conditions or in specialized cell types, two factors have been generally accepted as bona fide DNA sensors, IFNγ-inducible protein 16 (IFI16) and cyclic GMP-AMP synthase (cGAS) (Carty et al., 2021). IFI16 belongs to the family of pyrin and HIN domain-containing (PYHIN) proteins and can be found in the nucleus or the cytoplasm, depending on the cell type.

The extensively studied PRR cGAS senses DNA of cellular and viral origin, including reverse transcribed cDNA of RNA viruses. Upon binding of cytoplasmic dsDNA, cGAS synthesizes the second messenger cGAMP, which binds and activates the stimulator of IFN genes (STING) which is located in the endoplasmic reticulum (Nakaya et al. 2017). Subsequently IRF3 (Interferon Regulatory Factor 3), is phosphorylated and activated by TNK-binding kinase1 (TBK1). IRF3 phosphorylated and activated translocates in the nucleus inducing the type 1 IFN response, considered the key molecule in the antiviral response (H. Yang et al. 2017) (Fig. 16 B). Notably, type 1 INF can be expressed ubiquitously.
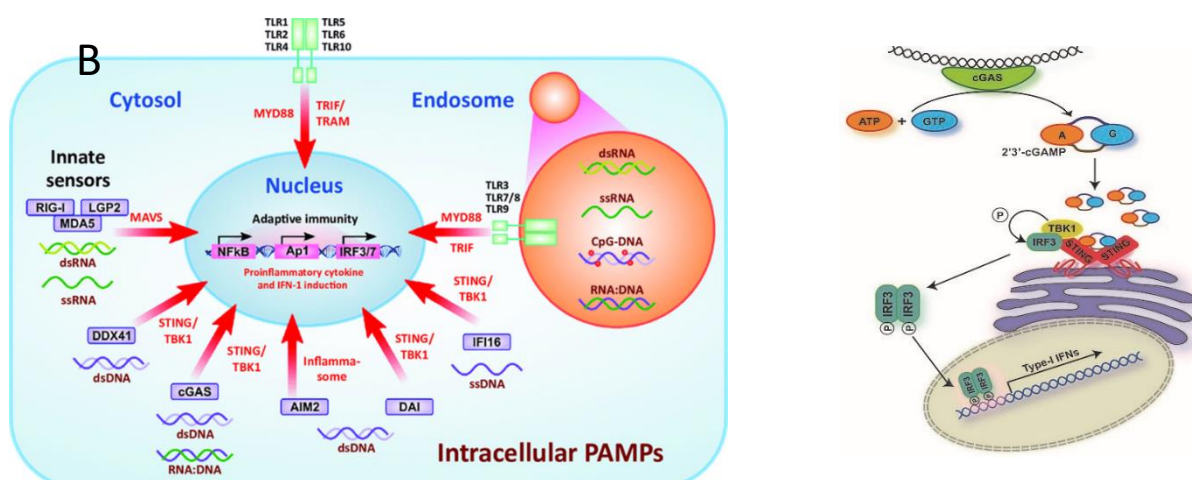
Figure 16. A. Pathways involved in the cytosolic nucleic acids sensing. B cGAS-STING-IRF3 pathway

The most compelling evidence for a LINE-1-associated pattern inducing inflammatory responses has been collected for LINE-1 DNA. Increasing evidence now suggesting that excess reverse-transcribed LINE-1 DNA triggers innate immune reactions via the cGAS/STING pathway. Most studies, however, identified LINE-1 ssDNA accumulation as the most likely PAMP, and it is still unclear as to how cGAS, a known dsDNA sensor, is stimulated by LINE1 ssDNA. The most likely explanation would be that cGAS senses secondary structures, such as stem loop formations, in LINE-1 ssDNA or partially double-stranded LINE-1 cDNA, possibly resulting from aberrant reverse transcription and integration processes. In an alternative explanation, the retroelement-derived nucleic acid triggering the cGAS-mediated immune response is dsDNA and the presence of immunostimulatory dsDNA might only be overshadowed by excess ssDNA accumulation.

Different nucleic acids of LINE-1 and Alu elements can be sensed by pattern recognition receptors during retrotransposition (Fig. 17).
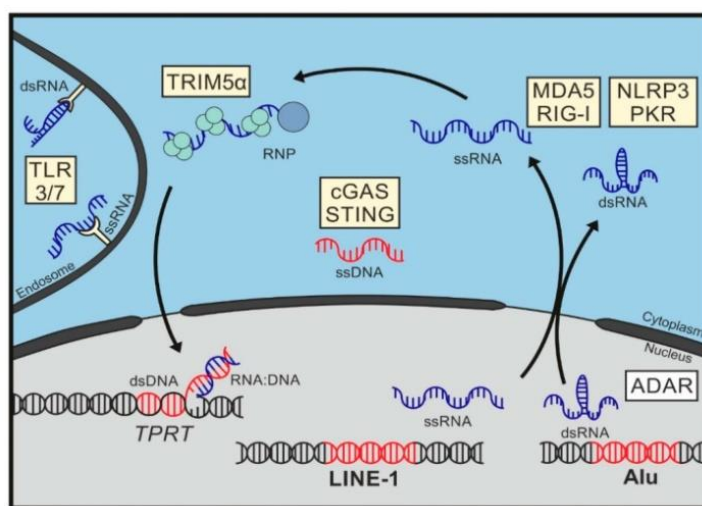
Figure 17. LINE-1 and Alu elements can be sensed by pattern recognition receptors during retrotransposition.

LINE-1 single-stranded DNA (ssDNA) has been shown to accumulate in the cytoplasm, triggering an activation of the cyclic GMP-AMP synthase (cGAS)-STING pathway. It

has been suggested that LINE1 ssDNAs are products of aberrant reverse transcription, which are exported to the cytoplasm (Lagisquet et al., 2021).

Recently, it was reported that mice deficient for SIRT6 exhibit a severely shortened lifespan, growth retardation, and highly elevated LINE1 activity (Simon et al., 2019). SIRT6 is a stress responsive protein deacetylase and a mono-ADP-ribosylase that is involved on the packaging the L1 DNA into transcriptionally silent heterochromatin. SIRT6-deficient cells and tissues accumulate abundant cytoplasmic L1 cDNA, which triggers strong type I IFN response via activation of cGAS.

SIRT6 knockout (KO) mice show a strong activation of L1, suggesting a role for L1 misexpression in their age-related phenotypes.

Remarkably, nucleoside reverse-transcriptase inhibitors, which inhibit L1 retrotransposition, significantly improved health and lifespan of SIRT6 knockout mice and completely rescued type I IFN response (Simon et al., 2019) (Fig. 18).
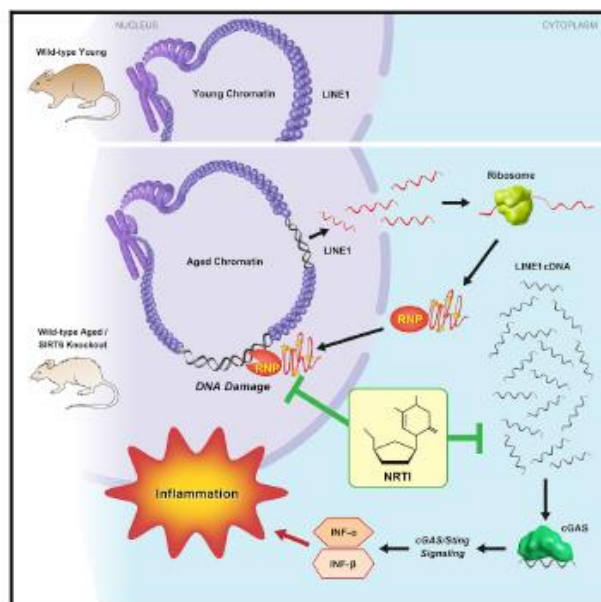
Fig. 18 (Simon et al., 2019). Cytoplasmic accumulation of LINE1 cDNA copies induced a type I IFN response, through the cGAS DNA sensing pathway, resulting in pathological inflammation. Inhibiting L1 replication significantly improved the health and lifespan of aged mice.

2. Purpose of the thesis

It was recently demonstrated that during cellular senescence retrotrasposable elements (TEs), like LINE-1 elements, can be transcriptionally derepressed activating the INF type 1 response. Hypomethylation of the LINE-1 promoter CpG islands, epigenetic modification induced by DNA damage and senescence-associated chromatin reorganization (lamin B-mediated) have been proposed as mechanism that can activate LINE-1 transcription and transposition during cellular senescence.

DNA and RNA sequencies derived by TEs can accumulate in cytoplasm of senescent cells. As a consequence, senescent cells could be chronically stimulated to activate an antiviral response, characterized by increased release of INF type 1, through the cGAS-STING-IRF3 molecular axis.

In this framework, a better understanding of the mechanisms involved in the accumulation of cytoplasmic DNA, including cDNA derived from TEs, in senescent cells, could help to underpinn some of the key features of aging process.

We will analyse the genome-wide methylation status of young and senescent human endothelial cells (HUVECs), to identify genomic regions characterized by significant demethylation in senescent cells, and we will search for the presence of demethylated CpG sites inside TEs sequences.

Rretrotrasposable activity of identifyed demethylated TEs will be investigated, analysing TEs RNA and DNA in senescent cells compared to younger ones. These analisys will be per formed on two cellular models involved in inflammatory responses, such as human endothelial cells and fibroblasts.

Finally, the abilities of TEs nucleic acids located in cytosol, to activate sensors inducing antiviral response characterized by INF type 1 sinthesys will be verified.

3. Materials and methods

3.1 Genome-wide DNA methylation analysis

Genomic DNA was extracted from young and senescence HUVECs (biological triplicates) using Qiagen's QiAmp mini kit following the manufacturer's recommendations. Bisulphite-conversion of 1 µg DNA was perfeomed using EZ DNA Methylation (Zymo Research, USA) and analysed with the Infinium HumanMethylationEPIC BeadChip (Illumina Inc., USA) accordingly to the manufacturer's instructions.

The IlluminaHumanMethylationEPICanno.ilm10b2.hg19_0.6.0.tar.gz manifest was employed to annotate the EPIC probes. Quality controls of raw and normalised data were performed using ShinyMethyl v1.18, available in Bioconductor 3.8.

Data normalisation included noob background correction and implemented functional normalisation of the Minfi function "preprocess Funnorm".

3.2 Characterisation of the senescence status of HUVEC and NHDF cells

HUVEC and NHDF senescence was characterised by analysing a number of well-established senescence biomarkers, comparing non senescent (young) cells, cells with an intermediate senescence status (middle) and old (senescent) cells. Compared with young cells, old cells were characterised by growth arrest, which was documented analysing cumulative population doublings (cPDs), telomere length (T/S), SA β-gal activity, mRNA trascription of cell cycle regulators p16 and p21; expression levels of miR-21, miR-146, miR-217 (Mensà, Guescini, Giuliani, Bacalini, et al. 2020).

3.3 Telomere lenght assesment

The telomere length was measured using the method previously described (Cawthon 2002).

Every PCR experiment included a calibrator.The calibrator was obtained diluting in DNAse free water a reference sample of genomic DNA (gDNA). The calibrator was used at a concentration of 3 ng/µl with serially dilutions (dilution factor of 1.68) to obtain eight different concentrations ranging from 50.4 ng to 1.25 ng.

To limit the variability between the different experiments, the tests with the telomere mix and the single copy gene (36B4) were carried out in the same plate.

The thermal profile used consists of the following cycles:

95°C x 10 sec

95°C x 5 sec ⎤
57°C x 15 sec ⎬ — 30 cycles
72°C x 20 sec ⎦

Each sample was analysed in duplicate, whereas the different dilutions of calibrator in tripled.

The T/S ratio (Telomere /Single copy gene) of each sample was determined ad previously described (Bonfigli et al., 2016).

3.4 Detection of SA β-galactosidase activity

The percentage of senescent cells, was assessed using Senescence Detection Kit (cat. no. K320, BioVision Inc., USA), that leverages the activity of the enzyme β-galactosidase at pH 6, characteristic of senescent cells.

β-galactosidase can split an organic compound the X-Gal, consisting of a galactose molecule bound to a substituted indole, producing galactose and 5-bromo-4-chloro-3-hydroxyndous. The latter is oxidized to 5,5'-dibromo-4,4'-dichloro-indigo, an insoluble blue compound. Cultured cells are removed from the soil washed with PBS (Phosphate buffer saline) 1X, and covered with 1ml of 'Fixative Solution'. After 15 minutes at room temperature, are carried out two more washes in PBS, then 1ml of 'Staining Solution' is added. Covered cells are incubated at 37°C overnight in a dry incubator before proceeding with the display under an optical microscope.

To define the senescence rate, each reading of 200 cells was made in triplicate; cells are defined as senescent when from the total of each reading, at least 60% are positive for β-Gal staining.

3.5 HUVEC and NHDF colture

An in vitro model of replicative cell senescence was established using long-term cultured Human Umbelical Vein Endothelial Cells (HUVECs) and Normal Human Dermal Fibroblasts (NHDFs). Cryopreserved HUVECs from pool of donors were purchased from Clonetics (Lonza, Switzerland) and cultured in endothelial basal medium (EBM-2, CC-3156, Lonza) supplemented with SingleQuot Bullet Kit (CC4176, Lonza) containing 0.1% human recombinant epidermal growth factor (rh-EGF), 0.04% hydrocortisone, 0.1% vascular endothelial growth factor (VEGF), 0.4% human recombinant fibroblast growth factor (rh-FGF-B), 0.1% insulin-like growth factor-1 with the substitution of arginine for glutamic acid at position 3 (R3-IGF-1), 0.1% ascorbic acid, 0.1% heparin, 0.1% gentamicin and amphotericin-B (GA-1000) and 2% fetal bovine serum (FBS).

Cryopreserved NHDFs from pool of donors were purchased from Clonetics (Lonza, Switzerland) and cultured in (FBM-2, CC-3131, Lonza) supplemented with SingleQuotes Bullet Kit (CC-4126, Lonza) containing 0.1% insulin, 0.1% Human Basic Fibroblast Growth Factor (hFGF-B), 0.1% gentamicin and amphotericin-B (GA-1000) and 2% fetal bovine serum (FBS).

HUVEC and NHDF Cells were both seeded at a density of 5000/cm2, sub-cultured when they reached 70–80% confluence, and maintained in a humidified atmosphere of 5% CO_2 at 37°C. All cells tested negative for mycoplasma infection. Before replating, harvested cells were counted using a haemocytometer. Population doublings (PDs) were calculated by the formula: (log10F – log10I)/log10, where F is the number of cells at the end of the passage and I is the number of seeded cells. Cumulative population doubling (cPD) was calculated as the sum of PD changes. Cells were cultured until the arrest of replication and classified based on SA β-Gal activity into Young (β-Gal < 5%), senescent (β-Gal > 60%) and middle aged (30%<β-Gal<40%).

3.6 Metylation analysis of specific loci

Extracted DNA deriving from young and senescent HUVECs, was bisulphite-converted and analysed by the Infinium Human MethylanEPIC Bead Chip. CLC Genomics WorkBench was used to align sequencing data with human genome, promoters and regulatory regions, while Repeatemasker (rpmsk), downloaded from USCS Genome, served to identify methylations within repeating sequences.

3.7 Gene density upstream and downstream demethylated sites

Gene density was calculated using the 'FlankBed' function of Galaxy, obtaining the sequences 500 Kbase upsteam and downstream of each CpG significantly demethyled in senescence cells, gene densities were divided into three groups: low gene density (1-10 genes), middle gene density (11-40 genes), high gene density (41-90 genes).

3.8 Primer design

Suitable primers were firstly identified using "Primer 3" then using the function "In silico PCR" of UCSC, was verified the unique recognition of a single sequence.

Primers sequences were further checked using "Mega-X" and aligning primers sequences with the genome, the positions of demethylated CPGs and the consensus sequences of LINE1, L1PA2 and L1HS.

The compatibility of the Tm of the primers pair and the length of the amplified was also verified.

3.9 Nuclear and cytoplasmic cell fractions division

One million of young, middle and old cells were pelleted and treated using the method described above (Asada et al. 2018) with some modifications. The pellet after adding four volumes of Lysis Buffer n1 (20mM HEPES, pH 7.4, 10mM KCl, 2mM MgCl2, 1mM DTT, and 1mM EDTA) was incubated in ice for 20 minutes. In order to facilitate cellular lysis, the pellet was passed 15 times through a 25-gauge needle and the suspension obtained centrifugated 2 times to 800 g for 5 minutes each. The pellet obtained, containing the nuclear fraction, was treated with a second lysis buffer (50mM HEPES, pH 8.0, 150mM NaCl, 10% glycerol, 1mM DTT, 2mM EDTA, 0.5% SDS, and 100µg/mL

proteinAse K (Sigma-Aldrich) and incubated 1 hour at 37°C for further extraction. The supernatant was further centrifuged for 10 minutes at 10000 g; the pellet obtained and containing the mitochondrial fraction has been discarded; the supernatant without further extraction steps was used as a cytoplasmic fraction.

The nuclear fraction for samples used in western blotting experiments was extracted using a modified Lysis Buffer No. 2, free of Proteinase K.

The use of Raw lysate:

The current procedures for quantitative extranuclear DNA analysis imply DNA purification with subsequent absolute quantification of various DNA sequences by quantitative real-time PCR (qPCR). Unfortunately, the DNA extraction is accompanied by some constraints, such as the risk of contamination or inconsistency, particularly when using samples with low concentrations. Moreover purification reagents may contain PCR inhibitors, minimizing the assay resolution or leading to false quantitative or qualitative outcomes (Huggett et al. 2008). The DNA yield is reduced to an uncertain extent, depending on the isolation method of choice and the fragment size of the DNA sequencies.

One approach to overcome the mentioned aspects restricting ccf-DNA but also cytosolic DNA measurement is the quantification directly in the raw sample, in our case in the raw lysate, like it has been recommended recently by Schwarzenbach (Umetani et al. 2006)(Schwarzenbach, Hoon, and Pantel 2011) in a published method for DNA quantification without prior DNA extraction.

Before proceeding with the experiments, to verify the absence of proteins that could infer with the analysis, the raw lysate was diluted serially. The concentration of each dilution was read in triplicate using Qubit, the reads average used to create a calibration line, whose R^2 resulted close to 1.

3.10 Quantitative RT-PCR of mature microRNAs

MiRNAs have been quantified using the TaqMan MicroRNA (Applied Biosystems) kit with some modifications. Total RNA has been retrotranscribed with the TaqMan MicroRNA kit. Five RT reaction microliters contained 1 µl of specific miR primer, 1.67 µl of RNA, 0.4 µl of dNTPs at the concentration of 10 mM, 0.3 µl of inverse transcribing, 0.5 µl of buffer 10x, 0.6 µl of diluted RNAse inhibitor 1:10 and 0.5 µl of H2O. The thermal profile of the backtransscription includes the following phases: 16°C for 30 min, 42°C for 30 min and 85°C for 5 min.

The next Real time qPCR was performed in 20 µl PCR reaction containing 1 µl taqman miR 20x, containing PCR primers and probes (5′-FAM); 10 µl of TaqMan Universal Master mix no UNG (Applied Biosystems) and 5 µl of RT product.

The reaction was first incubated at 95°C for 2 min followed by 40 cycles of 95°C for 15 s and 60°C for 1 min. The relative expression of miRNAs was calculated with the formula $2^{-\Delta\Delta Ct}$, where $\Delta Ct = Ct(miRNA) - Ct(RNU44)$.

3.11 p16, p21 and IFN1 mRNA expression level

For the gene expression, 1000 ng of purified RNA were retrotranscribed using PrimeScript™ RT reagent Kit with gDNA Eraser (Perfect Real Time) (TaKaRa), following the instructions indicated in the manual.

Real time qPCR rations were performed using a Rotor Gene Q (Qiagen, Germany) in a total reaction volume of 10 µl using TB Green Premix Ex Taq II. For each sample the reaction was performed in duplicate and each experiment included a template-free sample, to check contaminations or primers pairing events.

The mRNA expression was calculated using Actin as reference gene. mRNA expression levels were analyzed using the 2−ΔCt method. B.

In the table below are the primers sequences used, written in direction 5'-3', all primers were used at the concentration of 10 µM.

Actin-Fw	TGCTATCCCTGTACGCCTCT
Actin-Rv	GTGGTGGTGAAGCTGTAGCC
GAPDH-Fw	TGC ACC ACC AAC TGC TTA GC
GAPDH-Rv	GGC ATG GAC TGT GGT CAT GAG

p16-Fw	CAT AGA TGC CGC GGA AGG T
P16 Rv	CTA AGT TTC CCG AGG TTT CTC AGA
P21 Fw	TGGACCTGTCACTGTCTTGT
P21 Rv	TCCTGTGGGCGGATTAG
IFN1β-Fw	TGC TCT CCT GTT GTG CTT CT
IFN1β-Rv	CAT AGA TGG TCA ATG CGG CG
Actin-Fw	TGCTATCCCTGTACGCCTCT
Actin-Rv	GTGGTGGTGAAGCTGTAGCC

3.12 Expression of Alu, ORF2 and L1PA2 mRNAs

TEs expression levels were measured applying the same method described above for the mRNA expression of p16, p21 and INF type 1, with some changes. In the backtranscribed mix, the RT Primer Mix test tube was replaced with dT oligo.

During each backtranscription reaction, in parallel with the samples, were inserted a sample without template (no RT) and a calibrator, *i.e.* a sample with known concentration, prepared, diluted, rated and frozen before the start of the experiments, in order to verify the performance of each experiment and compare the data obtained in different Runs.

The primers sequences used for TEs analysis were reported In the table below, written in direction 5'-3'. All primers were used at the concentration of 10 µM.

L1PA2-Chr14-Rv	CCT CGC CTT GCT TCC ACT T
L1PA2-Chr14-Fw	CAG CTC AGG TCT ACA GCT CC
Alu Ya5-Rv	TCT CGA TCT CCT GAC CTC GT
Alu Cons-Fw	CGC CTG TAA TCC CAG CAC
ORFp2-Rv	CCG GCT TTG GTA TCA GAA TG
ORFp2-Fw	CAG CCG AAT CTA CCA GAG G
5S-Fw	CGA TCT CGT CTG ATC TC
5S-Rv	CTA CAG CAC CCG GTA TT

3.13 Western Blot

The proteins of the nuclear and cytoplasmic fractions were extracted using the RIPA buffer (NaCl 150mM, Tris 10mM pH7.2, 0.1% SDS, 1% Triton X-100, EDTA 5mM pH 8, protease inhibitors (Roche Applied Science, Indianapolis, IN).

A total of 30 ng lysate were used; the concentration of lysate proteins was determined using the Bradford colorimetric reaction (Sigma-Aldrich, Milan, Italy). Electrophoresis was performed using Mini-PROTEAN TGX Stain Free Gels precast gels, 4-15%, 12 well comb (Bio-Rad Laboratories, USA).

Membrane transfer was performed using Trans-Blot Turbo (Bio-Rad).

The membrane was then incubated the whole night at -4 degree, covered with a 5% milk solution and primary antibodies (Lamin A/C, Cell Signaling) (β-Actin,sc-47778, Santa Cruz). The secondary antibody, was added to the membranes after carefully rinsing them with abundant PBS in order to completely eliminate residues of primary non-legatose antibody. Incubation with secondary antibody took place for 1 hour at room temperature. The proteins were displayed using the chemiluminescent substrate "Clarity Western ECL substrate" (Bio-Rad)

*3.*14 RNA purification

The purification of RNA from cellular pellets of 300,000 cells took place using the "Total RNA Purification kit" (Norgen Biotek Corp, Thorold, ON, Canada) and following the indications in the user manual.

3.15 DNA Extraction

DNA extraction was carried out using the QIAamp® MinElute® ccfDNA Mini Kit (Qiagen, Netherlands) following the user manual instructions.

This extracton kit allows to recede fragmented nucleic acids that are as short as 20 bases less. In fact most of common extraction kits available on market purify DNA fragments up to 200 bp in length.

3.16 Determination of nucleic acid concentration

The concentration of DNA or RNA, according to the experiment, was defined using Qubit's Hight sensitivity (Thermo Fisher Scientifics) program; for each sample the reading was made in triplicate.

3.17 Statystical analysis and Graphs

Differences in methylation between youg and senescent cells were analysed applying Wilcoxon sign ranks, after Bonferroni's correction..

To verify the expression data significance, the student t-test for paired samples was used. Data with P-value <0.05 (*), P-value <0.01 (**) and P-value <0.001 (***) have been consideredas significant.

Statystical analysis was performed using IBM SPSS Statistics, version 25; graphs were obtained using GraphPad prism, version 8.

4. Results

4.1 Characterization of the senescence status of HUVECs and NHDF

The senescent status of HUVECs and NHDFs was characterized by analysing a number of well-established senescence-associated biomarkers. Non-senescent (young), intermediate (midway) and senescent (old) cells were analysed.

Compared with YOUNG cells, OLD cells, both HUVECs and NHDF, were characterized by growth arrest, which was documented by reduced cumulative population doublings (cPDs) (Fig. 1A and 1B), increased SA β-gal activity (Fig. 2A and 2B), progressive telomere shortening (Fig. 3A and 3B), and trascriptional upregulation of the cell cycle regulators p21 and p16(INK4a) (Fig.4A and 4B; HUVECs) (Fig. 5A and 5B; NHDF).
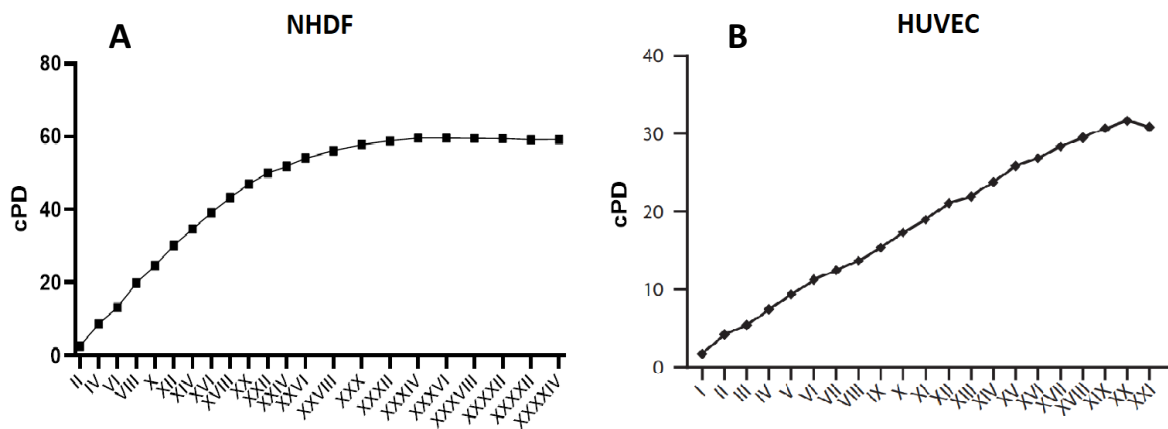
Figure 1A and B. Cumulative population doubling (cPD), respectively in NHDF (A) cells and HUVEC cells (B)
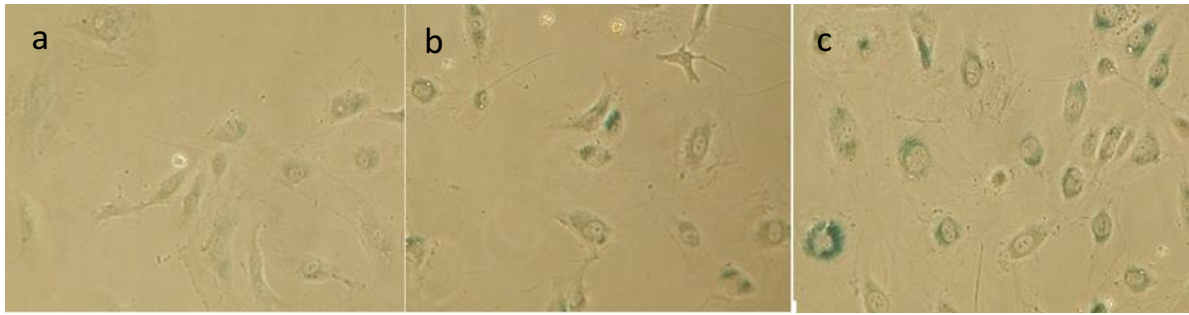
Figure 2A. SA-β-Gal staining of HUVEC cells. Young cells (a), midway cells (b) and senescent cells (c).
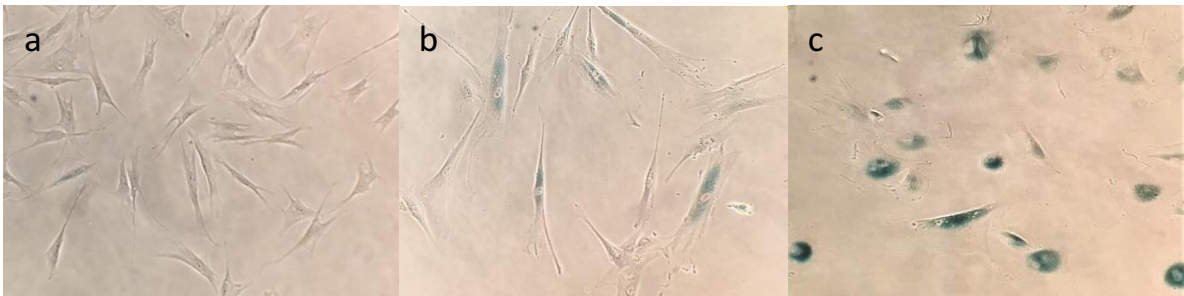
Figure 2B. SA-β-Gal staining of NHDF cells. Young cells (a), midway cells (b) and senescent cells (c).
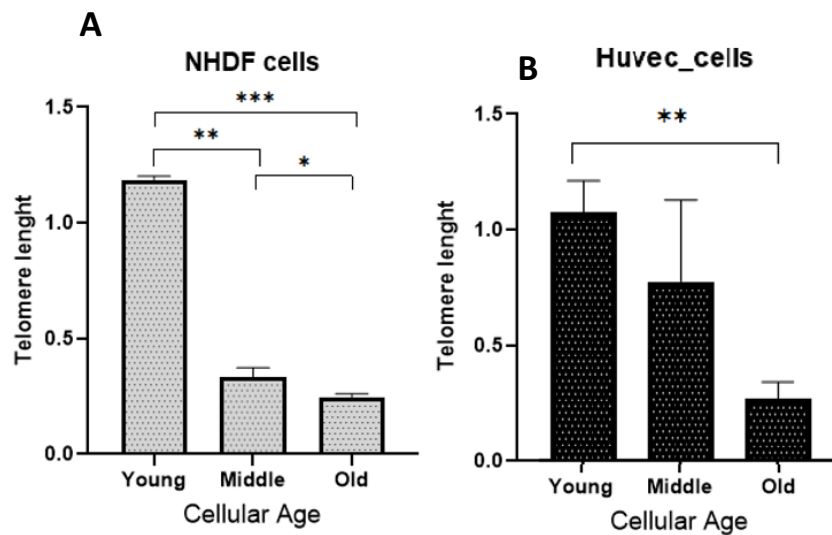
Figure 3A and 3B. Telomere lenght (T/S) respectively in NDHF (A) and HUVEC (B) cells
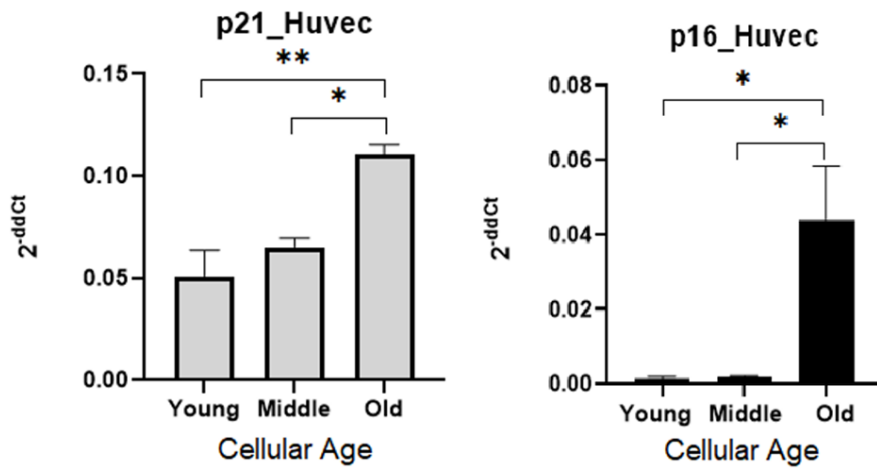
Figure 4A and 4B. Expression levels of p21 and p16 mRNA in HUVECs.
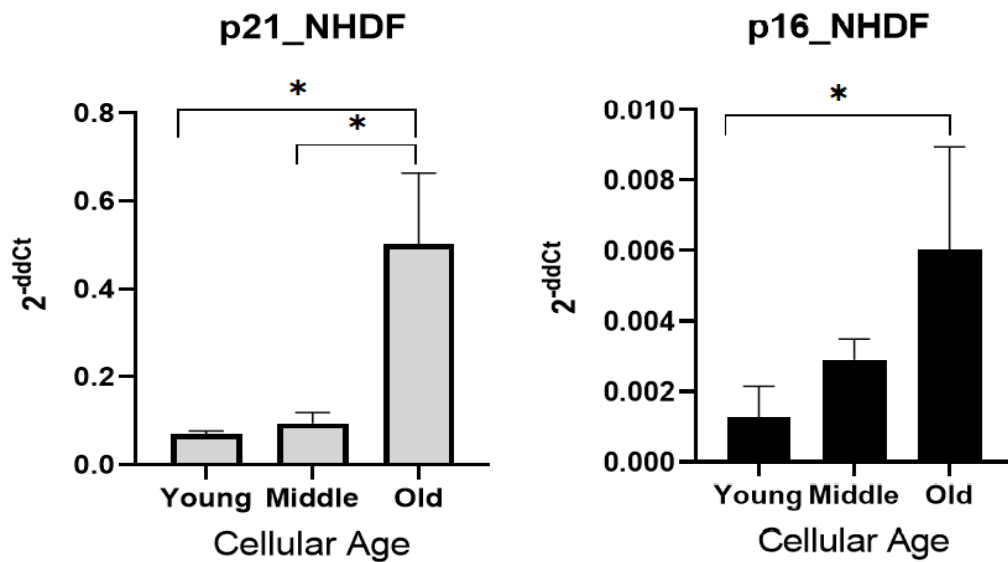
Figure 5A and 5B. Expression levels of p21 and p16 mRNA in NHDF.

Finally, the expression levels of innovative biomarkers of cellular senescence, *i.e.* three inflammammiRs, such as miR-21, miR-146a and miR-217, were analysed (Olivieri et al., 2015) (Mensà, et al., 2020).

Significant increased expression of miR-21 and miR-217 was observed in Old *vs.* Yung cells, both NHDF and HUVEC cells (Fig. 6A and 6B).

Regarding miR-146a expression, increasing trends were observed in Old vs Young NHDF and HUVEC cells.
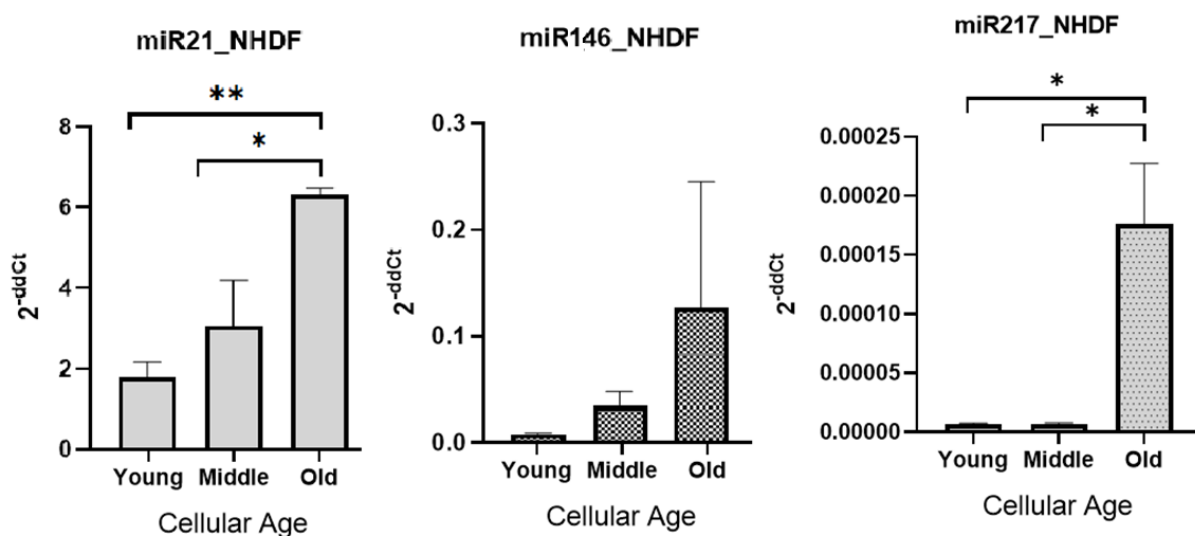
Figure 6A. MiR-21, miRNA-146a and miRNA-217 expression levels in youg, middle and old NHDF cells
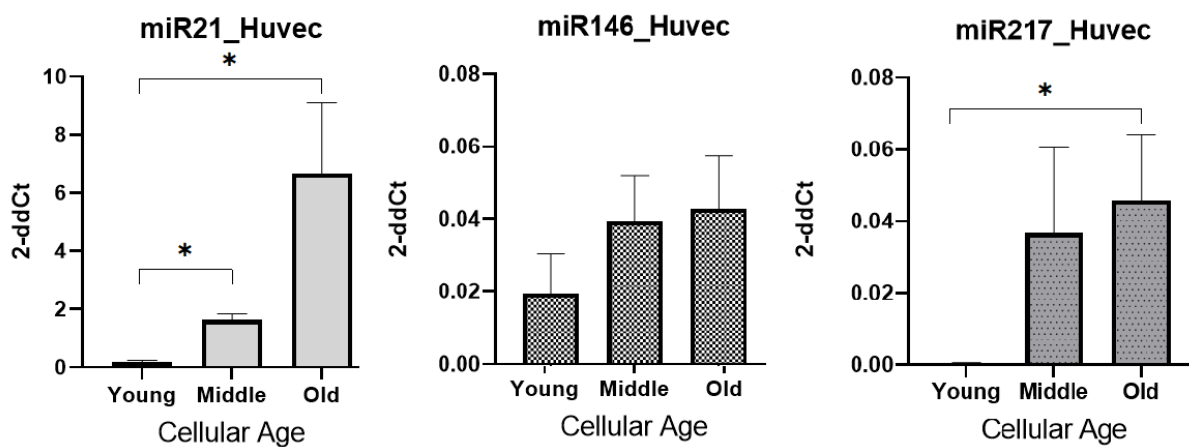
Figure 6B. MiR-21, miR-146a and miR-217 expression levels in youg, middle and old HUVEC cells

4.2 The genome wide methylation analysis of young and senescent HUVECs

The genome wide methylation analysis was initially carried out only on HUVEC cells, comparing Young and Old cells (Fig. 7).
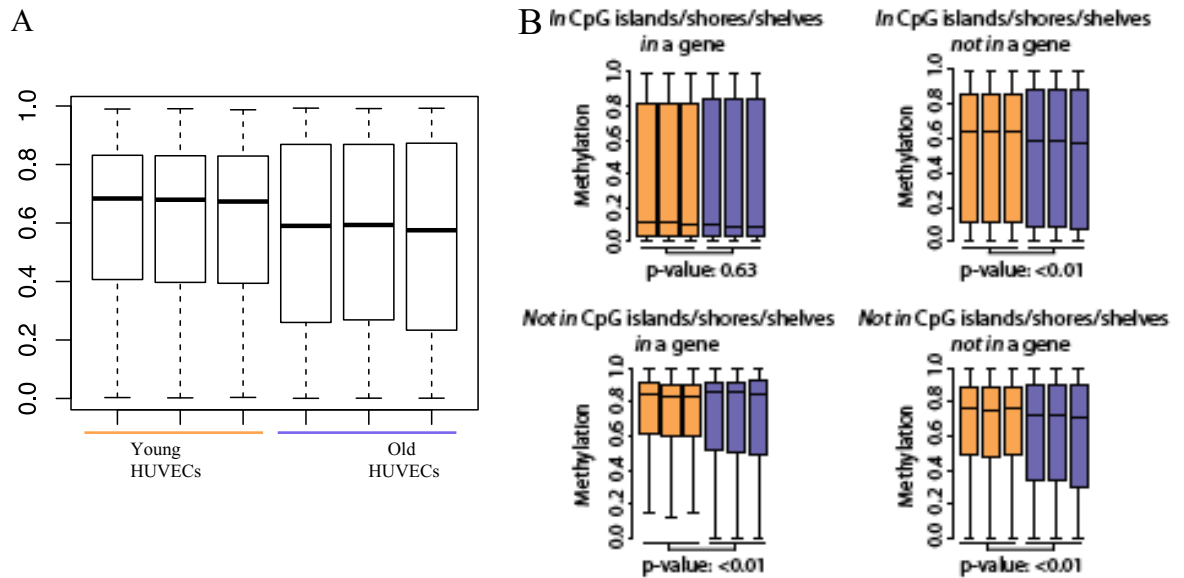
Figure 7 A and B. A CpG DNA methylation values anlysed by InfiniumEPIC probes in Young and Old HUVECs (data are showed as triplicates). B. The probes were divided in 4 groups according to their genomic location and t-test was applied to each group in order to compare mean beta values between Young and Senescent HUVECs.

Characterization and comparison of the epigenetic profile of Old and Young cells demonstrated a differential methylation state at 335,495 CpG sites (Fig. 7A); Old cells showed significant hypomethylation in "CpG island/shore/shelf regions located in intergenic regions" and significant hypermethylation of "single CpG island/shore/shelf in genes" (Fig. 7B).

A further analysis of the hypo and hypermethylated CpG sites in old compared to young HUVECs revealed an increased demethylated CpG in genomic regions characterized by low gene density, defined as "other" in Fig. 8.
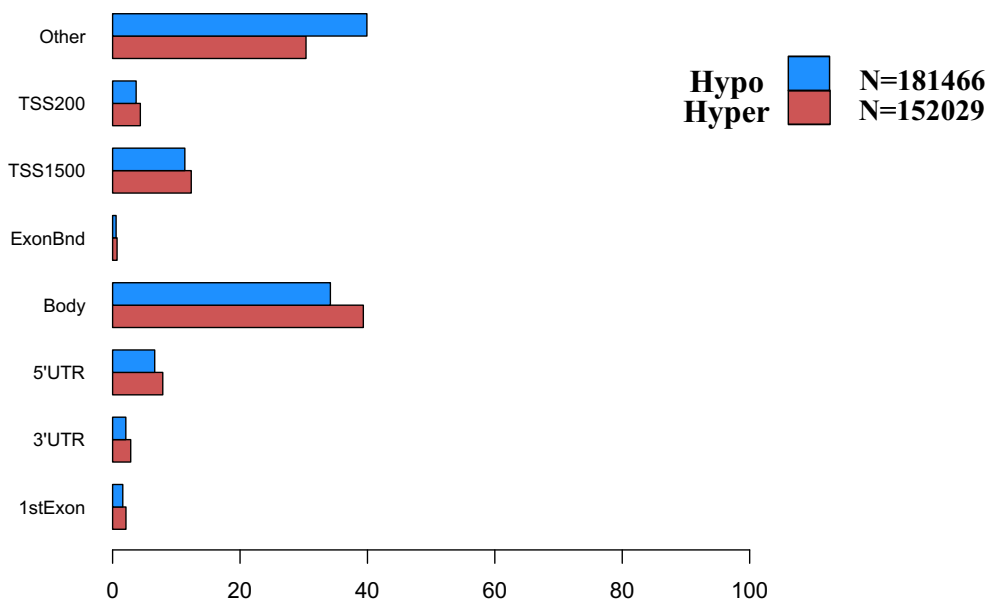
Figure 8. Genomic localization of hypomethylated and hypermethylated CpG locI in Old HUVECs compared to Young HUVECs.

To further investigate if the sequences characterized by increased senescence-associated demethylation belonging to transposable elements (TEs), the most significantly demethylated single CpG sites identifyed by genome-wide methylation analysis were mapped on the reference genome and annotated for their localization inside TEs sequences. CpGs with significant demethylation (> 50%) in senescent HUVECs compared to youger cells were considered in this analysis.

The analysis revealed that the most demethylated sequences within TEs in old HUVECs compared to younger cells belong to the LINE1 family, in particular to the three subfamilies L1M, L1P and L1Hs (Fig. 9).
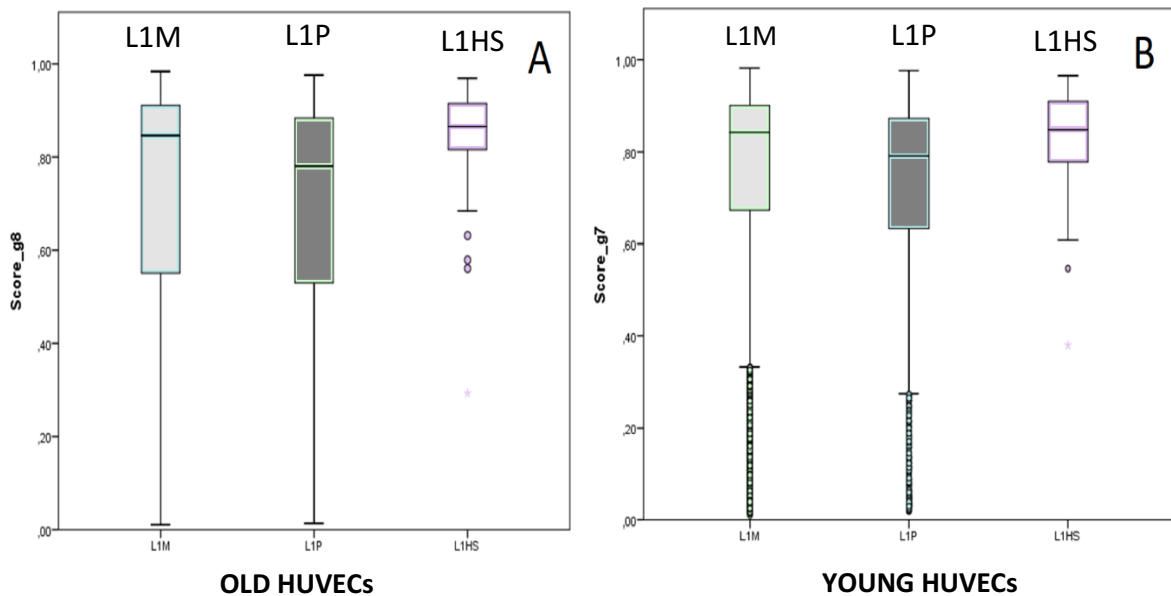
Figure 9. Methylation score of different LINE1 subfamilies, respectively in old (A) and young cells (B).

Significant differential methylation status was confirmed comparing CpGs inside the three LINE1 subfamilies identifyed (Fig. 9).

The length of these LINE1 subfamilies (L1M, L1P and L1HS) has been verified. Almost all the TEs have been found to be incomplete, lacking elements essential to their activity, therefore unable to retrotranspose. Importantly, an L1PA2 element (6053 bp long), located on chromosome 14, extending from position 46.352.411 to 46.358.464 was almost complete, lacking only few bases at 5'. L1PA2 are TE sequences not so active as the L1HS, but evolutionarily quite recent; they are chimeric and present the 5' promoter sequence typical of LINE1. The characteristics of this L1PA2, demethylated in senescent HUVECs and quite complete in sequence, suggest that it could be able to transpone.

Moreover, CpGs demethylation in old cells was significantly different in the three identifyed subfamilies. In detail, the L1M and L1P subfamilies were significantly more demethylated in senescent HUVECs than L1HS (p<0,0001), (Fig.10 A).

This analysis was performed including all CpG genomic sites identified by InfiniumEPIC probes, and mapped within the three analysed L1 subfamilies (L1M, L1P and L1HS).

In order to verify possible causes of the differential methylation status among the different LINE1 subfamilies, their genomic distribution was verified.

Analyzing the gene density of the LINE1 subfamilies regions, a significantly different distribution emerged between the L1HS (evolutionary young LINE1 subfamily) and L1M - L1P (evolutionary old LINE1 subfamilies) (p<0.0001) (Figure 10 B).
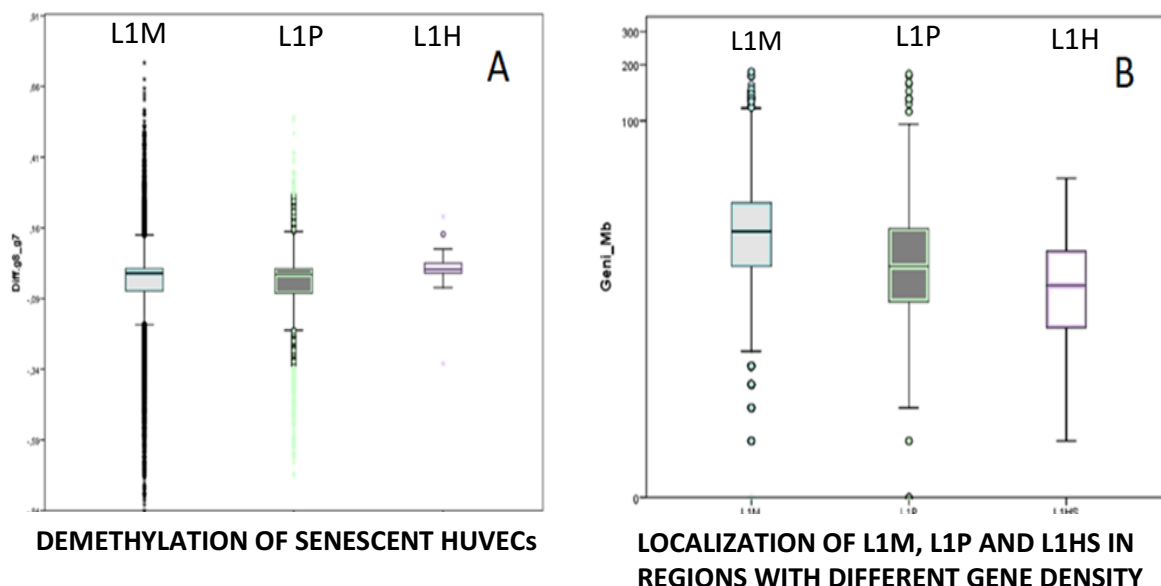
Figure 10. A Demethylation of the three LINEs subfamilies in old HUVECs. **B**. Localization of the three LINEs subfamilies in regions with different gene density.

L1HS demethylated CpG's are mainly represented in regions with low gene density, whereas demethylated L1M and L1P elements can be mapped both in areas with low and with high gene density (Fig. 11).

Conteggio

		Gene_density_class																	Totale
		1,00	2,00	3,00	4,00	5,00	6,00	7,00	8,00	9,00	10,00	11,00	12,00	13,00	14,00	15,00	16,00	18,00	
Subfamily_group	L1HS	28	18	10	2	2	0	0	0	0	0	0	0	0	0	0	0	0	60
	L1M	2330	6524	6787	3922	2013	1274	572	333	225	128	41	40	12	27	9	1	6	24244
	L1P	1099	1517	785	310	186	133	62	37	24	5	0	2	2	2	1	2	2	4169
Totale		3457	8059	7582	4234	2201	1407	634	370	249	133	41	42	14	29	10	3	8	28473

Figure 11. Distribution of the mainly demethylated LINE1 subfamilies in genomic regions with different gene density (Gene density classes). Gene density classes are defined based on the range of gene density, grouped in 18 classes from the lowest (class 1) to the highest (class 18) gene density.

More in detail, the L1M containing demethylated CpG sites in senescent HUVECs compared to younger cells, are more frequently surrounded by regions with low gene density (range from one to ten genes for Mbases) (Figure 12A, B and C).
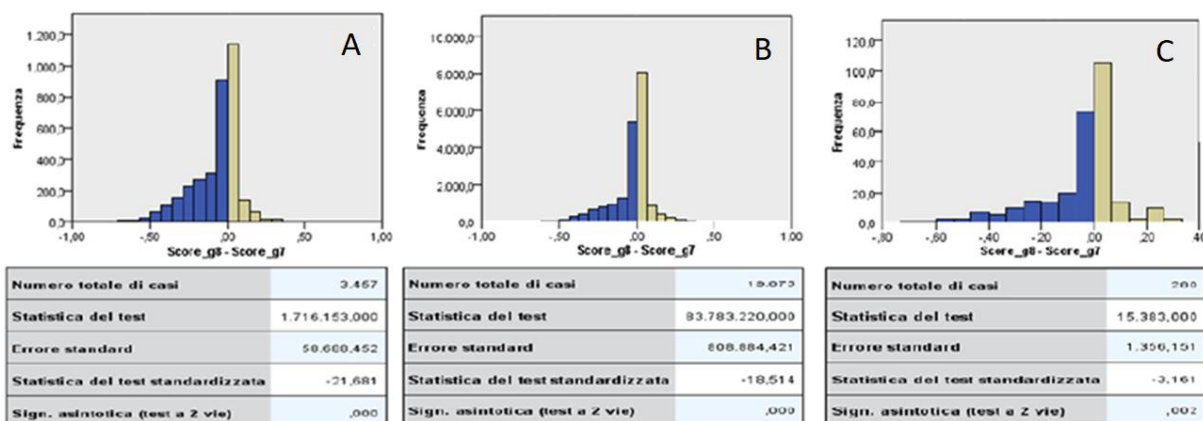
Figure 12. L1M subfamilies distributions of demethylatd CpGs, respectively in areas of low gene density (**A**), midway gene density (**B**), high gene density (**C**). The negative component (in blue) represents the percentage of demethylation (Wilcoxon signed-rank test).

Since recent data suggest that cellular senescence is characterized by a strong activation of the TEs (De Cecco et al. 2019) (Simon et al. 2019), we extend our analysis to the model of replicative senescent dermal fibroblasts (NHDF).

4.3 DNA, RNA sequencies of L1PA2 and ORF2 elements (belonging to LINE1 family) and Alu element (belonging to SINE subfamily).

To verify the hypothesis that L1 demethylation could be associated not only with L1 trascription/activation, but also with the retrotrascription of different TEs, such as SINE sequences that usually depend on ORF2 enzyme encoded by LINE sequences for

reverse transcription and retrotransposition, we anlysed both LINE1 (L1PA2 element previously identifyed and ORF2 element belonging to LINE1 family) and the SINE subfamily of Alu elements.

We select Alu elements since increased evidence suggested an association of this SINE family with cellular senescence process in fibroblast (De Cecco et al., 2019).

The analysis of RNA trascripts revealed significant increased expression of both Alu elements (Fig. 13) and ORF2 (Fig. 14), in HUVECs and NHDF senescent cells compared to the younger ones.
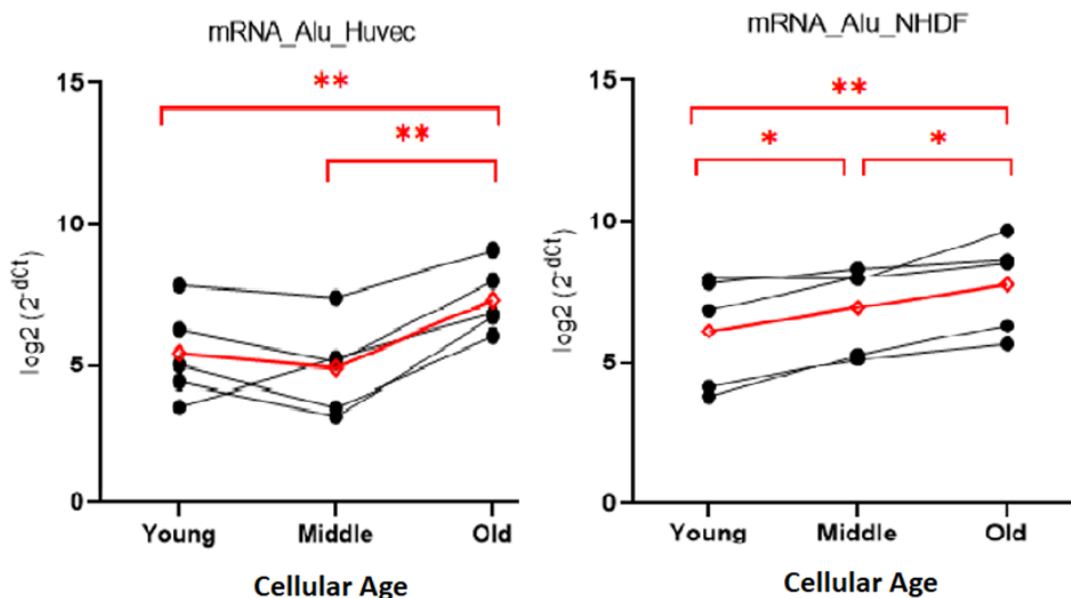
Figure 13. Relative expression of the Alu retrotransposable elements, in HUVEC and NHDF cells. The red line defines the average trend.
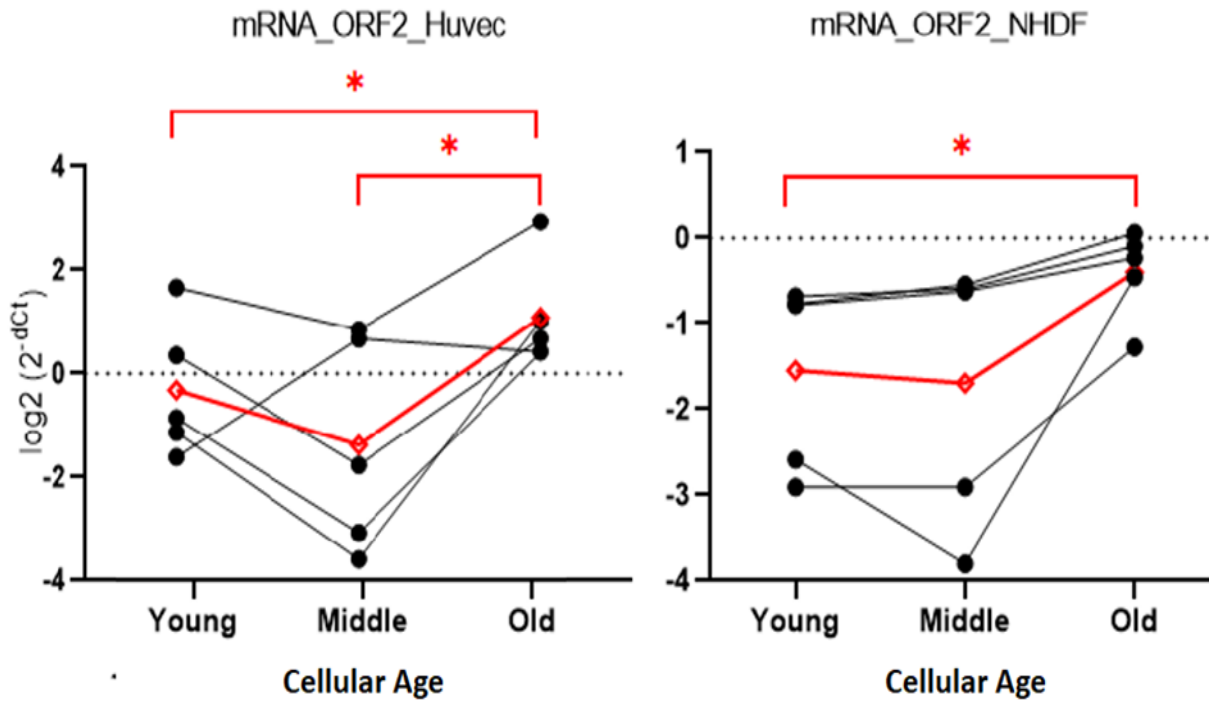
Figure 14. Relative expression of the ORF2 proteins in HUVEC and NHDF cells. The red line defines the average trend

On the other hand, no significant modulation of L1PA2 expression level was found in senescent cells. Notably, L1PA2 was identified by the previous analysis as the most demetylated full-length LINE1 element in senescent cells, suggesting that it could be potentially active (Fig.15).

Notably, L1PA2 RNA was detectable both in old and young cells, suggesting that this LINE sequence is effectively transcribed both in endothelial cells and fibroblasts.
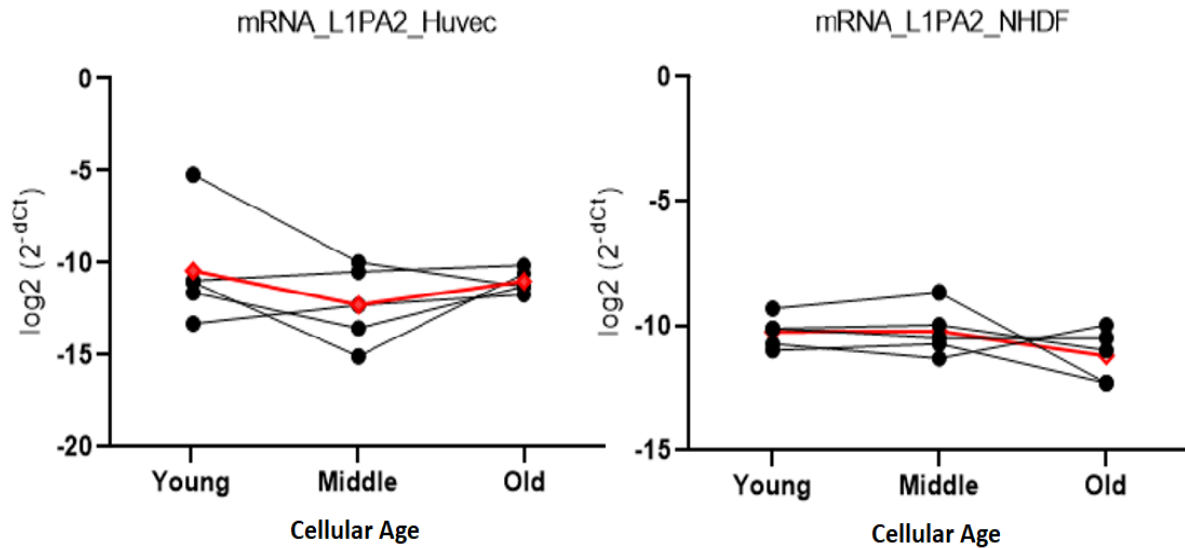
Figure 15. Relative expression of the retroelement L1PA2, mapped on Chromosome14. The red line shows the average trend.

In the next step, in order to clarify if the cytoplasm of senescent cells is enriched of TEs sequnces, we analysed the expression of the selected TEs both in the nuclear and cytosolic fractions.

An increase in TEs DNA copies in the nucleus could indicate an increase of the integrated sequences, while an increased amount of TEs DNA copies in the cytoplasm could indicate an increase in the retrotranscription process, which proceeds through a (c)DNA intermediate.

Nuclear and cytoplasmatic fractions were firstly tested to verify possible cross-contaminations, analysing the expression levels of the cytoplasmatic protein GAPDH, that is expected to be detectable mainly in cytosolic fraction, and the nuclear protein Lamin A/C, that is expected to be not detectable in cytosolic fraction. Western Blot analysis confirmed the absence of cross-contaminations between nuclear and cytoplasmatic fractions (Fig.16)

HUVECs   HNDFs

Figure 16A and 16B. A Protein (WB) analysis of LaminA/C in the nuclear (N) and cytoplasmic (C) fractions of HUVE and NHDF cells. B. RNA (PCR) analysis of Beta-Actin in the nuclear (N Act) and cytoplasmic (C Act) fractions of HUVEc and NHDF.
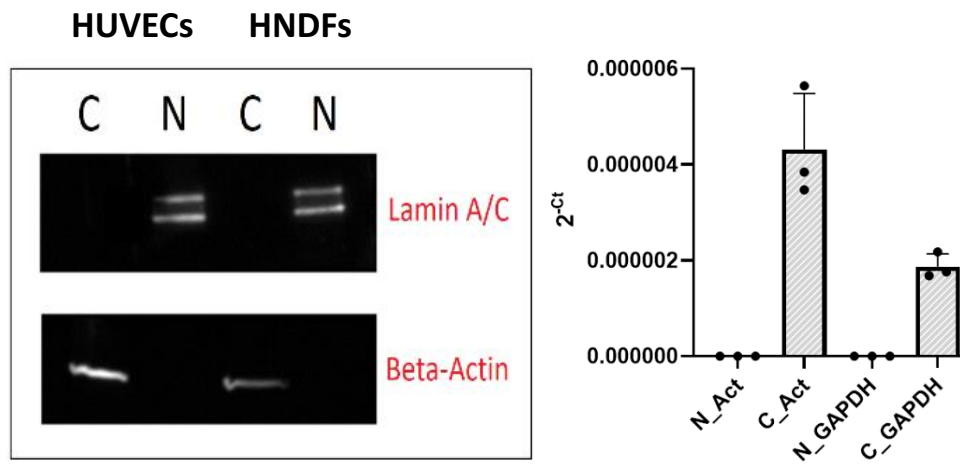
Regarding the cytoplasmatic fractions, significant increased levels of DNA sequences derived from Alu (Fig. 17), ORF2 (Fig. 18) and L1PA2 (Fig. 19) were observed in senescent NHDF.

In HUVEC significant increased levels of DNA sequences derived from ORF2 (Fig. 18) were observed in senescent cells.
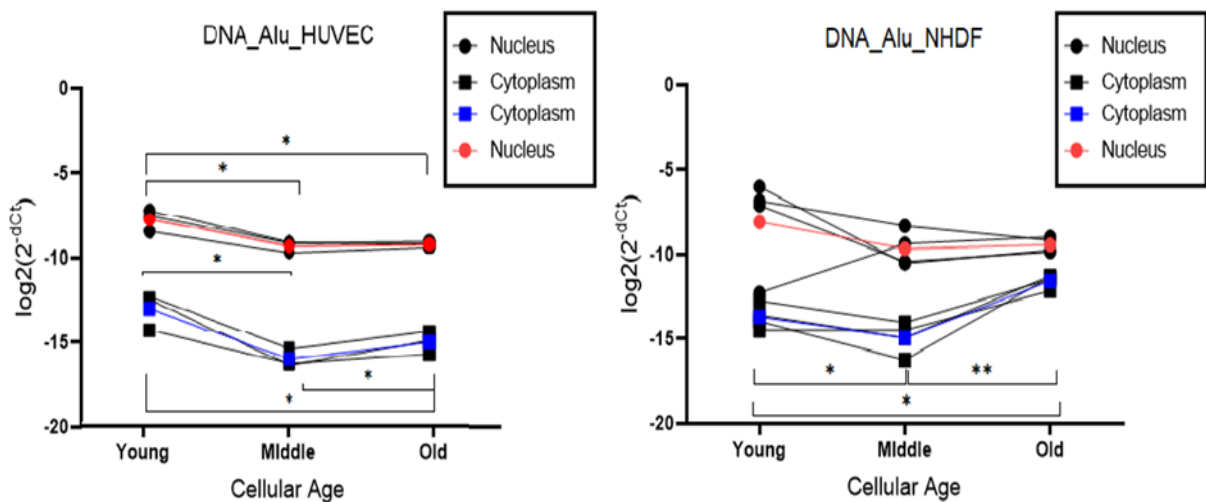
Figure 17. DNAs derived from Alu elements in citplasms and nuclei of HUVEC and NHDF cells. Red lines show the average trend in the nuclear fraction; blue lines show the average trend in the cytosolic fraction
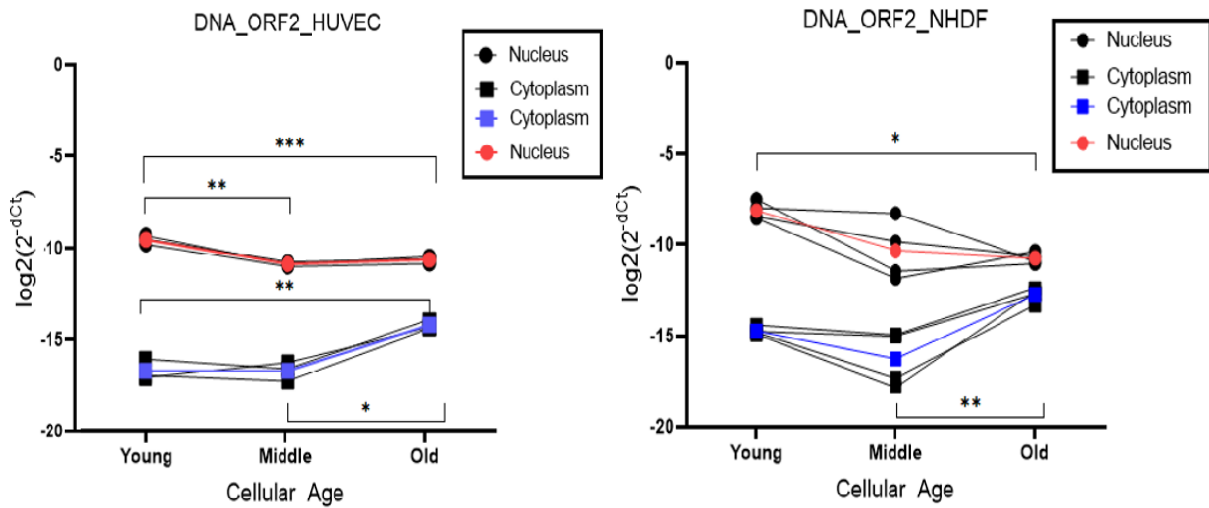
Figure 18. DNAs derived from ORF2 elements in cytoplasms and nuclei of HUVEC and NHDF cells. Red lines show the average trend in the nuclear fraction; blue lines show the average trend in the cytosolic fraction
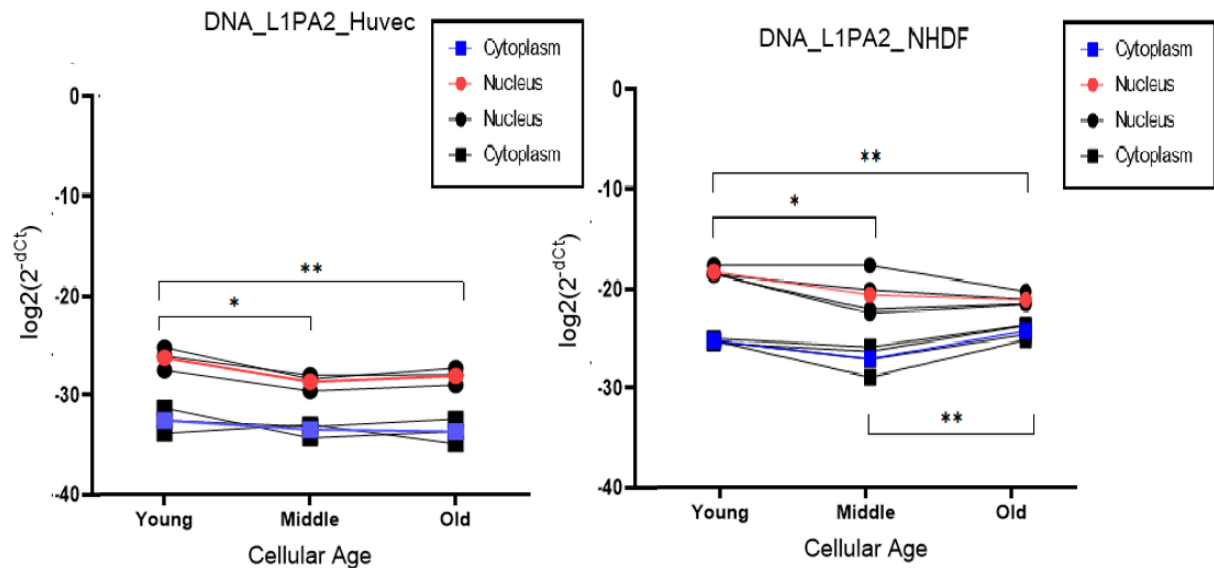
Figure 19. DNAs derived from L1PA2 subfamily elements in cytoplasms and nuclei of HUVEC and NHDF cells. Red lines show the average trend in the nuclear fraction; blue lines show the average trend in the cytosolic fraction

Regarding the nucler fraction, significant reduction of Alu (Fig. 17), ORF2 (Fig. 18) and L1PA2 (Fig. 19) DNA sequences was observed in senescent HUVECs, whereas in senescent NHDF significant reductions of ORF2 (Fig. 18) and L1PA2 (Fig. 19), but not of Alu (Fig. 17) sequences, were observed.

The increased abudance of cytoplasmic DNA of L1PA2 sequence but not of its mRNA, suggest a complex mechanism of LINE1 retrotrasposition in senescent cells. This mechanism deserves further investigations.

4.4 INF type 1 expression levels

Finally, we analysed the expression levels of IFN-1β. Significant increased expression levels were observed in senescent NHDF, but not in HUVEC cells (Fig. 20).
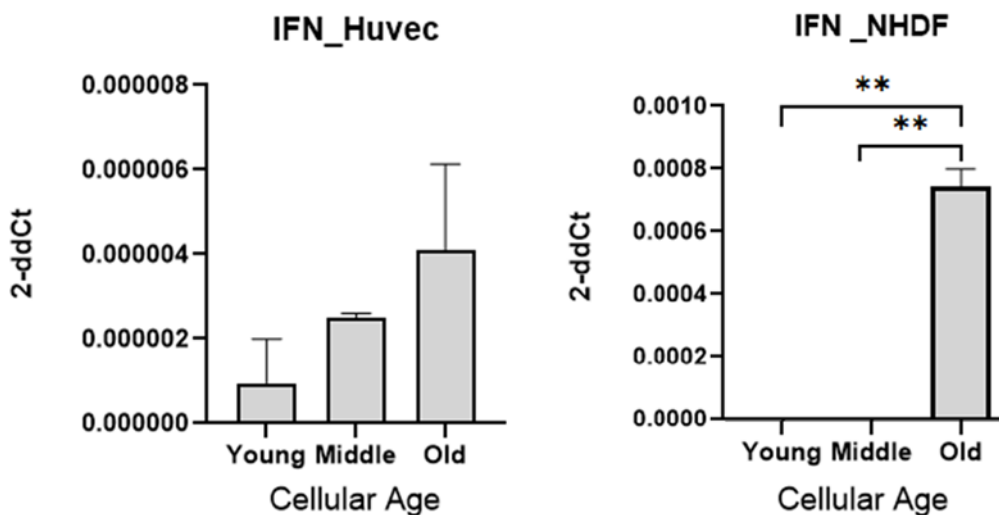
Figure 20. Expression levels of the IFN-1β in HUVEC and NHDF cells.

5. Discussion

This study analysed some epigenetic mechanisms that could be involved in the acquisition of the senescent phenotype in two well established cellular models of replicative senescence, such as human endothelial cells (HUVECs) and fibroblasts (HNDF).

Firstly, the genome-wide methylation analysis were performed in young and senescent HUVECs, revealing a global genome demethylation in senescent cells. The most significantly demethylated single CpG sites identifyed by genome-wide methylation analysis were then mapped on the reference genome and annotated for their localization inside TEs sequences. The analysis revealed that the most demethylated sequences within TEs in senescent HUVECs belong to the TE LINE1 family, in particular to the the three subfamilies L1M, L1P and L1HS. Interestingly, significant increased demethylated CpGs were identifyed in genomic regions with low coding gene density.

This first part of the analysis suggests that cells can adopt different mechanisms of self-defense against TEs, such as their methylation and the confination of potentially more active TEs sequences in regions with a reduced number of coding genes.

Increasing evidence suggested that LINE-1 methylation status can be related with aging and with the development of some ARDs, including type 2 diabetes mellitus (T2DM). A clear age associated decline in the methylation of LINE-1 was observed in cell-free DNA from peripheral blood (Erichsen et al., 2018). In healthy individuals this DNA fraction is suggested to derive from apoptotic cells, necrotic cells and from active cellular secretion of newly synthesized DNA (Bronkhorst et al., 2016).

These data suggest tha cellular genome-wide hypomethylation occurs in an age-dependent fashion in endothelial, epithelial and other body cells from various organs.

LINE-1 hypomethylation was also associated with a higher risk of worsening metabolic status, independent of other classic risk factors (Martin-Nunez et al., 2014). This discovery highlights the potential role for LINE-1 DNA methylation as a predictor of the risk of T2DM or other related metabolic disorders. Moreover, LINE-1 DNA methylation is associated with increased LDL cholesterol and decreased HDL cholesterol levels, and these metabolic changes increase the risk of cardiovascular disease (Pearce et al., 2012).

We further verified the integrity and completeness of the TEs containing demethylated CpGs in senescent cells. Almost all the TEs have been found to be incomplete and therefore unable to retrotranspose. Importantly, only L1PA2 element (6053 bp long) located on chromosome 14 was almost complete. L1PA2 are TE sequences not so active as the L1HS, but evolutionarily quite recent. The characteristics of this L1PA2, demethylated in senescent HUVECs and quite complete in sequence, suggest that it could be able to transpone.

Full-length LINE-1 transcription is driven by a CpG dinucleotide-rich internal promoter, and an hypomethylation of LINE-1 can cause their activation whit consequent retroelement transposition and chromosomal alteration (Saito et al., 2010). Therefore, after the analysis of TEs methylation, we further verified the expression levels of the L1PA2, and of other retroelements belong to SINE, like Alu sequences. In the human genome, L1 and Alu elements are the two most abundant families of TEs. Part of their high prevalence may be explained by the facts that L1s appear to be the only currently active autonomous TEs in the human genome, and that Alu elements can hijack the L1 machinery, expecially L1 ORF2, for the retrotrascriprion and transposition.

These analysis were performed both in HUVEC and in fibroblast (NHDF).

The analysis of the TEs RNA expression revealed a significant increase of both Alu and L1 ORF2 in senescent HUVEC and NHDF, but not of L1PA2, suggesting that even if L1PA2 is demethylated in senescent HUVECs, it is not actively trascribed.

The increased RNA copies of Alu and L1 ORF2 in senescent HUVEC and NHDF compared to younger cells, suggest a senescence-associated activation of these TEs.

To further investigate not only the expression but also the integration of the demethylated TEs in senescent cells, we analysed the DNA copy numbers in nuclear and cytosolic fractions of young and senescent cells.

An increased in nuclear TEs copy number could indicate an increase of the integrated sequences, while an increased amount of TEs DNA in the cytoplasm could suggest an increase in the retrotranscription process, which proceeds through a cDNA intermediate.

In senescent HUVECs significant reductions of L1PA2, Alu and ORF2 DNA sequences were observed in the nuclear fraction, in association with increased levels of ORF2 DNA in the cytoplasm.

In NHDF, significant reduction of L1PA2 was observed in the nucler fraction in association with increased levels of DNA sequences derived from Alu, ORF2 and L1PA2 in cytoplasm.

Overall, L1 ORF2 and Alu DNA copy number significantly increase in cytoplasm of senescet HUVECs and fibroblasts. Senescent cells are non mitotic cells, and the cell cycle dictates both where the LINE-1 complexes gather and when LINE-1 is active. LINE-1 enters the nucleus as the cell starts to divide and the membrane of the nucleus breaks down. The LINE-1 complexes are then retained in the nucleus while the membrane of the nucleus reforms. Later, as the cell duplicates its genetic material, LINE-1 starts to copy and paste itself. During this process, only LINE-1 RNA and

ORF2p were found in the nucleus. We observed and increased copy numbers of L1 RNA and Alu DNA in the cytosol of senescent cells, suggesting that the retrotrascription of these RNAs could occur in the cytosol thus increasing the copy number of cDNA derived by the retrotrascription of the RNA sequences.

Our results are in accordance with previous studies, showing that L1 ORF2 increased expression was associated to senescence-like state in cancer cell lines (Ardeljan et al., 2017), and in normal human fibroblasts and adult mesenchymal stem cells (Wallace et al., 2008).

The increased amount of L1PA2 DNA sequences (in cytosol) not associated with increased L1PA2 RNA abundance, a condition that we observed in senescent fibroblasts, could be explained by different mechanismss.

The increase in cytoplasmic L1PA2 DNA copies could depend from an increased retrotrascription activity. A second hypothesis involves a mechanism known as repetitive excision, previously described in plants (Li et al. 2017) and in bacteria (Lundblad and Kleckner 1985).

Transposon excision is a special case of deletion, promoted by the presence of large inverted repeats at the excision ends, with the release of a portion of DNA, that could contain TE..

This mechanism would be able to provide explanation for increased TEs DNA in cytosol and the decreased levels of the same sequences in the nucleus (Fig. 20). However, this second hypothesis cannot explain the increased demethylation observed in the genomic region of senescent cells containing TEs.
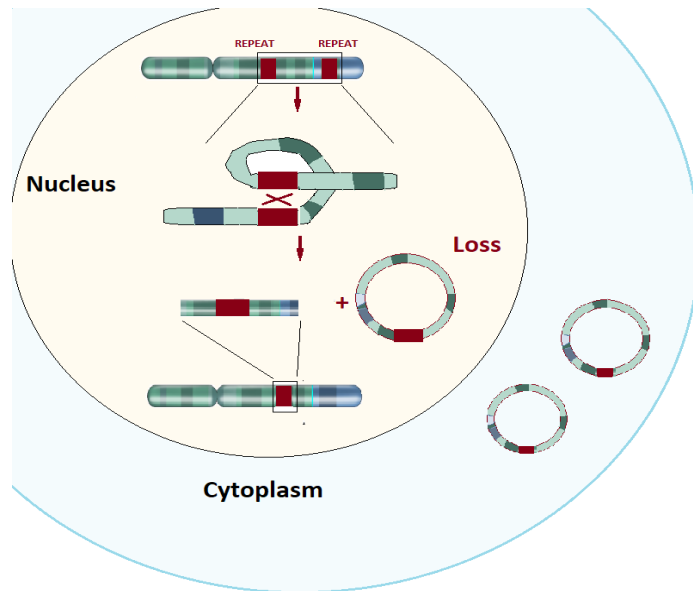
Figure 20. Repetitive excision mechanism of action

Overall, we observed an increased DNA abudance of Alu, ORF2 and L1PA2 in the cytoplasmic fractions, associated with a declining trends of the same sequences in the nuclear fractions of senescent human cells.

This general trend observed both in endothelial cells and fibroblasts during replicative senescence, could affect the secretome of senescent cells, thus modulating inflammaging and the development of ARDs.

Importantly, age-related reactivation of TEs was observed across species, including C. Elegans, Drosophila and mouse. Altered activity of specific TEs is also associated with multiple age-associated pathologies, such as cancer and neurodegenerative diseases, including Alzheimer Disease, amyotrophic lateral sclerosys and frontotemporal lobar degeneration (reviewed in Bravo et al., 2020).

Incresed evidence suggest that cytoplasmic nucleic acids can activate the cytoplasmic sensor of nucleic acids, thus activating an antiviral response promoting type 1 INF increased expression. More in detail, the accumulation of TEs in the cytoplasm could

trigger the cGAS-STING-IRF3 axis activation, thus inducing an increased trascription of type 1IFN genes (Hopfner and Hornung, 2020).

We observed that senescent NHDF showed increased type 1INF expression. Surprisingly, in senescent HUVECs, the type 1 INF expression was not significantly modulated compared to younger cells.

This result, suggest that some cell types, *i.e.* endothelial cells, could be "tolerant" during senescence to the increased amount of misplaced cytosolic nucleic acids, becoming more susceptible to viral infections. Alternatively, during the replicative senescence, cells hyperactivated by cytosolic nucleic acids could become apoptotic.

The demethylation of specific regions in the genome of senescent cells, could contribute to activate TEs, that can be transcribed as RNA, traslocated in cytplasms and retrotrascribed in cDNA, thus contributing to increase the pool of DNA, RNA and RNA:DNA hybrids molecules in cytoplasms of senescent cells.

Endothelial senescent cells, even in presence of an increased burden of cytosolic nucleic acids, do not activate the antiviral response, shifting towards a proinflammatory secretome rather than to the type 1 IFN associated antiviral response.

Overall our data suggest a complex cross-talk between different epigenetic mechanisms in cellular senescence, converging on the promotion and mainteinance of a proinflammatory secretoma that can spread proinflammatory molecules at paracrine and systemic levels, thus fuelling inflammaging and increasing the chances to develop the most common ARDs.

6. Bibliography

Ardeljan D, Taylor MS, Ting DT, Burns KH. The Human Long Interspersed Element-1 Retrotransposon: An Emerging Biomarker of Neoplasia. Clin Chem. 2017;63(4):816-822. doi: 10.1373/clinchem.2016.257444.

Asada, Ken, Keiya Ito, Daishi Yui, Hirokuni Tagaya, and Takanori Yokota. 2018. "Cytosolic Genomic DNA Functions as a Natural Antisense." *Scientific Reports*. https://doi.org/10.1038/s41598-018-26487-1.

Barzilai, Nir, Derek M. Huffman, Radhika H. Muzumdar, and Andrzej Bartke. 2012. "The Critical Role of Metabolic Pathways in Aging." *Diabetes*.

Bonfigli Anna Rita, Spazzafumo Liana, Prattichizzo Francesco, Bonafè Massimiliano, Mensà Emanuela, Micolucci Luigina, Giuliani Angelica, Fabbietti Paolo, Testa Roberto, Boemi Massimo, Lattanzio Fabrizia, Olivieri Fabiola. Leukocyte telomere length and mortality risk in patients with type 2 diabetes Oncotarget. 2016; 7(32): 50835–50844.

Bourque G, et al. Ten things you should know about transposable elements. Genome Biol. 2018. PMID: 30454069

Bravo JI, Nozownik S, Danthi PS, Benayoun BA. https://doi.org/10.2337/db11-1300. Transposable elements, circular RNAs and mitochondrial transcription in age-related genomic regulation. Development. 2020 Jun 11;147(11):dev175786. doi: 10.1242/dev.175786.

Brew, Bruce James, and Justin C. McArthur. 2020. "'A Man Is as Old as His Arteries' (Attributed to Thomas Sydenham, the English Hippocrates)." *Aids*. https://doi.org/10.1097/QAD.0000000000002414.

Bronkhorst A.J., Wentzel J.F., Aucamp J., van Dyk E., du Plessis L., Pretorius P.J.

Characterization of the cell-free DNA released by cultured cancer cells. BBA. 2016;1863:157–165

Brouha, Brook, Joshua Schustak, Richard M. Badge, Sheila Lutz-Prigge, Alexander H. Farley, John V. Morant, and Haig H. Kazazian. 2003. "Hot L1s Account for the Bulk of Retrotransposition in the Human Population." *Proceedings of the National Academy of Sciences of the United States of America*. https://doi.org/10.1073/pnas.0831042100.

Burns, Kathleen H., and Jef D. Boeke. 2012. "Human Transposon Tectonics." *Cell*. https://doi.org/10.1016/j.cell.2012.04.019.

Burton, Frank H., Daniel D. Loeb, Charles F. Voliva, Sandra L. Martin, Marshall H. Edgell, and Clyde A. Hutchison. 1986. "Conservation throughout Mammalia and Extensive Protein-Encoding Capacity of the Highly Repeated DNA Long Interspersed Sequence One." *Journal of Molecular Biology*. https://doi.org/10.1016/0022-2836(86)90235-4.

Campisi, Judith, and Fabrizio D'Adda Di Fagagna. 2007. "Cellular Senescence: When Bad Things Happen to Good Cells." *Nature Reviews Molecular Cell Biology*. https://doi.org/10.1038/nrm2233.

Cardelli, Maurizio, and Marchegiani Francesca. 2013. "Good, Bad, Mobile Elements: Genome's Most Successful 'Parasites' as Emerging Players in Cell and Organismal Aging." *Current Pharmaceutical Design*. https://doi.org/10.2174/1381612811319090021.

Cardelli M. The epigenetic alterations of endogenous retroelements in aging.Mech Ageing Dev. 2018 Sep;174:30-46. doi: 10.1016/j.mad.2018.02.002

Cawthon, Richard M. 2002. "Telomere Measurement by Quantitative PCR." *Nucleic*

Acids Research. https://doi.org/10.1093/nar/30.10.e47.

Cecco, Marco De, Takahiro Ito, Anna P. Petrashen, Amy E. Elias, Nicholas J. Skvir, Steven W. Criscione, Alberto Caligiana, et al. 2019. "L1 Drives IFN in Senescent Cells and Promotes Age-Associated Inflammation." *Nature*. https://doi.org/10.1038/s41586-018-0784-9.

"Characterization of L1-Ribonucleoprotein Particles - PubMed." n.d.

Carty M, Guy C, Bowie AG Detection of Viral Infections by Innate Immunity. Biochem Pharmacol. 2021 Jan; 183():114316.

Chen, Jian Min, Peter D. Stenson, David N. Cooper, and Claude Férec. 2005. "A Systematic Analysis of LINE-1 Endonuclease-Dependent Retrotranspositional Events Causing Human Genetic Disease." *Human Genetics*. https://doi.org/10.1007/s00439-005-1321-0.

Childs, Bennett G., Tyler J. Bussian, and Darren J. Baker. 2019. "Cellular Identification and Quantification of Senescence-Associated β-Galactosidase Activity in Vivo." *Methods in Molecular Biology*. https://doi.org/10.1007/978-1-4939-8931-7_4.

Collado, Manuel, Maria A. Blasco, and Manuel Serrano. 2007. "Cellular Senescence in Cancer and Aging." *Cell*. https://doi.org/10.1016/j.cell.2007.07.003.

Cost, Gregory J., Qinghua Feng, Alain Jacquier, and Jef D. Boeke. 2002. "Human L1 Element Target-Primed Reverse Transcription in Vitro." *EMBO Journal*. https://doi.org/10.1093/emboj/cdf592.

Cruzen, Christina, and Ricki J. Colman. 2009. "Effects of Caloric Restriction on Cardiovascular Aging in Non-Human Primates and Humans." *Clinics in Geriatric Medicine*. https://doi.org/10.1016/j.cger.2009.07.001.

Deininger, Prescott L., and Mark A. Batzer. 1999. "Alu Repeats and Human Disease." *Molecular Genetics and Metabolism*. https://doi.org/10.1006/mgme.1999.2864.

"DNA Modification, Differentiation, and Transformation - PubMed." n.d.

Eipel, Monika, Felix Mayer, Tanja Arent, Marcelo R.P. Ferreira, Carina Birkhofer, Uwe Gerstenmaier, Ivan G. Costa, Stefanie Ritz-Timme, and Wolfgang Wagner. 2016. "Epigenetic Age Predictions Based on Buccal Swabs Are More Precise in Combination with Cell Type-Specific DNA Methylation Signatures." *Aging*. https://doi.org/10.18632/aging.100972.

Erichsen L, Beermann A, Arauzo-Bravo MJ, Hassan M, Dkhil MA, Al-Quraishy S, Hafiz TA, Fischer JC, Santourlidis S. Genome-wide hypomethylation of LINE-1 and Alu retroelements in cell-free DNA of blood is an epigenetic biomarker of human aging. Saudi J Biol Sci. 2018;25:1220-1226. doi: 10.1016/j.sjbs.2018.02.005.

Fontana, Luigi, Linda Partridge, and Valter D. Longo. 2010. "Extending Healthy Life Span-from Yeast to Humans." *Science*. https://doi.org/10.1126/science.1172539.

Fülöp, Tamas, Gilles Dupuis, Jacek M. Witkowski, and Anis Larbi. 2016. "The Role of Immunosenescence in the Development of Age-Related Diseases." *Revista de Investigacion Clinica*.

Furano, Anthony V. 2000. "The Biological Properties and Evolutionary Dynamics of Mammalian LINE-1 Retrotransposons." *Progress in Nucleic Acid Research and Molecular Biology*. https://doi.org/10.1016/s0079-6603(00)64007-2.

"Genomic Instability--an Evolving Hallmark of Cancer - PubMed." n.d.

Gorenjak, Vesna, Samina Akbar, Maria G. Stathopoulou, and Sophie Visvikis-Siest.

2018. "The Future of Telomere Length in Personalized Medicine." *Frontiers in Bioscience - Landmark*. https://doi.org/10.2741/4664.

Green, Douglas R., Lorenzo Galluzzi, and Guido Kroemer. 2011. "Mitochondria and the Autophagy-Inflammation-Cell Death Axis in Organismal Aging." *Science*. https://doi.org/10.1126/science.1201940.

Gu, Tong J., Xiang Yi, Xi W. Zhao, Yi Zhao, and James Q. Yin. 2009. "Alu-Directed Transcriptional Regulation of Some Novel MiRNAs." *BMC Genomics*. https://doi.org/10.1186/1471-2164-10-563.

Guillozet, . A L, S Weintraub, D C Mash, M M Mesulam, and ; T Gomez-Isla. 1993. "Mitochondrial DNA Mutations, Oxidative Stress, and Apoptosis in Mammalian Aging." *Proc. Natl. Acad. Sci. U.S.A*.

Guo, Caiwei, Hyun Hwan Jeong, Yi Chen Hsieh, Hans Ulrich Klein, David A. Bennett, Philip L. De Jager, Zhandong Liu, and Joshua M. Shulman. 2018. "Tau Activates Transposable Elements in Alzheimer's Disease." *Cell Reports*. https://doi.org/10.1016/j.celrep.2018.05.004.

Hannum, Gregory, Justin Guinney, Ling Zhao, Li Zhang, Guy Hughes, Srini Vas Sadda, Brandy Klotzle, et al. 2013. "Genome-Wide Methylation Profiles Reveal Quantitative Views of Human Aging Rates." *Molecular Cell*. https://doi.org/10.1016/j.molcel.2012.10.016.

Hayflick, L., and P. S. Moorhead. 1961. "The Serial Cultivation of Human Diploid Cell Strains." *Experimental Cell Research*. https://doi.org/10.1016/0014-4827(61)90192-6.

Hekimi, Siegfried, Jérôme Lapointe, and Yang Wen. 2011. "Taking a 'Good' Look at Free Radicals in the Aging Process." *Trends in Cell Biology*.

https://doi.org/10.1016/j.tcb.2011.06.008.

Hopfner KP, Hornung V. Molecular mechanisms and cellular functions of cGAS-STING signalling. Nat Rev Mol Cell Biol. 2020 Sep;21(9):501-521. doi: 10.1038/s41580-020-0244-x

Horvath, Steve. 2013. "DNA Methylation Age of Human Tissues and Cell Types." *Genome Biology*. https://doi.org/10.1186/gb-2013-14-10-r115.

Houtkooper, Riekelt H., Carles Cantó, Ronald J. Wanders, and Johan Auwerx. 2010. "The Secret Life of NAD+: An Old Metabolite Controlling New Metabolic Signaling Pathways." *Endocrine Reviews*. https://doi.org/10.1210/er.2009-0026.

Huggett, Jim F., Tanya Novak, Jeremy A. Garson, Clare Green, Stephen D. Morris-Jones, Robert F. Miller, and Alimuddin Zumla. 2008. "Differential Susceptibility of PCR Reactions to Inhibitors: An Important and Unrecognised Phenomenon." *BMC Research Notes*. https://doi.org/10.1186/1756-0500-1-70.

"Inflamm-Aging." n.d.

Jang, Ji Yong, Arnon Blum, Jie Liu, and Toren Finkel. 2018. "The Role of Mitochondria in Aging." *Journal of Clinical Investigation*. https://doi.org/10.1172/JCI120842.

Jones, Meaghan J., Sarah J. Goodman, and Michael S. Kobor. 2015. "DNA Methylation and Healthy Human Aging." *Aging Cell*. https://doi.org/10.1111/acel.12349.

Kane, Alice E., and David A. Sinclair. 2019. "Epigenetic Changes during Aging and Their Reprogramming Potential." *Critical Reviews in Biochemistry and Molecular Biology*. https://doi.org/10.1080/10409238.2019.1570075.

Khan, Hameed, Arian Smit, and Stéphane Boissinot. 2006. "Molecular Evolution and Tempo of Amplification of Human LINE-1 Retrotransposons since the Origin of Primates." *Genome Research*. https://doi.org/10.1101/gr.4001406.

Khodosevich, Konstantin, Yuri Lebedev, and Eugene Sverdlov. 2002. "Endogenous Retroviruses and Human Evolution." *Comparative and Functional Genomics*. https://doi.org/10.1002/cfg.216.

Kramerov DA, Vassetzky NS Origin and evolution of SINEs in eukaryotic genomes. Heredity (Edinb). 2011 Dec; 107(6):487-95).

Lagisquet J, Zuber K, Gramberg T. Recognize Yourself—Innate Sensing of Non-LTR Retrotransposons Viruses. 2021; 13(1): 94. doi: 10.3390/v13010094

Li, Shu Fen, Ting Su, Guang Qian Cheng, Bing Xiao Wang, Xu Li, Chuan Liang Deng, and Wu Jun Gao. 2017. "Chromosome Evolution in Connection with Repetitive Sequences and Epigenetics in Plants." *Genes* 8 (10). https://doi.org/10.3390/genes8100290.

Liu, Ruiqi, Fei Xu, Siwei Bi, Xueshan Zhao, Bangsheng Jia, and Ying Cen. 2019. "Mitochondrial DNA-Induced Inflammatory Responses and Lung Injury in Thermal Injury Murine Model: Protective Effect of Cyclosporine-A." *Journal of Burn Care and Research*. https://doi.org/10.1093/jbcr/irz029.

Loo, Tze Mun, Kenichi Miyata, Yoko Tanaka, and Akiko Takahashi. 2020. "Cellular Senescence and Senescence-Associated Secretory Phenotype via the CGAS-STING Signaling Pathway in Cancer." *Cancer Science*. https://doi.org/10.1111/cas.14266.

López-Otín, Carlos, Maria A. Blasco, Linda Partridge, Manuel Serrano, and Guido Kroemer. 2013. "The Hallmarks of Aging." *Cell*.

https://doi.org/10.1016/j.cell.2013.05.039.

Luan, Dongmei D., Malka H. Korman, John L. Jakubczak, and Thomas H. Eickbush. 1993. "Reverse Transcription of R2Bm RNA Is Primed by a Nick at the Chromosomal Target Site: A Mechanism for Non-LTR Retrotransposition." *Cell*. https://doi.org/10.1016/0092-8674(93)90078-5.

Lundblad, V., and N. Kleckner. 1985. "Mismatch Repair Mutations of Escherichia Coli K12 Enhance Transposon Excision." *Genetics*. https://doi.org/10.1093/genetics/109.1.3.

Maiese, Kenneth. 2016. "Forkhead Transcription Factors: New Considerations for Alzheimer's Disease and Dementia." *Journal of Translational Science*. https://doi.org/10.15761/jts.1000146.

Marioni, Riccardo E., Matthew Suderman, Brian H. Chen, Steve Horvath, Stefania Bandinelli, Tiffany Morris, Stephan Beck, et al. 2019. "Tracking the Epigenetic Clock across the Human Life Course: A Meta-Analysis of Longitudinal Cohort Data." *Journals of Gerontology - Series A Biological Sciences and Medical Sciences*. https://doi.org/10.1093/gerona/gly060.

Martin-Nunez, G. M., Rubio-Martin, E., Cabrera-Mulero, R., Rojo-Martinez, G., Olveira, G., Valdes, S., et al. (2014). Type 2 diabetes mellitus in relation to global LINE-1 DNA methylation in peripheral blood: a cohort study. Epigenetics 9, 1322–1328. doi: 10.4161/15592294.2014.969617

Meduri, G. Umberto, and Charles R. Yates. 2004. "Systemic Inflammation-Associated Glucocorticoid Resistance and Outcome of ARDS." *Annals of the New York Academy of Sciences*. https://doi.org/10.1196/annals.1321.004.

Mensà, Emanuela, Michele Guescini, Angelica Giuliani, Maria Giulia Bacalini, Deborah Ramini, Giacomo Corleone, Manuela Ferracin, et al. 2020. "Small Extracellular Vesicles Deliver MiR-21 and MiR-217 as pro-Senescence Effectors to Endothelial Cells." *Journal of Extracellular Vesicles*. https://doi.org/10.1080/20013078.2020.1725285.

Mensà, Emanuela, Michele Guescini, Angelica Giuliani, and Maria Giulia. 2020. "Small Extracellular Vesicles Deliver MiR-21 and MiR-217 as pro-Senescence Effectors to Endothelial Cells." *Journal of Extracellular Vesicles* 9 (1). https://doi.org/10.1080/20013078.2020.1725285.

Mensà, Emanuela, Silvia Latini, Deborah Ramini, Gianluca Storci, Massimiliano Bonafè, and Fabiola Olivieri. 2019. "The Telomere World and Aging: Analytical Challenges and Future Perspectives." *Ageing Research Reviews*. https://doi.org/10.1016/j.arr.2019.01.004.

Min, Byungkuk, Kyuheum Jeon, Jung Sun Park, and Yong Kook Kang. 2019. "Demethylation and Derepression of Genomic Retroelements in the Skeletal Muscles of Aged Mice." *Aging Cell*. https://doi.org/10.1111/acel.13042.

Nakaya, Yuki, Jingtao Lilue, Spyridon Stavrou, Eileen A. Moran, and Susan R. Ross. 2017. "AIM2-like Receptors Positively and Negatively Regulate the Interferon Response Induced by Cytosolic DNA." *MBio*. https://doi.org/10.1128/mBio.00944-17.

Nelson, Glyn, James Wordsworth, Chunfang Wang, Diana Jurk, Conor Lawless, Carmen Martin-Ruiz, and Thomas von Zglinicki. 2012. "A Senescent Cell Bystander Effect: Senescence-Induced Senescence." *Aging Cell*. https://doi.org/10.1111/j.1474-9726.2012.00795.x.

Olivieri, Fabiola, Maria Cristina Albertini, Monia Orciani, Artan Ceka, Monica Cricca,

Antonio Domenico Procopio, and Massimiliano Bonafè. 2015. "DNA Damage Response (DDR) and Senescence: Shuttled Inflamma-MiRNAs on the Stage of Inflamm-Aging." *Oncotarget* 6 (34): 35509–21. https://doi.org/10.18632/oncotarget.5899.

Pace, John K., and Cédric Feschotte. 2007. "The Evolutionary History of Human DNA Transposons: Evidence for Intense Activity in the Primate Lineage." *Genome Research*. https://doi.org/10.1101/gr.5826307.

Pal, Sangita, and Jessica K. Tyler. 2016. "Epigenetics and Aging." *Science Advances*. https://doi.org/10.1126/sciadv.1600584.

Partridge, Linda, Matias Fuentealba, and Brian K. Kennedy. 2020. "The Quest to Slow Ageing through Drug Discovery." *Nature Reviews Drug Discovery*. https://doi.org/10.1038/s41573-020-0067-7.

Pearce, M. S., McConnell, J. C., Potter, C., Barrett, L. M., Parker, L., Mathers, J. C., et al. (2012). Global LINE-1 DNA methylation is associated with blood glycaemic and lipid profiles. Int. J. Epidemiol. 41, 210–217. doi: 10.1093/ije/dys020

Puca, Annibale Alessandro, Chiara Spinelli, Giulia Accardi, Francesco Villa, and Calogero Caruso. 2018. "Centenarians as a Model to Discover Genetic and Epigenetic Signatures of Healthy Ageing." *Mechanisms of Ageing and Development*. https://doi.org/10.1016/j.mad.2017.10.004.

Quan, Yue, Yanguo Xin, Geer Tian, Junteng Zhou, and Xiaojing Liu. 2020. "Mitochondrial ROS-Modulated MtDNA: A Potential Target for Cardiac Aging." *Oxidative Medicine and Cellular Longevity*. https://doi.org/10.1155/2020/9423593.

Rera, Michael, Sepehr Bahadorani, Jaehyoung Cho, Christopher L. Koehler, Matthew Ulgherait, Jae H. Hur, William S. Ansari, Thomas Lo, D. Leanne Jones, and David W. Walker. 2011. "Modulation of Longevity and Tissue Homeostasis by the Drosophila PGC-1 Homolog." *Cell Metabolism*. https://doi.org/10.1016/j.cmet.2011.09.013.

Rodier, Francis, and Judith Campisi. 2011. "Four Faces of Cellular Senescence." *Journal of Cell Biology*. https://doi.org/10.1083/jcb.201009094.

Rojas, Diego Montiel, Andreas Nilsson, Elodie Ponsot, Robert J. Brummer, Susan Fairweather-Tait, Amy Jennings, Lisette C.P.G.M. de Groot, et al. 2018. "Short Telomere Length Is Related to Limitations in Physical Function in Elderly European Adults." *Frontiers in Physiology*. https://doi.org/10.3389/fphys.2018.01110.

Salminen, Antero, and Kai Kaarniranta. 2012. "AMP-Activated Protein Kinase (AMPK) Controls the Aging Process via an Integrated Signaling Network." *Ageing Research Reviews*. https://doi.org/10.1016/j.arr.2011.12.005.

Schwarzenbach, Heidi, Dave S.B. Hoon, and Klaus Pantel. 2011. "Cell-Free Nucleic Acids as Biomarkers in Cancer Patients." *Nature Reviews Cancer*. https://doi.org/10.1038/nrc3066.

Shaw, Albert C., Samit Joshi, Hannah Greenwood, Alexander Panda, and Janet M. Lord. 2010. "Aging of the Innate Immune System." *Current Opinion in Immunology*. https://doi.org/10.1016/j.coi.2010.05.003.

Simon, Matthew, Michael Van Meter, Julia Ablaeva, Zhonghe Ke, Raul S. Gonzalez, Taketo Taguchi, Marco De Cecco, et al. 2019. "LINE1 Derepression in Aged Wild-Type and SIRT6-Deficient Mice Drives Inflammation." *Cell Metabolism*. https://doi.org/10.1016/j.cmet.2019.02.014.

Srikanta, Deepa, Shurjo K. Sen, Charles T. Huang, Erin M. Conlin, Ryan M. Rhodes, and Mark A. Batzer. 2009. "An Alternative Pathway for Alu Retrotransposition Suggests a Role in DNA Double-Strand Break Repair." *Genomics*. https://doi.org/10.1016/j.ygeno.2008.09.016.

Stetson, Daniel B., Joan S. Ko, Thierry Heidmann, and Ruslan Medzhitov. 2008. "Trex1 Prevents Cell-Intrinsic Initiation of Autoimmunity." *Cell*. https://doi.org/10.1016/j.cell.2008.06.032.

An integrated map of structural variation in 2,504 human genomes.

Sudmant PH, Rausch T, Gardner EJ, Handsaker RE, Abyzov A, Huddleston J, Zhang Y, Ye K, Jun G, Fritz MH, Konkel MK, Malhotra A, Stütz AM, Shi X, Casale FP, Chen J, Hormozdiari F, Dayama G, Chen K, Malig M, Chaisson MJP, Walter K, Meiers S, Kashin S, Garrison E, Auton A, Lam HYK, Mu XJ, Alkan C, Antaki D, Bae T, Cerveira E, Chines P, Chong Z, Clarke L, Dal E, Ding L, Emery S, Fan X, Gujral M, Kahveci F, Kidd JM, Kong Y, Lameijer EW, McCarthy S, Flicek P, Gibbs RA, Marth G, Mason CE, Menelaou A, Muzny DM, Nelson BJ, Noor A, Parrish NF, Pendleton M, Quitadamo A, Raeder B, Schadt EE, Romanovitch M, Schlattl A, Sebra R, Shabalin AA, Untergasser A, Walker JA, Wang M, Yu F, Zhang C, Zhang J, Zheng-Bradley X, Zhou W, Zichner T, Sebat J, Batzer MA, McCarroll SA, 1000 Genomes Project Consortium., Mills RE, Gerstein MB, Bashir A, Stegle O, Devine SE, Lee C, Eichler EE, Korbel JO Nature. 2015 ; 526(7571):75-81.

Takahashi, Akiko, Tze Mun Loo, Ryo Okada, Fumitaka Kamachi, Yoshihiro Watanabe, Masahiro Wakita, Sugiko Watanabe, et al. 2018. "Downregulation of Cytoplasmic DNases Is Implicated in Cytoplasmic DNA Accumulation and SASP

in Senescent Cells." *Nature Communications*. https://doi.org/10.1038/s41467-018-03555-8.

Tan, Rong, and Li Lan. 2016. "Guarding Chromosomes from Oxidative DNA Damage to the Very End." *Acta Biochimica et Biophysica Sinica*. https://doi.org/10.1093/abbs/gmw040.

"Telomeres and Aging - Telomere Shortening - T.A. Sciences®." n.d.

Thijssen, Dick H.J., Sophie E. Carter, and Daniel J. Green. 2016. "Arterial Structure and Function in Vascular Ageing: Are You as Old as Your Arteries?" *Journal of Physiology*. https://doi.org/10.1113/JP270597.

Thomas, Charles A., Leon Tejwani, Cleber A. Trujillo, Priscilla D. Negraes, Roberto H. Herai, Pinar Mesci, Angela Macia, Yanick J. Crow, and Alysson R. Muotri. 2017. "Modeling of TREX1-Dependent Autoimmune Disease Using Human Stem Cells Highlights L1 Accumulation as a Source of Neuroinflammation." *Cell Stem Cell*. https://doi.org/10.1016/j.stem.2017.07.009.

Umetani, Naoyuki, Joseph Kim, Suzanne Hiramatsu, Howard A. Reber, Oscar J. Hines, Anton J. Bilchik, and Dave S.B. Hoon. 2006. "Increased Integrity of Free Circulating DNA in Sera of Patients with Colorectal or Periampullary Cancer: Direct Quantitative PCR for ALU Repeats." *Clinical Chemistry*. https://doi.org/10.1373/clinchem.2006.068577.

Wallace NA, Belancio VP, Deininger PL. L1 mobile element expression causes multiple types of toxicity. Gene. 2008 Aug 1;419(1-2):75-81. doi: 10.1016/j.gene.2008.04.013

Wang, Ke, and Daniel J. Klionsky. 2011. "Mitochondria Removal by Autophagy." *Autophagy*. https://doi.org/10.4161/auto.7.3.14502.

Worman, Howard J., and Susan Michaelis. 2018. "Permanently Farnesylated Prelamin a, Progeria, and Atherosclerosis." *Circulation*. https://doi.org/10.1161/CIRCULATIONAHA.118.034480.

Wu, X., and S. M. Burgess. 2004. "Integration Target Site Selection for Retroviruses and Transposable Elements." *Cellular and Molecular Life Sciences*. https://doi.org/10.1007/s00018-004-4206-9.

Yang, Allen S., Marcos R.H. Estécio, Ketan Doshi, Yutaka Kondo, Eloiza H. Tajara, and Jean Pierre J. Issa. 2004. "A Simple Method for Estimating Global DNA Methylation Using Bisulfite PCR of Repetitive DNA Elements." *Nucleic Acids Research*. https://doi.org/10.1093/nar/gnh032.

Yang, Hui, Hanze Wang, Unyao Ren, Qi Chen, and Zhijian J. Chena. 2017. "CGAS Is Essential for Cellular Senescence." *Proceedings of the National Academy of Sciences of the United States of America*. https://doi.org/10.1073/pnas.1705499114.

Yoshimura, Yuichi, Mats A. Holmberg, Predrag Kukic, Camilla B. Andersen, Alejandro Mata-Cabana, S. Fabio Falsone, Michele Vendruscolo, Ellen A.A. Nollen, and Frans A.A. Mulder. 2017. "MOAG-4 Promotes the Aggregation of α-Synuclein by Competing with Self-Protective Electrostatic Interactions." *Journal of Biological Chemistry*. https://doi.org/10.1074/jbc.M116.764886.

Zhao, Le, Yong-Tao Duan, Ping Lu, Zhi-Juan Zhang, Xiao-Ke Zheng, Jun-Lei Wang, and Wei-Sheng Feng. 2019. "Epigenetic Targets and Their Inhibitors in Cancer Therapy." *Current Topics in Medicinal Chemistry*. https://doi.org/10.2174/1568026619666181224095449.

Cell Death &
Differentiation

ARTICLE

Genomic stability, anti-inflammatory phenotype, and up-regulation of the RNAseH2 in cells from centenarians

Gianluca Storci[1,2,3] · Sabrina De Carolis[1,3] · Alessio Papi[4] · Maria Giulia Bacalini[5] · Noémie Gensous [1] ·
Elena Marasco[1] · Anna Tesei[6] · Francesco Fabbri[6] · Chiara Arienti[6] · Michele Zanoni[6] · Anna Sarnelli[7] ·
Spartaco Santi[8,9] · Fabiola Olivieri[10,11] · Emanuela Mensà[10] · Silvia Latini[10] · Manuela Ferracin [1] · Stefano Salvioli[1] ·
Paolo Garagnani [1] · Claudio Franceschi[5] · Massimiliano Bonafè[1,3,6]

Abstract
Current literature agrees on the notion that efficient DNA repair favors longevity across evolution. The DNA damage response machinery activates inflammation and type I interferon signaling. Both pathways play an acknowledged role in the pathogenesis of a variety of age-related diseases and are expected to be detrimental for human longevity. Here, we report on the anti-inflammatory molecular make-up of centenarian's fibroblasts (low levels of IL-6, type 1 interferon beta, and pro-inflammatory microRNAs), which is coupled with low level of DNA damage (measured by comet assay and histone-2AX activation) and preserved telomere length. In the same cells, high levels of the RNAseH2C enzyme subunit and low amounts of RNAseH2 substrates, i.e. cytoplasmic RNA:DNA hybrids are present. Moreover, RNAseH2C locus is hypo-methylated and RNAseH2C knock-down up-regulates IL-6 and type 1 interferon beta in centenarian's fibroblasts. Interestingly, RNAseH2C locus is hyper-methylated in vitro senescent cells and in tissues from atherosclerotic plaques and breast tumors. Finally, extracellular vesicles from centenarian's cells up-regulate RNAseH2C expression and dampen the pro-inflammatory phenotype of fibroblasts, myeloid, and cancer cells. These data suggest that centenarians are endowed with restrained DNA damage-induced inflammatory response, that may facilitate their escape from the deleterious effects of age-related chronic inflammation.

Introduction

Human longevity represents the capability of exceptional individuals to reach the extreme limits of human lifespan while avoiding age-related diseases, such as atherosclerosis and cancer [1]. A common feature of age-related diseases is

✉ Gianluca Storci
gianluca.storci@unibo.it

✉ Massimiliano Bonafè
massimiliano.bonafe@unibo.it

1 Department of Experimental, Diagnostic and Specialty Medicine, University of Bologna, Bologna, Italy

2 Interdepartmental Centre "L. Galvani" (CIG), University of Bologna, Bologna, Italy

3 Center of Applied Biomedical Research (CRBA), Policlinico Universitario S. Orsola-Malpighi, Bologna, Italy

4 Department of Biological, Geological and Environmental Science, University of Bologna, Bologna, Italy

5 IRCCS Istituto delle Scienze Neurologiche di Bologna, Bologna, Italy

6 Istituto Scientifico Romagnolo per lo Studio e la Cura dei Tumori (IRST), IRCCS, Biosciences Laboratory, Meldola (Forlì), Italy

7 Medical Physics Unit, Istituto Scientifico Romagnolo per lo Studio e la Cura dei Tumori (IRST), IRCCS, Meldola, Italy

8 Institute of Molecular Genetics, National Research Council (CNR), Bologna, Italy

9 IRCCS, Rizzoli Orthopedic Institute, Bologna, Italy

10 Department of Clinical and Molecular Sciences, DISCLIMO, Università Politecnica delle Marche, Ancona, Italy

11 Center of Clinical Pathology and Innovative Therapy, Italian National Research Center on Aging, INRCA-IRCCS, Ancona, Italy

the activation of inflammatory pathways that recalls the systemic pro-inflammatory status that develops with age, named inflamm-aging [2]. Studies on centenarians convey that such long-living subjects escape the majority of age-related diseases and avoid the detrimental effects of inflamm-aging [1, 2]. An explanation of such phenomenon stands in the genetic and epigenetic make-up of such exceptional individuals that may restrain the activation of the innate immunity/inflammation in response to lifelong stress [2]. As it occurs across evolution, individuals that attain longevity are likely to be endued with a peculiar capability to repair DNA damage, thus maintaining genomic integrity lifelong [1, 2]. In our previous investigation, we showed that centenarians are endowed with well-preserved telomeres [3] and a highly efficient DNA repair response (DDR) mainly due to the activation of 53BP1-dependent non-homologous end joining (NHEJ) mechanism [4]. DNA damage is a powerful trigger of inflammation and type I interferon (IFNalpha/beta) signaling [5–7]. Recent literature shed light on the importance of cytoplasmic nucleic acid sensors in DNA-damage response [6]. Indeed, upon DNA damage, nucleic acids are misplaced into the cytoplasm, whereby they engage evolutionary-conserved sensors that trigger inflammation and IFNalpha/beta pathways [6, 7]. This mechanism is pathogenic in rare diseases called interferonopathies [8], but it is expected to be also linked to common age-related autoimmune diseases, such as systemic lupus erythematosus and psoriasis [8, 9]. The cytoplasmic misplacement of nucleic acids recently gained importance in explaining the onset of the senescent associated pro-inflammatory secretome [10]. In particular, it was demonstrated that the absence of the cytosolic DNA sensor cGAS incapacitates chronic DDR activation to elicit senescence [11]. The relationship between cell senescence and systemic aging is a major matter of debate. Indeed, senescent cells are likely to constitute a minor population in aged tissues [12]. However, owing to their capability of secreting a huge amount of inflammatory mediators they may contribute to systemic inflammation and thus to inflamm-aging [13]. Moreover, current literature pinpoints that the ablation/injection of few senescent cells is enough to reduce/increase progeric features at systemic level in the mice [14, 15]. Here, we hypothesize that centenarians may be endowed with a molecular setting that allows them to maintain genomic stability while avoiding the activation of DNA damage associated inflammatory/INFbeta response. To this purpose, we measured the level of DNA damage in dermal fibroblasts (DF) from centenarian's cells under basal and upon stress (gamma radiations) and their capability to express interleukin-6 (IL-6, "the cytokine for gerontologist") [16], a major predictor of morbidity and mortality in aged people [17]. In the same experimental setting, we measured INFbeta, owing to that type I interferon is triggered by DNA damage and it elicits systemic progeric features in the mouse model [18]. In particular, we then assessed the level of highly pro-inflammatory species such as cytoplasmic RNA:DNA hybrids [6, 19, 20] in fibroblasts of people of different ages and the expression of the cognate degrading enzyme RNAseH2 [8]. Indeed, the degradation of RNA:DNA hybrids is a crucial physiologic phenomenon to preserve normal cell functioning and RNA:DNA hybrids accumulation elicit INFalpha/beta signaling, genomic instability, and telomere derangement in a variety of cellular models [8, 21, 22]. Finally, owing to the fact that extra-cellular vesicles (EV) take part in inflammation and INFalpha/beta activation [23–25], we assessed the capability of EV from centenarian's fibroblasts to modulate inflammatory activation in a variety of recipient cells.

Materials and methods

Cell cultures

Primary DF (Supplementary Table 1) were obtained from healthy young (18–40 years), old (58–98 years), and centenarian (>99 years, Supplementary Table 2) subjects. DF were cultured in 10% FCS DMEM (Euroclone, Milan, Italy). All the experiments were performed between the 3rd and 6th in vitro passage. DF were collected upon signed informed consent. The study was approved by the local Ethics Committee (S. Orsola-Malpighi Hospital Prot. n. 2006061707, amendment 08/11/2011; Fondazione IRCCS Cà Granda Ospedale Maggiore Policlinico, Prot. n. 2035, amendment 30/11/2011; University of Calabria 9/9/2004 amendment on 24/11/2011). Early passages and senescent human embryonic diploid lung fibroblasts were cultured as previously described [26]. THP1 cells were maintained in 20% FCS RPMI 1640 medium. Cells were seeded in 24-well plates at a density of 500.000 cells/ml. For M1–M2 monocyte polarization assay, THP1 were exposed to 1×10^3 CD9+ EV/cell for 72 h. MCF-7 cells were cultured in 10% RPMI 1640 medium. MCF-7 MS were generated by seeding single cell suspension ($1–5 \times 10^3$ cells per well) in low attachment plates filled with MammoCult™ (Stem Cell Technologies, Vancouver, Canada) and assessed at day 7 [27]. HUVECs were cultured as previously described [28].

Exposure of DF to DNA damaging agents

DF were exposed to a single radiation dose of 7.5 Gy using the linear acceleration Elekta Synergy Platform system (Elekta Oncology Systems, Stockholm, Sweden) as previously described [29]. DNA damage was evaluated 72 h after treatment. Doxorubicin (Sigma, St. Louis, MO) was used at a concentration of 5 μM for 24 h.

Comet assay

The assay was performed according to the manufacturer's protocol (Comet Assay, Trevigen, Gaithersburg, MD). Briefly, at the end of the treatments, 5×10^5 cells were suspended in LMA agarose (at 37 °C) at a ratio of 1:10 (v/v), and 75 µl were immediately transferred onto the comet slide. The slides were immersed for 1 h at 4 °C in a lysis solution, washed in the dark for 1 h at room temperature in alkaline solution, then electrophoresed for 30 min at 20 V. Slides were immersed twice in dH$_2$O for 5 min each, then dipped in 70% ethanol and stained with the Silver Staining Kit (Trevigen). The extent of DNA damage was evaluated quantitatively by Olympus IX51 microscope 10×, Olympus Corporation, Tokyo, Japan, by scoring at least 100 nucleoids of different categories, using the free software Cell Profiler (version 2.1.1). Percentage of DNA in the tail for different categories of comets was expressed.

Confocal microscopy analysis

Cells were fixed and permeabilized with ice-cold methanol for 10′ and acetone for 1′ on ice, blocked with 2% BSA, and incubated with primary anti-S9.6 antibody (1:100 dilution, Kerafast, Boston, MA, USA) and secondary goat anti-mouse Alexa Fluor 488 (1:250; Life Technologies). Alternatively, cells were fixed with paraformaldehyde 4% for 20 min at room temperature and incubated overnight at 4 °C with anti Rad51 diluted 1:100 (Millipore, Milan, Italy). The confocal imaging was performed with a Nikon A1 confocal laser scanning microscope, equipped with a 60×, 1.4 NA objective and with 405, 488, and 561 nm laser lines. Rad51 foci were enumerated using Fiji (ImageJ).

Transient gene knock-down and over-expression

RNAseH2C (HSS149830) and Snai2/Slug (HSS109993/109995/185949) specific siRNA, the GC matched content control (siSCR) were transiently transfected with lipofectamine 2000 (Life Technologies, Carlsbad, CA, USA) following manufacturer instructions. All transfections were performed onto 70% confluent cells. The cells were harvested after 72 h of siRNA transfection and stored in TRIzol® (Life Technologies, Carlsbad, CA, USA).

Real-time PCR analysis

Total RNA was extracted from cells using TRIzol® (Life Technologies, Carlsbad, CA, USA). TaqMan probes for Rad51, Snai2/Slug, IL-6, RNAseH2A/B/C, interferon beta-1, TREX1, IL-1, PPRalpha, PPRgamma, RXRalpha, Alox-15, Jagged-1, IL-10, CD163, CD68, and glucuronidase were purchased from Life Technologies (Carlsbad, CA,

USA). Quantitative PCR analysis was performed on Light-Cycler using iQ software (BIORAD, Hercules, CA, USA), mRNA levels were calculated with the 2^{-ddct} method.

Telomere length assessment

Telomere length was measured as telomere-to-single copy gene ratio (T/S), using quantitative real-time PCR as previously described [30] with some modifications. For cellular samples, 5 µl aliquots containing 20 ng DNA and 10 µl of master mix per sample were processed. For EV samples, 5 µl aliquots containing 0.8 ng DNA and 10 µl of master mix per sample were processed. For each standard curve, one reference DNA sample was diluted serially in water by 1.68-fold dilution to produce 5 DNA concentrations ranging from 30 to 2 ng in 5 µl. To reduce inter-assay variability, the telomere and the single-copy gene (36B4) were analyzed on the same plate. Primer sequences and concentrations for telomere and 36B4 were as previously described [30]. The thermal cycling profile was: (1) one cycle of 10 s at 95 °C; (2) 30 cycles of 5 s at 95 °C, 15 s at 57 °C, and 20 s at 72 °C. Measurements were performed in duplicate and reported as T/S ratio relative to a calibrator sample (Roche, Milano, Italy) to allow comparison across runs. EV telomeric sequences were quantified based on the RT-PCR CT, without the comparison with single gene copy. To date no single gene copy was described in EV. The real-time Chromo4 MJ Research system (Bio-Rad Laboratories, Hercules, CA, USA) was used for all PCRs. The coefficients of variation within duplicates of the telomere and single-gene assay were 2% and 1.8%, respectively. Approximately 30% of the samples were repeated on different plates to assess T/S measurement reproducibility. The inter-assay coefficient of variation was <10%. All analyses were blind. The correlation coefficient between T/S and the telomere restriction fragment was $R^2 = 0.88$

ELISA test

IL-6 ELISA was performed with Quantikine ELISA kit for human IL-6 (R&D System, Minneapolis, MN, USA) according to manufacturer instructions. Concentrations of Maresin 1 and Resolvin D1 (RvD1) in cell culture supernatants were measured using commercially available ELISA kits (Cayman Chemical Co., Ann Arbor, MI, USA) according to manufacturer instructions.

Western blot analysis

Proteins were extracted with radio-immunoprecipitation assay buffer, with the exception of γ-H2AX extraction which was performed by adding HCl to the lysis buffer [10 mmol/L HEPES (pH 7.9); 1.5 mmol/L MgCl$_2$; 10 mmol/L

KCl] to a final concentration of 0.2 mol/L. The following antibodies were used: anti-actin (C4—Santa Cruz, CA); anti-phospho-(gamma)-Histone H2AX (Ser139, clone JBW301, Millipore, Billerica, MA, USA); anti-Rad51, clone 3C10 (Millipore); anti-Snai2/Slug (L40C6, Cell Signalling, Beverly, MA, USA); anti-RNAseH2C (Proteintech, IL, USA), and anti-actin (clone C4, Santa Cruz, CA, USA) as loading control.

DNA methylation analysis

DNA methylation of RNAseH2C locus (genomic region: chr11:65,486,750–65,487,179, GRCh37/hg19) was evaluated using the EpiTYPER assay (Agena Bioscience). Briefly, the EZ-96 DNA Methylation Kit (Zymo Research Corporation) was used to perform bisulfite-conversion of 500 ng of genomic DNA. This treatment specifically converts unmethylated cytosines to uracils, while methylated cytosines remain unaffected. Ten nanograms of converted DNA were amplified using the following primers for bisulfite-converted DNA: RNAseH2C_F_aggaagagagATGGGGTTGAGGATAGTTTAAAAAG; RNASEH2C_R_cagtaatacgactcactatagggagaaggctCCCAATAAAAAAACTCTTCACAACA. PCR products were then processed and analyzed according to EpiTYPER protocol. The following Gene Expression Omnibus datasets were analyzed for RNAseH2C methylation according to Illumina HumanMethylation450 BeadChip array measurements: GSE40279, which includes whole-blood DNA methylation data from 656 healthy subjects with age ranging from 19 to 101 years; GSE46394, which includes DNA methylation data from 15 atherosclerotic lesion tissues and matched normal aortic tissue, plus 19 carotid atherosclerotic samples; GSE66695, which includes DNA methylation data from 40 normal and 80 breast cancer samples.

Small RNA seq analysis

Small RNA libraries were prepared from 6 DF samples using TruSeq Small RNA Library PrepKit v2 (Illumina, RS-200-0012/24/36/48), according to manufacturer's indications. Briefly, 35 ng of purified RNA were linked to RNA 3′ and 5′ adapters, converted to cDNA and amplified using Illumina primers containing unique indexes for each sample. Each library was quantified using Agilent Bioanalyzer and High Sensitivity DNA kit (Agilent, 5067-4626) and an equal amount of libraries were pooled together. A size-selection was performed to keep fragments between 130 and 160 bp. After ethanol precipitation, the library pool was quantified with Agilent High Sensitivity DNA kit, diluted to 1.8 pM and sequenced using NextSeq® 500/550 High Output Kit v2 (75 cycles) (Illumina, FC-404-2005) on

Illumina NextSeq500 platform. Raw base-call data generated from the Illumina NextSeq500 system were demultiplexed by Illumina BaseSpace Sequence Hub (https://basespace.illumina.com/home/index) and converted to FASTQ format. After a quality check, which was performed with FastQC tool (https://www.bioinformatics.babraham.ac.uk/projects/fastqc/), the adapter sequences were trimmed using Cutadapt (http://cutadapt.readthedocs.io/en/stable/index.html). In this step, sequences shorter than 10 nucleotides were also removed. Read mapping was performed using STAR algorithm (https://www.ncbi.nlm.nih.gov/pubmed/23104886). The reference genome was constituted by human microRNAs sequences from the miRbase 21 database (http://www.mirbase.org/). Counts of raw mapped reads were obtained using the htseq-count script from the HTSeq tools (http://www-huber.embl.de/HTSeq/doc/overview.html); raw counts were further normalized using DESeq2 bioconductor package (http://bioconductor.org/packages/release/bioc/html/DESeq2.html). Data were analyzed using Genespring GX software v. 14.8 (Agilent Technologies). Differentially expressed miRNAs were identified using moderated t-test (FDR 10% with Benjamini–Hochberg correction), principal component analysis and cluster analysis, with Manhattan correlation, were performed using GeneSpring GX software.

CD9+ exosome isolation and phenotypization from DF supernatants

CD9+ exosomes from young, old, and centenarians DF supernatants were isolated by CD9 immunobeads isolation kit (HansaBioMed Life Sciences Ltd.; cod: HBM-BOLC-CC/20-1) according to manufacturer's protocol. EVs were diluted to approximately 1 ml of PBS, loaded into the sample chamber of an LM10 unit (Nanosight, Malvern, UK) and three videos of either 30 or 60 s were recorded of each sample. Exosomal-surface antigens were investigated with the MACSPlex Exosome kit (Miltenyi Biotec GmbH, Gladbach, Germany). Briefly, after isolation, exosomes were diluted in MACSPlex buffer and stained according to manufacturer instructions. The samples were analyzed with a FACSCanto flow cytometer (Beckton Dickinson). At least 10.000 events per sample were recorded. Data were analyzed with FACSDiva software. The median fluorescence values plotted in the graph were background corrected and normalized on CD63/81/9 median signal intensity. Negative values were excluded from the plot.

Statistical analysis

The exact p-value was calculated by un-paired t-test (two groups comparisons) and one-way ANOVA (>2 groups

Fig. 1 Reduced level of interleukin-6 and high genetic stability in cells from centenarians. **a** IL-6 ELISA test in aged people (old) and centenarians (cen) DF supernatants. **b** Real-time PCR analysis of IL-6 mRNA level in old and cen DF (left panel) and peripheral blood mononuclear cells, PBMC (right panel). **c** IL-6 mRNA level in old and cen DF exposed to gamma rays (7.5 Gy). **d** IL-6 mRNA level in old and cen DF exposed to doxorubicin (5 μM for 24 h); data are presented as mean ± s.d.
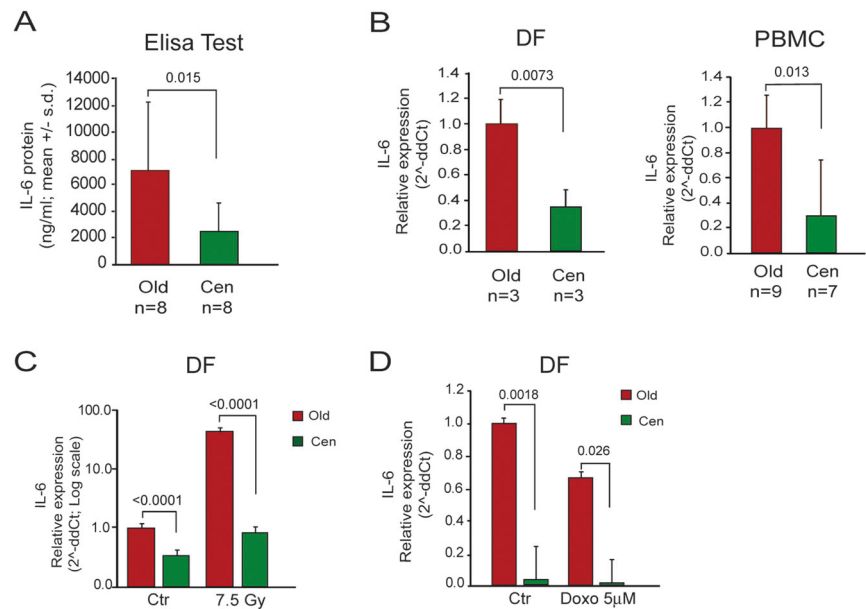
comparisons). Post-hoc *t*-test values were corrected for multiple comparisons according to Bonferroni correction. The statistical analysis was performed with GraphPad Prism 6 software.

Results

Reduced level of interleukin-6 and DNA damage in cells from centenarians

The first observation of our investigation regards the reduced IL-6 protein level in the supernatant of centenarian's primary DF compared to supernatants from aged people ones (Fig. 1a). The finding above was confirmed by real-time PCR analysis, which also conveyed reduced IL-6 mRNA level in DF and peripheral blood mononuclear cells (PBMC) from centenarians, as compared to aged people (Fig. 1b). These data led us to reason that cells from centenarians are characterized by a restrained pro-inflammatory phenotype. To further confirm this finding, we performed small RNA-seq analysis (Supplementary Figure 1a). The data obtained revealed the down-regulation of a variety of inflammation-related microRNAs (such as miR146a, miR155a, miR21, miR125a, and miR125b) that have been previously associated with age-related diseases [31, 32]. Moreover, anti-inflammatory micro-RNAs such as miR508-3p, miR532-5p, and miR335-5p [33–35] were up-regulated in centenarian's DF (Supplementary Figure 1a). We then tested if such a peculiar molecular set-up persisted even after the induction of a DNA damage: upon exposure to a single radiation dose of 7.5 Gy of gamma rays, we

substantiate that centenarian's DF show a dramatically hampered capability to express IL-6, with respect to cells from old subjects (2 folds vs 80 folds, Fig. 1c). Similar results were observed when DF were exposed to doxorubicin (Fig. 1d). These data indicate that centenarian's cells are endowed with hampered pro-inflammatory response to DNA damaging agents. This finding is in agreement with our previous observation that centenarian's DF have a high capability to promptly repair DNA damage [4]. In our set of centenarian's DF, we found a low level of overall DNA damage measured by comet assay (Fig. 2a). Importantly, such behavior was persistent even after a dose of 7.5 Gy of gamma rays (Fig. 2b). Notably, low levels of the DNA double strand breaks (DSB) sensor Ser139-phosphorylated γ-H2AX were present in centenarian's DF in basal conditions as well as upon doxorubicin exposure compared to aged people DF (Fig. 2c). Interestingly, we previously reported that centenarian's DF display a prompt recovery from oxidative stress-induced DNA damage associated with an up-regulation of the DNA damage repair protein 53BP1 [4] which promotes the error-prone NHEJ machinery and switches-off the error-free homologous (HR) DNA repair mechanism [4, 36]. Accordingly, we observed a substantial decrease of the major player of HR protein, i.e., Rad51 in centenarian's DF compared to old people ones as assessed by western blot and real-time PCR analysis (Fig. 2d). This observation was confirmed by confocal microscopy analysis, showing a decrease of Rad51 positive foci in centenarian's DF even upon a dose of 7.5 Gy of gamma rays (Fig. 2e). Finally, since telomeres are major source of DNA damage signaling and HR is a major mechanism of telomere maintenance, we assessed telomere length in DF by PCR
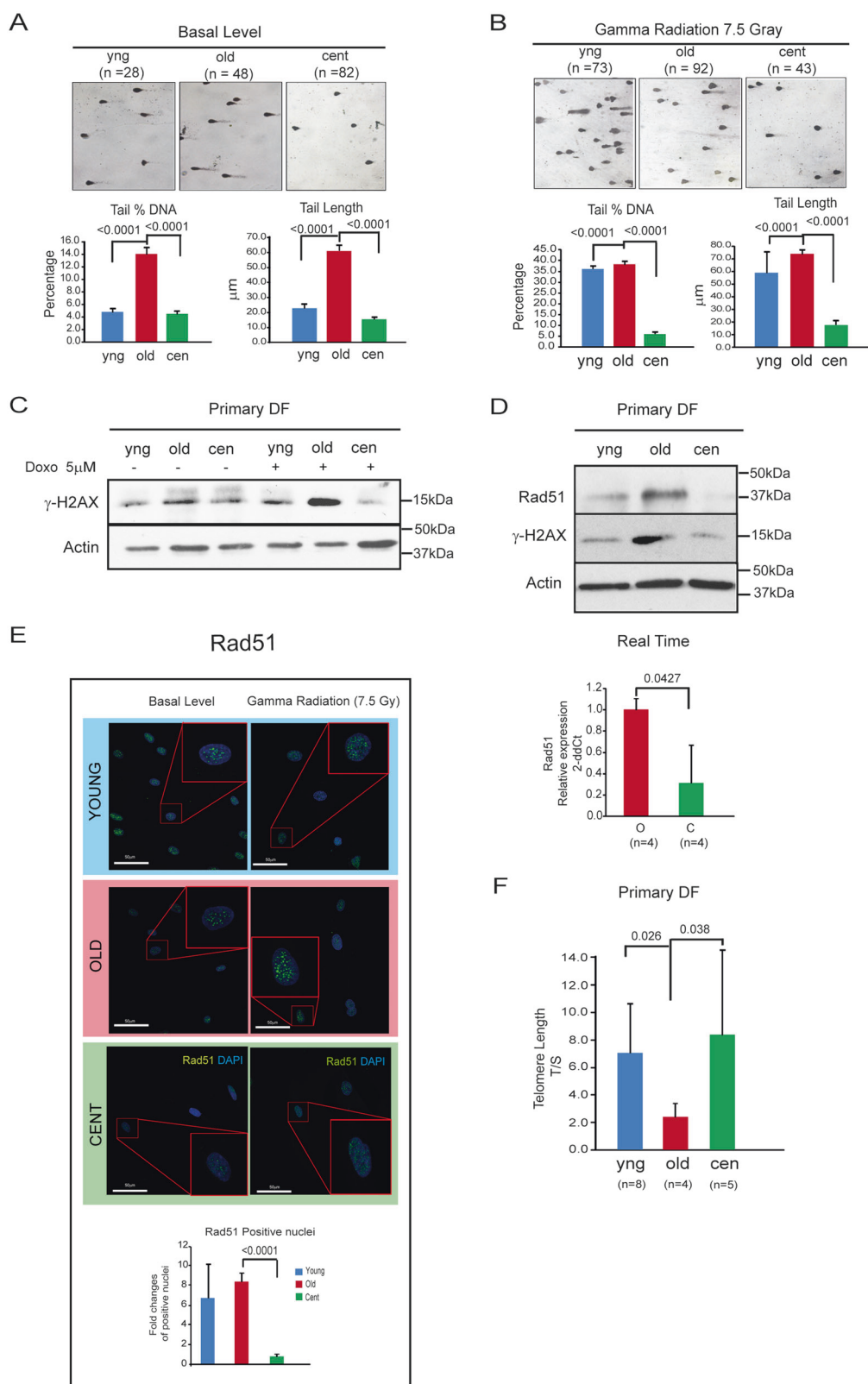
analysis. In keeping with previous observations [3], we found that centenarian's DF display higher than expected telomere length, being more similar to young people than old people ones (Fig. 2f). These data show that blunted inflammatory activation in centenarian's DFs is accompanied by a remarkable genomic stability.

◀ **Fig. 2** Reduced level of DNA damage in cells from centenarians. **a** Comet assay in young (yng), aged (old), and centenarians (cen) DF under basal condition. **b** Comet assay in yng, old, and cen DF upon 7.5 Gy of gamma radiation exposure. **c** Phospho-serine139-γ-H2AX (γ-H2AX) and actin protein level in yng, old, and cen DF treated or untreated with 5 μM doxorubicin for 24 h. **d** Rad51, γ-H2AX, and actin protein level in DF from yng, old, and cen, and Rad51 mRNA level in old and cen DF. **e** Confocal microscopy analysis of Rad51 in yng, old, cen DF at basal condition and upon exposure of 7.5 Gy of gamma radiation. **f** Telomere/single copy gene ratio (T/S) in DNA from yng ($n = 8$), old ($n = 4$), cen ($n = 5$) DF; data are presented as mean ± s.d.

High level of RNAseH2C and low level of RNA:DNA hybrids in cells from centenarians

DNA damage is a powerful trigger of type I interferon signaling [6, 37]. In this regard, DF from centenarians showed a reduced expression of IFNbeta and IL-6 in comparison to old people cells, while the levels of these cytokines in DF from young subjects were remarkably similar to those of centenarians (Fig. 3a). Notably, an up-regulation of the IFN-regulated gene TREX1 was observed in aged people compared to young and centenarian ones (Fig. 3b). DNA damage elicits inflammation and type I interferon by displacing nucleic acids into the cytoplasm [6, 38]. Cytoplasmic RNA:DNA hybrids are likely to play a substantial role in the above mechanism [19, 20]. These molecules are mainly processed by RNAseH2 enzyme [8, 21]. Remarkably, all three components of the RNAseH2 enzymatic complex were up-regulated in centenarian's DF compared to old people (Fig. 3c). In particular, the up-regulation of RNAseH2C enzyme subunit in centenarian's cells was confirmed by western blot analysis (Fig. 3c). Accordingly, the amount of RNA:DNA hybrids, assessed by confocal microscopy analysis, were reduced in the cytoplasm of centenarian's DF, with respect to old people's ones (Fig. 3d). Moreover, after exposure to a dose of 7.5 Gy of gamma rays, a dramatic increase in the amount of RNA:DNA hybrids was observed in the cytoplasm of young and old people's DF, but not in centenarian's ones (Fig. 3d). Importantly, we observed an opposite relationship between RNAseH2C and IL-6 expression in cells exposed to a dose of 7.5 Gy of gamma rays (Fig. 3e, f). In centenarian's cells, the transient knock-down of RNAseH2C led to a marked dose-dependent increase of IL-6 and INFbeta expression (Fig. 3g). These data indicate that the anti-inflammatory phenotype of centenarian's cells is associated with RNAseH2C over-expression.

RNAseH2C locus methylation in senescent cells and human pathologic tissues

Prompted by the above-described results, we measured RNAseH2C expression in senescent cells [5]. In this latter, an activation of inflammatory and type I interferon signaling due to the misplacement of nucleic acids into the cytoplasm has been recently found [10, 11]. A down-regulation of RNAseH2 subunits expression and a significant up-regulation of IFNbeta were also observed in senescent primary human umbilical endothelial cells (HUVEC) compared to non-senescent ones (Fig. 4a). Accordingly, reduced RNAseH2C expression in senescent fetal lung fibroblasts [26] was found in comparison to early passage cells (Fig. 4b). Epigenetic age-related changes are deeply involved in the aging process [38]. We thus measured DNA methylation at RNAseH2C locus by EpiTYPER (Fig. 4c). A marked hypo-methylation of the first 3 CpG sites of the investigated amplicon was observed in centenarian's DF (Fig. 4d). In PBMC, we also observed an age-related decrease in the methylation level of RNAseH2C locus at cg11637721 site, which corresponds to the CpG3 site in the EpiTYPER assay (Fig. 4e). Intriguingly, senescent lung fibroblasts displayed a higher degree of methylation at the same RNAseH2C CpG sites that were hypo-methylated in centenarian's DF (Fig. 4f). We thus reasoned that RNAseH2C gene methylation may be increased in pathologic tissues. To verify this assumption, we searched Gene Expression Omnibus (GEO) database for DNA methylation datasets and analyzed data from GSE46394 and GSE66695 (see Materials and methods). The analysis conveyed that the RNAseH2C CpG site cg11637721 is hyper-methylated in tissues obtained from atherosclerotic plaques (Fig. 4g) and breast cancer tissues, compared to cognate healthy ones (Fig. 4h). These data indicate that disease-free longevity is associated with an un-methylated state of RNAseH2C locus.

Anti-inflammatory activity of extracellular vesicles (EV) from centenarians

EV have been recently reported to modulate inflammatory and type I interferon signaling pathways [23, 39]. To test the role of EV in our experimental setting, CD9+ EV were isolated from young, old, and centenarian's DF supernatants, counted by Nanosight and phenotypically characterized by FACS analysis (Supplementary Figure 2a). EV were then administered to primary DF of people of different ages, THP1 myelo-monocytic and MCF-7 breast cancer cells (Fig. 5a). We found that EV from centenarians reduced IL-6 expression and induced RNAseH2C in young people's DF, as well in THP1 and MCF-7 cells (Fig. 5b, c, Supplementary Figure 2b). In THP1 cells exposed to centenarian's EV, we observed an over-expression of M2-polarization markers (CD68, CD163, IL-10, and PPAR-gamma) and an up-regulation of anti-inflammatory enzyme (Alox-15) and RXRalpha transcription factor (Fig. 5d, e). A parallel down-regulation of IFNbeta, of the pro-inflammatory cytokine IL-1beta and of PPR-alpha transcription factor were also observed (Fig. 5f). Such an anti-inflammatory capacity of
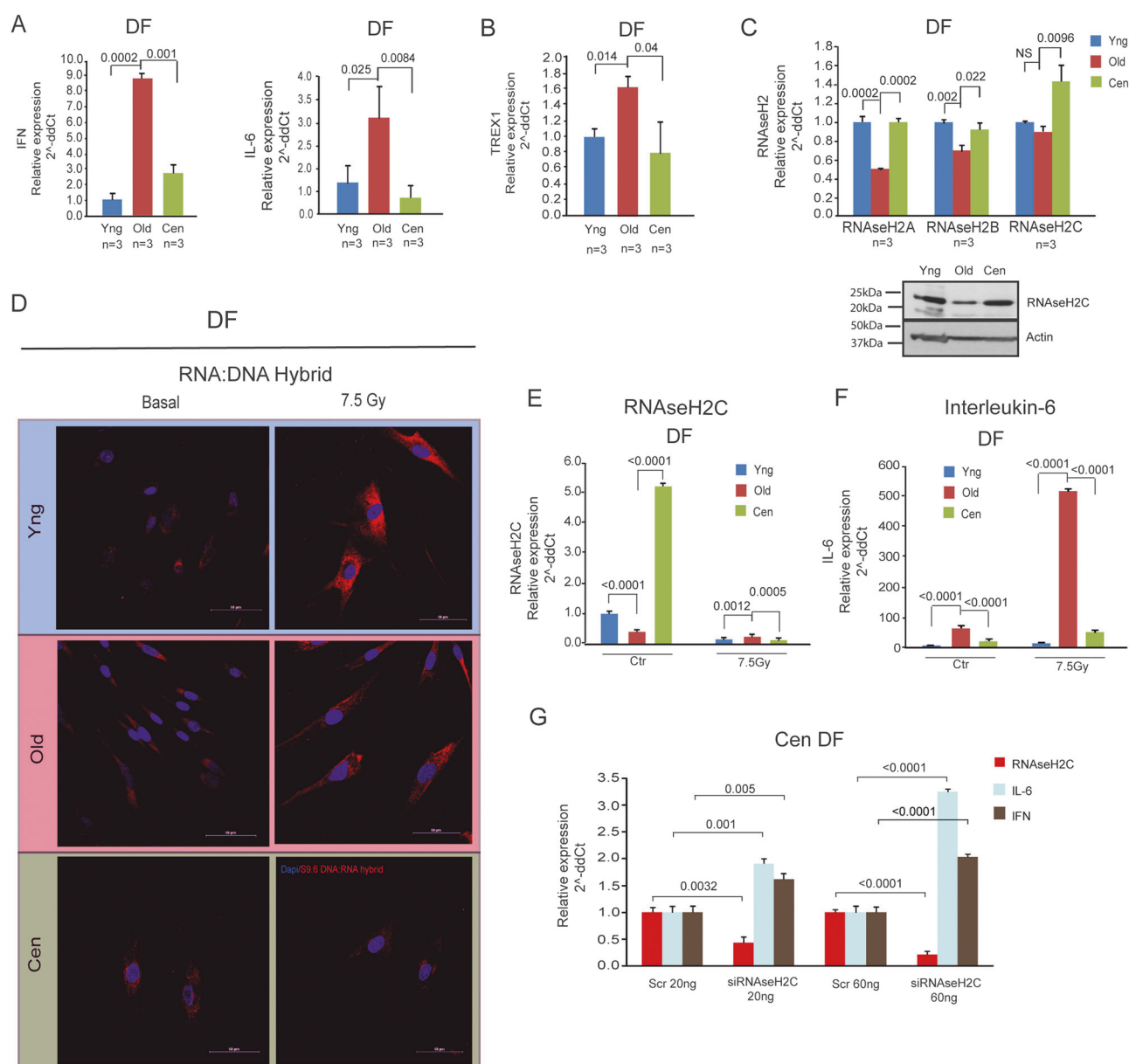
Fig. 3 High level of RNAseH2C and low level of RNA:DNA hybrids in cells from centenarians. **a** IFN and IL-6 mRNA level in DF from young (yng), aged (old), and centenarian (cen) in a different set of samples respect to Fig. 1b. **b** TREX1 mRNA level in yng, old, and cen DF. **c** RNAseH2A-H2B-H2C mRNA level in yng, old, and cen DF; RNAseH2C and actin protein level in yng, old, and cen DF. **d** Confocal microscopy analysis of RNA:DNA hybrids (S9.6 antibody) in yng, old, and cen DF under basal or upon 7.5 Gy gamma radiation exposure. **e** RNAseH2C mRNA level in yng, old, and cen DF under basal or upon 7.5 Gy gamma radiation exposure. **f** IL-6 mRNA level in yng, old, and cen DF under basal or upon 7.5 Gy gamma radiation exposure. **g** IL-6, IFN, and RNAseH2C mRNA level in cen DF upon RNAseH2C knock-down (20 and 60 ng siRNA); data are presented as mean ± s.d.

centenarian's EV was confirmed by the high levels of pro-resolving mediators (maresin-1 and resolvin D1) in THP1 cells administered with centenarian's EV and exposed to a dose of 7.5 Gy of gamma rays (Fig. 5g). The telomere has been previously characterized among the DNA sequences endowed with peculiar anti-inflammatory activity [40–42]. Interestingly, we observed that EV from centenarians contained more than expected amounts of TTAGGG telomeric repeats (Fig. 5h). These data point at the capability

of centenarians EV to exert anti-inflammatory activity in recipient cells.

Discussion

This paper reports an anti-inflammatory molecular make-up in DF from centenarians. Indeed, as compared to aged people DF, such cells disclose low levels of the pro-inflammatory

A HUVEC

B Lung Fibroblast

C

D DF RNAseH2C Locus

E CpG3 RNAseH2C Methylation by Age (GSE 40279)

F Lung Fibroblast RNAseH2C

G CpG3 RNAseH2C Methylation (GSE46394)

H CpG3 RNAseH2 in Breast Cancer (GSE 66695)
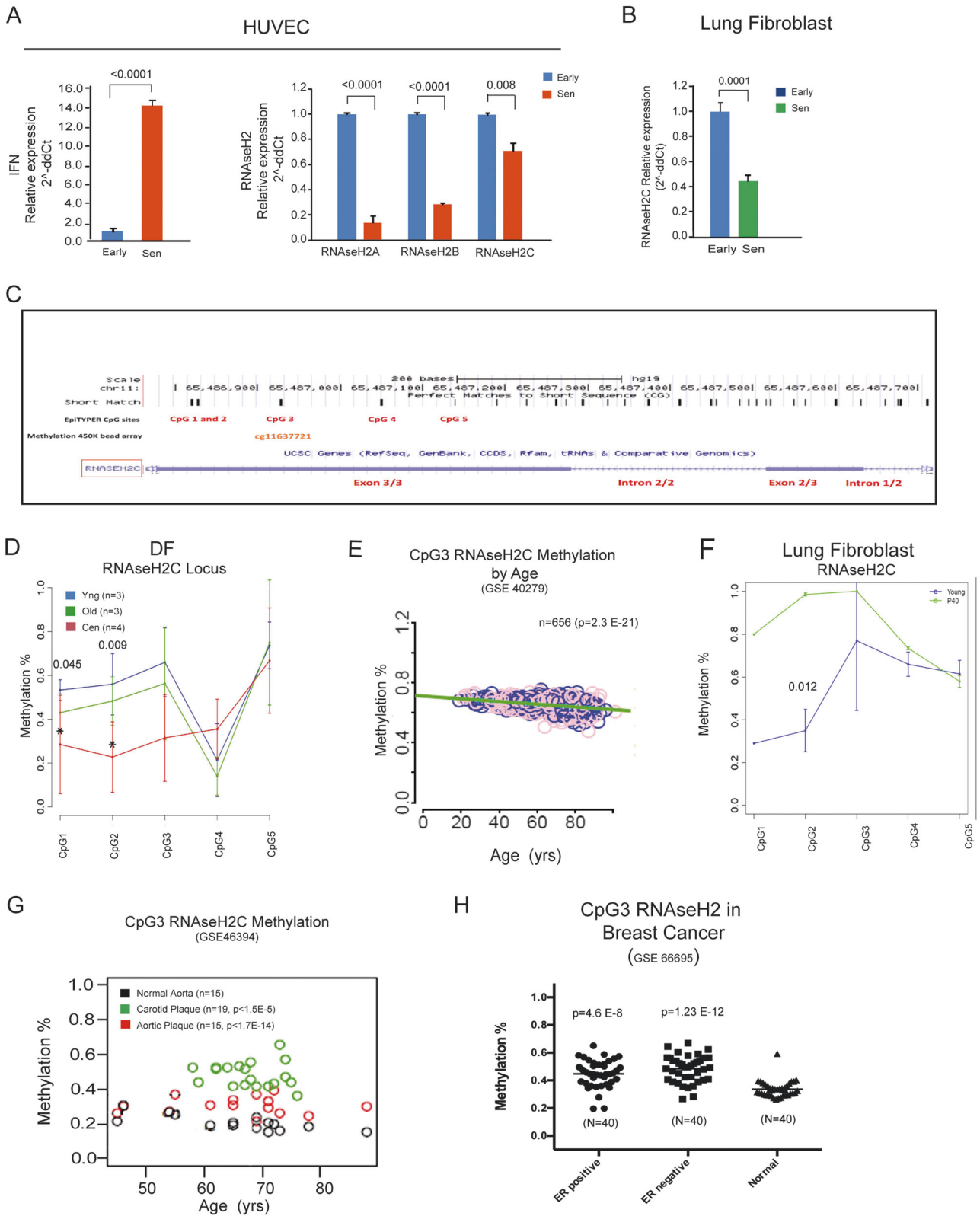
cytokine IL-6, low expression of INFbeta, as well as an anti-inflammatory microRNA pattern. In particular, microRNA associated with inflammatory age-related diseases such as miR146b, mir21, miR125a/b, miR155a [31, 32] are down-regulated, whereas anti-inflammatory microRNA such as miR508-3p, miR532-5p, and miR335-5p [33–35] are

Fig. 4 Opposite correlation of RNAseH2C locus methylation with longevity and age-related diseases. **a** RNAseH2C and IFN mRNA level in early passage and senescent HUVEC cells. **b** RNAseH2C mRNA level in early and senescent (sen) lung fibroblasts. **c** UCSC view (human GRCh37/hg19) of the RNaseH2C CpG locus explored with EpiTYPER assay and Illumina Infinium 450K corresponding probes. **d** Percent of methylation for each RNAseH2C CpG unit, measured in young (yng), aged (old), and centenarian (cen) DF. **e** Percent of methylation of the Illumina Infinium 450K CpG3 unit probe in whole-blood of people of different ages. **f** Percent of methylation for each RNAseH2C CpG unit, in early and sen human embryonic diploid lung fibroblasts. **g** Percent of methylation of the Illumina Infinium 450K CpG3 unit probe in normal aortic, aortic, and carotid atherosclerotic samples (dataset GSE46394). **h** Box plot analysis of percent methylation of CpG3 unit probe in normal and ER-positive or ER-negative breast cancer samples (dataset GSE66695); data are presented as mean ± s.d.

up-regulated. These data suggest that the molecular set-up of centenarians may allow these individuals to avoid or postpone inflamm-aging, i.e., the seemingly unavoidable activation of the inflammatory response that occurs during life [2]. Such exceptional individuals are the living proof that it is possible to reach the extreme limits of human lifespan by escaping the detrimental effects of major age-related dysfunctions and diseases [1]. These latter (e.g., atherosclerosis, diabetes, and cancer), albeit extremely heterogeneous, share an inflammatory pathogenesis [12]. Along the myriads of mechanism that may ignite inflammation, DNA damage response has emerged as a crucial trigger of pro-inflammatory/INF alpha/beta response [8, 20, 21, 43]. DNA damage is associated with inflammation in a variety of physiologic and pathologic conditions [6, 8, 37, 43, 44]. Here we show a remarkable low level of DNA damage in cells from centenarians, i.e., almost absent comet tails and barely detectable levels of γ-H2AX phosphorylation, even after exposure to DNA damaging agents. These peculiar features associate with a well-preserved telomere length. All these evidence extend and confirm previous reports [3, 4], showing that centenarians are likely to be endowed with the peculiar capability to repair DNA damage, an activity that is associated with longevity across evolution [45]. Based on the tight relationship between inflammation and DNA damage, the maintenance of the genome is expected to shelter the individuals from a variety of inflammatory diseases, and to prevent or post-pone inflamm-aging. Recent literature shows that DNA damage-induced inflammation and type I interferon signaling depend upon the displacement of nucleic acids into the cytoplasm, where they engage cognate sensors [6, 8, 13, 37]. The phenomenon has been recently linked to the induction of the pro-inflammatory secretome of senescent cells [10]. A particular kind of DNA damage-induced misplaced nucleic acids are RNA:DNA hybrids [6, 19]. Here we show that cells from centenarians are almost devoid of cytoplasmic RNA:DNA hybrids even upon the exposure to gamma radiations. Accordingly, the enzyme

involved in the clearance of RNA:DNA hybrids, namely RNAseH2, is strongly up-regulated in cells from centenarians. Then we report that the knock-down of RNAseH2C elicits IL-6 and IFNbeta expression, thus demonstrating that the up-regulation of this enzyme plays a role in the anti-inflammatory set-up of centenarian's cells. These data are in agreement with current literature showing that RNAseH2C mutations that impair cytoplasmic RNA:DNA hybrids degradation are major trigger for the inflammatory/IFN response [8]. Notably, RNA:DNA hybrids are essential intermediates of the HR-dependent repair of telomere ends but must be proficiently removed to ensure genomic and telomeric stability [46]. Noteworthy, cells of centenarians display almost undetectable levels of Rad51 protein, the major player of HR, thus suggesting that they may act as HR-deficient cells. This apparently paradoxical finding, perfectly fits with our previous observation that centenarian's cells show the up-regulation of 53BP1, the major mediator of NHEJ, that switches off Rad51 expression and function [36]. In such a peculiar genetic background, the up-regulation of the RNAseH2 enzyme, by promoting RNA:DNA hybrid degradation, is likely assuring genomic stability and telomere maintenance [47]. In this regard, the unbalancing of DNA-repair mechanisms towards NHEJ, associated with higher expression of RNAseH2, is expected to be advantageous for human longevity as it may ensure adequate DNA repair, while avoiding the deleterious effects of Rad51-generated RNA:DNA hybrids [48]. As far as the Rad51 down-regulation in centenarian's cells, based on our previous observations [26], we observed an up-regulation of Rad51 repressor SLUG, whose down-regulation up-regulated Rad51 mRNA level (Supplementary Figure 3a-b). Noteworthy, SLUG expression was also capable to up-regulate RNAseH2C expression (Supplementary Figure 3c). Though these data may be considered preliminary, it may be speculated that SLUG-dependent mechanisms may control DNA stability and the cognate inflammatory response in aging by modulating RNAseH2 expression. In this regard, we provide evidence that the expression of *RNAseH2C* is epigenetically regulated. In particular, *RNAseH2C* is hypo-methylated in centenarians, but hyper-methylated in atherosclerotic plaques and breast cancer tissues. Notably, all these cell types represent pathologic conditions associated with aging and with the up-regulation of inflammatory response [12, 48]. Importantly, our data on the positive relationship between RNAseH2C and longevity are reinforced by literature data showing that RNAseH-dependent RNA:DNA hybrids clearance extends lifespan in the yeast [49]. Moreover, RNAseH2C locus (as well as IL-6 receptor) were identified in a recent genome-wide analysis on human longevity as potential polymorphisms that may explain part of the inter-individual variability in attaining healthy aging and longevity [50]. A major conundrum in aging studies is the relationship between the mechanisms of cellular (in vitro) senescence and those occurring in vivo, at
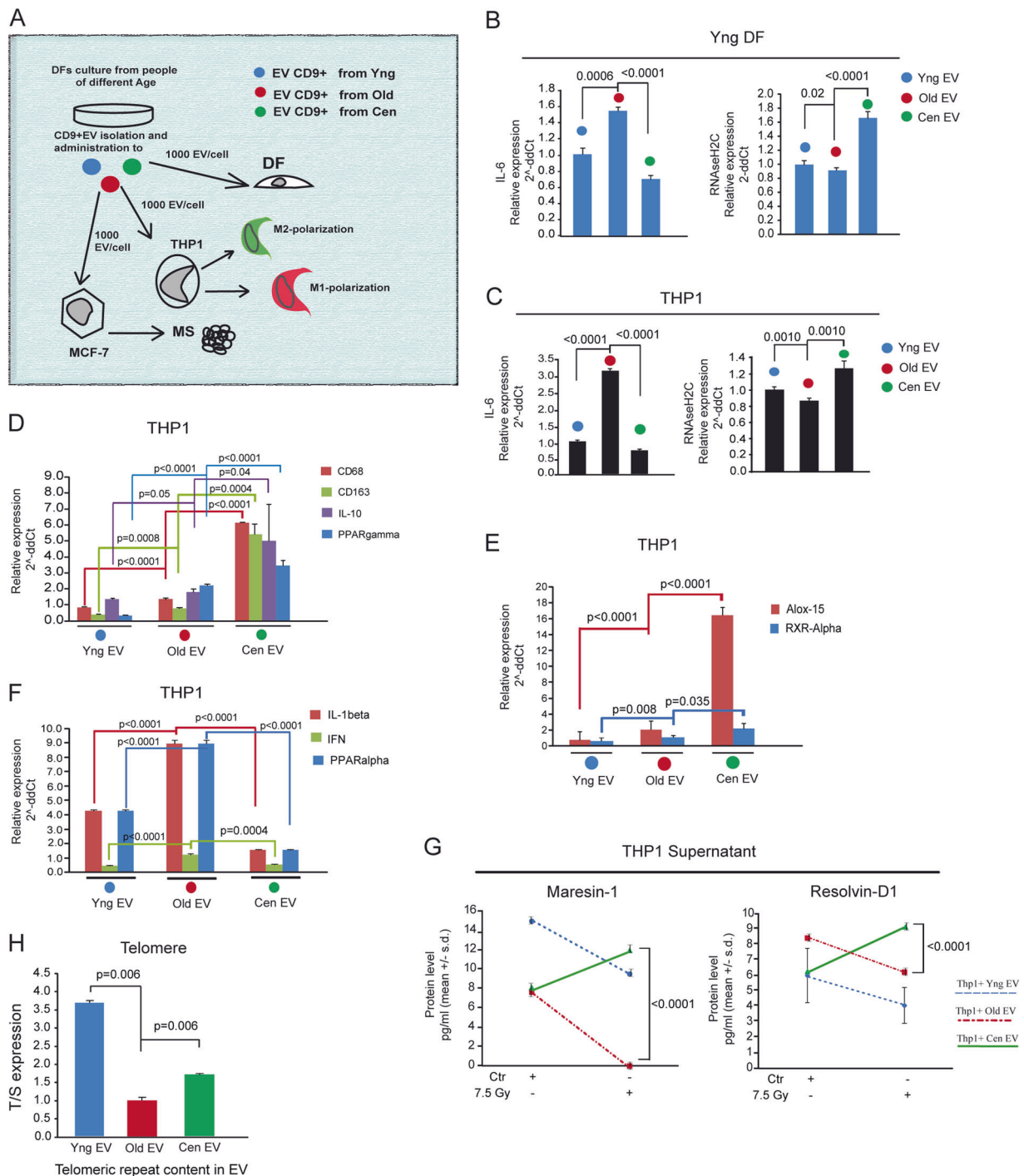
Fig. 5 Anti-inflammatory activity of extracellular vesicles from centenarians. **a** Schematic of the experimental design showing CD9+ EV isolated from young (yng), aged (old), and centenarian (cen) DF and administered to DF, THP1 myelomonocitic cells, and MCF-7 breast cancer cell lines (See Supplementary Figure 2). **b** IL-6 and RNAseH2C mRNA level in DF exposed to yng-EV, old-EV, cen-EV. **c** IL-6 and RNAseH2C mRNA level in THP1 cells exposed to yng-EV, old-EV, cen-EV. **d** IL-10, CD163, CD68, and PPARgamma mRNA level in THP1 cells administered with yng-EV, old-EV, cen-EV. **e** Alox-15 and RXR-alpha mRNA level in THP1 cells exposed to yng-EV, old-EV, cen-EV. **f** IFN, IL-1beta, and PPARalpha mRNA level in THP1 cells administered with yng-EV, old-EV, cen-EV. **g** ELISA test of Maresin1 and Resolvin D1 on the supernatant of THP1 cells administered with yng-EV, old-EV, cen-EV under basal or upon 7.5 Gy gamma radiation exposure. **h** Real-time PCR analysis of telomeric repeat (T/S) in EV isolated from of yng, old, cen DF; data are presented as mean ± s.d.

cell and systemic level [14]. In this regard, the accrual of senescent cells, albeit it sets up a minor pool even in aged tissues, has been reported to be sufficient to elicit progeric features in vivo [13]. In particular, the ablation of senescent cells in genetically-engineered mice or via the administration of a set of purposely-named drugs (i.e., senolytics) halts the onset of aging features in vivo [14, 51, 52]. Accordingly, the transplant of few senescent cells into adult mice causes tissue dysfunctions that can be reversed upon the administration of senolytics [14]. As far as the relationship between in vitro senescence in vivo aging is concerned, here we found that in vitro senescent cells convey low expression of RNAseH2C and high RNAseH2C locus methylation. This molecular set-up is expected to facilitate the accumulation in the cytoplasm of nucleic acids (RNA:DNA hybrids in this case) that activate inflammatory/type I interferon signaling in these cells [10, 11, 39]. Nevertheless, cells from centenarians show high levels of RNAseH2C expression and low level of RNAseH2C locus methylation and of RNA:DNA hybrid in the cytoplasm. This molecular make-up seems to favor longevity, at least in part by dampening inflammatory/type I interferon signaling in such cells. In regard to the relationship between cellular and systemic aging features, in this paper we show that centenarian's cells can cast anti-inflammatory signals to other cell types, such as fibroblasts, monocytes, and cancer cells, via EV. Such subcellular nano-scaled structures have been extensively characterized [24] and contain a wealth of cellular components, including nucleic acids [34]. In all cellular models here tested, EV isolated from centenarian's DF are capable to induce RNAseH2C and reduce IL-6 expression. EV from centenarians also skew monocyte polarization towards the M2 phenotype which exhibits anti-inflammatory, pro-resolution, and reparative capability [53]. These data are reinforced by our observation regarding the capability of EV from centenarians to up-regulate two omega 3–derived lipid mediators, Resolvin-D1 and Maresin, which are tightly linked to the M2 macrophage phenotype [54, 55]. These anti-inflammatory mediators are currently regarded as molecules with a powerful capability to taper inflammation and to promote tissue integrity and repair [55]. Interestingly, EV from centenarians administered to MCF-7 grown in vitro as 3D cultures (mammospheres, MS) [54], blunted MS growth and reduced the level of the IL-6 dependent MS growth factor JAG1 (Supplementary Figure 4a and 4b) [54]. These data suggest that EV from long-living individuals may halt or thwart cancer cell growth. The amount of RNA in EV did not allow us to assess whether the microRNA content of such EV may propagate the anti-inflammatory phenotype to target cells. However, as a support of the centenarian's EV anti-inflammatory activity we could demonstrate the presence of higher than expected telomeric DNA sequences TTAGGG in centenarian's EV. Indeed, extracellular telomere sequences exert potent inhibitory activity on inflammation/type I

interferon signaling [56, 57]. These data suggest that EV may spread the anti-inflammatory set-up of centenarian's cells at a systemic level, thus providing cues on the molecular mechanisms that taper inflamm-aging and promote disease-free longevity in humans.

Compliance with ethical standards

Conflict of interest The authors declare that they have no conflict of interest.

References

1. Franceschi C, Bonafe M. Centenarians as a model for healthy aging. Biochem Soc Trans. 2003;31:457–61.
2. Franceschi C, Bonafè M, Valensin S, Olivieri F, De Luca M, Ottaviani E, et al. Inflammaging. An evolutionary perspective on immunosenescence. Ann N Y Acad Sci. 2000;908:244–54.
3. Mondello C, Petropoulou C, Monti D, Gonos ES, Franceschi C, Nuzzo F. Telomere length in fibroblasts and blood cells from healthy centenarians. Exp Cell Res. 1999;248:234–42.
4. Lattanzi G, Ortolani M, Columbaro M, Prencipe S, Mattioli E, Lanzarini C, et al. Lamins are rapamycin targets that impact human longevity: a study in centenarians. J Cell Sci. 2014;127:147–57.
5. Rodier F, Coppe JP, Patil CK, Hoeijmakers W, Munoz DP, Raza SR, et al. Persistent DNA damage signalling triggers senescence-associated inflammatory cytokine secretion. Nat Cell Biol. 2009;11:973–79.
6. Shen YJ, Le Bert N, Chitre AA, Ko CX, Nga XH, Ho SS, et al. Genome-derived cytosolic DNA mediates type I interferon-dependent rejection of B cell lymphoma cells. Cell Rep. 2015;11:460–73.
7. Schlee M, Hartmann G. Discriminating self from non-self in nucleic acid sensing. Nat Rev Immunol. 2016;16:566–80.
8. Crow YJ, Manel N. Aicardi–Goutieres syndrome and the type I interferonopathies. Nat Rev Immunol. 2015;15:429–40.
9. Molès JP, Griez A, Guilhou JJ, Girard C, Nagot N, Van de Perre P, et al. Cytosolic RNA:DNA duplexes generated by endogenous reverse transcriptase activity as autonomous inducers of skin inflammation in psoriasis. PLoS One. 2017;12:e0169879.
10. Gluck S, Guey B, Gulen MF, Wolter K, Kang TW, Schmacke NA, et al. Innate immune sensing of cytosolic chromatin fragments through cGAS promotes senescence. Nat Cell Biol. 2017;19:1061–70.

11. Yang H, Wang H, Ren J, Chen Q, Chen ZJ. cGAS is essential for cellular senescence. Proc Natl Acad Sci USA. 2017;114: E4612–20.

12. Childs BG, Durik M, Baker DJ, van Deursen JM. Cellular senescence in aging and age-related disease: from mechanisms to therapy. Nat Med. 2015;21:1424–35.

13. Franceschi C, Campisi J. Chronic inflammation (inflammaging) and its potential contribution to age-associated diseases. J Gerontol A Biol Sci Med Sci. 2014;69:S4–9.

14. Xu M, Pirtskhalava T, Farr JN, Weigand BM, Palmer AK, Weivoda MM, et al. Senolytics improve physical function and increase lifespan in old age. Nat Med. 2018;24:1246–56.

15. Zhu Y, Tchkonia T, Pirtskhalava T, Gower AC, Ding H, Giorgadze N, et al. The Achilles' heel of senescent cells: from transcriptome to senolytic drugs. Aging Cell. 2015;14:644–58.

16. Ershler WB. Interleukin-6: a cytokine for gerontologists. J Am Geriatr Soc. 1993;41:176–81.

17. Knupfer H, Preiss R. Significance of interleukin-6 (IL-6) in breast cancer (review). Breast Cancer Res Treat. 2007;102:129–35.

18. Yu Q, Katlinskaya YV, Carbone CJ, Zhao B, Katlinski KV, Zheng H, et al. DNA-damage-induced type I interferon promotes senescence and inhibits stem cell function. Cell Rep. 2015;11: 785–97.

19. Koo CX, Kobiyama K, Shen YJ, LeBert N, Ahmad S, Khatoo M, et al. RNA polymerase III regulates cytosolic RNA:DNA hybrids and intracellular microRNA expression. J Biol Chem. 2015;290: 7463–73.

20. Mankan AK, Schmidt T, Chauhan D, Goldeck M, Höning K, Gaidt M, et al. Cytosolic RNA:DNA hybrids activate the cGAS-STING axis. EMBO J. 2014;33:2937–46.

21. Günther C, Kind B, Reijns MA, Berndt N, Martinez-Bueno M, Wolf C, et al. Defective removal of ribonucleotides from DNA promotes systemic autoimmunity. J Clin Invest. 2015;125: 413–24.

22. Keskin H, Storici F. Defects in RNase H2 stimulate DNA break repair by RNA reverse transcribed into cDNA. MicroRNA. 2015;4:109–16.

23. Kitai Y, Kawasaki T, Sueyoshi T, Kobiyama K, Ishii KJ, Zou J, et al. DNA-containing exosomes derived from cancer cells treated with topotecan activate a STING-dependent pathway and reinforce antitumor immunity. J Immunol. 2017;198:1649–59.

24. Tkach M, Théry C. Communication by extracellular vesicles: where we are and where we need to go. Cell. 2016;164:1226–32.

25. Eitan E, Green J, Bodogai M, Mode NA, Baek R, Jorgensen MM, et al. Age-related changes in plasma extracellular vesicle characteristics and internalization by leukocytes. Sci Rep. 2017; 7:1342.

26. Bacalini MG, Deelen J, Pirazzini C, De Cecco M, Giuliani C, Lanzarini C, et al. Systemic age-associated DNA hypermethylation of ELOVL2 gene: in vivo and in vitro evidences of a cell replication process. J Gerontol A Biol Sci Med Sci. 2017; 72:1015–23.

27. Storci G, Bertoni S, De Carolis S, Papi A, Nati M, Ceccarelli C, et al. Slug/beta-catenin-dependent proinflammatory phenotype in hypoxic breast cancer stem cells. Am J Pathol. 2013;183: 1688–97.

28. Prattichizzo F, Giuliani A, Recchioni R, Bonafe M, Marcheselli F, De Carolis S, et al. Anti-TNF-alpha treatment modulates SASP and SASP-related microRNAs in endothelial cells and in circulating angiogenic cells. Oncotarget. 2016;7:11945–58.

29. Tesei A, Sarnelli A, Arienti C, Menghi E, Medri L, Gabucci E, et al. In vitro irradiation system for radiobiological experiments. Radiat Oncol. 2013;8:257.

30. Cawthon RM. Telomere measurement by quantitative PCR. Nucleic Acids Res. 2002;30:e47.

31. Olivieri F, Rippo MR, Procopio AD, Fazioli F. Circulating inflamma-miRs in aging and age-related diseases. Front Genet. 2013;4:121.

32. Kim SW, Ramasamy K, Bouamar H, Lin AP, Jiang D, Aguiar RC. MicroRNAs miR-125a and miR-125b constitutively activate the NF-kappaB pathway by targeting the tumor necrosis factor alpha-induced protein 3 (TNFAIP3, A20). Proc Natl Acad Sci USA. 2012;109:7865–70.

33. Jia-Xing Z, Zhen-Hua C, Dong-Liang C, Xiao-Peng T, Chen-Yuan W, Zhi-Wei Z, et al. LINC01410-miR-532-NCF2-NF-kB feedback loop promotes gastric cancer angiogenesis and metastasis. Oncogene. 2018;37:2660–75.

34. Gao XL, Li JQ, Dong YT, Cheng EJ, Gong JN, Qin YL, et al. Upregulation of microRNA-335-5p reduces inflammatory responses by inhibiting FASN through the activation of AMPK/ULK1 signaling pathway in a septic mouse model. Cytokine. 2018;110:466–78.

35. Huang T, Kang W, Zhang B, Wu F, Dong Y, Tong JH, et al. miR-508-3p concordantly silences NFKB1 and RELA to inactivate canonical NF-kappaB signaling in gastric carcinogenesis. Mol Cancer. 2016;15:9.

36. Ciccia A, Elledge SJ. The DNA damage response: making it safe to play with knives. Mol Cell. 2010;40:179–204.

37. Erdal E, Haider S, Rehwinkel J, Harris AL, McHugh PJ. A pro-survival DNA damage-induced cytoplasmic interferon response is mediated by end resection factors and is limited by Trex1. Genes Dev. 2017;31:353–69.

38. Horvath S, Pirazzini C, Bacalini MG, Gentilini D, Di Blasio AM, Delledonne M, et al. Decreased epigenetic age of PBMCs from Italian semi-supercentenarians and their offspring. Aging (Albany NY). 2015;7:1159–70.

39. Takahashi A, Okada R, Nagao K, Kawamata Y, Hanyu A, Yoshimoto S, et al. Exosomes maintain cellular homeostasis by excreting harmful DNA from cells. Nat Commun. 2017;8:15287.

40. Gursel I, Gursel M, Yamada H, Ishii KJ, Takeshita F, Klinman DM. Repetitive elements in mammalian telomeres suppress bacterial DNA-induced immune activation. J Immunol. 2003;171: 1393–00.

41. Shirota H, Gursel I, Gursel M, Klinman DM. Suppressive oligodeoxynucleotides protect mice from lethal endotoxic shock. J Immunol. 2005;174:4579–83.

42. Goldfarb IT, Adeli S, Berk T, Phillippe M. Fetal and placental DNA stimulation of TLR9: a mechanism possibly contributing to the pro-inflammatory events during parturition. Reprod Sci. 2017;25:788–96.

43. Brégnard C, Guerra J, Déjardin S, Passalacqua F, Benkirane M, Laguette N. Upregulated LINE-1 activity in the fanconi anemia cancer susceptibility syndrome leads to spontaneous pro-inflammatory cytokine production. EBioMedicine. 2016;8: 184–94.

44. Bonafè M, Storci G, Franceschi C. Inflamm-aging of the stem cell niche: breast cancer as a paradigmatic example: breakdown of the multi-shell cytokine network fuels cancer in aged people. Bioessays. 2012;34:40–9.

45. MacRae SL, Zhang Q, Lemetre C, Seim I, Calder RB, Hoeijmakers J, et al. Comparative analysis of genome maintenance genes in naked mole rat, mouse, and human. Aging Cell. 2015;14: 288–91.

46. Ohle C, Tesorero R, Schermann G, Dobrev N, Sinning I, Fischer T. Transient RNA–DNA hybrids are required for efficient double-strand break repair. Cell. 2016;167:1001–13.

47. Balk B, Maicher A, Dees M, Klermund J, Luke-Glaser S, Bender K, et al. Telomeric RNA–DNA hybrids affect telomere-length dynamics and senescence. Nat Struct Mol Biol. 2013;20: 1199–205.

48. Wahba L, Gore SK, Koshland D. The homologous recombination machinery modulates the formation of RNA–DNA hybrids and associated chromosome instability. eLife. 2013;2:e00505.

49. Salvi JS, Chan JN, Szafranski K, Liu TT, Wu JD, Olsen JB, et al. Roles for Pbp1 and caloric restriction in genome and lifespan maintenance via suppression of RNA–DNA hybrids. Dev Cell. 2014;30:177–91.

50. Pilling LC, Kuo CL, Sicinski K, Tamosauskaite J, Kuchel GA, Harries LW, et al. Human longevity: 25 genetic loci associated in 389,166 UK biobank participants. Aging (Albany NY). 2017;9: 2504–20.

51. Baker DJ, Wijshake T, Tchkonia T, LeBrasseur NK, Childs BG, van de Sluis B, et al. Clearance of p16Ink4a-positive senescent cells delays ageing-associated disorders. Nature. 2011;479:232–6.

52. Baar MP, Brandt RMC, Putavet DA, Klein JDD, Derks KWJ, Bourgeois BRM, et al. Targeted apoptosis of senescent cells restores tissue homeostasis in response to chemotoxicity and aging. Cell. 2017;169:132–47.

53. Mantovani A, Biswas SK, Galdiero MR, Sica A, Locati M. Macrophage plasticity and polarization in tissue repair and remodelling. J Pathol. 2013;229:176–85.

54. Sansone P, Storci G, Tavolari S, Guarnieri T, Giovannini C, Taffurelli M, et al. IL-6 triggers malignant features in mammospheres from human ductal breast carcinoma and normal mammary gland. J Clin Invest. 2007;117:3988–02.

55. Serhan CN. Pro-resolving lipid mediators are leads for resolution physiology. Nature. 2014;510:92–101.

56. Marwaha V, Chen YH, Helms E, Arad S, Inoue H, Bord E, et al. T-oligo treatment decreases constitutive and UVB-induced COX-2 levels through p53- and NFkappaB-dependent repression of the COX-2 promoter. J Biol Chem. 2005;280: 32379–88.

57. Steinhagen F, Zillinger T, Peukert K, Fox M, Thudium M, Barchet W, et al. Suppressive oligodeoxynucleotides containing TTAGGG motifs inhibit cGAS activation in human monocytes. Eur J Immunol. 2018;48:605–11.

Review

The telomere world and aging: Analytical challenges and future perspectives

Emanuela Mensà[a], Silvia Latini[a], Deborah Ramini[a], Gianluca Storci[b,c], Massimiliano Bonafè[b,c,d], Fabiola Olivieri[a,e,*]

[a] Department of Clinical and Molecular Sciences, DISCLIMO, Università Politecnica delle Marche, Ancona, Italy
[b] Department of Experimental, Diagnostic and Specialty Medicine, University of Bologna, Bologna, Italy
[c] Interdepartmental Centre "L. Galvani" (CIG), University of Bologna, Bologna, Italy
[d] Istituto Scientifico Romagnolo per lo Studio e la Cura dei Tumori (IRST), IRCCS, Biosciences Laboratory, Meldola, Italy
[e] Center of Clinical Pathology and Innovative Therapy, IRCCS INRCA, Ancona, Italy

A B S T R A C T

Telomeres, the terminal nucleoprotein structures of eukaryotic chromosomes, play pleiotropic functions in cellular and organismal aging. Telomere length (TL) varies throughout life due to the influence of genetic factors and to a complex balancing between "shortening" and "elongation" signals. Telomerase, the only enzyme that can elongate a telomeric DNA chain, and telomeric repeat-containing RNA (TERRA), a long non-coding RNA involved in looping maintenance, play key roles in TL during life. Despite recent advances in the knowledge of TL, TERRA and telomerase activity (TA) biology and their measurement techniques, the experimental and theoretical issues involved raise a number of problems that should carefully be considered by researchers approaching the "telomere world". The increasing use of such parameters – hailed as promising clinically relevant biomarkers – has failed to be paralleled by the development of automated and standardized measurement technology. Consequently, associating given TL values to specific pathological conditions involves on the one hand technological issues and on the other clinical-biological issues related to the planning of clinically relevant association studies. Addressing these issues would help avoid major biases in association studies involving TL and a number of outcomes, especially those focusing on psychological and bio-behavioral variables. The main challenge in telomere research is the development of accurate and reliable measurement methods to achieve simple and sensitive TL, TERRA, and TA detection. The discovery of the localization of telomeres and TERRA in cellular and extracellular compartments had added an additional layer of complexity to the measurement of these age-related biomarkers. Since combined analysis of TL, TERRA and TA may well provide more exhaustive clinical information than a single parameter, we feel it is important for researchers in the various fields to become familiar with their most common measurement techniques and to be aware of the respective merits and drawbacks of these approaches.

1. Introduction

Telomeres, the terminal nucleoprotein structures of eukaryotic chromosomes, have a key role in protecting chromosomal DNA ends (Blackburn, 1990). Mounting evidence suggests that they play pleiotropic functions that are not simply related to the maintenance of chromosome homeostasis, but also to the regulation of gene expression and the modulation of stress-related signaling pathways (Blackburn, 2005). Telomere length (TL) is species-specific and heritable (Chiang et al., 2010); therefore, its value at any time depends on genetic characteristics and on the balance between "shortening" and "elongation" signals (Honig et al., 2015). Shortening signals come from a variety of

stressors like repeated cell division, nuclease activation, oxidative damage, DNA replication, and transcriptional stress (Blackburn et al., 2015). Elongation signals are capable of activating telomerase or alternative lengthening of telomeres (ALT); the latter mechanism relies on recombination-mediated telomere elongation and can be induced by telomere-specific DNA damage (Hu et al., 2016). Telomerase is an RNA-protein complex that extends telomeric DNA at the 3′ ends of chromosomes through telomerase reverse transcriptase (TERT) and integral template-containing telomerase RNA (TER) (Jiang et al., 2018). Telomerase is responsible for the preservation of replicative potential in most eukaryotic cells and is involved in pleiotropic functions that range from TL maintenance and genome stability to tissue renewal and

mitochondrial protection (Li et al., 2018a, 2018b). TL is a marker of the metabolic activity and pluripotency state of embryonic stem cells (Wang et al., 2017a). In embryonic cell lines telomerase is activated and keeps TL constant; in adult stem cells its limited activity and provides only partial compensation for telomere shortening (TS); and in somatic cells it is usually not activated. As a result, during somatic cellular and organismal aging shortening outpaces elongation. Telomeres that have reached a critical length become dysfunctional and activate a DNA damage response which leads to a senescence phenotype characterized by reduced proliferative ability and the acquisition of a secretory proinflammatory phenotype (SASP) (d'Adda di Fagagna et al., 2003).

TL has long been known to be critically involved in cellular aging as a consequence of replication and/or the action of a wide range of stressors, but is also being extensively investigated in relation to organismal aging. Although cell senescence does not necessarily equate with aging of an organism, TS has been observed in both conditions (reviewed in Zhu et al., 2018), and TL has been investigated as a biomarker of aging *per se* and as a risk factor for the development and progression of the most common age-related diseases (ARDs) (Jose et al., 2017).

Recent insights into telomere biology and function indicate that telomeric repeat-containing RNA (TERRA), a long non-coding RNA, is involved in the telomere looping maintenance mechanism (Graf et al., 2017). An inverse correlation has been documented between TL and TERRA both *in vitro* and *in vivo*. According to two hypotheses that have been advanced to explain it, TERRA transcription could facilitate 5′-3′ nuclease activity at the chromosome ends (Pfeiffer and Lingner, 2012), or TS could induce TERRA expression to coordinate telomerase molecule recruitment and activity at the shortest telomeres (Cusanelli et al., 2013).

Notably, telomere DNA, TERRA, and telomerase are not independent molecules; in fact, their structures and temporal relationships are closely regulated by complexes such as shelterin, small nucleolar RNAs (snoRNAs), and small nucleolar ribonucleoproteins (snoRNPs), besides the transcription machinery (Blasco et al., 1999; Gomez et al., 2012). Even though the latter molecules are capable of affecting endpoint TL, the present work focuses on telomeres, TERRA, and telomerase activity (TA).

Despite recent advances, there are a number of outstanding issues related to the knowledge and measurement technology of TL, TERRA, and TA. The most important are: i) the accuracy of the methods employed to measure TL, TERRA, and TA in biomedical research; ii) their strengths and weaknesses; iii) the scope for their improvement; iv) the chemical-clinical variables to be correlated with TL in association studies of aging and ARDs; and v) the need for human longitudinal studies to evaluate the ability of specific approaches (pharmaceutical, nutraceutical) to reverse TS during aging.

Addressing these issues would help avoid major biases in association studies addressing TL and a wide range of outcomes (Montpetit et al., 2014).

This work describes the analytical caveats and criticisms regarding the various TL, TERRA, and TA measurement methods. Since not all protocols are appropriate (or recommended) for epidemiological and longitudinal ARD studies, and some approaches may be applicable only to tumor tissue, the paper focuses on the methods that are suitable for clinical and epidemiological applications.

We will also describe and discuss the localization of telomere and telomere-related sequences in the cellular and extracellular compartment, since localization adds an additional layer of complexity to telomere, TERRA, and TA measurement.

2. Localization of telomere and telomere-related sequences

Recent studies have highlighted a number of possible localizations of telomeric sequences, including the cellular and extracellular compartment (Fig. 1). In cells, telomere sequences can be detected in the nucleus, the chromosome ends and interstitial loci (Smith et al., 2018), and the cytoplasm (Cohen et al., 2010; Zhang et al., 2017a). Localizations in the extracellular compartment include exosomes (Li et al., 2008; Zinkova et al., 2017).

An increased number of telomeric sequences has been described in the cytoplasm of stressed cells in physiological as well as pathological conditions (Kuttler and Mai, 2007; Byrd et al., 2016). Telomeric circles (t-circles or c-circles) are extrachromosomal duplex or single-stranded circular DNA molecules composed of (CCCTAA)(n) sequences. Integration of t-circles in telomere repeats at the chromosome ends results in telomere elongation; circular DNA forms can also be involved in the rapid elongation of DNA ends in rolling-circle replication processes (Nabetani and Ishikawa, 2011).

T-circles, which can be found in human immortalized and cancer cells, rely on ALT pathways or high TA (Tokutake et al., 1998). In fact, in cells showing high TA, extrachromosomal telomeric DNA circles can be excised from the overextended chromosomal ends and released outside the nucleus (Pickett et al., 2009). T-circles have been detected in blood from patients with ALT + tumors; their analysis may have clinical value for their diagnosis and management (Henson et al., 2009). Importantly, t-circles are also found in healthy tissue (Tomaska et al., 2009).

Recent evidence indicates that telomeric sequences are also found in cell-free (cf)-DNA, including biofluids such as plasma and serum (Zinkova et al., 2017). Most of the DNA found in such biofluids is associated to nanovesicles, mainly exosomes, (Fernando et al., 2017; Németh et al., 2017).

TERRA, the long non-coding RNA molecules deriving from transcription of telomeric/subtelomeric regions, is enriched with 5′-(UUAGGG)-3′ repetitions that are complementary to AATCCC, the strand opposite to TTAGGG sequences. TERRA can therefore combine with AATCCC strands, generating three-stranded nucleic acid structures that contain a DNA:RNA hybrid molecule and a displaced DNA strand (Balk et al., 2014). These structures are localized at the level of R-loops and are involved in telomere homeostasis (Toubiana and Selig, 2018). In contrast, UUTCCC molecules, the RNA sequence complementary to TTAGGG, are not related to telomere DNA:RNA hybrids in human cells.

Notably, cf-TERRA – which is shorter (measuring about 200 nt) and more stable than TERRA associated to telomeric DNA in the nucleus – has also been detected in extracellular vesicles. These characteristics suggest that some extrachromosomal telomere-related sequences may be RNA and/or DNA:RNA hybrids (Wang and Lieberman, 2016) (see Fig. 1).

In eukaryotic cells, telomeres and TERRA can fold into G-quadruplexes (G4s), which are characterized by four G combined through non-canonical Hoogsten hydrogen bonding to generate planar structures called tetrads (Martadinata et al., 2011; Wang et al., 2018a) (see Fig. 1). Two or more tetrads can overlap and interact with each other *via* π-stacking, generating stable G4s. Experimental studies and bioinformatics predictions support the view that G4s are involved in several cellular functions such as telomeric DNA elongation, recombination, and transcription, and RNA post-transcriptional mechanisms (Cammas and Millevoi, 2017).

Whereas the location of telomere sequences and TERRA in the nucleus is well known, it is more difficult to describe the cytoplasmic localization of telomere repeats and TERRA.

It has been hypothesized that a cytoplasmic location of TAGGG may exert a suppressive effect on innate immune cells due to their ability to form G4s (Gursel et al., 2003). Colocalization of CpG DNA with toll-like receptor (TLR) 9 in endosomal vesicles is disrupted by TTAGGG telomeric repetitive elements, although cell binding and uptake remain unchanged, suggesting that specific host-derived molecules can downregulate the innate immune response elicited by a TLR ligand.

While cytoplasmic (cy-) or cf-telomeric sequences seem to restrain inflammation, TERRA found in extracellular fractions can stimulate innate immune signaling (Wang et al., 2015). TERRA can be activated
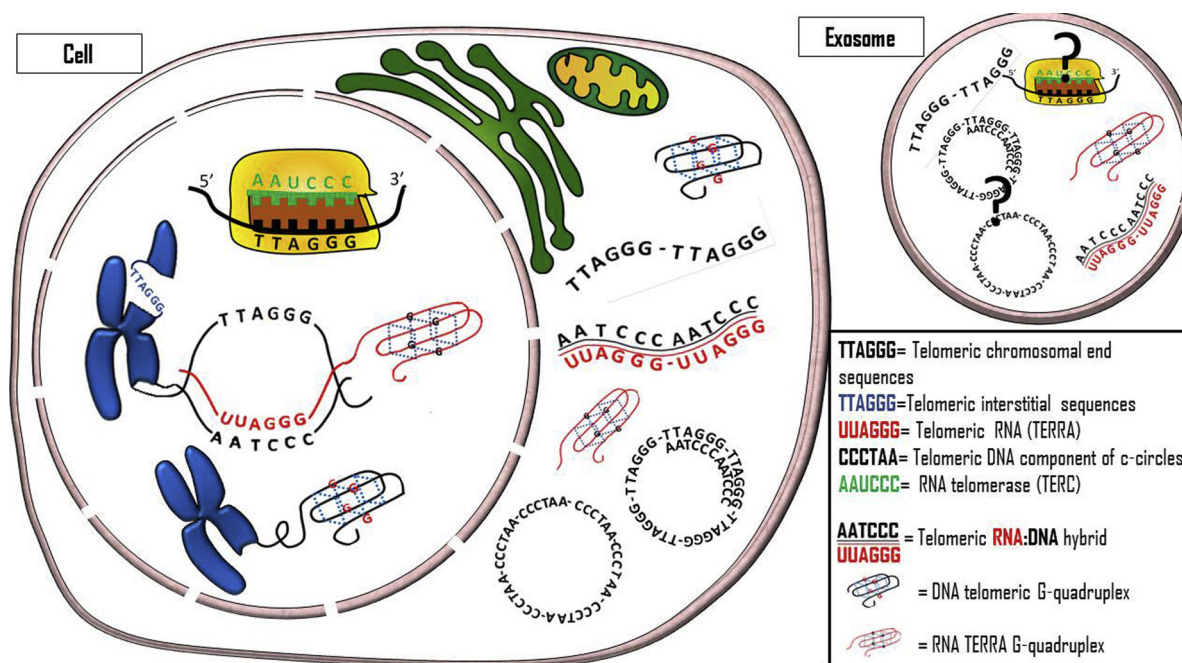
Fig. 1. Telomere-related molecules in cells (nucleus and cytoplasm) and exosomes.
Telomeric sequences can have a number of possible localizations not only in cells (nucleus and cytoplasm) but also in nanovesicles.
DNA, TERRA, DNA:RNA hybrids, and telomerase are not independent molecules: their structures and temporal relationships are closely regulated by key complexes such as shelterin and snoRNPs, besides the transcription machinery. However, these important parameters cannot be depicted here.

through a p53-response element embedded in a retrotransposon-like repeat found in human subtelomeres. TERRA secretion in extracellular vesicles serves as a danger signal, inducing the production of inflammatory cytokines in neighboring cells (Wang et al., 2017c). These findings suggest that TERRA may be part of the innate immune response to viral infection and that exosomes containing cf-TERRA carry a telomere-associated molecular pattern and telomere-specific alarmin from dysfunctional telomeres to the extracellular environment to elicit an inflammatory response (Wang and Lieberman, 2016).

Recently, we have hypothesized that telomeric sequences may be important components of the cy- and cf-DNA payload and that changes in a variety of biochemical features of cy- and cf-DNA (*e.g.* the proportion of DNA hybridized with RNA and the amount of 5-methyl-deoxy-cytosine and 8-oxo-deoxy-guanosine) can affect the ability of these DNA pools to ignite the innate immune system (Storci et al., 2018).

Notably, the localization of telomeric sequences in the cellular and extracellular compartment adds a further layer of complexity to telomere measurement, because different extraction/separation procedures may affect their reciprocal amounts (Komosa et al., 2015).

3. Telomeres and aging

A number of epidemiological studies have found a significant association linking telomere attrition, aging, and several biological outcomes including morbidity and mortality (Gorenjak et al., 2018; Gao et al., 2018). Short leukocyte TL (LTL) has been identified as an independent risk factor for functional decline in elderly European populations (Montiel Rojas et al., 2018) and has been found to be associated to altered fatty acid metabolism and increased oxidative stress in human aging (Zierer et al., 2016). Epidemiological studies provide support for a putative effect of dietary components and exercise on TL and the aging process (Mundstock et al., 2015a; Freitas-Simoes et al., 2018). An association has also been reported between telomere attrition and body mass index gain, suggesting potential pathways linking adiposity and aging outcomes (Müezzinler et al., 2016; Wulaningsih

et al., 2018). However, these associations have been described in works performed with different methodological approaches, of which few were prospective; adequately powered randomized controlled trials are therefore warranted. For all these reasons, the causal relationships between important functional parameters and TL remain an open question (Mundstock et al., 2015b; Pérez et al., 2017).

Recent evidence suggests that TL may not be a useful clinical marker of functional aging in older adult populations, whereas it may play a crucial role in longitudinal studies involving young and middle-aged populations (Brown et al., 2018). Since the trajectories of aging begin to diverge as early as in young adulthood (Belsky et al., 2015), it is critical to assess the contribution of telomere-related variations to the diverse aging pathways. Although telomeres shorten during aging, different cell types may have a diverse telomere attrition rate (TAR), *i.e.* a different rate of tissue and organ aging. A yearly TAR of ˜25 base pairs during aging has been reported in blood leukocytes, mononuclear cells, and isolated T and B lymphocytes (Müezzinler et al., 2013), whereas high interindividual TAR variation has been described in some longitudinal studies (Chen et al., 2011; Lin et al., 2015).

The marked heterogeneity of health outcomes seen in older individuals suggests that although "chronological" age is a major risk factor for functional impairment, "biological" age may be a more accurate predictor of the rate of aging (Lowsky et al., 2014). TL is currently the most extensively investigated biological age predictor, although new predictors, *e.g.* the epigenetic clock, are emerging (Jylhävä et al., 2017). Mounting evidence suggests that the various biological age predictors may reflect different aspects of the aging process, even though links between the various biomarkers are likely (Vetter et al., 2018). At present, the most stimulating area in telomere research is the study of how progressive TS induces epigenetic alterations and changes in gene expression associated to human healthy and unhealthy aging (Shay, 2018). In this scenario, combinations of the diverse predictors may shed light on the complexity of the aging process and help to improve the estimation of aging trajectories. Composite scores integrating molecular and physiological data have been proposed to measure biological aging in humans (Khan et al., 2017; Belsky et al.,
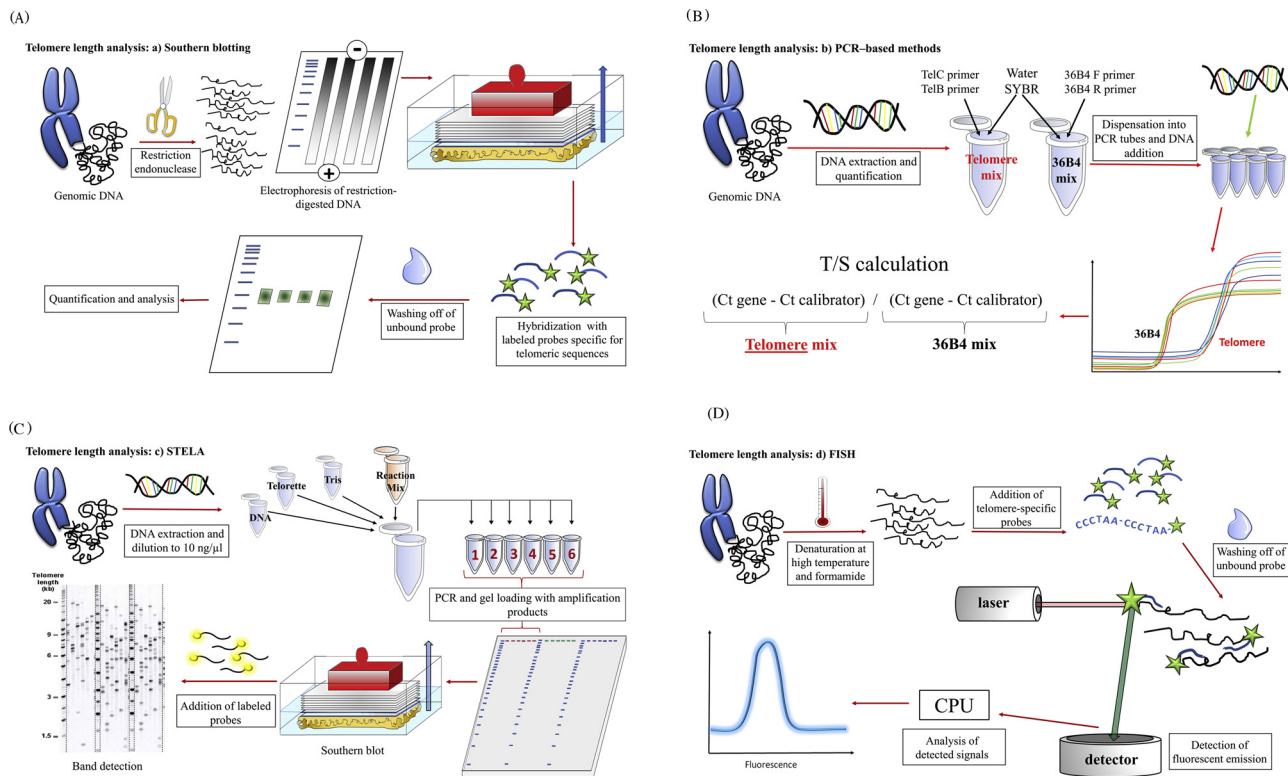
Fig. 2. Most commonly used techniques employed to measure TL.
Schematic representation of the most common techniques employed to measure TL: 2a) Southern blotting-RTF; 2b) PCR-based methods; 2c) STELA; 2d) FISH.

2018).

Growing evidence also suggests that the association of LTL to functional impairment, *i.e.* frailty, may be driven by the unfavorable effect of having short telomeres, rather than reflect a linear dose-response relationship. Short telomeres, rather than TL *per se*, may thus be an informative biomarker of aging and ARDs (Montiel Rojas et al., 2018; Haapanen et al., 2018). Several findings indicate that short telomeres precede the clinical manifestation of the most common ARDs, such as type 2 diabetes and atherosclerotic disease (Toupance et al., 2017).

Overall, even though the factors involved in TAR and the pleiotropic roles of telomeres are not entirely clear, TL is being widely used as a biomarker of the aging process, and intense effort is being devoted to translating TL values into information that can be employed in clinical practice (Hastings et al., 2017). However, translation from the bench to the beside is being hampered by a number of biological factors, including the dependence of TL on genetic, epigenetic, environmental and behavioral factors, as well as by technical aspects such as pre-analytical issues and poor standardization of TL measurement techniques (Danese and Lippi, 2018). With regard to the latter question, since current measurement methods have been developed for use in molecular biology laboratories, reliable and robust TL estimation requires a high level of technical understanding and competence. Since researchers involved in areas other than cell biology, including physiology, psychology, evolution and ecology, have become interested in telomere biology and dynamics (Nussey et al., 2014; Conklin et al., 2018), we feel it is important for all those who work in these varied fields to become familiar with the most common TL measurement techniques and to be aware of their respective advantages and drawbacks.

4. Measurement of telomere length: analytical caveats

A variety of techniques are employed to measure TL; they include: i)

Southern blot analysis of terminal restriction fragments (TRFs), which measures the length distribution and average TL in biological samples; ii) fluorescence *in situ* hybridization (FISH), including Q-FISH and flow-FISH; iii) polymerase chain reaction (PCR)-based methods like quantitative (q)PCR, Single TElomere Length Analysis (STELA), and Telomere Shortest Length Assay (TeSLA); and iv) whole genome sequencing (WGS)-based techniques.

Although Southern blotting is the gold standard technique for TL measurement, the methods used most frequently in clinical and epidemiological studies are qPCR and FISH. Since the correlations among Southern blotting, FISH, and qPCR data from different laboratories can show different strength, laboratory-specific internal validation is clearly essential (Khincha et al., 2017).

The most commonly used matrix for TL measurement is still venous blood, although less invasive DNA collection methods are increasingly used. However, too little is known about how TL values relate in different samples. A recent study of three matrices – whole venous blood, finger-prick dried blood spot (DBS) and saliva – has shown that DBS and saliva are viable alternatives to invasive venous blood draws (Stout et al., 2017). Notably, TL values were higher in saliva than in whole blood or DBS.

Notably, all TL measurement techniques have been developed at a time when telomeric sequences were believed to be measureable only in the nucleus of eukaryotic cells. Now that TL has been found to provide much more complex biological information, it would be useful to distinguish between TL measured in the nucleus and in the other intra- and extracellular compartments. The difficulty of applying some of the techniques devised for the nucleus to sequences found in extra-chromosomal compartments suggests the need for novel technical approaches.

Since all TL measurement methods suffer from considerable weaknesses, several analytical caveats must be resolved before they can be put to routine use (Tarik et al., 2018; Lai et al., 2017, 2018).

The most commonly used methods and their technical drawbacks

are briefly reviewed below and depicted in Fig. 2 (**2a,** Southern blotting- TRF; **2b,** PCR-based methods; **2c,** STELA; **2d** FISH).

4.1. Terminal restriction fragment (TRF) technique

This is a modified Southern blotting approach that measures the TL range in a cell population using the TRF length distribution expressed in kilobases (Fig. 2a) (Harley et al., 1990; Ouellette et al., 2000). It is one of the earliest TL assessment tools and has become the gold standard in telomere biology. DNA is extracted, digested, resolved by gel electrophoresis, transferred to a membrane, hybridized with labeled probes, and quantified. Though precise and highly accurate, it requires a considerable amount of intact genomic DNA and provides only an average TL for a population of cells (Kimura et al., 2010). The use of this time-consuming, expensive, and labor-intensive technique, which also requires high DNA concentrations, is therefore generally limited to studies involving limited number of samples. Southern blot analysis has recently been proposed to monitor the addition of telomeric sequences to single, newly generated telomeres *in vivo* (Bonetti and Longhese, 2018).

4.2. qPCR technique

qPCR is widely used in epidemiological studies, because it quickly provides mean relative TL (RTL) and requires small amounts of DNA (about 20 ng/reaction) (Fig. 2b). Introduced by Cawthon (2009), it achieves telomeric DNA detection through fluorescent signals (T) using partially mismatched primers. Telomeric DNA is normalized to a single-copy housekeeping gene (S) amplified in the same sample, and the T/S ratio is computed as a measure of RTL. A successive, improved version, Monochrome Multiplex Real-Time PCR (MMQPCR), requires a smaller amount of DNA. Amplification of both telomeric DNA and the single-copy gene in the same well of a plate reduce variability compared with monoplex PCR. Since the use of single-copy genes does not ensure optimal data normalization in cancer DNA, new primer sets have been developed to obtain a more precise evaluation of RTL (Dahlgren et al., 2018).

The chief drawback of measuring TL by qPCR is primer design. The repetitive nature of telomeres involves that primers can crosslink, giving rise to dimers and non-specific PCR signal. The problem can be overcome using samples with a good initial amount of template, since low template concentrations may generate non-specific signal. However, intra- and intersample variability can be high, and the wide range of the coefficient of variation described by a number of studies suggests limited reproducibility (Martin-Ruiz et al., 2015). Moreover, certain methodological conditions are known to affect TL measurement. For instance, some PCR master mixes can influence result specificity and consistency (Jiménez and Forero, 2018). Given the availability of different PCR mixes, the presence of stabilizers for the newly synthesized double-stranded DNA should carefully be checked (Wang et al., 2004). Another limitation of qPCR is that it provides a relative value (RTL) *per* genome rather than an absolute value in kilobases. This is a problem, given the limited number of comparative studies that have been conducted to validate qPCR with the gold standard Southern blotting. Although significant positive correlations have been reported between TL measured by qPCR and Southern blotting, experimental discrepancies do impact TL analysis, requiring optimization of PCR conditions (Tarik et al., 2018). Notably, the difficulty of comparing RTL values entails that only trends can be compared between studies.

Despite these important caveats, TL measurement by PCR is the most widely used method in epidemiological studies, and blood and saliva are the most common matrices in studies of large numbers of samples. The Genetic Epidemiology Research on Adult Health and Aging (GERA) has analyzed TL in 110,266 DNA specimens extracted from saliva (Lapham et al., 2015) using a novel high-throughput robotic system for TL and informatics analysis. Samples were run in triplicate

along with control samples; within-sample variability was limited by employing thresholds to eliminate outlying measurements. Interestingly about 99% of samples passed all quality control measures. Another common matrix used for TL measurement by qPCR is leukocytes. LTL analyzed in 12,199 adults participating in two population-based prospective cohort studies in Europe (ESTHER) and the United States (Nurses' Health Study) was found to be associated to all-cause, cardiovascular disease (CVD), and cancer mortality (Mons et al., 2017).

Notably, DNA extraction methods have a pronounced influence on TL values, which in some circumstances can result in spurious or lost associations in epidemiological studies (Raschenberger et al., 2016). A recent meta-analysis of LTL and all-cause mortality suggests that the accuracy of the TL measurement technique used affects risk assessment (Wang et al., 2018b). Whereas qPCR provides reliable TL analysis in blood and saliva, this is not true of cancer cell DNA, because use of single-copy genes in conditions of genomic instability, which is typical of cancer cells, may affect the accuracy of normalization. Dedicated primer sets have recently been developed to achieve RTL measurement in cancer cells (Dahlgren et al., 2018).

The discovery of cf-DNA/RNA has raised the problem of detecting telomeric sequences in samples, such as microvesicles and exosomes, that contain very diluted template sequences, since in these cases qPCR efficiency may also be reduced. Moreover, no single-copy genes have yet been validated for cf-telomere estimation.

A more detailed description is required for STELA (Fig. 2c), which allows assessing the length of a chromosome subset, and TeSLA, which enables TL measurement in the subset of the shortest telomeres, *i.e.* those induced by sudden TS due not to cell replication but to breaks resulting from the action of stressors (Lai et al., 2017). TeSLA has been developed to overcome the problems posed by telomere repeat sequences (TRSs) in detecting abrupt TS in a single chromosome. STELA is labor-intensive and unsuitable for testing large numbers of samples. However, STELA data may have prognostic implications in the clinical assessment of disease cells, *e.g.* to predict clinical outcome in patients with chronic lymphocytic leukemia (Lin et al., 2014) or myelodysplastic syndrome (Williams et al., 2017).

4.3. Probe-based non-PCR methods

Probe-based TL assays, which involve the use of probes for telomeres (T) and a reference gene (R) for a given DNA sample, may provide a cost-effective approach to measure TL in extracted DNA samples (Kibriya et al., 2014). A novel, accurate, high-throughput, pooled-sample multiplex Luminex assay suitable for large-scale studies has recently been described (Jasmine et al., 2018).

4.4. Fluorescence in-situ hybridization (FISH) techniques: Q-FISH and flow-FISH

Q-FISH is a molecular cytogenetic method that can be employed to obtain information from metaphase or interphase cells, depending on the sequence of the fluorochrome-conjugated probe used. FISH methods can be used to measure TL in subsets of cells separated from fresh blood or from tissues (Fig. 2d) (Perner et al., 2003). Whereas the telomeres of each chromosome arm can provide heterogeneous staining results due to a different number of telomeric repeats, those found on the two sister chromatids generally display nearly identical intensities. The use of telomeric probes allows probe binding to its target to be identified by a distinct fluorescent signal within the cell nucleus. Synthetic DNA/RNA analogs capable of binding to DNA/RNA in a sequence-specific manner have been proved to yield more sensitive and specific TL measurements than DNA probes (Marchesini et al., 2016).

Since correct interpretation of the fluorescence signal requires a fluorescence microscope, FISH techniques require expensive equipment that may not be available at all laboratories.

Flow-FISH, first described in 1998 (Rufer et al., 1998), utilizes the

quantitative properties of telomere-specific probe retention to quantify median fluorescence in a population of cells *via* use of a flow cytometer instead of a fluorescence microscope. TL measurement by flow-FISH can have clinical relevance in specific clinical indications and selected settings, *e.g.* patients with mutations in some inherited genes (Alder et al., 2018). Flow-FISH has demonstrated excellent diagnostic sensitivity in measuring TL in patients with short telomere syndrome (STS). STSs are accelerated aging syndromes caused by heritable gene mutations which result in TS. For instance, RTL measurement by qPCR is not optimal to diagnose dyskeratosis congenital, an STS characterized by inherited bone marrow failure and cancer susceptibility caused by germline mutations in telomere biology genes (Gadalla et al., 2016); in these patients LTL analysis by flow-FISH is the recommended molecular diagnostic test (Gutierrez-Rodrigues et al., 2014). Flow-FISH can also be applied to measure TL in stored samples.

4.5. Whole genome sequence (WGS)-based technique

WGS-based TL measurement supplies reliable sequencing reads from telomeres (Castle et al., 2010; Parker et al., 2012). However, their standard alignment to the reference sequence provides limited information on the region of origin, due to the repetitive nature of telomeric regions and to the fact that in the human reference sequence the ends of most chromosomes are simply stretches of Ns, which stand for unknown nucleotides. Methods have been developed to measure average TL from whole genome or exome shotgun sequence data (Ding et al., 2014) and to provide simultaneous TL measurement and global transcriptome analysis in the same cell (Wang et al., 2017a). The chief challenge for using next-generation sequences (NGSs) to measure TL is the need for bioinformatics expertise and softwares to decipher massive datasets. Several bioinformatics tools that adopt different approaches to identify, quantify, and normalize telomeric reads – like Motif_counter, TelSeq, Computel, qMotif, and Telomerecat – have been designed to determine telomere content and TL from NGS data (Lee et al., 2017; Farmery et al., 2018). Direct comparison of these WGS-based telomere measurement tools has shown that their best motifs all yielded similar performances when used to measure telomere content (Lee et al., 2017). In contrast, calculations using the best motif for TelSeq and Computel, the two tools that produce a TL estimate, were significantly lower and did not correlate well with TL measurements by TRF analysis (Lee et al., 2017).

Other important factors that should be considered when comparing WGS-based telomere measurement techniques are tool accessibility, ease of tool use, the time required to analyze one sample, and multi-threading ability (Lee et al., 2017).

Telomere Dysfunction-Induced Foci (TIF) (Takai et al., 2003; de Lange, 2002; Karlseder et al., 1999) and Extrachromosomal DNA (Tokutake et al., 1998; Cohen and Méchali, 2002; Cesare and Griffith, 2004; Henson et al., 2009; Schvartzman et al., 2013; Komosa et al., 2015; Moye et al., 2015; Henson et al., 2017) analysis are not quantitative techniques and are not optimized for epidemiological studies. Separation of extrachromosomal DNA depends on sample preparation, DNA/RNA extraction procedures, and DNAse or RNase treatment, according to the compartment being assessed.

4.6. TL heterogeneity

TL heterogeneity has been detected in various cell types, including stem and cancer cells and can directly influence the frequency with which chromosomes undergo telomeric fusion and subsequent breakage-fusion-bridge cycles (Londoño-Vallejo, 2004). Single-cell analysis technology has recently been developed and effectively employed to investigate TL heterogeneity. Single-cell analysis of TL, *i.e.* STELA, where each amplicon is derived from a single telomeric molecule from a single cell, can disclose the full detail of TL distribution. Notably, STELA measures TL within the length ranges observed in

senescent cells (Garcia-Martin et al., 2017), providing a new tool to explore the relationship between TL and the aging process.

5. TERRA and aging

The role of TERRA has been an outstanding issue in telomere biology for the past decade, mainly due to lack of knowledge of its loci. New insights suggest that TERRA molecules can be transcribed from nearly all telomeres in mammalian cells, always in centromere to telomere direction; they also suggest the involvement of subtelomeric regions – transcriptionally active genomic regions that give rise to long non-coding RNAs whose size ranges from 100 to 9 kb according to the position of the transcription starting site (Diman and Decottignies, 2018). These transcripts often display a cap structure added at the 5′ end, and only 7% of these transcripts are polyadenylated (Oliva-Rico and Herrera, 2017).

Cf-TERRA sequences have also been detected in human blood and serum, especially as exosome-associated molecules: the secretory phenotype characterized by release of cf-TERRA has been called TASP (TERRA-associated secretory phenotype) (Wang et al., 2015). Since high TERRA levels may be detected in human tumor tissue, they may prove to be innovative cancer biomarkers (Arora et al., 2014).

Notably, TERRA forms RNA:DNA hybrids at the chromosome ends and can fold into G-quadruplexes (Balk et al., 2014). Experimental evidence has shown that TERRA can also form higher-order structures based on parallel G4 units (Martadinata et al., 2011).

A mounting number of human diseases are being associated to abnormal G4 RNA regulation, suggesting the potential relevance of G4s to human health. Recent work supports the notion that G4s in the promoter regions of oncogene and telomere DNA could be therapeutic targets in cancer patients (Kaulage et al., 2018).

5.1. Measurement of TERRA: analytical caveats

The major problem in TERRA measurement is that transcription can start from the subtelomeric regions of all chromosomes. A number of primers specific for different subtelomeric regions have been used, including primers matching the 1q, 2q, 3p, 7p, 10p, 10q, 12q 13q, 14q, 15q, 17p,17q, 18p, XqYq, and XpYp chromosome, (Feretzaki and Lingner, 2017; Wang et al., 2015). However, some loci seem to be more involved in TERRA transcription than others. Chromosomes 20q and Xp have been suggested to be the main TERRA loci in human cells (Montero et al., 2016).

The techniques used most commonly to quantify TERRA sequences are briefly described below and are depicted in Fig. 3 (**3a,** RT-PCR; **3b,** Northern blotting; **3c,** RNA dot blotting; and **3d,** G-quadruplex detection with specific antibodies).

5.1.1. RT-qPCR

RT-qPCR is currently the fastest and most practical quantitative analysis technique for TERRA measurement.

The initial reverse transcription that yields cDNA can require a different amount of starting RNA, depending on the sample (Feretzaki and Lingner, 2017). DNAse treatment is required after RNA extraction (Iglesias et al., 2011), to ensure the quality and concentration of the starting sample, which can greatly affect results. Contamination with salt, ethanol, or proteins can strongly influence the performance of the downstream application.

Reverse transcription primers can be five repetitions of the oligonucleotide CCCTAA, random hexamers, or different set of primers. Poly-T, which is frequently used for reverse transcription of mRNA, is unsuitable due to the lack of TERRA transcript polyadenylation. GAPDH, U6snRNA, 36B4, GUSB, actin, and 18S have been described as suitable reference genes.
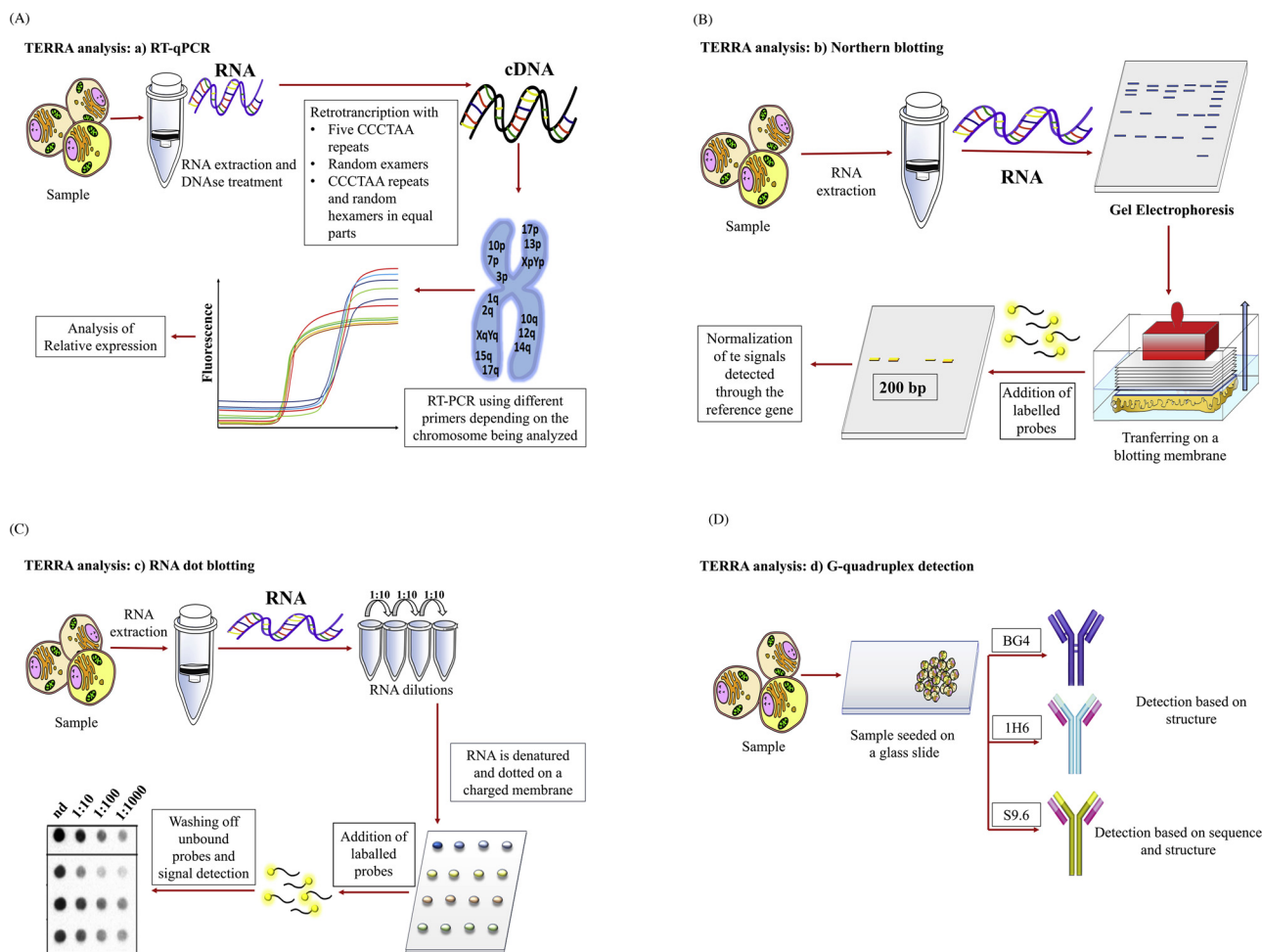
Fig. 3. Most commonly used techniques employed to quantify TERRA sequences.
Schematic representation of the three most common techniques employed to measure TERRA: 3a) RT-PCR; 3b) Northern blotting; 3c) RNA dot blotting (a simplification of Northern blotting that does not require gel electrophoresis); 3d) G-quadruplex detection with specific antibodies. G-quadruplex can be detected using engineered antibodies, such as clones 1H6 and BG4, which have specificity for the structure, or S9.6, which has specificity for structure and sequence.

5.1.2. Northern blotting

Northern blotting can detect the overall amount of TERRA transcripts, but unlike RT-qPCR it cannot measure minor changes in transcription or quantify TERRA levels in single chromosomes (Feretzaki and Lingner, 2017).

RNA extracted from samples is denatured and electrophoresed on agarose formamide gel, since the size of cf-TERRA is about 200 bp. Next, RNA can be transferred onto a blotting membrane and cross-linked to it using UV radiation. For RNA detection, the blot is hybridized using labeled probes specific for TERRA sense and antisense strands; 18S and U6 RNA have been used for normalization (Wang et al., 2015).

5.1.3. RNA dot blotting

RNA dot blotting is a simplification of Northern blotting. It does not require gel electrophoresis and it makes it possible to analyze different samples with different concentrations in a single test.

Extracted RNA is denatured using high temperatures or denaturing solutions, dotted on a charged nylon transfer membrane, and cross-linked to it by UV radiation. Subsequent steps involve a radiolabeled probe, washes in buffer to remove excess probe, and RNAse A treatment to eliminate single-strand RNA. The most common probes for TERRA detection are CCCTAA repeats labeled at their 5′ end with ^{32}P-γ-ATP by T4 polynucleotide kinase (Koskas et al., 2017).

5.1.4. RNA-FISH

RNA-FISH is used to analyze the cellular localization of TERRA by hybridizing detergent-extracted nuclei with a fluorescently labeled probe. It can even be used after immunofluorescence. Different probes, including C-rich peptidonucleic acid (PNA) coupled with a cyanine 3 fluorochrome, a fluorescently labeled probe containing CCCTAA repeats, or a light switching pyrene probe, can be used for hybridization to identify TERRA G4s in living cells (Koskas et al., 2017; Xu et al., 2010).

5.1.5. Detection of G-quadruplexes

G4s can be detected using engineered antibodies, such as clones 1H6 and BG4, which have specificity for the structure, not the sequence. These antibodies are used to detect the cellular localization of G4s by immunofluorescence. Since detection is based on structure, different types of G4s, *e.g.* DNA:RNA (hybrids), RNA-RNA, and DNA-DNA, can be identified.

Other critical aspects concern the labeling obtained with BG4 using different fixatives. Cytoplasmic TERRA is preferentially detected by fixation with PFA-Triton X-100, whereas nuclear quadruplexes (TERRA or DNA-DNA) can be detected by MeOH fixation (Laguerre et al., 2016). S9.6 is another monoclonal antibody with high affinity for DNA-RNA G4s formed at R-loops, because it is both structure- and sequence-specific. Maximum affinity is obtained with 52% of GC in the target sequence, whereas weak or no binding is obtained with amounts lower

than 25% or higher than 75% (König et al., 2017). Unfortunately, commercial kits including these antibodies are currently not available.

6. TA activity and aging

Telomerase is the only enzyme that can elongate a telomeric DNA chain to compensate for TS. It is different from other polymerases, because it involves a distinctive, reiterative reuse of an internal single-stranded telomeric template (Wu et al., 2017). Notably, the human TERT gene may be capable of autoregulation, because it is located very close to the telomere end of the chromosome, ~1.2 Mb from the 5p end.

Most somatic cells lack TA; exceptions include embryonic tissue, stem cells, reproductive organs, and some rapidly regenerating tissues. Since TA is seen in 80–90% of tumor cells, its value as a diagnostic/prognostic tumor marker has prompted the development of reliable and standardized assays. As noted above, in somatic cells TA usually declines after birth; the successive cell divisions gradually lead to TS and trigger cellular senescence (Kim and Shay, 2018).

Most studies have investigated cells that express high levels of TERT, such as immortalized and cancer cells. However, TA regulation is a dynamic process also in normal human cells, suggesting that active telomere maintenance is required for the proliferation of normal cells (Masutomi et al., 2003). However, the role of telomerase in normal senescent cells has not been analyzed in depth. Reduced TERT protein levels and reduced TA have been described in senescent primary cultures of adult human dermal fibroblasts (HDFs) (Yehuda et al., 2017).

Telomerase activation/replacement has potential in treating patients with telomere maintenance deficiency syndrome as well as in tissue engineering approaches designed to treat degenerative conditions that are associated to normal aging. Telomerase-deficient mice have been proposed as a model to study the adverse cellular and organismal consequences of widespread DNA damage signaling activation *in vivo*. Telomerase reactivation in such mice extends TL, reduces DNA damage signaling, and eliminates degenerative phenotypes in multiple organs (Jaskelioff et al., 2011). Conversely, clinical research work is focusing on telomerase inhibition therapies to treat tumors, which induce telomerase overexpression by overcoming the short telomere barrier to unrestricted proliferation (Fleisig and Wong, 2007). Since telomerase-complex components are upregulated in most tumor cells, TERT restriction is a potential therapeutic option (Kim et al., 1994). Given that most somatic cells show low TA, selective inactivation of telomerase expression in cancer cells fails to influence most normal cells, suggesting that telomerase is a good target for cancer therapy (Sprouse et al., 2012).

TA is also considered as a biomarker for cardiovascular aging and CVD. Recent studies suggest a link between statins and telomere biology that may be explained by the anti-inflammatory actions of statins (Strazhesko et al., 2016).

Overall, TL and TA regulation is a complex and dynamic process that is impaired in patients with ARDs.

A greater understanding of the mechanisms underpinning telomerase regulation and the development of reliable TA assessment technologies is essential to help research in therapeutic strategies for telomerase modulation. A number of TA determination techniques, including those devised most recently, are described below. However, not all of them are suitable for epidemiological and clinical studies.

6.1. TA measurement: analytical caveats

TA detection assays can be divided into two main groups: those based on direct detection of telomerase products and those based on different systems of product amplification (Skvortsov et al., 2011). New bioanalytical methods based on direct detection of telomerase products, such as PCR-free assays, isothermal amplification, and Single Molecule Stochastic Binding assay, have recently been applied to TA detection not only in cells and tissues, but also in body fluids (Zhang et al., 2017a,

2017b; Su et al., 2017).

Multiple approaches have also been proposed to assess telomerase gene activity, including engagement of TERT alternative splicing, TERT gene amplification, and epigenetic changes (reviewed in Shay, 2016). Interestingly, some human TERT mutations/deletions have been associated to premature aging diseases, and patients carrying mutations in genes crucial for telomere maintenance show accelerated aging phenotypes (Chu et al., 2016). Recently, alterations in the gene encoding human TERT have been identified as points of interest for elucidating the oncogenic mechanism of several different cancer types (Bollam et al., 2018).

6.2. TA determination assays based on direct detection of telomerase products

6.2.1. TA detection using direct incorporation of a radioactively labeled substrate

The earliest TA detection method was based on the use of radioactive labeling without additional amplification (Blackburn et al., 1989). The method is still employed for qualitative determination of TA in cell line extracts. Since radioactive substances are complex and dangerous to use, new methods that do not use radioactive substances have been developed. Some of these approaches are briefly described in Table 1a.

6.3. TA detection assays based on telomerase product amplification

6.3.1. Telomere repeat amplification protocol (TRAP)

The Telomere Repeat Amplification Protocol (TRAP) is a widely used assay to determine TA in mammalian cells, tissues, and other biological samples (Kim et al., 1994). It involves three steps: extension, amplification, and detection of telomerase products. In the extension step, telomeric repeats are added to the telomerase substrate. In the amplification step, the extension products are amplified by PCR using specific primers (Wege et al., 2003). In the detection step, TA is estimated by electrophoretic analysis of the extension products. However, since amplification is often associated to poor reproducibility and high background, it is unsuitable for diagnostic applications. The main analytical challenges include throughput, the replacement of radioactive labels with non-labeled compounds, the reduction of the amount of side product, the elimination of primer-dimer artifacts and of false-positive amplification products, and the reduction of intra- and inter-sample variation (Wu et al., 2000; Skvortsov et al., 2011). Techniques employed to quantify telomerase activity (TA) were depicted in Fig. 4.

The main changes made to the basic TRAP protocol are summarized in Table 1b.

7. Biological variables related to TL, TERRA, and TA

Although TL is the area characterized by the largest number of applications, it is likely that similar biological, disease-mediated processes will be found to be relevant to TERRA and TA, which are interconnected.

Age, gender, and ethnicity have been found to be significantly associated to TL; for instance, the female gender and an African or Hispanic origin have been associated to a predisposition to have longer telomeres compared to the male gender and a European origin (Gardner et al., 2014; Hansen et al., 2016). Significant but weak correlations have also been described between LTL and hematological parameters (Meyer et al., 2016). A number of biomarkers related to a variety of physiological processes are also strongly associated to accelerated TS; however, the complex relationships between TL and the other chemical and clinical biomarkers are only beginning to be understood (Barrett et al., 2015).

The significant associations between inflammaging and telomere attrition, reported by several studies, suggest that TS is related to an

Table 1a

Some of the most relevant modification of TA detection assays based on direct detection of telomerase products.

Modifications of TA detection assays based on direct detection of telomerase products	Brief description of the protocol	References
Surface Plasmon Resonance (SPR)	Surface Plasmon Resonance (SPR) can be applied to measure small local changes in refractive index on metal layers, linked directly to alterations in concentration on the surface. Biotin-conjugated oligonucleotides containing telomeric repeats can be immobilized on the surface of a sensor pretreated with streptavidin (). The oligomers associated with the telomerase extracts can be elongated and TA can be calculated by measuring the SPR signals. The main limiting factors are reaction time and sample concentration.	Maesawa et al., 2003
Detection of telomerase activity using oligo-modified magnetic particles and nuclear magnetic resonance (NMR)	Another physical phenomenon employed for TA detection is nuclear magnetic resonance (NMR). Through a complementary interaction, the magnetic particles bind the telomeric sequences synthesized by telomerase. The spin-spin relaxation time is measured by a relaxometer. Since the formation of an organized nanoparticle ensemble involves a change in the magnetic relaxation time of surrounding water molecules, the magnetic field increases in presence of nanoparticle ensembles and decreases with non-ordered ones. Since the change reaches half of the maximum after 30 seconds and plateaus after 40-60 minutes, the analysis is fast, sensitive, and high-throughput.	Grimm et al., 2004
Quartz crystal microbalance technique (QCM)	This highly sensitive method involves microgravimetric analysis of TA based on the piezoelectric effect of quartz. The application of an alternating current promotes the oscillation of a quartz crystal, whose resonance frequency is then determined. Ligands on the crystal surface in a liquid environment can induce a reduction in resonance frequency. Telomerase induces oligonucleotide binding to the sensor's surface.	Pavlov et al., 2004.
Biobarcode assay	This approach uses magnetic particles, *i.e.* gold spheres, and two types of oligonucleotides, complementary and non complementary to telomerase-synthesized DNA. Binding of the electroactive complex $[Ru(NH_3)_6]^{3+}$ to the non-complementary telomerase-synthesized DNA chain permits quantitative detection. The method can measure TA in cell line extracts but is not used in tissues.	Li et al., 2010; Skvortsov et al., 2011
Optical biosensor assay	The assay is based on the change in the refraction index induced by the amount of telomerase products detected on the surface of the optical biosensor in real time. A three-oligonucleotide system, *i.e.* a "cassette system" including a sequence complementary to the RNA template of telomerase modifies the sensor surface to avoid steric impediments and to ensure process reversibility.	Buckle et al., 1996; Schmidt et al., 2002; Kulla and Katz, 2008
Quantum dots	Nanoparticles are conductor or semiconductor particles that represent quantum dots (QDs) in quantitative TA detection. Similar to the way a photon can be emitted during the transition of an atom between energy levels, a photon can be emitted during a transition in a quantum blot. In this system, photon absorption and emission occur at specific wavelengths that are related to QD size (smaller nanoparticles correspond to higher wavelengths). A modification involving a thio group at the end of the telomere oligonucleotide bound to the QD makes it capable of fluorescence when it absorbs a quantum with a wavelength of 400 nm and emits a quantum with wavelength of 560 nm. When a modified fluorescent oligonucleotide, TR-dUTP, is incorporated into telomerase DNA products bound to the QD, a fluorescence energy transfer occurs with a higher wavelength (610 nm). This method is not recommended for clinical materials.	Patolsky et al., 2003; Zavari-Nematabad et al., 2017; Li et al., 2018a, 2018b
Graphene oxide (GO)-based fluorescent nanosensor	A fluorescent DNA is adsorbed on a GO surface that can bind dye-labeled single-stranded DNA (ssDNA) complementary to the telomeric repeated sequence and efficiently quench the fluorescence of the dye *via* fluorescence resonance energy transfer (FRET). It is a rapid, sensitive and specific approach to detect telomerase activity.	Zhang et al., 2018

Brief description of NMR, SPR, QCM, Biobarcode assay, Optical biosensor assay, Quantum dots, Graphene oxide (GO)-based fluorescent nanosensor protocols.

enhanced susceptibility to the development and progression of ARDs, such as type 2 diabetes, CVD, and cancer (Bonfigli et al., 2016; Testa et al., 2011; Wang et al., 2016; Jose et al., 2017). With regard to cancer, long telomeres have been associated to an increased risk of several cancers; however, emerging data suggest that short telomeres might predict poor survival in cancer patients (Zhang et al., 2015; Rachakonda et al., 2018). Association studies of TL and cancer have identified significant, but not clinically relevant, differences in TL between cases and controls (Savage, 2018). A recent meta-analysis has highlighted that the inconsistent effect of TL on cancer outcomes may be due to different measurement methods (Adam et al., 2017; Wang et al., 2017b). Therefore, standardization of TL measurement and reporting has the potential to enhance the prognostic value of TL in human diseases.

A significant relationship, reported among exposure to factors promoting inflammation or oxidative stress (smoking) and shorter telomeres (Astuti et al., 2017), has been confirmed in the offspring of smoking mothers (Oerther and Lorenz, 2018). A recently described association between accelerated telomere attrition and marked weight gain in middle life suggests the importance of lifetime weight management to preserve functional telomeres (Hang et al., 2018). Nonetheless, the inconsistent effects of weight loss on TL and DNA repair indicate that interventions and assays should be reassessed (Himbert et al., 2017).

Different age-related telomere attrition trajectories and circulating inflammatory cytokine levels have been described in aging individuals (Lustig et al., 2017). This is not unexpected, since a number of stressors, including infectious agents, microbiota composition, cellular senescence, and misplaced nucleic acids (DNA/RNA), can promote TS in immune cells as well as in other somatic cells, fueling inflammation. These stressors are so closely interconnected that the respective effects are difficult to unravel. This could be one of the weakness of the studies exploring the relationship linking stressors, inflammaging, and TL: only the integrated analysis of a number of components in the same

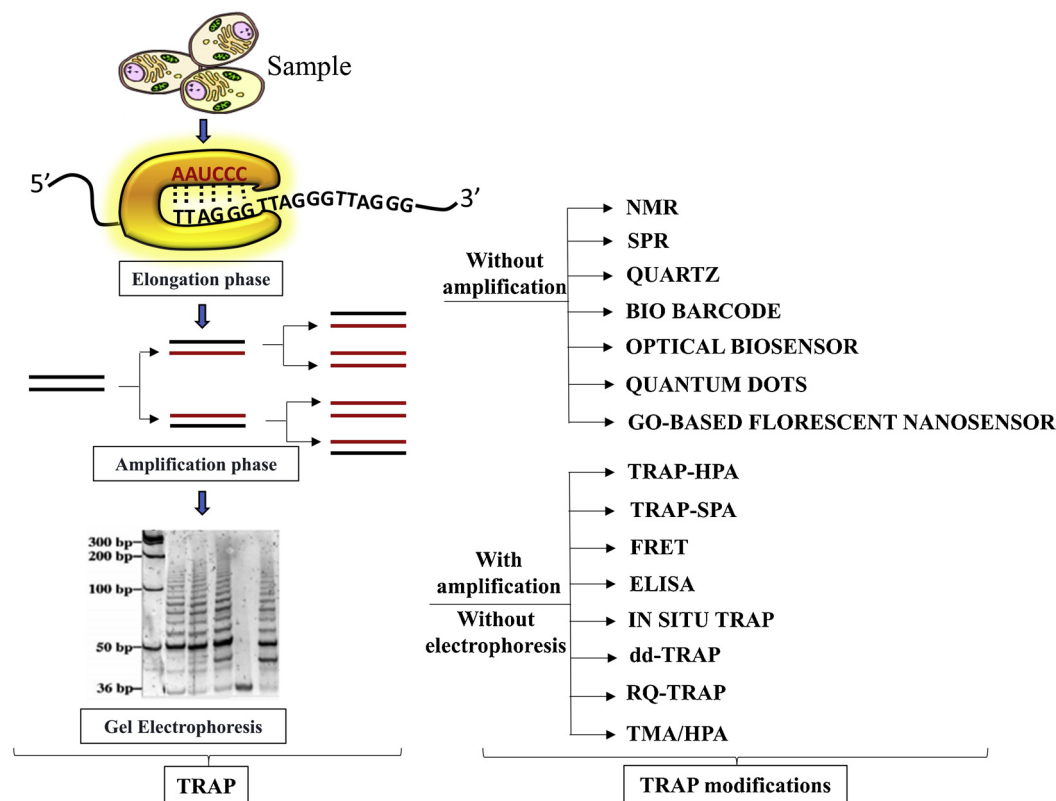## Techniques employed to quantify telomerase activity (TA)

Fig. 4. Techniques employed to quantify telomerase activity (TA).
Schematic representation of the most common techniques employed to measure TA. The methods are grouped into two major categories: those based on direct detection of telomerase products and those based on different systems of amplification of these products (TRAP-based methods).

subjects/patients could clarify the issue. Moreover, the complex signaling affecting telomere balance during life requires multivariate analysis approaches to test for associations between TL and multiple biological variables; bias should be minimized especially in association studies involving TL and ARDs and TL and psychological and bio-behavioral variables.

TL measurement is also a useful approach to evaluate the pathogenicity of the genetic variants associated to telomere-related disorders. STSs are often caused by heritable gene mutations that result in decreased TL (Norberg et al., 2018). Their diverse clinical presentation – like bone marrow failure and idiopathic pulmonary fibrosis associated to gene mutations involving TERT, TERC, and other genes – make STSs a diagnostic challenge (Mangaonkar and Patnaik, 2018). Large-scale molecular epidemiological studies have uncovered novel associations between ARDs such as CVD, cancer, and impaired mental health, and both TL and common genetic variants in telomere biology genes (Savage, 2018).

Finally, it is conceivable that RNA-dependent factors will constitute additional biological variables for TERRA and TA measurement, both of which are RNA-dependent.

Advantages and disadvantages (sensitivity, specificity, number of samples that can be managed, ease to use and suitability for clinical studies) are reported in Table 2 for telomere length (TL), telomeric repeat-containing RNA (TERRA) and telomerase activity (TA) measurement techniques.

8. Conclusion

The outstanding challenge in telomere research is the development of accurate and reliable measurement methods ensuring simple and sensitive TL, TERRA, and TA detection. Reaching these goals requires

guidelines for the development of standardized and automated measurement procedures. Studies of the reproducibility, accuracy, reliability, and sensitivity of the different TL, TERRA, and TA measurement methods at independent laboratories should be encouraged. Bench to bedside translation of biological metrics related to the telomere world requires the establishment of normal range values as well as critical values for interpretation. This is essential not only in studies of individual molecules, but also to shed light on the associations of TL, TERRA, and TA with physiological, psychological, and bio-behavioral phenomena and human pathological conditions. These tasks are complex and the data provided by the latest studies are not always clear and conclusive. For these reasons TL, TERRA, and TA are still not included in everyday clinical practice. Nevertheless, considerable progress has been made, and researchers are increasingly close to finding the solutions for better and faster measurement. Importantly, researchers undertaking the study of telomeres should be aware of the methodological problems involved in TL, TERRA, and TA analysis. Careful consideration is warranted when selecting measurement methods for research or clinical studies.

Notably, most of the sample material used for epidemiological studies is extracted banked DNA and/or RNA. Since the results of TL and TERRA measurement are affected by extraction methods and degradation, sample quality checks are critical for correct measurement and data interpretation.

Furthermore, RNA species detection in cells depends on metabolic activity, and although it may not be detectable in resting blood, it may be detected in tumor samples.

What is essential for future studies of the "telomere world" is that researchers publish full details of their methods and the quality control thresholds they employ. Notably, it is critical to be familiar with the relationships between telomeres and a number of other variables if

Table 1b

Some of the most relevant modifications made to the basic TRAP protocol.

Modifications of TRAP protocol	Brief description of the protocol	References
*TRAP with a post-PCR hybridization protection protocol (**TRAP-HPA**)*	TRAP-HPA uses a probe labeled with covalently bound chemiluminescent acridine to detect DNA after amplification and provides high-throughput semi-quantitative determination of TA.	Hirose et al., 1997; Fajkus, 2006
*Scintillation proximity assay (**TRAP-SPA**)*	TRAP-SPA enables detection of amplification products thought the conjugation of telomerase products with biotin and amplification in presence of [3 H] TTP. Semi-quantitative determination can be obtained in large series of tissue and cell line extracts. The main drawbacks are the use of tritium and PCR artifacts.	Savoysky et al., 1996; Fajkus,2006
*TRAP with Fluorescence Resonance Energy Transfer (**FRET**)*	FRET uses two primers (amplifluors) whose hairpin structure contains a donor (fluorescein) and an acceptor (4'-dimethylaminophenyl-azobenzoic acid. Its main advantages include the absence of radioisotopes, the limited volume of the elongation products, the elimination of post-PCR processing, the reduction of carryover contamination risk, and fast analysis.	Uehara et al., 1999; Ding et al., 2010; Kawamura et al., 2014; Fajkus,2006
*TRAP combined with Enzyme-Linked Immunosorbent Assay (**ELISA**)*	TRAP-ELISA is a colorimetric qualitative and semi-quantitative assay, where biotin conjugation of telomere-imitating oligonucleotide (TS) primers permits binding of amplified DNA to streptavidin-coated microplates. This step is followed by DNA denaturation and hybridization with digoxigenin (DIG)-labeled probes specific for telomeric sequences. The addition of polyclonal DIG antibodies conjugated to horseradish peroxidase prompts the colorimetric reaction and enables TA detection. Some commercial kits include positive and negative internal standards. Since TRAP-ELISA is fast and allows analyzing multiple samples in a single run, it is the most commonly used assay for TA determination in screening studies.	Fajkus, 2006; Wu et al., 2000; Sue et al., 2014
***In situ* TRAP**	In *in situ* TRAP the cell suspensions are immobilized on silane-coated slides. PCR commonly uses FITC-labeled primers, and the final analysis is made under a fluorescence microscope. Fluorescence intensity and localization are employed to determine TA in individual cells (cancer cells usually show bright fluorescence). *In situ* TRAP can also be used to obtain a semi-quantitative determination of TA in tissue sections.	Skvortsov et al., 2011; Fajkus, 2006
*Droplet Digital Telomere Repeat Amplification Protocol (**ddTRAP**)*	This is a two-step assay where cell lysates are analyzed by droplet digital PCR (ddPCR). It involves the same steps as a conventional TRAP assay, except that the PCR products are detected by ddPCR. This system has improved the throughput, sensitivity, and reproducibility of the TRAP assay. As a consequence, it can test a variety of cell types, including cell lines and primary adult human cells, without radioactive compounds but with comparable sensitivity.	Ludlow et al., 2018; Fajkus, 2006
*Real-time Quantitative TRAP (**RQ-TRAP**)*	Real-time Quantitative TRAP (RQ-TRAP) uses fluorescent dyes (*e.g.* PicoGreen or SYBR Green) to quantify double-stranded DNA products in the PCR elongation and amplification steps. Its main advantage is that TA quantification is achieved without any additional time-consuming steps besides sample extraction and real-time cycling. The assay provides accurate TA measurement, hence highly effective TA monitoring in cultured cells, and can be used to analyze multiple samples. Its main disadvantages are the inhibitory effects of PCR contaminants, the possibility that PCR reaction saturation in the final step may level small TA differences compared to the results of conventional TRAP, and the risk of false-positive signals.	Wege et al., 2003; Gelmini et al., 1998; Hou et al., 2001; Saldanha et al., 2003; Hou et al., 2001; Skvortsov et al., 2011; Fajkus, 2006
*TRAP with isothermic transcription-mediated amplification (**TMA/HPA**)*	This approach provides a semi-quantitative determination of TA based on the presence of a polymerase that uses synthesized DNA as a matrix for RNA synthesis. Telomerase-synthesized DNA contains an additional sequence acting as a substrate for reverse primer hybridization. This tecnique also avoids the necessity of performing and evaluating polyacrylamide gel electrophoresis of reaction products and it is characterized by high sensitivity (1-1000 cells). Its main advantage is that it does not require sample heating. The assay is sensitive to the presence of RNase.	Saldanha et al., 2003; Skvortsov et al., 2011

Brief description of TRAP HPA, TRAP-SPA, FRET, ELISA, *in situ* TRAP, ddTRAP, RQ-TRAP and TMA/HPA protocols.

errors generated by confounding variables that are not controlled for are to be avoided.

Starting from the most recent evidence in telomere biology, we hypothesize that combined TL, TERRA, and TA analysis may provide highly reliable information to estimate the rate of cell, tissue and organismal aging and the risk of ARD development (Kim and Shay, 2018). TL, TERRA, and TA have been associated singly to aging and a number of common ARDs, yet no studies have evaluated them in an integrated way, either using cellular or organismal models.

Although red blood cells and platelets are a significant source of exosomes from blood, different cell types can release exosomes into human plasma/serum, including endothelial cells, monocytes and astrocytes (Goetzl et al., 2017; Goetzl et al., 2016; Halim et al., 2016).

Plasma exosomes released by endothelial cells and monocytes should be extensively investigated for telomeres and TERRA content, especially in patients with ARDs.

9. Future perspective

A new geriatric medicine branch, geroscience, postulates that it should be possible to delay the aging process and the onset of the most common chronic ARDs (Vaiserman and Lushchak, 2017), and mounting evidence suggests that the human healthspan could be increased by nutraceutical or pharmaceuticals approaches (Gurău et al., 2018; Klimova et al., 2018). The hypothesis has prompted the organization of geroscience-guided therapeutic trials, *e.g.* TAME (Targeting Aging with

Table 2

Advantages and disadvantages of the most common TL, TERRA, and TA measurement techniques.

	Tecnique	Time efficient	Sensitivity	Specificity	Reproducibility	Easy to use	Suited for clinical studies	References
TL	STELA/TeSLA	No	High	High	High	No	No	Lai et al., 2018; Martin-Ruiz et al., 2015.
	(q)PCR	Yes	Low	Intermediate	Intermediate	Yes	Yes	Gutierrez-Rodrigues et al., 2014; Martin-Ruiz et al., 2015.
	Southern blot	No	Intermediate	High	High	Yes	No	Tarik et al., 2018; Martin-Ruiz et al., 2015.
	FISH-qFISH-Flow	No	Intermediate	Intermediate	Intermediate	Yes	No	Baerlocher et al., 2002
	FISH	Yes	High	High	High	Yes	Yes	Gutierrez-Rodrigues et al., 2014
	WGS	No	High	High	High	No	Yes	Lee et al., 2017
TERRA	RT-qPCR	Yes	High	Intermediate	–	Yes	Yes	Feretzaki and Lingner, 2017
	Northern Blot	No	Low	High	–	Yes	No	Feretzaki and Lingner, 2017
	RNA dot blotting	Yes	Low	High	–	Yes	No	Koskas et al., 2017
	RNA-FISH	Yes	High	Intermediate	–	Yes	No	Koskas et al., 2017; Xu et al., 2010
TA	Classic	No	Intermediate	Intermediate	Low	Yes	No	Ohuchida et al., 2005; Fajkus, 2006
	HPA	No	Intermediate	Intermediate	Low	Yes	No	Hirose et al., 1997; Fajkus, 2006
	SPA	No	Intermediate	Intermediate	Low	No	No	Savoysky et al., 1996; Fajkus,2006
		Yes	Intermediate	Intermediate	Intermediate	Yes	Yes	Uehara et al., 1999; Ding et al., 2010; Kawamura et al., 2014; Fajkus,2006
		Yes	High	High	Intermediate	Yes	Yes	Wu et al., 2000; Sue et al., 2014; Fajkus, 2006
		Yes	High	High	Intermediate	Yes	No	Skvortsov et al., 2011; Fajkus, 2006
		Yes	High	High	High	Yes	Yes	Ludlow et al., 2018; Fajkus, 2006
		Yes	High	Intermediate	High	Yes	Yes	Wege et al., 2003; Gelmini et al., 1998; Hou et al., 2001; Saldanha et al., 2003; Hou et al., 2001; Skvortsov et al., 2011; Fajkus, 2006
		Yes	High	High	–	Yes	No	Saldanha et al., 2003; Skvortsov et al., 2011
	SPR	Yes	Intermediate	Intermediate	High	Yes	No	Maesawa et al., 2003
	NMR	Yes	High	Intermediate	High	No	No	Grimm et al., 2004.
	QCM	Yes	High	Intermediate	High	No	No	Pavlov et al., 2004.
	Biobarcode	No	High	High	Intermediate	Yes	No	Li et al., 2010; Skvortsov et al., 2011
	Optical biosensor	Yes	High	High	High	Yes	No	Buckle et al., 1996; Schmidt et al., 2002; Kulla and Katz, 2008
	Quantum dots	No	High	High	–	Yes	No	Patolsky et al., 2003; Zavari-Nematabad et al., 2017; Li et al., 2018a, 2018b
	GO-based fluorescent nanosensor	Yes	High	High	–	Yes	Yes	Zhang et al., 2018

Advantages and disadvantages (sensitivity, specificity, number of samples that can be managed and ease to use) are reported for telomere length (TL), telomeric repeat-containing RNA (TERRA), and telomerase activity (TA) measurement techniques.

-Not yet addressed.

MEtformin) (Justice et al., 2018). However, ongoing studies highlight the scarcity of well-vetted "rate of aging" biomarkers for human studies and the need for such biomarkers to move from the assessment of chronological age to the evaluation of physiological age (Kohanski et al., 2016; Sierra and Kohanski, 2017).

Cutting-edge technologies for TL, TERRA, and TA measurement are still in their infancy, but they promise great future discoveries through method improvements and the multiplication of laboratories offering them. Technological advances are expected to provide fast, automated, and standardized measurement of TL, TERRA, and TA in the same sample not only in cells and tissues, but in all biological fluids and circulating vesicles. These new technologies are expected to provide more concordant data in association studies both with regard to aging *per se* and to a number of ARDs.

Conflicts of interest

None.

Authors' contributions

Emanuela Mensà, Silvia Latini, Deborah Ramini and Gianluca Storci wrote the paper, which was revised by Massimiliano Bonafè and Fabiola Olivieri.

Acknowledgment

References

Adam, R., Díez-González, L., Ocaña, A., Šeruga, B., Amir, E., Templeton, A.J., 2017. Prognostic role of telomere length in malignancies: a meta-analysis and meta-regression. Exp. Mol. Pathol. 102, 455–474. https://doi.org/10.1016/j.yexmp.2017.05.010.

Alder, J.K., Hanumanthu, V.S., Strong, M.A., DeZern, A.E., Stanley, S.E., Takemoto, C.M., Danilova, L., Applegate, C.D., Bolton, S.G., Mohr, D.W., Brodsky, R.A., Casella, J.F., Greider, C.W., Jackson, J.B., Armanios, M., 2018. Diagnostic utility of telomere length testing in a hospital-based setting. Proc. Natl. Acad. Sci. U. S. A. 115, E2358–E2365. https://doi.org/10.1073/pnas.1720427115.

Arora, R., Lee, Y., Wischnewski, H., Brun, C.M., Schwarz, T., Azzalin, C.M., 2014. RNaseH1 regulates TERRA-telomeric DNA hybrids and telomere maintenance in ALT tumour cells. Nat. Commun. 21, 5–5220.

Astuti, Y., Wardhana, A., Watkins, J., Wulaningsih, W., PILAR Research Network, 2017. Cigarette smoking and telomere length: a systematic review of 84 studies and meta-analysis. Environ. Res. 158, 480–489.

Baerlocher, G.M., Mak, J., Tien, T., Lansdorp, P.M., 2002. Telomere length measurement by fluorescence in situ hybridization and flow cytometry: tips and pitfalls. Cytometry 47, 89–99.

Balk, B., Dees, M., Bender, K., Luke, B., 2014. The differential processing of telomeres in response to increased telomeric transcription and RNA-DNA hybrid accumulation. RNA Biol. 11, 95–100.

Barrett, J.H., Iles, M.M., Dunning, A.M., Pooley, K.A., 2015. Telomere length and common disease: study design and analytical challenges. Hum. Genet. 134, 679–689.

Belsky, D.W., Caspi, A., Houts, R., Cohen, H.J., Corcoran, D.L., Danese, A., Harrington, H., Israel, S., Levine, M.E., Schaefer, J.D., Sugden, K., Williams, B., Yashin, A.I., Poulton, R., Moffitt, T.E., 2015. Quantification of biological aging in young adults. Proc. Natl. Acad. Sci. U. S. A. 112, E4104–10. https://doi.org/10.1073/pnas.1506264112.

Belsky, D.W., Moffitt, T.E., Cohen, A.A., Corcoran, D.L., Levine, M.E., Prinz, J.A., Schaefer, J., Sugden, K., Williams, B., Poulton, R., Caspi, A., 2018. Eleven telomere, epigenetic clock, and biomarker-composite quantifications of biological aging: do they measure the same thing? Am. J. Epidemiol. 187, 1220–1230.

Blackburn, E.H., 1990. Telomeres: structure and synthesis. J. Biol. Chem. 265,

5919–5921.

Blackburn, E.H., 2005. Telomeres and telomerase: their mechanisms of action and the effects of altering their functions. FEBS Lett. 579, 859–862.

Blackburn, E.H., Greider, C.W., Henderson, E., Lee, M.S., Shampay, J., Shippen-Lentz, D., 1989. Recognition and elongation of telomeres by telomerase. Genome 31, 553–560.

Blackburn, E.H., Epel, E.S., Lin, J., 2015. Human telomere biology: a contributory and interactive factor in aging, disease risks, and protection. Science 350, 1193–1198.

Blasco, M.A., Gasser, S.M., Lingner, J., 1999. Telomeres and telomerase. Genes Dev. 13, 2353–2359.

Bollam, S.R., Berens, M.E., Dhruv, H.D., 2018. When the ends are really the beginnings: targeting telomerase for treatment of GBM. Curr. Neurol. Neurosci. Rep. 18, 15.

Bonetti, D., Longhese, M.P., 2018. Analysis of de novo telomere addition by southern blot. Methods Mol. Biol. 1672, 363–373.

Bonfigli, A.R., Spazzafumo, L., Prattichizzo, F., Bonafè, M., Mensà, E., Micolucci, L., Giuliani, A., Fabbietti, P., Testa, R., Boemi, M., Lattanzio, F., Olivieri, F., 2016. Leukocyte telomere length and mortality risk in patients with type 2 diabetes. Oncotarget 7, 50835–50844. https://doi.org/10.18632/oncotarget.10615.

Brown, L., Zhang, Y., Mitchel, C., Ailshire, J., 2018. Does telomere length indicate biological, physical and cognitive health among older adults? Evidence from the health and retirement study. J. Gerontol. A Biol. Sci. Med. Sci. https://doi.org/10.1093/gerona/gly001.

Buckle, M., Williams, R.M., Negroni, M., Buc, H., 1996. Real time measurements of elongation by a reverse transcriptase using surface plasmon resonance. Proc. Natl. Acad. Sci. U. S. A. 93, 889–894.

Byrd, A.K., Zybailov, B.L., Maddukuri, L., Gao, J., Marecki, J.C., Jaiswal, M., Bell, M.R., Griffin, W.C., Reed, M.R., Chib, S., Mackintosh, S.G., MacNicol, A.M., Baldini, G., Eoff, R.L., Raney, K.D., 2016. Evidence that G-quadruplex DNA accumulates in the cytoplasm and participates in stress granule assembly in response to oxidative stress. J. Biol. Chem. 291, 18041–18057.

Cammas, A., Millevoi, S., 2017. RNA G-quadruplexes: emerging mechanisms in disease. Nucleic Acids Res. 45, 1584–1595.

Castle, J.C., Biery, M., Bouzek, H., Xie, T., Chen, R., Misura, K., Jackson, S., Armour, C.D., Johnson, J.M., Rohl, C.A., Raymond, C.K., 2010. DNA copy number, including telomeres and mitochondria, assayed using next-generation sequencing. BMC Genomics 11, 244.

Cawthon, R.M., 2009. Telomere length measurement by a novel monochrome multiplex quantitative PCR method. Nucleic Acids Res. 37, e21.

Cesare, A.J., Griffith, J.D., 2004. Telomeric DNA in ALT cells is characterized by free telomeric circles and heterogeneous t-loops. Mol. Cell. Biol. 24, 9948–9957.

Chen, W., Kimura, M., Kim, S., Cao, X., Srinivasan, S.R., Berenson, G.S., 2011. Longitudinal versus cross-sectional evaluations of leukocyte telomere length dynamics: age-dependent telomere shortening is the rule. J. Gerontol. A Biol. Sci. Med. Sci. 66, 312–319.

Chiang, Y.J., Calado, R.T., Hathcock, K.S., Lansdorp, P.M., Young, N.S., Hodes, R.J., 2010. Telomere length is inherited with resetting of the telomere set-point. Proc. Natl. Acad. Sci. U. S. A. 107, 10148–10153.

Chu, T.W., MacNeil, D.E., Autexier, C., 2016. Multiple mechanisms contribute to the cell growth defects imparted by human telomerase insertion in fingers domain mutations associated with premature aging diseases. J. Biol. Chem. 291, 8374–8386.

Cohen, S., Méchali, M., 2002. Formation of extrachromosomal circles from telomeric DNA in Xenopus laevis. EMBO Rep. 3, 1168–1174.

Cohen, S., Agmon, N., Sobol, O., Segal, D., 2010. Extrachromosomal circles of satellite repeats and 5S ribosomal DNA in human cells. Mob. DNA 1, 11.

Conklin, Q.A., King, B.G., Zanesco, A.P., Lin, J., Hamidi, A.B., Pokorny, J.J., Álvarez-López, M.J., Cosín-Tomás, M., Huang, C., Kaliman, P., Epel, E.S., Saron, C.D., 2018. Insight meditation and telomere biology: the effects of intensive retreat and the moderating role of personality. Brain Behav. Immun. 70, 233–245. https://doi.org/10.1016/j.bbi.2018.03.003.

Cusanelli, E., Romero, C.A., Chartrand, P., 2013. Telomeric noncoding RNA TERRA is induced by telomere shortening to nucleate telomerase molecules at short telomeres. Mol. Cell 51, 780–791.

d'Adda di Fagagna, F., Reaper, P.M., Clay-Farrace, L., Fiegler, H., Carr, P., Von Zglinicki, T., Saretzki, G., Carter, N.P., Jackson, S.P., 2003. A DNA damage checkpoint response in telomere-initiated senescence. Nature 426, 194–198.

Dahlgren, P.N., Bishop, K., Dey, S., Herbert, B.S., Tanaka, H., 2018. Development of a new monochrome multiplex qPCR method for relative telomere length measurement in Cancer. Neoplasia 20, 425–431.

Danese, E., Lippi, G., 2018. Telomere length: is the future in our "ends"? Ann. Transl. Med. 6, 280. https://doi.org/10.21037/atm.2018.06.24.

de Lange, T., 2002. Protection of mammalian telomeres. Oncogene 21, 532–540.

Diman, A., Decottignies, A., 2018. Genomic origin and nuclear localization of TERRA telomeric repeat-containing RNA: from Darkness to Dawn. FEBS J. 285, 1389–1398.

Ding, C., Li, X., Ge, Y., Zhang, S., 2010. Fluorescence detection of telomerase activity in cancer cells based on isothermal circular strand-displacement polymerization reaction. Anal. Chem. 82, 2850–2855.

Ding, Z., Mangino, M., Aviv, A., Spector, T., Durbin, R., UK10K Consortium, 2014. Estimating telomere length from whole genome sequence data. Nucleic Acids Res. 42, e75.

Fajkus, J., 2006. Detection of telomerase activity by the TRAP assay and its variants and alternatives. Clin. Chim. Acta 371, 25–31.

Farmery, J.H.R., Smith, M.L., NIHR BioResource - Rare Diseases, Lynch, A.G., 2018. Telomerecat: a ploidy-agnostic method for estimating telomere length from whole genome sequencing data. Sci. Rep. 8, 1300.

Feretzaki, M., Lingner, J., 2017. A practical qPCR approach to detect TERRA, the elusive telomeric repeat-containing RNA. Methods 114, 39–45.

Fernando, M.R., Jiang, C., Krzyzanowski, G.D., Ryan, W.L., 2017. New evidence that a large proportion of human blood plasma cell-free DNA is localized in exosomes. PLoS One 12, e0183915.

Fleisig, H.B., Wong, J.M., 2007. Telomerase as a clinical target: current strategies and potential applications. Exp. Gerontol. 42, 102–112.

Freitas-Simoes, T.M., Ros, E., Sala-Vila, A., 2018. Telomere length as a biomarker of accelerated aging: is it influenced by dietary intake? Curr. Opin. Clin. Nutr. Metab. Care 21, 430–436.

Gadalla, S.M., Khincha, P.P., Katki, H.A., Giri, N., Wong, J.Y., Spellman, S., Yanovski, J.A., Han, J.C., De Vivo, I., Alter, B.P., Savage, S.A., 2016. The limitations of qPCR telomere length measurement in diagnosing dyskeratosis congenital. Mol. Genet. Genomic Med. 4, 475–479.

Gao, X., Zhang, Y., Mons, U., Brenner, H., 2018. Leukocyte telomere length and epigenetic-based mortality risk score: associations with all-cause mortality among older adults. Epigenetics 13, 846–857. https://doi.org/10.1080/15592294.2018.1514853.

Garcia-Martin, I., Janssen, A.B., Jones, R.E., Grimstead, J.W., Penketh, R.J.A., Baird, D.M., John, R.M., 2017. Telomere length heterogeneity in placenta revealed with high-resolution telomere length analysis. Placenta 59, 61–68. https://doi.org/10.1016/j.placenta.2017.09.007.

Gardner, M., Bann, D., Wiley, L., Cooper, R., Hardy, R., Nitsch, D., Martin-Ruiz, C., Shiels, P., Sayer, A.A., Barbieri, M., Bekaert, S., Bischoff, C., Brooks-Wilson, A., Chen, W., Cooper, C., Christensen, K., De Meyer, T., Deary, I., Der, G., Diez Roux, A., Fitzpatrick, A., Hajat, A., Halaschek-Wiener, J., Harris, S., Hunt, S.C., Jagger, C., Jeon, H.S., Kaplan, R., Kimura, M., Lansdorp, P., Li, C., Maeda, T., Mangino, M., Nawrot, T.S., Nilsson, P., Nordfjall, K., Paolisso, G., Ren, F., Riabowol, K., Robertson, T., Roos, G., Staessen, J.A., Spector, T., Tang, N., Unryn, B., van der Harst, P., Woo, J., Xing, C., Yadegarfar, M.E., Park, J.Y., Young, N., Kuh, D., von Zglinicki, T., Ben-Shlomo, Y., Halcyon study team, 2014. Gender and telomere length: systematic review and meta-analysis. Exp. Gerontol. 51, 15–27.

Gelmini, S., Caldini, A., Becherini, L., Capaccioli, S., Pazzagli, M., Orlando, C., 1998. Rapid, quantitative nonisotopic assay for telomerase activity in human tumors. Clin. Chem. 44, 2133–2138.

Goetzl, E.J., Mustapic, M., Kapogiannis, D., Eitan, E., Lobach, I.V., Goetzl, L., Schwartz, J.B., Miller, B.L., 2016. Cargo proteins of plasma astrocyte-derived exosomes in Alzheimer's disease. FASEB J. 30, 3853–3859.

Goetzl, E.J., Schwartz, J.B., Mustapic, M., Lobach, I.V., Daneman, R., Abner, E.L., Jicha, G.A., 2017. Altered cargo proteins of human plasma endothelial cell-derived exosomes in atherosclerotic cerebrovascular disease. FASEB J. 31, 3689–3694.

Gomez, D.E., Armando, R.G., Farina, H.G., Menna, P.L., Cerrudo, C.S., Ghiringhelli, P.D., Alonso, D.F., 2012. Telomere structure and telomerase in health and disease (review). Int. J. Oncol. 41, 1561–1569. https://doi.org/10.3892/ijo.2012.1611.

Gorenjak, V., Akbar, S., Stathopoulou, M.G., Visvikis-Siest, S., 2018. The future of telomere length in personalized medicine. Front. Biosci. (Landmark Ed) 23, 1628–1654.

Graf, M., Bonetti, D., Lockhart, A., Serhal, K., Kellner, V., Maicher, A., Jolivet, P., Teixeira, M.T., Luke, B., 2017. Telomere length determines TERRA and R-Loop regulation through the cell cycle. Cell 170, 72–85.

Grimm, J., Perez, J.M., Josephson, L., Weissleder, R., 2004. Novel nanosensors for rapid analysis of telomerase activity. Cancer Res. 64, 639–643.

Gurău, F., Baldoni, S., Prattichizzo, F., Espinosa, E., Amenta, F., Procopio, A.D., Albertini, M.C., Bonafè, M., Olivieri, F., 2018. Anti-senescence compounds: a potential nutraceutical approach to healthy aging. Ageing Res. Rev. 46, 14–31. https://doi.org/10.1016/j.arr.2018.05.001.

Gursel, I., Gursel, M., Yamada, H., Ishii, K.J., Takeshita, F., Klinman, D.M., 2003. Repetitive elements in mammalian telomeres suppress bacterial DNA-induced immune activation. J. Immunol. 171, 1393–1400.

Gutierrez-Rodrigues, F., Santana-Lemos, B.A., Scheucher, P.S., Alves-Paiva, R.M., Calado, R.T., 2014. Direct comparison of Flow-FISH and qPCR as diagnostic tests for telomere length measurement in humans. PLoS One 9, e113747.

Haapanen, M.J., Perälä, M.M., Salonen, M.K., Guzzardi, M.A., Iozzo, P., Kajantie, E., Rantanen, T., Simonen, M., Pohjolainen, P., Eriksson, J.G., von Bonsdorff, M.B., 2018. Telomere length and frailty: the helsinki birth cohort study. J. Am. Med. Dir. Assoc. 19, 658–662. https://doi.org/10.1016/j.jamda.2018.05.011.

Halim, A.T., Ariffin, N.A., Azlan, M., 2016. Review: the multiple roles of monocytic microparticles. Inflammation 39, 1277–1284.

Hang, D., Nan, H., Kværner, A.S., De Vivo, I., Chan, A.T., Hu, Z., Shen, H., Giovannucci, E., Song, M., 2018. Longitudinal associations of lifetime adiposity with leukocyte telomere length and mitochondrial DNA copy number. Eur. J. Epidemiol. 33, 485–495.

Hansen, M.E., Hunt, S.C., Stone, R.C., Horvath, K., Herbig, U., Ranciaro, A., Hirbo, J., Beggs, W., Reiner, A.P., Wilson, J.G., Kimura, M., De Vivo, I., Chen, M.M., Kark, J.D., Levy, D., Nyambo, T., Tishkoff, S.A., Aviv, A., 2016. Shorter telomere length in Europeans than in Africans due to polygenetic adaptation. Hum. Mol. Genet. 25, 2324–2330.

Harley, C.B., Futcher, A.B., Greider, C.W., 1990. Telomeres shorten during ageing of human fibroblasts. Nature 345, 458–460.

Hastings, W.J., Shalev, I., Belsky, D.W., 2017. Translating Measures of Biological Aging to Test Effectiveness of Geroprotective Interventions: What Can We Learn from Research on Telomeres? Front. Genet. 8, 164.

Henson, J.D., Cao, Y., Huschtscha, L.I., Chang, A.C., Au, A.Y., Pickett, H.A., Reddel, R.R., 2009. DNA C-circles are specific and quantifiable markers of alternative-lengthening-of-telomeres activity. Nat. Biotechnol. 27, 1181–1185.

Henson, J.D., Lau, L.M., Koch, S., Martin La Rotta, N., Dagg, R.A., Reddel, R.R., 2017. The C-Circle assay for alternative-lengthening-of-telomeres activity. Methods 114, 74–84.

Himbert, C., Thompson, H., Ulrich, C.M., 2017. Effects of intentional weight loss on markers of oxidative stress, DNA repair and telomere length - a systematic review. Obes. Facts 10, 648–665.

Hirose, M., Abe-Hashimoto, J., Ogura, K., Tahara, H., Ide, T., Yoshimura, T., 1997. A

rapid, useful and quantitative method to measure telomerase activity by hybridization protection assay connected with a telomeric repeat amplification protocol. J. Cancer Res. Clin. Oncol. 123, 337–344.

Honig, L.S., Kang, M.S., Cheng, R., Eckfeldt, J.H., Thyagarajan, B., Leiendecker-Foster, C., Province, M.A., Sanders, J.L., Perls, T., Christensen, K., Lee, J.H., Mayeux, R., Schupf, N., 2015. Heritability of telomere length in a study of long-lived families. Neurobiol. Aging 36, 2785–2790.

Hou, M., Xu, D., Björkholm, M., Gruber, A., 2001. Real-time quantitative telomeric repeat amplification protocol assay for the detection of telomerase activity. Clin. Chem. 47, 519–524.

Hu, Y., Shi, G., Zhang, L., Li, F., Jiang, Y., Jiang, S., Ma, W., Zhao, Y., Songyang, Z., Huang, J., 2016. Switch telomerase to ALT mechanism by inducing telomeric DNA damages and dysfunction of ATRX and DAXX. Sci. Rep. 6, 32280.

Iglesias, N., Redon, S., Pfeiffer, V., Dees, M., Lingner, J., Luke, B., 2011. Subtelomeric repetitive elements determine TERRA regulation by Rap1/Rif and Rap1/Sir complexes in yeast. EMBO Rep. 12, 587–593.

Jaskelioff, M., Muller, F.L., Paik, J.H., Thomas, E., Jiang, S., Adams, A.C., Sahin, E., Kost-Alimova, M., Protopopov, A., Cadiñanos, J., Horner, J.W., Maratos-Flier, E., Depinho, R.A., 2011. Telomerase reactivation reverses tissue degeneration in aged telomerase-deficient mice. Nature 469, 102–106.

Jasmine, F., Shinkle, J., Sabarinathan, M., Ahsan, H., Pierce, B.L., Kibriya, M.G., 2018. A novel pooled-sample multiplex luminex assay for high-throughput measurement of relative telomere length. Am. J. Hum. Biol. 30, e23118. https://doi.org/10.1002/ajhb.23118.

Jiang, J., Wang, Y., Sušac, L., Chan, H., Basu, R., Zhou, Z.H., Feigon, J., 2018. Structure of telomerase with telomeric DNA. Cell 173, 1179–1190.

Jiménez, K.M., Forero, D.A., 2018. Effect of master mixes on the measurement of telomere length by qPCR. Mol. Biol. Rep. 45, 633–638.

Jose, S.S., Bendickova, K., Kepak, T., Krenova, Z., Fric, J., 2017. Chronic inflammation in immune ageing: role of pattern recognition receptor crosstalk with the telomere complex? Front. Immunol. 8, 1078.

Justice, J.N., Ferrucci, L., Newman, A.B., Aroda, V.R., Bahnson, J.L., Divers, J., Espeland, M.A., Marcovina, S., Pollak, M.N., Kritchevsky, S.B., Barzilai, N., Kuchel, G.A., 2018. A framework for selection of blood-based biomarkers for geroscience-guided clinical trials: report from the TAME Biomarkers Workgroup. Geroscience. https://doi.org/10.1007/s11357-018-0042-y.

Jylhävä, J., Pedersen, N.L., Hägg, S., 2017. Biological age predictors. EBioMedicine 21, 29–36. https://doi.org/10.1016/j.ebiom.2017.03.046.

Karlseder, J., Broccoli, D., Dai, Y., Hardy, S., de Lange, T., 1999. p53- and ATM-dependent apoptosis induced by telomeres lacking TRF2. Science 283, 1321–1325.

Kaulage, M.H., Maji, B., Pasadi, S., Ali, A., Bhattacharya, S., Muniyappa, K., 2018. Targeting G-quadruplex DNA structures in the telomere and oncogene promoter regions by benzimidazole–carbazole ligands. Eur. J. Med. Chem. 148, 178–194.

Kawamura, K., Yaku, H., Miyoshi, D., Murashima, T., 2014. A simple "add and measure" FRET-based telomeric tandem repeat sequence detection and telomerase assay method. Org. Biomol. Chem. 12, 936–941.

Khan, S.S., Singer, B.D., Vaughan, D.E., 2017. Molecular and physiological manifestations and measurement of aging in humans. Aging Cell 16, 624–633. https://doi.org/10.1111/acel.12601.

Khincha, P.P., Dagnall, C.L., Hicks, B., Jones, K., Aviv, A., Kimura, M., Katki, H., Aubert, G., Giri, N., Alter, B.P., Savage, S.A., Gadalla, S.M., 2017. Correlation of leukocyte telomere length measurement methods in patients with dyskeratosis congenita and in their unaffected relatives. Int. J. Mol. Sci. 18 pii: E1765.

Kibriya, M.G., Jasmine, F., Roy, S., Ahsan, H., Pierce, B., 2014. Measurement of telomere length: a new assay using QuantiGene chemistry on a Luminex platform. Cancer Epidemiol. Biomarkers Prev. 23, 2667–2672.

Kim, W., Shay, J.W., 2018. Long-range telomere regulation of gene expression: telomere looping and telomere position effect over long distances (TPE-OLD). Differentiation 99, 1–9.

Kim, N.W., Piatyszek, M.A., Prowse, K.R., Harley, C.B., West, M.D., Ho, P.L., Coviello, G.M., Wright, W.E., Weinrich, S.L., Shay, J.W., 1994. Specific association of human telomerase activity with immortal cells and cancer. Science 266, 2011–2015.

Kimura, M., Stone, R.C., Hunt, S.C., Skurnick, J., Lu, X., Cao, X., Harley, C.B., Aviv, A., 2010. Measurement of telomere length by the Southern blot analysis of terminal restriction fragment lengths. Nat. Protoc. 5, 1596–1607. https://doi.org/10.1038/nprot.2010.124.

Klimova, B., Novotny, M., Kuca, K., 2018. Anti-aging drugs - prospect of longer life? Curr. Med. Chem. 25, 1946–1953. https://doi.org/10.2174/0929867325666171129215251.

Kohanski, R.A., Deeks, S.G., Gravekamp, C., Halter, J.B., High, K., Hurria, A., Fuldner, R., Green, P., Huebner, R., Macchiarini, F., Sierra, F., 2016. Reverse geroscience: how does exposure to early diseases accelerate the age-related decline in health? Ann. N. Y. Acad. Sci. 1386, 30–44. https://doi.org/10.1111/nyas.13297.

Komosa, M., Root, H., Meyn, M.S., 2015. Visualization and quantitative analysis of extrachromosomal telomere-repeat DNA in individual human cells by Halo-FISH. Nucleic Acids Res. 43, 2152–2163.

König, F., Schubert, T., Längst, G., 2017. The monoclonal S9.6 antibody exhibits highly variable binding affinities towards different R-loop sequences. PLoS One 12, e0178875.

Koskas, S., Decottignies, A., Dufour, S., Pezet, M., Verdel, A., Vourc'h, C., Faure, V., 2017. Heat shock factor 1 promotes TERRA transcription and telomere protection upon heat stress. Nucleic Acids Res. 45, 6321–6333.

Kulla, E., Katz, E., 2008. Biosensor techniques used for determination of telomerase activity in Cancer cells. Sensors (Basel) 8, 347–369.

Kuttler, F., Mai, S., 2007. Formation of non-random extrachromosomal elements during development, differentiation and oncogenesis. Semin. Cancer Biol. 17, 56–64.

Laguerre, A., Wong, J.M., Monchaud, D., 2016. Direct visualization of both DNA and RNA quadruplexes in human cells via an uncommon spectroscopic method. Sci. Rep. 6, 32141.

Lai, T.P., Zhang, N., Noh, J., Mender, I., Tedone, E., Huang, E., Wright, W.E., Danuser, G., Shay, J.W., 2017. A method for measuring the distribution of the shortest telomeres in cells and tissues. Nat. Commun. 8, 1356.

Lai, T.P., Wright, W.E., Shay, J.W., 2018. Comparison of telomere length measurement methods. Philos. Trans. R. Soc. Lond., B, Biol. Sci. 373, 20160451.

Lapham, K., Kvale, M.N., Lin, J., Connell, S., Croen, L.A., Dispensa, B.P., Fang, L., Hesselson, S., Hoffmann, T.J., Iribarren, C., Jorgenson, E., Kushi, L.H., Ludwig, D., Matsuguchi, T., McGuire, W.B., Miles, S., Quesenberry, C.P.Jr., Rowell, S., Sadler, M., Sakoda, L.C., Smethurst, D., Somkin, C.P., Van Den Eeden, S.K., Walter, L., Whitmer, R.A., Kwok, P.Y., Risch, N., Schaefer, C., Blackburn, E.H., 2015. Automated assay of telomere length measurement and informatics for 100,000 subjects in the genetic epidemiology research on adult health and aging (GERA) cohort. Genetics 200, 1061–1072. https://doi.org/10.1534/genetics.115.178624.

Lee, M., Napier, C.E., Yang, S.F., Arthur, J.W., Reddel, R.R., Pickett, H.A., 2017. Comparative analysis of whole genome sequencing-based telomere length measurement techniques. Methods 114, 4–15.

Li, B., Jog, S.P., Reddy, S., Comai, L., 2008. WRN controls formation of extrachromosomal telomeric circles and is required for TRF2DeltaB-mediated telomere shortening. Mol. Cell. Biol. 28, 1892–1904.

Li, Y., Liu, B., Li, X., Wei, Q., 2010. Highly sensitive electrochemical detection of human telomerase activity based on bio-barcode method. Biosens. Bioelectron. 25, 2543–2547.

Li, C.C., Hu, J., Lu, M., Zhang, C.Y., 2018a. Quantum dot-based electrochemical biosensor for stripping voltammetric detection of telomerase at the single-cell level. Biosens. Bioelectron. 122, 51–57. https://doi.org/10.1016/j.bios.2018.09.049.

Li, Y., Pan, G., Chen, Y., Yang, Q., Hao, T., Zhao, L., Zhao, L., Cong, Y., Diao, A., Yu, P., 2018b. Inhibitor of the human telomerase reverse trancriptase (hTERT) gene promoter induces cell apoptosis via a mitochondrial-dependent pathway. Eur. J. Med. Chem. 145, 370–378.

Lin, T.T., Norris, K., Heppel, N.H., Pratt, G., Allan, J.M., Allsup, D.J., Bailey, J., Cawkwell, L., Hills, R., Grimstead, J.W., Jones, R.E., Britt-Compton, B., Fegan, C., Baird, D.M., Pepper, C., 2014. Telomere dysfunction accurately predicts clinical outcome in chronic lymphocytic leukaemia, even in patients with early stage disease. Br. J. Haematol. 167, 214–223. https://doi.org/10.1111/bjh.13023.

Lin, Y., Damjanovic, A., Metter, E.J., Nguyen, H., Truong, T., Najarro, K., 2015. Age-associated telomere attrition of lymphocytes in vivo is co-ordinated with changes in telomerase activity, composition of lymphocyte subsets and health conditions. Clin. Sci. (Lond.) 128, 367–377.

Londoño-Vallejo, J.A., 2004. Telomere length heterogeneity and chromosome instability. Cancer Lett. 212, 135–144.

Lowsky, D.J., Olshansky, S.J., Bhattacharya, J., Goldman, D.P., 2014. Heterogeneity in healthy aging. J. Gerontol. A Biol. Sci. Med. Sci. 69, 640–649.

Ludlow, A.T., Shelton, D., Wright, W.E., Shay, J.W., 2018. ddTRAP: a method for sensitive and precise quantification of telomerase activity. Methods Mol. Biol. 1768, 513–529.

Lustig, A., Liu, H.B., Metter, E.J., An, Y., Swaby, M.A., Elango, P., Ferrucci, L., Hodes, R.J., Weng, N.P., 2017. Telomere shortening, inflammatory cytokines, and anti-cytomegalovirus antibody follow distinct age-associated trajectories in humans. Front. Immunol. 8, 1027.

Maesawa, C., Inaba, T., Sato, H., Iijima, S., Ishida, K., Terashima, M., Sato, R., Suzuki, M., Yashima, A., Ogasawara, S., Oikawa, H., Sato, N., Saito, K., Masuda, T., 2003. A rapid biosensor chip assay for measuring of telomerase activity using surface plasmon resonance. Nucleic Acids Res. 31 E4-4.

Mangaonkar, A.A., Patnaik, M.M., 2018. Short telomere syndromes in clinical practice: bridging bench and bedside. Mayo Clin. Proc. 93, 904–916.

Marchesini, M., Matocci, R., Tasselli, L., Cambiaghi, V., Orleth, A., Furia, L., Marinelli, C., Lombardi, S., Sammarelli, G., Aversa, F., Minucci, S., Faretta, M., Pelicci, P.G., Grignani, F., 2016. PML is required for telomere stability in non-neoplastic human cells. Oncogene 35, 1811–1821.

Martadinata, H., Heddi, B., Lim, K.W., Phan, A.T., 2011. Structure of long human telomeric RNA (TERRA): G-quadruplexes formed by four and eight UUAGGG repeats are stable building blocks. Biochemistry 50, 6455–6461.

Martin-Ruiz, C.M., Baird, D., Roger, L., Boukamp, P., Krunic, D., Cawthon, R., Dokter, M.M., van der Harst, P., Bekaert, S., de Meyer, T., Roos, G., Svenson, U., Codd, V., Samani, N.J., McGlynn, L., Shiels, P.G., Pooley, K.A., Dunning, A.M., Cooper, R., Wong, A., Kingston, A., von Zglinicki, T., 2015. Reproducibility of telomere length assessment: an international collaborative study. Int. J. Epidemiol. 44, 1673–1683. https://doi.org/10.1093/ije/dyu191.

Masutomi, K., Yu, E.Y., Khurts, S., Ben-Porath, I., Currier, J.L., Metz, G.B., Brooks, M.W., Kaneko, S., Murakami, S., DeCaprio, J.A., Weinberg, R.A., Stewart, S.A., Hahn, W.C., 2003. Telomerase maintains telomere structure in normal human cells. Cell 114, 241–253.

Meyer, A., Salewsky, B., Buchmann, N., Steinhagen-Thiessen, E., Demuth, I., 2016. Relative leukocyte telomere length, hematological parameters and Anemia - data from the Berlin aging study II (BASE-II). Gerontology 62, 330–336. https://doi.org/10.1159/000430950.

Mons, U., Müezzinler, A., Schöttker, B., Dieffenbach, A.K., Butterbach, K., Schick, M., Peasey, A., De Vivo, I., Trichopoulou, A., Boffetta, P., Brenner, H., 2017. Leukocyte telomere length and all-cause, cardiovascular disease, and Cancer mortality: results from individual-participant-Data meta-analysis of 2 large prospective cohort studies. Am. J. Epidemiol. 185, 1317–1326. https://doi.org/10.1093/aje/kww210.

Montero, J.J., López de Silanes, I., Graña, O., Blasco, M.A., 2016. Telomeric RNAs are essential to maintain telomeres. Nat. Commun. 7, 12534.

Montiel Rojas, D., Nilsson, A., Ponsot, E., Brummer, R.J., Fairweather-Tait, S., Jennings,

A., de Groot, L.C.P.G.M., Berendsen, A., Pietruszka, B., Madej, D., Caumon, E., Meunier, N., Malpuech-Brugère, C., Guidarelli, G., Santoro, A., Franceschi, C., Kadi, F., 2018. Short Telomere Length Is Related to Limitations in Physical Function in Elderly European Adults. Front. Physiol. 9, 1110. https://doi.org/10.3389/fphys.2018.01110. eCollection 2018.

Montpetit, A.J., Alhareeri, A.A., Montpetit, M., Starkweather, A.R., Elmore, L.W., Filler, K., Mohanraj, L., Burton, C.W., Menzies, V.S., Lyon, D.E., Jackson-Cook, C.K., 2014. Telomere length: a review of methods for measurement. Nurs. Res. 63, 289–299.

Moye, A.L., Porter, K.C., Cohen, S.B., Phan, T., Zyner, K.G., Sasaki, N., Lovrecz, G.O., Beck, J.L., Bryan, T.M., 2015. Telomeric G-quadruplexes are a substrate and site of localization for human telomerase. Nat. Commun. 6, 7643.

Müezzinler, A., Zaineddin, A.K., Brenner, H., 2013. A systematic review of leukocyte telomere length and age in adults. Ageing Res. Rev. 12, 509–519.

Müezzinler, A., Mons, U., Dieffenbach, A.K., Butterbach, K., Saum, K.U., Schick, M., Stammer, H., Boukamp, P., Holleczek, B., Stegmaier, C., Brenner, H., 2016. Body mass index and leukocyte telomere length dynamics among older adults: results from the ESTHER cohort. Exp. Gerontol. 74, 1–8. https://doi.org/10.1016/j.exger.2015.11.019.

Mundstock, E., Zatti, H., Louzada, F.M., Oliveira, S.G., Guma, F.T., Paris, M.M., Rueda, A.B., Machado, D.G., Stein, R.T., Jones, M.H., Sarria, E.E., Barbé-Tuana, F.M., Mattiello, R., 2015a. Effects of physical activity in telomere length: systematic review and meta-analysis. Ageing Res. Rev. 22, 72–80. https://doi.org/10.1016/j.arr.2015.02.004.

Mundstock, E., Sarria, E.E., Zatti, H., Mattos Louzada, F., Kich Grun, L., Herbert Jones, M., Guma, F.T., Mazzola In Memoriam, J., Epifanio, M., Stein, R.T., Barbé-Tuana, F.M., Mattiello, R., 2015b. Effect of obesity on telomere length: Systematic review and meta-analysis. Obesity 23 (Silver Spring), 2165–2174. https://doi.org/10.1002/oby.21183.

Nabetani, A., Ishikawa, F., 2011. Alternative lengthening of telomeres pathway: re-combination-mediated telomere maintenance mechanism in human cells. J. Biochem. 149, 5–14. https://doi.org/10.1093/jb/mvq119.

Németh, A., Orgovan, N., Sódar, B.W., Osteikoetxea, X., Pálóczi, K., Szabó-Taylor, K.É., Vukman, K.V., Kittel, Á., Turiák, L., Wiener, Z., Tóth, S., Drahos, L., Vékey, K., Horvath, H., Buzás, E.I., 2017. Antibiotic-induced release of small extracellular ve-sicles (exosomes) with surface-associated DNA. Sci. Rep. 7, 8202.

Norberg, A., Rosén, A., Raaschou-Jensen, K., Kjeldsen, L., Moilanen, J.S., Paulsson-Karlsson, Y., Baliakas, P., Lohi, O., Ahmed, A., Kittang, A.O., Larsson, P., Roos, G., Degerman, S., Hultdin, M., 2018. Novel variants in Nordic patients referred for ge-netic testing of telomere-related disorders. Eur. J. Hum. Genet. 26, 858–867.

Nussey, D.H., Baird, D., Barrett, E., Boner, W., Fairlie, J., Gemmell, N., Hartmann, N., Horn, T., Haussmann, M., Olsson, M., Turbill, C., Verhulst, S., Zahn, S., Monaghan, P., 2014. Measuring telomere length and telomere dynamics in evolutionary biology and ecology. Methods Ecol. Evol. 5, 299–310.

Oerther, S., Lorenz, R., 2018. State of the science: using telomeres as biomarkers during the first 1,000 days of life. West. J. Nurs. Res. https://doi.org/10.1177/0193945918762806.

Ohuchida, K., Mizumoto, K., Ogura, Y., Ishikawa, N., Nagai, E., Yamaguchi, K., Tanaka, M., 2005. Quantitative assessment of telomerase activity and human telomerase re-verse transcriptase messenger RNA levels in pancreatic juice samples for the diag-nosis of pancreatic cancer. Clin. Cancer Res. 11, 2285–2292.

Oliva-Rico, D., Herrera, L.A., 2017. Regulated expression of the lncRNA TERRA and its impact on telomere biology. Mech. Ageing Dev. 167, 16–23.

Ouellette, M.M., Liao, M., Herbert, B.S., Johnson, M., Holt, S.E., Liss, H.S., Shay, J.W., Wright, W.E., 2000. Subsenescent telomere lengths in fibroblasts immortalized by limiting amounts of telomerase. J. Biol. Chem. 275, 10072–10076.

Parker, M., Chen, X., Bahrami, A., Dalton, J., Rusch, M., Wu, G., Easton, J., Cheung, N.K., Dyer, M., Mardis, E.R., Wilson, R.K., Mullighan, C., Gilbertson, R., Baker, S.J., Zambetti, G., Ellison, D.W., Downing, J.R., Zhang, J., Pediatric Cancer Genome Project, 2012. Assessing telomeric DNA content in pediatric cancers using whole-genome sequencing data. Genome Biol. 13, R113.

Patolsky, F., Gill, R., Weizmann, Y., Mokari, T., Banin, U., Willner, I., 2003. Lighting-up the dynamics of telomerization and DNA replication by CdSe-ZnS quantum dots. J. Am. Chem. Soc. 125, 13918–13919.

Pavlov, V., Xiao, Y., Gill, R., Dishon, A., Kotler, M., Willner, I., 2004. Amplified chemi-luminescence surface detection of DNA and telomerase activity using catalytic nu-cleic acid labels. Anal. Chem. 76, 2152–2156.

Pérez, L.M., Amaral, M.A., Mundstock, E., Barbé-Tuana, F.M., Guma, F.T.C.R., Jones, M.H., Machado, D.C., Sarria, E.E., Marques E Marques, M., Preto, L.T., Epifanio, M., Meinem Garbin, J.G., Mattiello, R., 2017. Effects of diet on telomere length: sys-tematic review and meta-analysis. Public Health Genomics 20, 286–292. https://doi.org/10.1159/000486586.

Perner, S., Brüderlein, S., Hasel, C., Waibel, I., Holdenried, A., Ciloglu, N., 2003. Quantifying telomere lengths of human individual chromosome arms by centromere-calibrated fluorescence in situ hybridization and digital imaging. Am. J. Pathol. 163, 1751–1756.

Pfeiffer, V., Lingner, J., 2012. TERRA promotes telomere shortening through exonuclease 1-mediated resection of chromosome ends. PLoS Genet. 8, e1002747.

Pickett, H.A., Cesare, A.J., Johnston, R.L., Neumann, A.A., Reddel, R.R., 2009. Control of telomere length by a trimming mechanism that involves generation of t-circles. EMBO J. 28, 799–809.

Rachakonda, S., Srinivas, N., Mahmoudpour, S.H., Garcia-Casado, Z., Requena, C., Traves, V., Soriano, V., Cardelli, M., Pajnova, D., Molven, A., Gruis, N., Nagore, E., Kumar, R., 2018. Telomere length and survival in primary cutaneous melanoma patients. Sci. Rep. 8, 10947. https://doi.org/10.1038/s41598-018-29322-9.

Raschenberger, J., Lamina, C., Haun, M., Kollerits, B., Coassin, S., Boes, E., Kedenko, L., Köttgen, A., Kronenberg, F., 2016. Influence of DNA extraction methods on relative telomere length measurements and its impact on epidemiological studies. Sci. Rep. 6, 25398. https://doi.org/10.1038/srep25398.

Rufer, N., Dragowska, W., Thornbury, G., Roosnek, E., Lansdorp, P.M., 1998. Telomere length dynamics in human lymphocyte subpopulations measured by flow cytometry. Nat. Biotechnol. 16, 743–747.

Saldanha, S.N., Andrews, L.G., Tollefsbol, T.O., 2003. Analysis of telomerase activity and detection of its catalytic subunit, hTERT. Anal. Biochem. 315, 1–21.

Savage, S.A., 2018. Beginning at the ends: telomeres and human disease. F1000Res. 7https://doi.org/10.12688/f1000research.14068.1. pii: F1000.

Savoysky, E., Akamatsu, K., Tsuchiya, M., Yamazaki, T., 1996. Detection of telomerase activity by combination of TRAP method and scintillation proximity assay (SPA). Nucleic Acids Res. 24, 1175–1176.

Schmidt, P.M., Matthes, E., Scheller, F.W., Bienert, M., Lehmann, C., Ehrlich, A., Bier, F.F., 2002. Real-time determination of telomerase activity in cell extracts using an optical biosensor. Biol. Chem. 383, 1659–1666.

Schvartzman, J.B., Martínez-Robles, M.L., Hernández, P., Krimer, D.B., 2013. Plasmid DNA topology assayed by two-dimensional agarose gel electrophoresis. Methods Mol. Biol. 1054, 121–132.

Shay, J.W., 2016. Role of telomeres and telomerase in aging and Cancer. Cancer Discov. 6, 584–593.

Shay, J.W., 2018. Telomeres and aging. Curr. Opin. Cell Biol. 52, 1–7. https://doi.org/10.1016/j.ceb.2017.12.001.

Sierra, F., Kohanski, R., 2017. Geroscience and the trans-NIH geroscience interest group, GSIG. Geroscience 39, 1–5. https://doi.org/10.1007/s11357-016-9954-6.

Skvortsov, D.A., Zvereva, M.E., Shpanchenko, O.V., Dontsova, O.A., 2011. Assays for detection of telomerase activity. Acta Naturae 3, 48–68.

Smith, E.D., Garza-Gongora, A.G., MacQuarrie, K.L., Kosak, S.T., 2018. Interstitial telo-meric loops and implications of the interaction between TRF2 and lamin A/C. Differentiation 102, 19–26.

Sprouse, A.A., Steding, C.E., Herbert, B.S., 2012. Pharmacological regulation of telomerase and its clinical potential. J. Cell. Mol. Med. 16, 1–7. https://doi.org/10.1111/j.1582-4934.2011.01460.x.

Storci, G., De Carolis, S., Olivieri, F., Bonafè, M., 2018. Changes in the biochemical taste of cytoplasmic and cell-free DNA are major fuels for inflamm-aging. Semin. Immunol. https://doi.org/10.1016/j.smim.2018.08.003. pii: S1044-5323(18)30070-30078.

Stout, S.A., Lin, J., Hernandez, N., Davis, E.P., Blackburn, E., Carroll, J.E., Glynn, L.M., 2017. Validation of minimally-invasive sample collection methods for measurement of telomere length. Front. Aging Neurosci. 9, 397. https://doi.org/10.3389/fnagi.2017.00397.

Strazhesko, I.D., Tkacheva, O.N., Akasheva, D.U., Dudinskaya, E.N., Plokhova, E.V., Pykhtina, V.S., Kruglikova, A.S., Kokshagina, N.V., Sharashkina, N.V., Agaltsov, M.V., Kashtanova, D.A., Vygodin, V.A., Ozerova, I.N., Skvortsov, D.A., Vasilkova, D., Boytsov, S.A., 2016. Atorvastatin therapy modulates telomerase activity in patients free of atherosclerotic cardiovascular diseases. Front. Pharmacol. 7, 347.

Su, X., Li, Z., Yan, X., Wang, L., Zhou, X., Wei, L., Xiao, L., Yu, C., 2017. Telomerase activity detection with amplification-free single molecule stochastic binding assay. Anal. Chem. 89, 3576–3582.

Sue, M.J., Yeap, S.K., Omar, A.R., Tan, S.W., 2014. Application of PCR-ELISA in molecular diagnosis. Biomed Res. Int. 2014, 653014.

Takai, H., Smogorzewska, A., de Lange, T., 2003. DNA damage foci at dysfunctional telomeres. Curr. Biol. 13, 1549–1556.

Tarik, M., Ramakrishnan, L., Sachdev, H.S., Tandon, N., Roy, A., Bhargava, S.K., Pandey, R.M., 2018. Validation of quantitative polymerase chain reaction with Southern blot method for telomere length analysis. Future Sci. OA 4, FSO282.

Testa, R., Olivieri, F., Sirolla, C., Spazzafumo, L., Rippo, M.R., Marra, M., Bonfigli, A.R., Ceriello, A., Antonicelli, R., Franceschi, C., Castellucci, C., Testa, I., Procopio, A.D., 2011. Leukocyte telomere length is associated with complications of type 2 diabetes mellitus. Diabet. Med. 28, 1388–1394. https://doi.org/10.1111/j.1464-5491.2011.03370.x.

Tokutake, Y., Matsumoto, T., Watanabe, T., Maeda, S., Tahara, H., Sakamoto, S., Niida, H., Sugimoto, M., Ide, T., Furuichi, Y., 1998. Extra-chromosomal telomere repeat DNA in telomerase-negative immortalized cell lines. Biochem. Biophys. Res. Commun. 247, 765–772.

Tomaska, L., Nosek, J., Kramara, J., Griffith, J.D., 2009. Telomeric circles: universal players in telomere maintenance? Nat. Struct. Mol. Biol. 16, 1010–1015. https://doi.org/10.1038/nsmb.1660.

Toubiana, S., Selig, S., 2018. DNA:RNA hybrids at telomeres - when it is better to be out of the (R) loop. FEBS J. 285, 2552–2566. https://doi.org/10.1111/febs.14464.

Toupance, S., Labat, C., Temmar, M., Rossignol, P., Kimura, M., Aviv, A., Benetos, A., 2017. Short telomeres, but not telomere attrition rates, are associated with carotid atherosclerosis. Hypertension. 70, 420–425.

Uehara, H., Nardone, G., Nazarenko, I., Hohman, R.J., 1999. Detection of telomerase activity utilizing energy transfer primers: comparison with gel- and ELISA-based detection. Biotechniques. 26, 552–558.

Vaiserman, A., Lushchak, O., 2017. Implementation of longevity-promoting supplements and medications in public health practice: achievements, challenges and future per-spectives. J. Transl. Med. 15, 160. https://doi.org/10.1186/s12967-017-1259-8.

Vetter, V.M., Antje, M., Karbasiyan, M., Steinhagen-Thiessen, E., Hopfenmüller, W., Demuth, 2018. Epigenetic clock and relative telomere length represent largely dif-ferent aspects of aging in the Berlin Aging Study II (BASE-II). J. Gerontol. A Biol. Sci. Med. Sci. https://doi.org/10.1093/gerona/gly184.

Wang, Z., Lieberman, P.M., 2016. The crosstalk of telomere dysfunction and inflamma-tion through cell-free TERRA containing exosomes. RNA Biol. 13, 690–695.

Wang, Y., Prosen, D.E., Mei, L., Sullivan, J.C., Finney, M., Vander Horn, P.B., 2004. A novel strategy to engineer DNA polymerases for enhanced processivity and improved performance in vitro. Nucleic Acids Res. 32, 1197–1207.

Wang, Z., Deng, Z., Dahmane, N., Tsai, K., Wang, P., Williams, D.R., Kossenkov, A.V., Showe, L.C., Zhang, R., Huang, Q., Conejo-Garcia, J.R., Lieberman, P.M., 2015. Telomeric repeat-containing RNA (TERRA) constitutes a nucleoprotein component of extracellular inflammatory exosomes. Proc. Natl. Acad. Sci. U. S. A. 112, E6293–300.

Wang, J., Dong, X., Cao, L., Sun, Y., Qiu, Y., Zhang, Y., Cao, R., Covasa, M., Zhong, L., 2016. Association between telomere length and diabetes mellitus: a meta-analysis. J. Int. Med. Res. 44, 1156–1173. https://doi.org/10.1177/0300060516667132.

Wang, H., Zhang, K., Liu, Y., Fu, Y., Gao, S., Gong, P., Wang, H., Zhou, Z., Zeng, M., Wu, Z., Sun, Y., Chen, T., Li, S., Liu, L., 2017a. Telomere heterogeneity linked to metabolism and pluripotency state revealed by simultaneous analysis of telomere length and RNA-seq in the same human embryonic stem cell. BMC Biol. 15, 114.

Wang, W., Zheng, L., Zhou, N., Li, N., Bulibu, G., Xu, C., Zhang, Y., Tang, Y., 2017b. Meta-analysis of associations between telomere length and colorectal cancer survival from observational studies. Oncotarget 8, 62500–62507. https://doi.org/10.18632/oncotarget.20055.

Wang, Z., Deng, Z., Tutton, S., Lieberman, P.M., 2017c. The telomeric response to viral infection. Viruses. 9https://doi.org/10.3390/v9080218. pii: E218.

Wang, Z., Li, J., Liu, J.P., 2018a. Effects of cation charges on the binding of stabilizers with human telomere and TERRA G-quadruplexes. J. Biomol. Struct. Dyn. https://doi.org/10.1080/07391102.2018.1471416.

Wang, Q., Zhan, Y., Pedersen, N.L., Fang, F., Hägg, S., 2018b. Telomere length and all-cause mortality: a meta-analysis. Ageing Res. Rev. 48, 11–20. https://doi.org/10.1016/j.arr.2018.09.002.

Wege, H., Chui, M.S., Le, H.T., Tran, J.M., Zern, M.A., 2003. SYBR Green real-time telomeric repeat amplification protocol for the rapid quantification of telomerase activity. Nucleic Acids Res. 31, E3–3.

Williams, J., Heppel, N.H., Britt-Compton, B., Grimstead, J.W., Jones, R.E., Tauro, S., Bowen, D.T., Knapper, S., Groves, M., Hills, R.K., Pepper, C., Baird, D.M., Fegan, C., 2017. Telomere length is an independent prognostic marker in MDS but not in de novo AML. Br. J. Haematol. 178, 240–249. https://doi.org/10.1111/bjh.14666.

Wu, Y.Y., Hruszkewycz, A.M., Delgado, R.M., Yang, A., Vortmeyer, A.O., Moon, Y.W., Weil, R.J., Zhuang, Z., Remaley, A.T., 2000. Limitations on the quantitative determination of telomerase activity by the electrophoretic and ELISA based TRAP assays. Clin. Chim. Acta 293, 199–212.

Wu, R.A., Upton, H.E., Vogan, J.M., Collins, K., 2017. Telomerase mechanism of telomere synthesis. Annu. Rev. Biochem. 86, 439–460.

Wulaningsih, W., Kuh, D., Wong, A., Hardy, R., 2018. Adiposity, telomere length, and telomere attrition in midlife: the 1946 british birth cohort. J. Gerontol. A Biol. Sci. Med. Sci. 73, 966–972. https://doi.org/10.1093/gerona/glx151.

Xu, Y., Suzuki, Y., Ito, K., Komiyama, M., 2010. Telomeric repeat-containing RNA structure in living cells. Proc. Natl. Acad. Sci. U. S. A. 107, 14579–14584.

Yehuda, S., Yanai, H., Priel, E., Fraifeld, V.E., 2017. Differential decrease in soluble and DNA-bound telomerase in senescent human fibroblasts. Biogerontology. 18, 525–533. https://doi.org/10.1007/s10522-017-9688-6.

Zavari-Nematabad, A., Alizadeh-Ghodsi, M., Hamishehkar, H., Alipour, E., Pilehvar-Soltanahmadi, Y., 2017. Development of quantum-dot-encapsulated liposome-based optical nanobiosensor for detection of telomerase activity without target amplification. Anal. Bioanal. Chem. 409, 1301–1310. https://doi.org/10.1007/s00216-016-0058-z.

Zhang, C., Chen, X., Li, L., Zhou, Y., Wang, C., Hou, S., 2015. The association between telomere length and Cancer prognosis: evidence from a meta-analysis. PLoS One 10, e0133174. https://doi.org/10.1371/journal.pone.0133174.

Zhang, T., Zhang, Z., Li, F., Hu, Q., Liu, H., Tang, M., Ma, W., Huang, J., Songyang, Z., Rong, Y., Zhang, S., Chen, B.P., Zhao, Y., 2017a. Looping-out mechanism for resolution of replicative stress at telomeres. EMBO Rep. 18, 1412–1428. https://doi.org/10.15252/embr.201643866.

Zhang, X., Lou, X., Xia, F., 2017b. Advances in the detection of telomerase activity using isothermal amplification. Theranostics. 7, 1847–1862.

Zhang, L., Peng, J., Hong, M.F., Chen, J.Q., Liang, R.P., Qiu, J.D., 2018. A facile graphene oxide-based fluorescent nanosensor for the in situ "turn-on" detection of telomerase activity. Analyst. 143, 2334–2341.

Zhu, Y., Liu, X., Ding, X., Wang, F., Geng, X., 2018. Telomere and its role in the aging pathways: telomere shortening, cell senescence and mitochondria dysfunction. Biogerontology. https://doi.org/10.1007/s10522-018-9769-1.

Zierer, J., Kastenmüller, G., Suhre, K., Gieger, C., Codd, V., Tsai, P.C., Bell, J., Peters, A., Strauch, K., Schulz, H., Weidinger, S., Mohney, R.P., Samani, N.J., Spector, T., Mangino, M., Menni, C., 2016. Metabolomics profiling reveals novel markers for leukocyte telomere length. Aging (Albany NY) 8, 77–94.

Zinkova, A., Brynychova, I., Svacina, A., Jirkovska, M., Korabecna, M., 2017. Cell-free DNA from human plasma and serum differs in content of telomeric sequences and its ability to promote immune response. Sci. Rep. 7, 2591.

Taylor & Francis
Taylor & Francis Group

RESEARCH ARTICLE

      OPEN ACCESS   Check for updates

Small extracellular vesicles deliver miR-21 and miR-217 as pro-senescence effectors to endothelial cells

Emanuela Mensà [a]*, Michele Guescini [b]*, Angelica Giuliani [a]*, Maria Giulia Bacalini [c], Deborah Ramini [a], Giacomo Corleone [d], Manuela Ferracin [e], Gianluca Fulgenzi [a], Laura Graciotti [a], Francesco Prattichizzo [f], Leonardo Sorci [g], Michela Battistelli [b], Vladia Monsurrò [h], Anna Rita Bonfigli [i], Maurizio Cardelli [j], Rina Recchioni [k], Fiorella Marcheselli [k], Silvia Latini [a], Serena Maggio [b], Mirco Fanelli [l], Stefano Amatori [l], Gianluca Storci [e], Antonio Ceriello [f], Vilberto Stocchi [b], Maria De Luca [m], Luca Magnani [d], Maria Rita Rippo [a], Antonio Domenico Procopio [a,k], Claudia Sala [n], Iva Budimir [n], Cristian Bassi [o], Massimo Negrini [o], Paolo Garagnani [e,p,q], Claudio Franceschi [c,r], Jacopo Sabbatinelli [a], Massimiliano Bonafè [e]* and Fabiola Olivieri [a,k]*

aDepartment of Clinical and Molecular Sciences, Università Politecnica delle Marche, Ancona, Italy; bDepartment of Biomolecular Sciences, University of Urbino Carlo Bo, Urbino, Italy; cIRCCS Istituto delle Scienze Neurologiche di Bologna, Bologna, Italy; dDepartment of Surgery and Cancer, Imperial College London, London, UK; eDepartment of Experimental, Diagnostic, and Specialty Medicine, University of Bologna, Bologna, Italy; fIRCCS MultiMedica, Milano, Italy; gDepartment of Materials, Environmental Sciences and Urban Planning, Università Politecnica delle Marche, Ancona, Italy; hDepartment of Medicine, University of Verona, Verona, Italy; iScientific Direction, IRCCS INRCA, Ancona, Italy; jAdvanced Technology Center for Aging Research, Scientific Technological Area, IRCCS INRCA, Ancona, Italy; kCenter of Clinical Pathology and Innovative Therapy, IRCCS INRCA, Ancona, Italy; lDepartment of Biomolecular Sciences, Molecular Pathology Laboratory "Paola", University of Urbino Carlo Bo, Fano, Italy; mDepartment of Nutrition Sciences, University of Alabama at Birmingham, Birmingham, USA; nDepartment of Physics and Astronomy, University of Bologna, Bologna, Italy; oDepartment of Morphology, Surgery & Experimental Medicine, and Laboratory for the Technologies of Advanced Therapies, Tecnopolo, University of Ferrara, Ferrara, Italy; pClinical Chemistry, Department of Laboratory Medicine, Karolinska Institutet at Huddinge University Hospital, Stockholm, Sweden; qPersonal Genomics S.r.l., Verona, Italy; rLobachevsky State University of Nizhny Novgorod, Nizhny Novgorod, Russia

ABSTRACT

The role of epigenetics in endothelial cell senescence is a cutting-edge topic in ageing research. However, little is known of the relative contribution to pro-senescence signal propagation provided by microRNAs shuttled by extracellular vesicles (EVs) released from senescent cells. Analysis of microRNA and DNA methylation profiles in non-senescent (control) and senescent (SEN) human umbilical vein endothelial cells (HUVECs), and microRNA profiling of their cognate small EVs (sEVs) and large EVs demonstrated that SEN cells released a significantly greater sEV number than control cells. sEVs were enriched in miR-21-5p and miR-217, which target DNMT1 and SIRT1. Treatment of control cells with SEN sEVs induced a miR-21/miR-217-related impairment of DNMT1-SIRT1 expression, the reduction of proliferation markers, the acquisition of a senescent phenotype and a partial demethylation of the locus encoding for miR-21. MicroRNA profiling of sEVs from plasma of healthy subjects aged 40–100 years showed an inverse U-shaped age-related trend for miR-21-5p, consistent with senescence-associated biomarker profiles. Our findings suggest that miR-21-5p/miR-217 carried by SEN sEVs spread pro-senescence signals, affecting DNA methylation and cell replication.

Introduction

Cellular senescence is considered as a hallmark of ageing and a major risk factor for the development of the most common age-related diseases (ARDs) [1]. Senescent cells (SCs) are characterised by a significantly reduced replicative potential and by the acquisition of a pro-inflammatory senescence-associated secretory phenotype (SASP) [2], which involves the paracrine induction of a senescent state in younger cells through a "bystander effect" [3]. Since this effect fuels inflammaging – the systemic, low-grade, chronic inflammation that accompanies human ageing [4] – it appears to be a critical step in SC accumulation during organismal ageing [5]. The clinical relevance of inflammaging in ARD development and progression has become clearly established [6]. SC clearance and attenuation of the bystander effect have been proposed

---

CONTACT Jacopo Sabbatinelli ✉ j.sabbatinelli@pm.univpm.it 🖃 Department of Clinical and Molecular Sciences, Università Politecnica Delle Marche, Via Tronto 10/A, Ancona, Italy

*These authors contributed equally

🅙 Supplemental data for this article can be accessed here.

as innovative therapeutic approaches to address, ameliorate or prevent a range of human disorders [7–10]. In this framework, unravelling the contribution of the epigenetic mechanisms involved in the senescence process would be a major step forward [11]. Considerable effort is being devoted to discriminating the effects of several epigenetic mechanisms, including DNA methylation and long and small non-coding RNA activity, on the modulation of the transcriptional programme leading to cellular senescence [12,13]. Senescence-associated (SA) genome-wide hypomethylation has been described in SCs, whereas the expression and activity of DNA methyltransferase 1 (DNMT1) decline with ageing [14]. DNMT1 is involved in maintaining the methylation pattern and works with Sirtuin 1 (SIRT1), an enzyme exerting mono-ADP ribosyltransferase or deacetylase activity, in ensuring genome integrity and in exerting pro-longevity effects [15,16]. As a result, DNMT and SIRT activators/inhibitors are being investigated as therapeutic agents against ARDs [17].

Senescence modulation by microRNAs (miRNAs) is a major senescence-related epigenetic mechanism. This has been suggested, among other findings, by the identification of discrete miRNA signatures associated with senescence in different cell types [18] and by the fact that living cells can actively release extracellular vesicles (EVs), which contain different species and amounts of non-coding RNAs. EVs comprise large particles (lEVs; also known as micro-vesicles) and small particles (sEVs or exosomes) and differ both in their intra-cellular origin and in the cargo they transport [19]. lEVs and sEVs seem to reflect the molecular characteristics of their cells of origin and to modulate the phenotype of recipient cells both in a paracrine and in a systemic manner [20,21]. Despite the major contribution to organismal ageing demonstrated for EVs and their miRNA cargo [22,23], too little is known of the effect of ageing on human EV content, on the miRNA repertoire shuttled by SCs and their cognate EVs, and on circulating EVs. Evidence from a variety of cellular models suggests that the senescence phenotype is characterised by increased EV secretion [24–26], although circulating EV concentrations seem to decline with age, possibly as a consequence of increased internalisation by immune cells [27]. Notably, the pro-inflammatory effects of EVs released from SCs seem to be related to their DNA/RNA cargo, which suggests that EVs belong to the SC secretome [25,26,28]. Recently, the effects of EVs have been explored in relation to vascular ageing [28]. EVs from the plasma of elderly subjects and from senescent endothelial cells (ECs) promote vascular calcification [29], reduce the bone formation rate [30] and

reprogram monocytes towards a pro-inflammatory phenotype [31].

Altogether, our knowledge of the *in vivo* effects of cellular senescence is quite limited. Moreover, the heterogeneous senescence phenotypes characterising living animals entail that there are currently no wholly reliable universal markers to identify senescent ECs *in vivo* [32].

This study was devised to unravel the relative contribution of EVs released from senescent ECs in spreading pro-senescence signals to proliferating cells via their miRNA cargo. Based on the evidence that the *in vitro* replicative senescence of ECs substantially mimics the progressive age-related impairment of endothelial function described *in vivo* [33], we set out to identify the miRNAs that are differentially expressed in senescent and non-senescent human umbilical vein endothelial cells (HUVECs) and their cognate EVs (lEVs and sEVs). We then correlated the miRNA levels with the methylation state of their genetic loci and assessed their interactions with the enzymes involved in the maintenance of the methylation pattern during ageing. Finally, we compared the SA-miRNAs isolated from EVs released from senescent HUVECs with the miRNAs showing a differential expression in circulating EVs obtained from subjects of different ages.

Materials and methods

Cell lines and cell culture

An *in vitro* model of replicative cell senescence was established using long-term cultured HUVECs and human aortic endothelial cells (HAECs). Cryopreserved HUVECs and HAECs obtained from pool of donors were purchased from Clonetics (Lonza, Switzerland) and cultured in endothelial basal medium (EBM-2, CC-3156, Lonza) supplemented with SingleQuot Bullet Kit (CC-4176, Lonza) containing 0.1% human recombinant epidermal growth factor (rh-EGF), 0.04% hydrocortisone, 0.1% vascular endothelial growth factor (VEGF), 0.4% human recombinant fibroblast growth factor (rh-FGF-B), 0.1% insulin-like growth factor-1 with the substitution of arginine for glutamic acid at position 3 (R3-IGF-1), 0.1% ascorbic acid, 0.1% heparin, 0.1% gentamicin and amphotericin-B (GA-1000) and 2% foetal bovine serum (FBS). Cells were seeded at a density of 5000/cm^2, sub-cultured when they reached 70–80% confluence, and maintained in a humidified atmosphere of 5% CO_2 at 37°C. All cells tested negative for mycoplasma infection. Before replating, harvested cells were counted using a haemocytometer. Population doublings (PDs) were calculated by the formula: $(\log_{10}F - \log_{10}I)/\log_{10}2$, where F is the number of

cells at the end of the passage and *I* is the number of seeded cells. Cumulative population doubling (cPD) was calculated as the sum of PD changes. Cells were cultured until the arrest of replication and classified based on SA β-Gal activity into control (CON, SA β-Gal < 5%) and senescent (SEN, SA β-Gal > 60%) cells. For the drug-induced senescence model, HUVECs and HAECs were treated with doxorubicin hydrochloride (Sigma Aldrich, Italy) at 50 nM for 24 h and were harvested following a 72-h recovery period with fresh medium.

Biomarkers of the HUVEC and HAEC senescent phenotype

SA β-galactosidase staining
SA β-galactosidase (β-gal) activity was assessed using Senescence Detection Kit (cat. no. K320, BioVision Inc., USA) as described previously [34].

Telomere length
Telomere length was analysed by quantitative PCR using Cawthon's method [35]. Genomic DNA was isolated from young and senescent HUVECs using Norgen's RNA/DNA Purification Kit (cat. no. 48,700, Norgen Biotek Corporation, Canada).

p16, IL-1β, IL-6, IL-8, DNMT1 and SIRT1 mRNA expression level
For mRNA gene expression, 1 µg of purified RNA was reverse-transcribed with OneScript® cDNA Synthesis Kit (Applied Biological Materials Inc., Canada) according to the manufacturer's instructions. qPCR reactions were conducted in a Rotor Gene Q 5plex HRM apparatus (Qiagen, Germany) in a 10 µl total reaction volume using TB Green Premix Ex Taq II (Clontech Laboratories, USA) according to the manufacturer's instructions. Each reaction was run in triplicate and always included a no-template control. The mRNA expression of the genes of interest was calculated using *GAPDH* as the reference gene.

mRNA expression levels were analysed by the $2^{-\Delta Ct}$ method. The value of the relative expression of the genes of interest is given as mean ± standard deviation (SD) of three independent experiments.

The primers sequences (written 5′-3′) were: p16, Fw: CATAGATGCCGCGGAAGGT, Rv: CTAAGTTTCCC GAGGTTTCTCAGA; IL-1β, Fw: CCAGCTACGAATC TCCGACC, Rv: TGGGGTGGAAAGGTTTGGA; IL-6, Fw: CCAGCTACGAATCTCCGACC, Rv: CATGGCC ACAACAATGACG; IL-8, Fw: TCTGCAGCTCTGTG TGTGAAGG, Rv: TGGGGTGGAAAGGTTTGGA; β-a ctin, Fw: TGCTATCCCTGTACGCCTCT, Rv: GTGGTGGTGAAGCTGTAGCC; DNMT1, Fw: AGA

ACGCCTTTAAGCGCCG; Rv: CCGTCCACTGCCAC CAAAT; SIRT1, Fw: AGGCCACGGATAGGTCCATA; Rv: GTGGAGGTATTGTTTCCGGC. Primer concentration was 200 nM.

p16, DNMT1 and SIRT1 protein quantification
In HUVECs, total proteins were purified using RIPA buffer (150 mM NaCl, 10 mM Tris, pH 7.2, 0.1% SDS, 1.0% Triton X-100, 5 mM EDTA, pH 8.0) containing a protease inhibitor cocktail (Roche Applied Science, USA). Protein concentration was determined using the Bradford method (Sigma-Aldrich, Italy). Total protein extracts (30 µg) were separated by SDS-PAGE and transferred to nitrocellulose membranes (Whatman, Germany). Membranes were blocked in phosphate-buffered saline (PBS) with 0.1% Tween 20 (PBS-T) containing 5% fat-free dry milk for 1 h and then incubated overnight at 4°C with primary antibodies targeting p16(Ink4a) (1:200; sc-377,412, Santa Cruz Biotechnology, USA), pH2AX (1:1000; #9718, Cell Signaling, USA), DNMT1 (1:1000; ab19905; Abcam, UK) and SIRT1 (1:1000; ab12193, Abcam), using β-actin (1:10,000; Santa Cruz Biotechnology) or α-tubulin (1:1000; #2144, Cell Signaling) as normalizers. All primary antibodies were probed with a secondary horseradish peroxidase (HRP)-conjugated antibody (Vector, USA). A chemiluminescence assay (ECL, Amersham, USA) was used for detection; the autoradiographic films thus obtained were quantified using ImageJ2 software [36]. Independent samples *t*-test was used to analyse the differences between samples. *p* values < 0.05 were considered significant.

Genome-wide DNA methylation analysis

Genomic DNA was extracted in triplicate from CON and SEN HUVECs using Qiagen's QiAmp mini kit following the manufacturer's recommendations.

Accordingly, 1 µg DNA was bisulphite-converted using EZ DNA Methylation (Zymo Research, USA) and analysed by the Infinium HumanMethylationEPIC BeadChip (Illumina Inc., USA) according to the manufacturer's instructions. The DNA methylation levels from the EPIC kit [37] were quantified by applying the workflow described for EPIC array analysis in the Minfi v1.28.3 vignette [38]. The IlluminaHumanMethylationEPICanno. ilm10b2.hg19_0.6.0.tar.gz manifest was employed to annotate the EPIC probes.

Quality control of raw and normalised data was performed with the ShinyMethyl v1.18 package, available in Bioconductor 3.8 [39]. Data normalisation included noob background correction [40] followed by functional normalisation implemented in the Minfi

function "preprocess Funnorm" [41]. Probes matching single nucleotide polymorphism (SNP) loci were not deployed for downstream analysis and were removed by running the Minfi function "dropLociWithSnps".

DNA methylation polymorphisms (DMPs) were assigned to a genomic category following the annotation available in the IlluminaHumanMethylationEPIC manifest under the column "UCSC_RefGene_Group". Probes not assigned to any category were classified as "others". DMPs were split into hyper- and hypo-methylated sites and plotted using an in-house-developed R script.

The methylation state of differentially expressed miRNAs (see below "Small RNAseq analysis [NGS] of cells and EVs") was inferred by evaluating the probes within −2 kb of the miRNA annotation start and +2 kb of their end in the hg19 genome assembly. DMPs associated with each miRNA were deployed to build a methylation state heatmap and linked to the miRNA expression state using an in-house-developed R script.

The methylation landscape of the *DNMT1* and *SIRT1* genes was characterised by estimating the normalised beta values of all probes occurring within −2 kb of the TSS of the gene and +2 kb of the gene end coordinate. Probes were classified by the "UCSC_RefGene_Group". Probes matching each genomic window were then plotted in boxplot format using an in-house-developed R script.

Electron microscopy analysis

HUVECs were plated on Aclar film (Ted Pella Inc., USA), sectioned tangential to the substrate and examined by TEM. HUVECs were fixed for 1 h at room temperature in 2.5 glutaraldehyde solution in 0.1 M cacodylate buffer (pH 7.4), post-fixed in 1% osmium tetroxide in the same buffer for 30 min at room temperature, dehydrated in an acetone series and embedded in epoxy resin (cat. no. 43,359, Sigma-Aldrich, Italy). Ultrathin (40 nm) sections were stained with lead citrate and uranyl acetate and examined in a Philips CM12 transmission electron microscope (Philips, Netherlands) at 100 kV. Scanning electron microscopy analysis was performed on HUVECs plated on Aclar film fixed and dehydrated as described above, critical point-dried (Balzers union cpd 020), gold-coated and imaged using a Philips XL20 microscope at 15 kV. The release of multi-vesicular bodies (MVBs) was evaluated by counting their number/μm^2 of cytoplasmic area in 24 CON and 22 SEN cells.

For TEM analysis of lEVs and sEVs, EVs were adsorbed to formvar carbon-coated 200 mesh grids (Agar Scientific Ltd., UK) for 2 min, gently washed with filtered PBS and immediately fixed on the grids with 2.5% glutaraldehyde for 1 min. The grids were incubated with 2% (w/v) sodium phosphotungstate for 1 min and observed in a Philips CM10 transmission electron microscope.

EV purification and characterisation (Nanosight tracking analysis and western blotting)

When CON and SEN HUVECs reached 70% confluence in T75 flasks, they were thoroughly washed with PBS and incubated in EGM-2 containing exosome-depleted FBS (cat. no. A2720801, Thermo Fisher Scientific, USA). Conditioned medium from 8′000′000 ± 1′000′000 cells was collected after 18 h and EVs (lEVs and sEVs) were purified by ultracentrifugation [42].

EVs released from SEN and CON cells were characterised according to the Minimal Information for Studies of Extracellular Vesicles guidelines, which were developed by the International Society for Extracellular Vesicles (ISEV) in 2018 [43]. Specifically, we (i) adopted the EV nomenclature suggested by the ISEV position papers; (ii) performed basic characterisation of the EV-releasing cells before the collection of conditioned medium (culturing condition details such as passage number, seeding density, confluence at harvest have been reported); (iii) employed a variety of techniques such as size-exclusion chromatography (SEC), serial ultracentrifugation or a combination of ultracentrifugation and density gradient separation to isolate EVs; (iv) characterised and quantified isolated EVs using nanoparticle tracking assay, transmission electron microscopy and western blot analysis using well-established markers (CD63, TSG101, calnexin).

EVs were purified by centrifugation at 1′000*g* for 15 min and then at 2′000*g* for 15 min to eliminate cell debris. Supernatants were further centrifuged at 18′000*g* for 30 min to obtain the lEV pellet. The resulting supernatant was pelleted by ultracentrifugation at 110′000*g* for 70 min. The sEV pellet was washed in 3 ml PBS, centrifuged again and resuspended in PBS.

EV amount and size was measured by NanoSight tracking analysis (NTA). sEVs and lEVs were loaded into the sample chamber of an LM10 unit (NanoSight, Malvern Instruments Ltd, UK). Three 30 or 60 s videos were recorded for each sample and analysed with NanoSight NTA 3.1 software. Data were expressed as mean ± SD of the three recordings. Samples containing a large number of particles were diluted before the analysis and the relative sEV and lEV concentration was calculated according to the dilution factor. Control beads (100 and 400 nm) were supplied by Malvern Instruments. EV lysates were prepared in RIPA buffer

containing a protease inhibitor cocktail (Roche Applied Science) and quantified using the Bradford method. Next, the lysates were subjected to SDS-PAGE and transferred to nitrocellulose membranes (Whatman). Membranes were then incubated with the primary antibodies overnight at 4°C. The following primary antibodies were used: calnexin (clone C4731, Sigma-Aldrich; 1:2000 dilution), TSG101 (ab125011, Abcam; 1:1000 dilution) and CD63 (ab59479, Abcam; 1:1000 dilution). After incubation with the specific HRP-conjugated antibody (Vector; 1:10,000 dilution), the chemiluminescent signal was detected using Clarity and/or Clarity Max (Bio-Rad, Italy). The autoradiographic films thus obtained were quantified using ImageJ2 software.

In order to exclude that protein-miRNA complexes could co-precipitate with EVs during the isolation procedure, we used a combination of density gradient separation and treatment of isolated vesicles with proteinase K 20 µg/ml to confirm that miR-21-5p is truly loaded into EVs. MiR-21-5p levels were not significantly different between the two conditions (miR-21-5p relative expression; control = 0.383 ± 0.050; proteinase K = 0.259 ± 0.063; n = 3; p = 0.185), confirming the intra-vesicular presence of the miRNAs.

Data regarding the EV-related aspects of the experiments conducted on HUVECs have been deposited to the EV-TRACK knowledge base (http://evtrack.org) [44] under accession number EV190105.

RNA extraction from HUVECs and EVs

Small RNAs (< 200 nucleotides) were extracted from HUVECs and sEV and lEV pellets using, respectively Norgen's total RNA Purification Kit and Total Exosome RNA & Protein Isolation Kit (Thermo Fisher Scientific) according to the manufacturer's protocol. Purified RNA was stored at −80°C until use.

Small RNA sequencing analysis (NGS) of HUVECs and EVs

CON and SEN cells, their EVs (lEVs and sEVs) and 12 samples of sEVs purified from plasma of four young, four elderly and four centenarian subjects were subjected to small RNA sequencing. RNA for the analysis was obtained from 6 ml of media from the culture of 2.000.000 CON cells and 1.600.000 SEN cells, in triplicate. TruSeq Small RNA Library PrepKit v2 (Illumina; RS-200-0012/24/36/48) was used for library preparation according to the manufacturer's indications. Briefly, 35 ng purified RNA was linked to RNA 3′ and 5′ adapters, converted to cDNA, and amplified using Illumina primers containing unique indexes for each sample. Each library was quantified using Agilent Bioanalyzer and High Sensitivity DNA Kit (cat. no. 5067-4626, Agilent Technologies, USA) and equal amounts of libraries were pooled together. Size selection allowed keeping 130–160 bp fragments. After ethanol precipitation, the library pool was quantified with Agilent High Sensitivity DNA Kit, diluted to 1.8 pM and sequenced using NextSeq® 500/550 High Output Kit v2 (75 cycles) (Illumina; FC-404-2005) on the Illumina NextSeq500 platform.

Raw base-call data generated by the Illumina NextSeq 500 system were demultiplexed using Illumina BaseSpace Sequence Hub (https://basespace.illumina.com/home/index) and converted to FASTQ format. After a quality check with FastQC (https://www.bioinformatics.babraham.ac.uk/projects/fastqc/), the adapter sequences were trimmed using Cutadapt (http://cutadapt.readthedocs.io/en/stable/index.html), which also removed sequences < 10 nucleotides. Reads were mapped using the STAR algorithm (https://www.ncbi.nlm.nih.gov/pubmed/23104886). The reference genome consisted of human miRNA sequences from the miRbase 21 database [45]. Raw counts from mapped reads were obtained using the htseq-count script from the HTSeq tools (http://www-huber.embl.de/HTSeq/doc/overview.html).

Raw counts were further normalised using DESeq2 bioconductor package (http://bioconductor.org/packages/release/bioc/html/DESeq2.html). NGS raw data are available through European Nucleotide Archive (http://www.ebi.ac.uk/) under accession number PRJEB33703.

MiRNAs expressed in SEN cells and their EVs were identified to obtain a normalised expression above the 40th percentile in at least one sample of the group.

Statistical analysis of NGS data

NGS data were analysed using Genespring GX software v14.8 (Agilent Technologies). The miRNAs showing a differential expression were identified by comparing SEN and CON cells using a fold change ≥ 1.5 filter and FDR 5% at moderated t-test with Benjamini-Hochberg correction. A fold change ≥ 1.3 with FDR 20% or 30% was used in lEV and sEV analysis, respectively. Cluster analysis was performed using GeneSpring GX software with Manhattan correlation as a similarity measure.

Quantitative PCR of mature miRNAs

MiRNA expression was measured by qPCR using the TaqMan miRNA assay (Catalogue #4427012 Thermo Fisher Scientific) as previously described [46].

Methylome analysis of loci coding for SA miRNAs

The sequences and genomic coordinates (GRCh38) of predicted hairpin precursor miRNAs were retrieved from miRbase 21 (Supplementary Table 7). The CpG nucleotide clusters (CpG islands) associated with miRNA genes within a distance of 2 kb were identified by visual inspection of the miRNA gene neighbourhood using the University of California Santa Cruz (UCSC) Genome Browser. Putative proximal promoter regions within 2 kb of the TSS were obtained from the database http://bicresources.jcbose.ac.in/zhumur/pirnaquest/.

Computational prediction of SA miRNA targets

To gain further insights into the relationship between SA miRNAs and the DNA methylation pattern of SEN cells, we explored the ability of SA miRNAs to target DNMT1 and/or SIRT1 using the StarBase v3.0 public platform (http://starbase.sysu.edu.cn) [47]. TargetScan, starBase and miRTarBase were used to predict potential miRNA-DNMT1/SIRT1 interactions. DIANA-mirPath v3 and Ingenuity Pathway Analysis (IPA) were used to identify the pathways targeted by SA miRNAs.

Uptake of sevs released from SEN HUVECs

An amount of 2×10^{11} sEVs has been collected from 6′000′000 of SEN HUVECs. sEVs released from SEN HUVECs were fluorescently labelled using PKH67 membrane dye (Sigma-Aldrich). Labelled sEVs were washed in 10 ml PBS, collected by ultracentrifugation and resuspended in PBS. Next, 10^9 sEVs were incubated with 5×10^4 recipient CON HUVECs for 4, 12, 18 and 24 h. An incubation time of 18 h was established to be optimal for sEV uptake by CON cells. Then, 10^9 sEVs released from SEN cells were incubated with 5×10^4 recipient CON HUVECs.

CON HUVECs were also treated for 18 h with sEVs transfected with miR-217 and miR-21-5p inhibitors (respectively, MH12774 and MH10206, Thermo Fisher Scientific). The transfection process was promoted by Exo-Fect kit (System Bio, USA) according to the manufacturer's recommendations. Briefly, sEVs were prepared for transfection by combining Exo-Fect solution, miRNA inhibitors, PBS and purified sEVs. The transfection solution was incubated at 37°C for 10 min and then put on ice. To stop the reaction, the EXoQuick-TC reagent supplied in the kit was added. After centrifuging for 3 min at 140,000 rpm, the supernatant was removed. The transfected sEVs pellet was suspended in 300 μl PBS and 150 μl of transfected sEVs were added to each well. The same method was used to load non-human cel-mir-39 into sEVs to assess the possibility of delivering miRNAs and their inhibitors through sEVs.

Assessment of the effects induced by SEN sEVs on CON cells

Immunofluorescence and western blot analysis of SIRT1 and DNMT1

CON HUVECs were seeded in BD Falcon chamber slides (cat. no. 354104; Falcon, USA) and treated with SEN sEVs and SEN sEVs transfected with miR-217 and miR-21-5p inhibitors as described above. Cells were washed twice with PBS and then fixed in 4% paraformaldehyde in PBS for 15 min at room temperature. After three washes in PBS they were incubated with 0.3% Triton X-100 in 2.5% bovine serum albumin (BSA) for 1 h at room temperature and then with KI67 antibody (dilution 1:150; Dako, Denmark), in 2.5% BSA overnight at 4°C. Cells were washed in PBS and incubated with secondary anti-rabbit Alexa Fluor 488 antibody (cat. no. 111-545-003, Jackson Laboratories, USA; dilution 1:200), at room temperature in 2% BSA for 1 h. After a wash in PBS, cells were stained with nuclear HOECHST 33,342 (cat. no. H-3570; Molecular Probes, USA) at 1:10,000 dilution in PBS for 5 min, coverslipped with Vectashield mounting medium (H-1200, Vector Laboratories) and viewed in a fluorescence microscope. Omission of the primary antibody resulted in lack of labelling, confirming the specificity of the antibody. The presence of senescence-associated heterochromatin foci (SAHF) was assessed by measuring the coefficient of variation (CV) of the HOECHST staining intensity in each nucleus. At least 200 nuclei have been assessed for each condition and each replicate using the using the CellProfiler image analysis software, version 3.1.9 [48].

The Ki67 proliferative index was expressed as a percentage based on the number of Ki67-positive cells.

Expression levels of PCNA and cyclins A, B1, D1

OneScript® cDNA Synthesis Kit was used to reverse-transcribe 1 μg of purified RNA according to the manufacturer's instructions. qPCR reactions were conducted on the Rotor Gene Q 5plex HRM apparatus in a 10 μl total reaction volume using TB Green Premix Ex Taq II (Clontech Laboratories) according to the manufacturer's recommendations. Each reaction was run in triplicate and included no-template controls. The mRNA expression of the genes of interest was calculated using GAPDH as the reference gene.

Relative mRNA levels were calculated with the $2^{-\Delta Ct}$ method. Relative expression values were reported as mean ± SD of three independent experiments.

Primer sequences (written 5′-3′) were: PCNA, Fw: CGGATACCTTGGCGCTAGTA, Rv: CACAGCTGT ACTCCTGTTCTGG; Cyclin D1, Fw: CCCTCGGT GTCCTACTTCAA, Rv: AGGAAGCGGTCCAGGTAG TT; Cyclin A, Fw: TTGAAGAAATATACCCCCCAG, Rv: AATGATTCAGGCCAGCTTTG; Cyclin B1, Fw: TTGGTGTCACTGCCATGTTT, Rv: TAAGCAAAAA GCTCCTGCTG.

Annexin V assay

Apoptosis was evaluated by annexin V staining followed by flow cytometry. Briefly, CON cells and CON cells treated with 10^9 SEN sEVs were plated in a 12-well plate at a density of 2×10^5 cells/well. Apoptosis was evaluated by staining cells with Annexin V and 7-AAD followed by fluorescence flow cytometry as described in Giuliani et al. [46]. The results were expressed as percentage of apoptotic cells out of total live cells.

Methylation status of MIR21 locus

Quantitative analysis of DNA methylation of the *MIR21* TSS200 region was performed using the EpiTYPER assay (Agena). Briefly, genomic DNA was bisulphite converted and the region chr17:57,918,197-57,918,709 (GRCh37/ hg19 assembly) was amplified using the following primers: Fwd: aggaagagagTTTATATAAGTGAAAGGATATTGG AGAGA; Rev: cagtaatacgactcactatagggagaaggctAAATAC CAAAATATCAAACAACCCA. PCR products were then processed according to standard EpiTYPER protocol. Each sample was analysed in triplicate.

Plasma samples and EV isolation

Plasma samples were obtained from 12 healthy subjects enrolled for the study. Subjects were considered healthy if they did not present type 1 or 2 diabetes, liver diseases, renal failure, history of cancer, neurodegenerative disorders, infectious or autoimmune diseases. Samples were collected at IRCCS INRCA (Ancona) and at Sant'Orsola University Hospital (Bologna). The procedure was approved by the respective ethics boards (Prot. no. 2006061707, amended on 08/11/2011). Written informed consent was collected from all participants. EVs were purified from 500 μl of plasma by qEVoriginal column (IZON, USA) according to the manufacturer's indications.

Statistical analysis

Principal component analysis (PCA) with varimax orthogonal rotation and Kaiser normalisation was performed to investigate possible common trends in the miRNAs contained in circulating EVs. Only miRNAs that were detected in at least one subject were included in the analysis. Scree plots and the Kaiser-Meyer-Olkin (KMO) test were applied to evaluate the suitability of the correlation matrix. Anti-image-correlation was assumed as adequate for KMO > 0.5. The number of factors to be retained was determined by examining the scree plots. Each retained factor was assigned a score, determined as the linear combination of each miRNA weighted by its respective PCA loading. Factor scores were tested for normality using the Shapiro-Wilk test and compared by one-way ANOVA followed by Tukey's multiple comparison test for pairwise comparisons. p values < 0.05 were deemed significant.

Results

Characterisation of the senescence status of HUVECs

HUVEC senescence was characterised by analysing a number of well-established senescence biomarkers in non-senescent (control, CON) and senescent (SEN) HUVECs.

Compared with CON cells, SEN cells were characterised by growth arrest, which was documented by reduced cumulative population doublings (cPDs) (Figure 1(a)), progressive telomere shortening (Figure 1(b)), increased SA β-gal activity (Figure 1 (c)), up-regulation of the cell cycle regulator p16 (INK4a) both at the transcriptional and the protein level (Figure 1(d,d')); up-regulation of phospho-histone H2AX (pH2AX), a biomarker of persistent DNA damage [49] (Figure 1(e)) and significantly increased mRNA transcription of the pro-inflammatory SASP components interleukin (IL)-1β, IL-6 and IL-8 (Figure 1(f–h)). A similar model of replicative senescence was replicated also in HAECs. Moreover, we established a model of drug-induced senescence by treating HUVECs and HAECs with 50 nM doxorubicin for 24 h. The characterisation of these additional models is reported in Supplementary Figure 1.

Human cell senescence is also marked by progressive, widespread genomic hypomethylation and focal hypermethylation at specific CpG sites [50]. Further characterisation and comparison of the epigenetic profile of SEN and CON cells demonstrated a differential methylation state at 335′495 CpG sites; in particular,
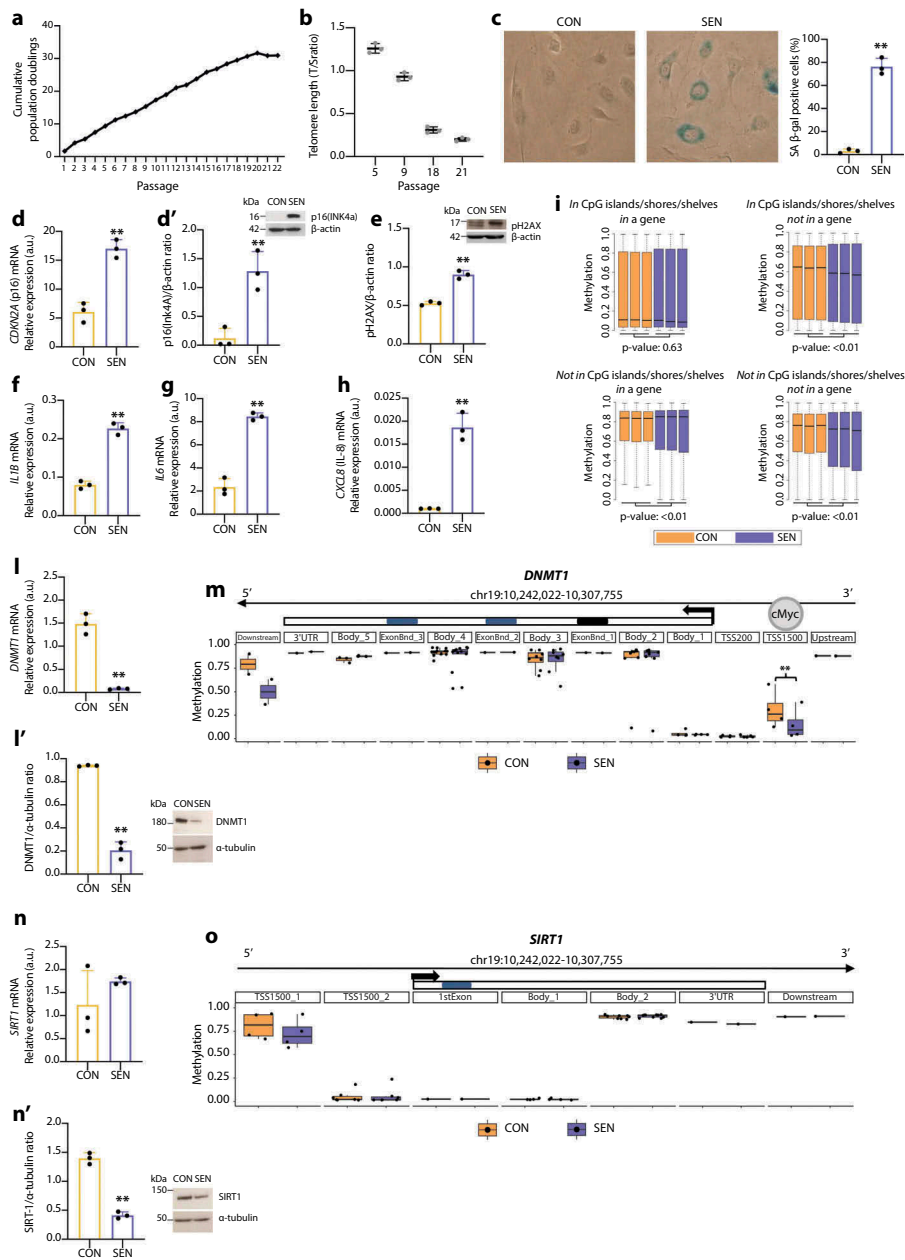
Figure 1. Characterisation of replicative senescence in human umbilical vein endothelial cells (HUVECs). (a) Cumulative population doubling (cPD) curves. (b) Telomere/single copy gene ratio (T/S) in DNA from HUVECs at different passages. (c) Representative positivity and quantification of the SA β-Gal staining in control (CON, < 10%) and senescent (SEN, > 60%) cells. (d) mRNA relative expression. (d') Western blot and densitometric analysis of p16(Ink4a) in CON and SEN cells. Protein expression values are reported as p16(Ink4)/β-actin ratio. (e) Western blot and densitometric analysis phospho-histone H2AX (pH2AX) in CON and SEN cells. Protein expression values are reported as pH2AX/β-actin ratio. (f) mRNA relative expression of interleukin (IL)-1β, (g) IL-6, (h) IL-8. (i) Boxplots of DNA methylation values of InfiniumEPIC probes in CON and SEN triplicates. The probes were divided in four groups according to their genomic location and t-test was applied to each group in order to compare mean beta values between CON and SEN. (l) mRNA relative expression. (l') Western blot and densitometric analysis of DNMT1 in CON and SEN cells. Protein expression values are reported as DNMT1/α-tubulin ratio. (m) Methylation status of CpGs among a genomic region covering the DNMT1 gene ± 2kb. The region is split in multiple windows based on Illumina Infinium annotation assigned to each CpG as reported in the Methods section. Methylation status of each window is represented with a boxplot. Each dot corresponds to the mean B value of an annotated CpG across the three replicates. Blue: SEN cells; Orange: CON cells. **, q-val < 0.01. Scale of the Methylation status corresponds to the B value. (n) mRNA relative expression. (n') Western blot and densitometric analysis of SIRT1 in CON and SEN cells. Protein expression values are reported as SIRT1/α-tubulin ratio. (o) Methylation status of CpGs among a genomic region covering the SIRT1 gene ± 2kb. The region is split in multiple windows based on Illumina Infinium annotation assigned to each CpG as reported in the Methods section. Methylation status of each window is represented with a boxplot. Each dot corresponds to an annotated CpG. Methylation status expressed in B value. Blue: SEN cells; Orange: CON cells. **, q-val < 0.01. For qPCR and western blot analysis data from three independent experiments are represented as mean ± SD. **, p < 0.01 from paired t-tests.

SEN cells showed significant hypomethylation in CpG island/shore/shelf regions located in intergenic regions and significant hypermethylation of non-CpG sites inside genes (Figure 1(i)).

Since DNMT1 and SIRT1 co-operate in maintaining the methylation pattern [15], we analysed their mRNA and protein levels and the methylation state of their loci in SEN and CON cells. We found that DNMT1 mRNA and protein levels were down-regulated in SEN cells (Figure 1(l,l')), even though methylation analysis disclosed significant loss of methylation at the *DNMT1* transcription start site (TSS)-1500 promoter region, which according to the ENCODE ChIP-Seq data binds the transcription factor c-MYC (Figure 1(m)). SIRT1 mRNA levels were similar in CON and SEN cells (Figure 1(n)); in contrast, the SIRT1 protein level was significantly reduced in SEN compared with CON cells (Figure 1(n')), despite the similar methylation state of SEN and CON cells (Figure 1(o)). These data suggest that during HUVEC replicative senescence DNMT1 and SIRT1 protein levels are modulated by post-transcriptional regulatory mechanisms.

Analysis of the senescence biomarkers confirmed that HUVECs aged in culture exhibit a senescent phenotype characterised by most of the established hallmarks of ageing [51]. This model can, therefore, be considered as an archetypal "*in vitro* model" of cellular senescence.

### Senescent HUVECs release more sEVs than control cells

We characterised the structure and content of EVs released from SEN and CON cells according to Minimal Information for Studies of Extracellular Vesicles guidelines, which were proposed by the International Society for Extracellular Vesicles (ISEV) in 2018 [43]. Scanning electron micrograph analysis of EVs released from SEN and CON cells demonstrated a significantly greater number of vesicular bodies emerging from the cell surface of SEN cells (Figure 2(a,b)). To purify these small (sEVs) and large (lEVs) EV fractions, sEVs and lEVs were collected after ultracentrifugation and further characterised by Nanoparticle Tracking Analysis (NTA), transmission electron microscopy (TEM) and western blot analysis of some relevant biomarkers. Representative distribution plots of sEVs and lEVs released from CON (Figure 2(c,d)) and SEN cells (Figure 2(c',d')) indicated that sEVs and lEVs had a different size distribution. Representative TEM images of sEVs and lEVs purified from CON and SEN (Figure 2 (e)) confirm their different size. Analysis of calnexin, TSG101 and CD63 membrane protein expression by western blotting demonstrated the efficient separation of supernatant-derived EV sub-populations: sEVs were positive for the exosomal markers CD63 and TSG101, whereas lEVs were positive for the endoplasmic reticulum marker calnexin (Figure 2(e')). Comparison of their number demonstrated that SEN and CON cells released more sEVs than lEVs. Moreover, NTA assay revealed that SEN cells released a threefold, significantly greater amount of sEVs (*t*-test for unpaired samples, $p < 0.01$) but a similar number of lEVs (Figure 2(f)) compared with CON cells. Notably, the size of sEVs and lEVs released from either cell type was not significantly different (Figure 2(g)). The increased release of sEVs from SEN cells was confirmed also in HUVECs undergoing drug-induced senescence following treatment with doxorubicin, and in HAECs undergoing both replicative and drug-induced senescence (Supplementary Figure 1d and 1d').

To further substantiate these data, multi-vesicular bodies (MVBs), a specialised subset of endosomes that contain sEVs, were identified and quantified in TEM images of SEN and CON HUVECs (Figure 2 (h)). A significantly greater number of MVBs at different stages of maturation was detected in SEN compared to CON cells (*t*-test for unpaired samples, $p < 0.01$) (Figure 2(i)).

MiRNome analysis of CON and SEN HUVECs and their cognate EVs

The expression of the whole miRNome was analysed in triplicate in SEN and CON cells and cognate lEVs and sEVs from different pools of donors. The list of all miRNAs thus detected is reported in Supplementary Table 1. The miRNAs showing a significant differential expression in sEVs and lEVs released from SEN cells and in SEN compared with CON cells are listed in Figure 3(a–c), respectively. The miRNAs showing a differential expression in sEVs, lEVs and their parental SEN cells, the relevant fold changes, Benjamini-Hochberg adjusted *p* values and the normalised expression in SEN and CON are reported in Supplementary Tables 2–4. The miRNAs showing a differential expression were used to cluster miRNAs and samples. The resulting heatmaps – of the miRNAs showing significant de-regulation in sEVs released from SEN cells, of the miRNAs showing significant de-regulation in lEVs released from SEN cells, and of the miRNAs showing significant de-regulation in SEN cells – are reported in Supplementary Figure 2a, 2b and 2c, respectively. Supplementary Tables 5 and 6 report miRNAs showing differential expression between SEN cells and their cognate sEVs and lEVs, respectively. As previously
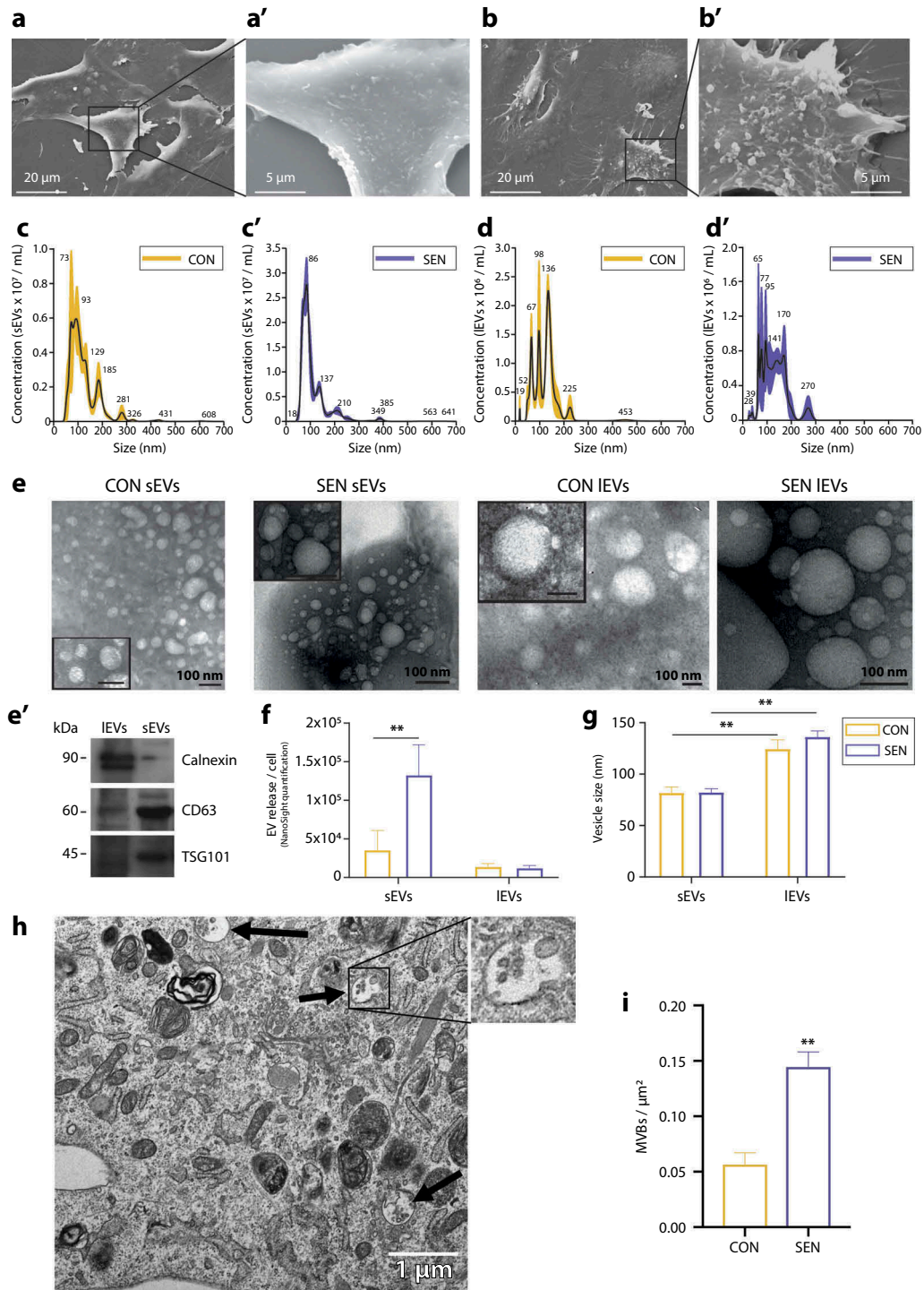
Figure 2. Characterisation of sEVs and lEVs released from CON and SEN cells. (a,a') SEM analysis of extracellular vesicles emerging from the CON cell plasmalemma. (b,b') SEM analysis of extracellular vesicles emerging from the SEN cell plasmalemma. Scale bars of 20 and 5 μm are applied for low and high magnification, respectively. (c) Average size distribution curve of sEVs released from (c) CON and (c') SEN cells. (d) Average size distribution curve of lEVs released from (d) CON and (d') SEN cells. EVs size was determined by NTA Nanoparticle Tracking Assay (NTA). Three 60 s videos were recorded for each sample, and NTA analysis settings kept constant between samples. The average concentration of vesicles was plotted against their size, with the black lines and the colour areas representing the fitting curve and the error bar, respectively. (e) Representative TEM analysis of sEVs and lEVs released into the culture media by CON and SEN cells with a scale bar of 100 nm. (e') Representative western blot analysis of calnexin, TSG101 and CD63 in isolated lEVs and sEVs. (f) Comparison of the number of sEVs and lEVs released per cell in CON and SEN cells as determined by NTA. (g) Comparison of the size of sEVs and lEVs released from CON and SEN cells as determined by NTA. Data from three independent experiments are represented as mean ± SD. **, $p < 0.01$ from paired t-tests. (h) Representative TEM photomicrograph of multi-vesicular bodies (MVBs) of SEN cells with a scale bar of 1 μm. (i) Comparison of the number of MVBs per μm² measured in n = 24 TEM images of CON and SEN cells. Data are represented as mean ± SD. **, $p < 0.01$ from unpaired t-test.
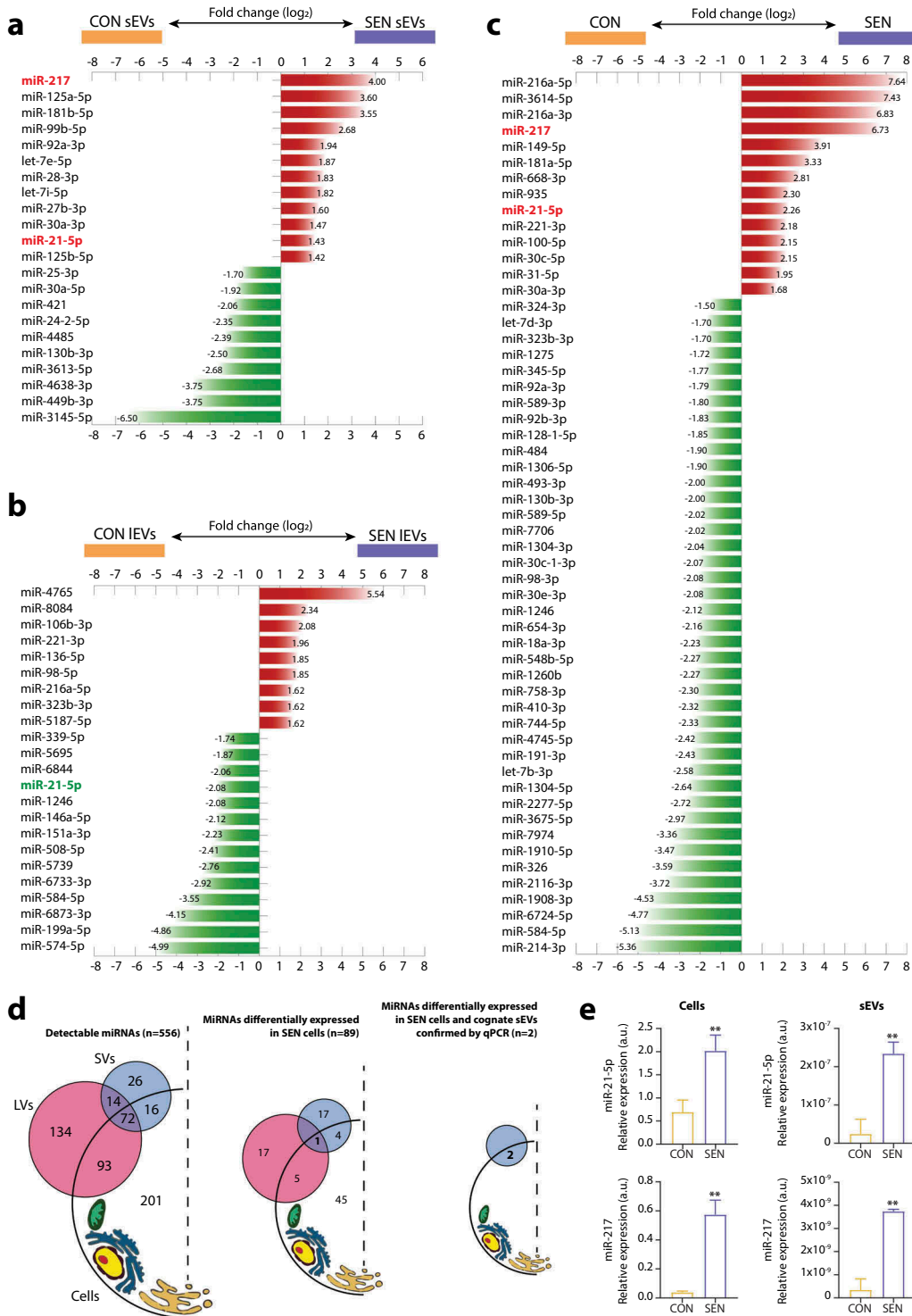
Figure 3. MiRNAs showing differential expression in SEN cells and cognate sEVs and lEVs. Bar charts reporting the (log₂) fold changes of the miRNAs showing a differential expression (a) in sEVs released from SEN cells, (b) in lEVs released from SEN cells and (c) in SEN cells. The miRNA de-regulation trend is indicated by bar colour; red, over-expression; green, under-expression in SEN sEVs/ SEN lEVs/SEN cells compared with CON sEVs/CON lEVs/CON cells, respectively. Only miR-21-5p (highlighted in red) showed significant SA de-regulation in SEN cells and cognate sEVs and lEVs. Data from small RNAseq of $n = 3$ independent replicates for each condition. MiRNAs showing a differential expression were identified by comparing SEN and CON cells using a fold change ≥ 1.5 filter and FDR 5% at moderated t-test with Benjamini-Hochberg correction. A fold change ≥ 1.3 with FDR 20% or 30% was used in lEV and sEV analysis, respectively. (d) Summary of the results of small RNAseq analysis on CON and SEN cells and cognate sEVs and lEVs. Briefly, 556 miRNAs were detected in at least one compartment (cells, sEVs and lEVs). Of the 355 miRNAs carried by EVs, only 42 (12%) were selectively packaged in sEVs; 86 (24%) were carried by both lEVs and sEVs and 227 (64%) were found only in lEVs. None of the miRNAs shared a common SA modulation trend in lEVs and sEVs. Only miR-21-5p was significantly de-regulated in both sEVs and lEVs released from SEN cells; however, it was over-expressed in sEVs and under-expressed in lEVs from the same SEN cell pool. (e) qPCR validation analysis of miR-21-5p and miR-217 in different pools of SEN cells and their cognate sEVs. Data from $n = 3$ independent experiments are represented as mean ± SD. **, $p < 0.01$ from unpaired t-test.

Table 1. MiRNAs commonly de-regulated in SEN cells and their EVs.

miRNA	Cells	sEVs	lEVs	CON normalised expression (log2)			SEN normalised expression (log2)		
				Cells	sEVs	lEVs	Cells	sEVs	lEVs
hsa-miR-21-5p	+	+	-	9.70	4.78	5.03	11.60	7.33	4.40
hsa-miR-217	+	+		5.88	2.11	0.95	9.38	5.47	0.31
hsa-miR-30a-3p	+	+		4.13	0.00	0.00	4.89	0.56	0.40
hsa-miR-130b-3p	-	-		7.05	1.82	1.11	6.06	0.50	0.82
hsa-miR-92a-3p	-	+		11.19	2.44	4.56	10.35	3.40	4.70
hsa-miR-221-3p	+		+	8.76	3.64	3.19	9.89	3.20	1.17
hsa-miR-216a-5p	+		+	2.09	0.98	0.00	5.02	0.07	0.70
hsa-miR-323b-3p	-		+	3.68	0.00	0.00	2.92	0.00	0.70
hsa-miR-584-5p	-		-	7.99	1.18	2.32	5.63	0.00	0.49
hsa-miR-1246	-		-	2.41	0.00	1.06	1.33	0.00	0.00

For each miRNA and condition, the log2 normalised expression values are reported for cells, sEVs, and lEVs. The reader is referred to Supplementary Tables 2–6 for detailed data on miRNAs differentially regulated across the various sample types. sEVs, small extracellular vesicles; lEVs, large extracellular vesicles; (+) over-expressed; (-) under-expressed.

reported [52], the levels of miRNAs loaded onto EVs are significantly lower compared to their parent cells.

Overall, 22 miRNAs were differentially expressed in sEVs released from SEN cells; of these, 12 (55%) were up-regulated and 10 (45%) were down-regulated (Figure 3(a)). Of the 55 miRNAs that were significantly modulated in SEN compared with CON cells 14 were up-regulated (25%) and 41 (75%) were down-regulated (Figure 3(c)). Only five miRNAs – miR-21-5p, miR-217, miR-30a-3p, miR-130b-3p and miR-92a-3p – were differentially expressed in sEVs and parental SEN cells (Table 1 and Figure 3(d)). Their analysis in a different batch of cells from a different pool of donors confirmed these findings. qPCR analysis confirmed the NGS data for miR-21-5p and miR-217 in cells and their sEVs (Figure 3(e)), whereas no differential expression was detected for miR-30a-3p, -92a-3p and -130b-3p (data not shown). The up-regulation of miR-21-5p and miR-217 in SEN cells and their cognate sEVs was confirmed also in HAECs undergoing replicative senescence, as well as in the model of drug-induced senescence established in both HUVECs and HAECs (Supplementary Figure 1(e,f,e',f')).

The results of miRNome analysis of SEN cells and cognate sEVs and lEVs are summarised in Figure 3(d).

miRNAs capable of targeting DNMT1 and SIRT1 and showing a differential expression in SEN cells and cognate EVs

To unravel the complex interaction between miRNA expression and methylation state in cells with the senescent phenotype we tried to establish which miRNAs capable of targeting DNMT1 and SIRT1 were significantly de-regulated in SEN cells and cognate EVs. Of the 12 miRNAs that were up-regulated in SEN sEVs, 4 – including miR-21-5p and miR-217 (Figure 4(a)) – were capable of targeting DNMT1 and/or SIRT1, whereas none of the nine miRNAs up-regulated in SEN lEVs

were able to target DNMT1 and/or SIRT1 (Figure 4(b)). Five of the 14 miRNAs showing up-regulation in SEN cells were able to target DNMT1 and/or SIRT1; of them, only miR-21-5p and miR-217 were also up-regulated in SEN sEVs (Figure 4(c)).

Surprisingly, SEN lEVs carried no up-regulated SA miRNAs targeting DNMT1 and/or SIRT1.

Altogether, these data suggest that miR-21-5p and miR-217 are the only miRNAs shuttled by SEN sEVs that are also expressed in SEN cells and are capable of targeting DNMT1 and SIRT1. This observation, coupled with the finding that SEN cells released three times more sEVs than CON cells, prompted further investigation on the effects of SEN sEVs on CON cells.

Methylation state of the loci coding for miRNAs showing differential expression in SEN and CON cells

To clarify whether miRNA expression in SEN cells was epigenetically regulated, we analysed the methylation state of the genetic loci encoding the miRNAs showing differential expression in SEN and CON cells. The genomic locations and sequences of the miRNAs showing significant down- or up-regulation in SEN cells are reported in Supplementary Table 5.

The methylation state was obtained by conducting a global methylation analysis, assessing CpG site methylation within 2000 bp upstream and downstream of each miRNA transcription start site (TSS).

The methylation changes observed at the loci encoding the 55 miRNAs showing significant de-regulation in SEN cells are reported in Figure 5(a). Principal component analysis (PCA) revealed significantly different methylation profiles of the miRNA genes that were differentially expressed in SEN compared with CON cells (Figure 5(b)); however, only about 50% showed SA methylation consistent with
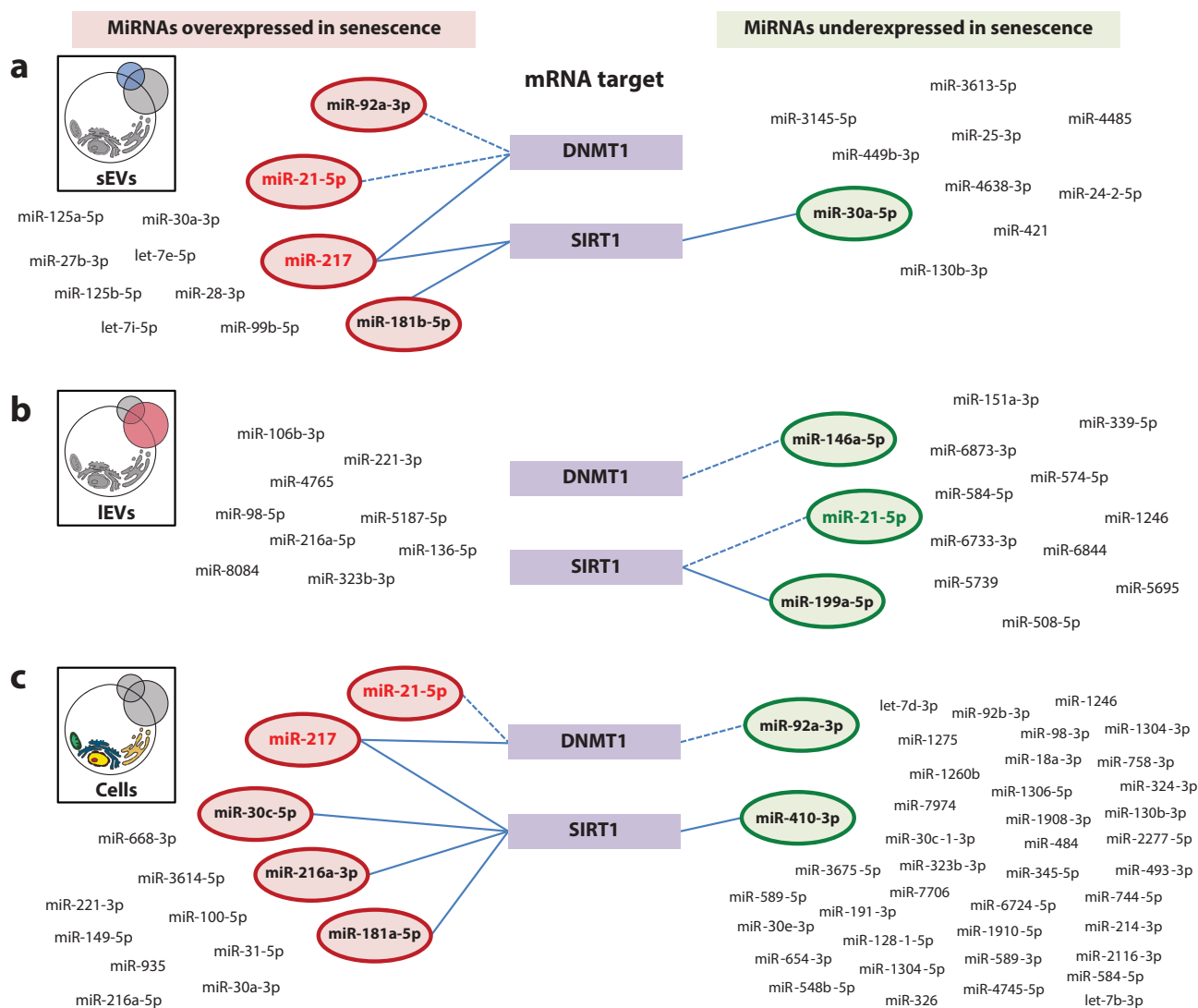
Figure 4. MiRNAs showing differential expression in SEN cells and their cognate sEVs and lEVs targeting DNMT1 and/or SIRT1. (a) MiRNAs showing over and under-expression in SEN sEVs compared with CON sEVs, (b) in SEN lEVs compared with CON lEVs, (c) and in SEN compared with CON cells targeting DNMT1 and/or SIRT1. Straight lines represent miRNA-mRNA interaction based on bioinformatic prediction from three different algorithms. Dotted lines represent miRNAs reducing DNMT1 activity by binding to its catalytic site, according to the report from Zhang et al. [54].

SA expression changes (Figure 5(c)). Of the miRNAs that exhibited differential methylation in SEN and CON cells, only miR-21-5p showed concordant DNA demethylation and RNA over-expression both in SEN cells and SEN sEVs (Figure 5(c)). The methylation state of miR-217 was not evaluated, because no CpG in the neighbourhood of its locus was covered by genome-wide methylome analysis.

Overall, in half of the loci encoding the miRNAs showing differential expression in SEN cells, the gene methylation and expression data were not consistent, suggesting that additional post-transcriptional regulation mechanisms are involved in the modulation of SA miRNAs. These data support the hypothesis of a complex interaction among different epigenetic mechanisms in inducing and maintaining a senescent phenotype.

SEN sEVs significantly reduce CON cell DNMT1 and SIRT1 levels and proliferation markers

Previous work has shown that miR-21-5p directly targets SIRT1 and indirectly down-regulates DNMT1 by targeting the *RASGRP1* gene, an upstream component of the Ras-MAPK pathway that regulates DNMT1 expression [53]. MiR-21-5p has also been demonstrated to inhibit DNMT1 activity by binding to its catalytic site [54]. As regards miR-217, it directly
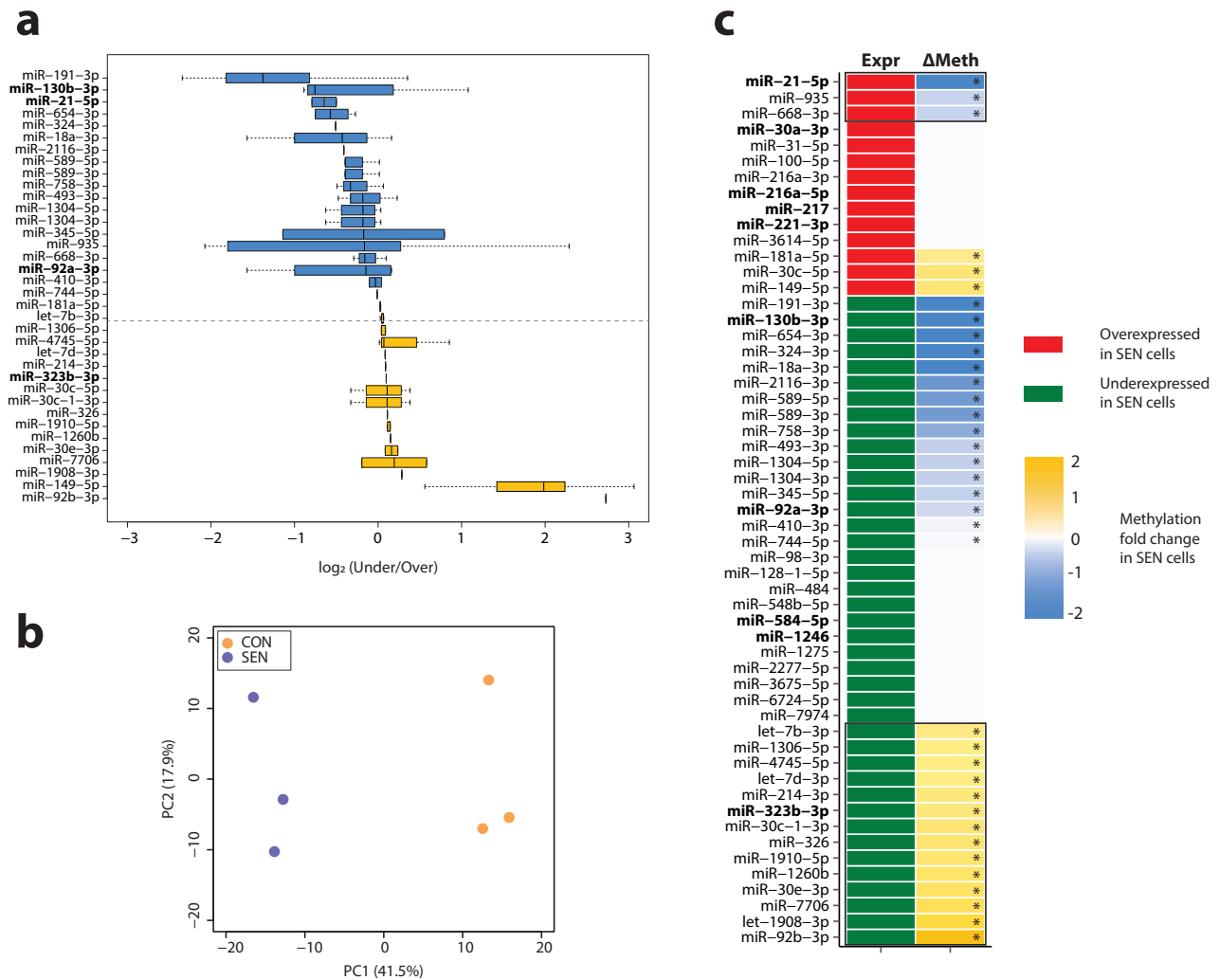
Figure 5. Methylation state of the loci encoding miRNAs showing a differential expression in SEN compared with CON cells. (a) Box plots showing the log2 B value fold change in SEN vs CON cells at CpG loci located within the coding regions of selected miRNA. Yellow: over-methylated CpG sites (median value); Blue: under-methylated CpG sites (median value). (b) PCA of DNA methylation values in CON and SEN triplicates, considering only the InfiniumEPIC probes mapping within 2000 bp upstream and downstream the miRNAs differentially expressed in SEN vs CON. The percentage of variance explained by the first and the second principal components is reported in brackets. (c) Figure summarising expression levels and methylation state of miRNAs showing a differential expression in SEN cells. MiRNAs showing expression concordant with the methylation state are enclosed in black lines. MiRNAs commonly de-regulated in SEN cells and their cognate sEVs and lEVs are highlighted in bold. Significantly methylated or unmethylated miRNAs are marked with (*).

targets DNMT1 in fibroblasts [55] and SIRT1 in endothelial cells [56].

Based on these findings, we assessed the functional potential of sEVs released from SEN cells to modulate DNMT1 and/or SIRT1 in CON cells. To do this, CON cells were treated with sEVs released from SEN cells. Their uptake was demonstrated by tracking sEVs with a fluorescent, membrane-permeable dye (Figure 6(a)). The possibility of delivering small RNAs through sEVs was further tested by loading non-human cel-miR-39 onto sEVs released from SEN cells. The latter treatment resulted in qPCR-detectable levels of cel-miR-39 in CON cells,

confirming the delivery of a considerable amount of cargo in this setting (Figure 6(b)). Treatment of CON cells with sEVs from SEN cells resulted in a significantly increased expression of miR-21-5p and miR-217 (Figure 6(c)). To evaluate whether this observation was related to the intracellular delivery of the copies of miR-21-5p and miR-217 loaded onto SEN sEVs or to the induction of the transcription of the two miRNAs in the recipient cells, we assessed the levels of pri-miR-21 using SEN cells as a positive control. Treatment of CON cells with SEN sEVs was not able to induce the up-regulation of pri-miR-21 (Figure 6(d)).
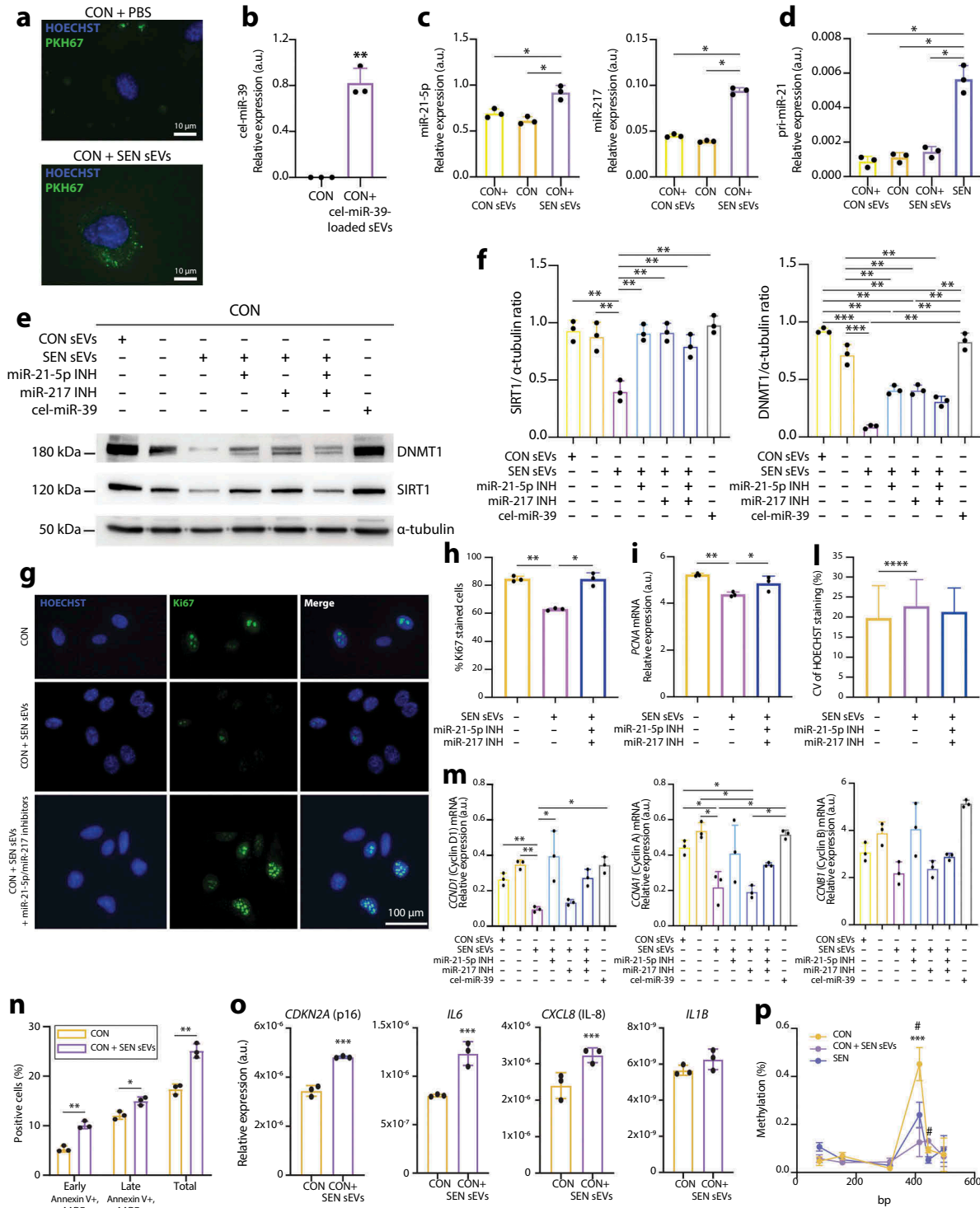
Figure 6. Modulation of DNMT1/SIRT1 and of replicative rate biomarkers induced in CON cells by treatment with sEVs released from SEN cells. (a) Immunofluorescence staining showing effective uptake in CON of sEVs released from SEN cells. sEVs were labelled with PKH67 green fluorescent dye. Scale bars of 10 μm are applied. (b) qPCR analysis of cel-miR-39 in CON cells treated with sEVs loaded with cel-miR-39. (c) qPCR analysis of miR-21-5p and miR-217 in CON cells treated with sEVs from SEN and with sEVs from CON. (d) qPCR analysis of pri-miR-21 in CON cells treated with sEVs from SEN and with sEVs from CON, and in SEN cells. (e) Western blots showing modulation of DNMT1 and SIRT1 protein levels in CON cells treated with sEVs released from SEN without and with miR-217 and miR-21 inhibitors. CON sEVs and cel-miR-39 were used as negative controls to exclude non-specific effects due to the treatment with sEVs and miRNAs, respectively. (f) Densitometric analysis of SIRT1 and DNMT1 protein level modulation in CON cells treated with sEVs released from SEN without and with miR-217 and miR-21 inhibitors. The effects of sEVs on SIRT1 and DNMT1 appear to be miR-21-5p- and miR-217-dependent. Protein expression values are reported as SIRT1/α-tubulin and SIRT1/α-tubulin ratios. (g) Immunofluorescence Ki67 staining of CON cells CON cells treated with sEVs released from SEN without and with miR-217 and

Treatment of CON cells with SEN sEVs also significantly reduced the expression of DNMT1 and SIRT1 (Figure 6(e,f)). This effect was not reproducible by treating CON cells with CON sEVs and was significantly rescued when SEN sEVs were loaded with miR-21-5p and miR-217 inhibitors, alone or combined (Figure 6(e,f)). This suggests that both miRNAs are involved in DNMT1 and SIRT1 modulation.

A reduction in CON cell replication ability, demonstrated by reduced Ki67 staining, was observed during the 18-h treatment with SEN sEVs (Figure 6(g, h)) and was associated with reduced PCNA (Figure 6 (i)), cyclin D1 and cyclin A (Figure 6(m)) expression. Importantly, the effects of SEN sEV uptake in CON cells appeared to be miR-21-5p-dependent. A trend towards the reduction of cyclin B mRNA was observed in treated CON cells, even if it did not reach statistical significance (Figure 6(m)). Notably, CON cells treated with SEN sEVs showed an increased formation of SAHF, as confirmed by the increased CV of the HOECHST staining intensity. This effect was not rescued by the addition of miR-21-5p/miR-217 inhibitors (Figure 6(l)).

We then performed Annexin V and 7-AAD staining and flow cytometry to quantify the rate of apoptosis in CON cells after treatment with SEN sEVs. As shown in Figure 6(n), the percentage of cells undergoing early (Annexin V+/7-AAD-) and late (Annexin V+/7-AAD +) apoptosis was significantly increased in CON cells treated with SEN sEVs compared with CON cells, demonstrating that SEN sEVs are able to induce apoptosis in CON cells after 18-h treatment.

Next, we evaluated whether treatment with SEN sEVs was capable of inducing a senescent phenotype in CON cells. A significant increase in the expression of p16, IL-6 and IL-8 mRNAs was observed, whereas no significant up-regulation of IL-1β mRNA was reported (Figure 6(o)).

As a final experiment, we assessed the methylation level of *MIR21* locus in CON and SEN cells, and in CON cells treated with SEN sEVs using the quantitative EpiTYPER assay. Treatment of CON cells with SEN sEVs was able to induce a significant demethylation of the fourth CpG site of the amplicon (corresponding to the microarray probe cg02515217, located in the TSS200 region), resulting in methylation levels comparable to those observed in SEN cells (Figure 6(p)).

Overall, SEN sEVs proved capable of modulating apoptosis and a number of key senescence features, i. e. cellular proliferation, SASP acquisition and DNMT1/SIRT1 expression. The effects on proliferation appear to be at least partly miR-21-5p-dependent, whereas those on DNMT1-SIRT1 expression appear to be dependent on miR-21-5p as well as miR-217. The down-regulation of DNMT1 in CON cells treated with SEN sEVs induced a partial demethylation of the *MIR21* locus which, however, was not associated to an increased transcription of miR-21-5p in treated cells.
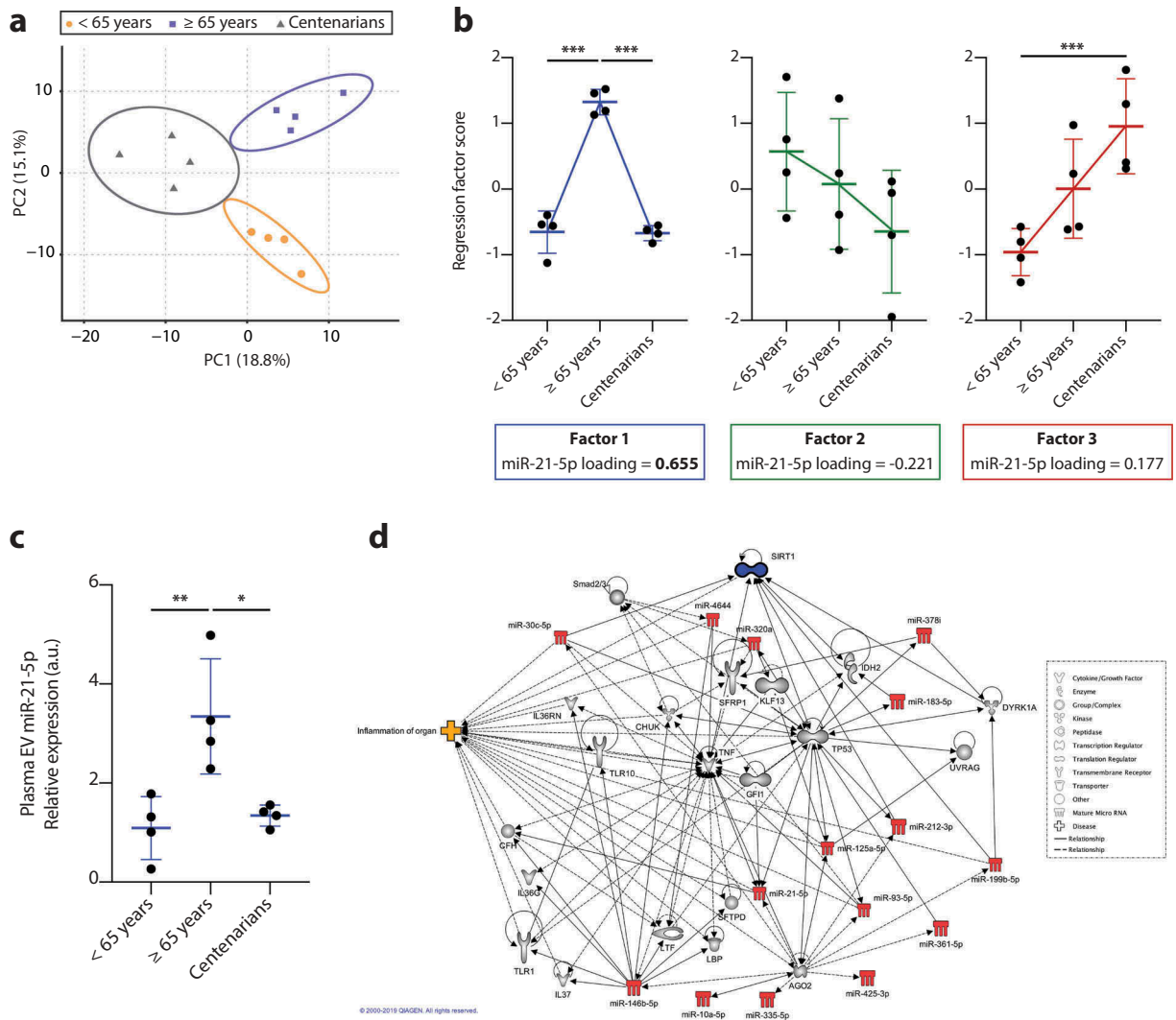
miRNA profiling in circulating EVs from healthy adults of different ages

The finding that SEN cells can spread pro-senescence signals via miRNAs carried by their sEVs suggested a further experiment, where EVs purified from plasma of 12 healthy adult donors of different ages were subjected to NGS analysis. Donors were grouped into three gender-matched age groups, young ($n = 4$), elderly ($n = 4$) and centenarians ($n = 4$), whose mean age was 50 ± 8 years, 74 ± 9 years and 102 ± 1 year, respectively. The demographic and clinical characteristics of the 12 donors are reported in Supplementary Table 8. There were no age-related differences in the number of sEVs purified from plasma among the groups ($p = 0.873$, data not shown). Of the 1186 miRNAs detected by the

miR-21 inhibitors. Scale bars of 100 µm are applied. (h) Quantification of Ki67-positive cells. (i) PCNA, (m) cyclin D1, cyclin A, cyclin B1 mRNA relative expression in CON cells treated with sEVs released from SEN cells without and with miR-217 and miR-21 inhibitors. (l) Evaluation of senescence-associated heterochromatin foci (SAHF) based on the calculation of the CV of the HOECHST staining in at least 200 nuclei of CON cells treated with sEVs without and with miR-217 and miR-21 inhibitors. Treatment of CON cells with sEVs released from SEN cells induced significant reduction of proliferation markers and the formation of SAHF. These effects were significantly reduced by treatment with sEVs released from SEN cells loaded with miR-21-5p inhibitor, suggesting that the effects of SEN sEVs on CON cell replication are, at least partly, miR-21-5p-dependent. (n) Assessment of apoptosis rate in CON cells treated with sEVs released from SEN cells. Annexin V+/AAD7- and annexin V+/7AAD + cells were respectively considered to be early- and late-apoptotic cells. (o) p16, IL-6, IL-8, IL-1β mRNA relative expression in CON cells treated with sEVs released from SEN cells. (p) Methylation status of the *MIR21* locus in SEN cells and in CON cells treated with sEVs released from SEN cells. The microarray probe cg02515217 is significantly under-methylated in SEN cells and in CON cells treated with SEN sEVs compared to CON cells. *, CON vs CON + SEN sEVs; #, CON vs SEN. Data from $n = 3$ independent experiments are represented as mean ± SD. */#, $p < 0.05$; **, $p < 0.01$; ***, $p < 0.001$ from one-way ANOVA followed by Tukey's multiple comparison test for pairwise comparisons.

Figure 7. Profiling of miRNAs identified in circulating EVs purified from plasma of healthy adult subjects of different ages. (a) PCA factor analysis with varimax rotation of 360 miRNAs detectable in at least two samples of at least one group of healthy donors. Rotation converged after 11 iterations and yielded 11 components with an eigenvalue > 1.0. Three components explaining more than 45% of the total variance were retained. PC1 and PC2, explaining respectively 18.8% and 15.1% of the total variance, are represented. Circles represent 95% confidence intervals. (b) Line plots showing the estimated marginal means for factors 1, 2 and 3 regression scores across the three age groups (<65 years, ≥65 years and centenarians). (c) qPCR validation of miR-21-5p levels in EVs from healthy donors. Data from four subjects in each age group are displayed as mean ± SD. *, $p < 0.05$; **, $p < 0.01$; ***, $p < 0.001$ from one-way ANOVA followed by Tukey's multiple comparison test for pairwise comparisons. (d) Ingenuity Pathway Analysis (IPA) on miRNAs loading on factor 1 with a score > 0.60 or < −0.60. Association of this dataset with the "diseases and disorders" IPA database revealed a significant enrichment of the subcategory "inflammation of organ".

analysis, 360 were expressed in EVs from at least two subjects in at least one group. These were included in the subsequent analysis. Age-related trends were identified by applying PCA with varimax rotation converging after 11 iterations and yielding 11 components with an eigenvalue > 1.0. Three components explaining more than 45% of the total variance were retained. The PCA plot (Figure 7(a)) indicates that PC1 and PC2 enable clear separation of the miRNA expression profiles of the three groups of subjects, explaining

respectively 18.8% and 15.1% of the total variance. The component loading for each miRNA is reported in Supplementary Table 9. Analysis of the factor scores reflecting the weighted level of the miRNAs expressed in the three groups identified an inverted U-shape distribution for factor 1, a slightly declining trend for factor 2 and a rising trend for factor 3 (Figure 7(b)). MiR-21-5p showed a strong loading on factor 1 (loading score = 0.655) (Figure 7(b)), whereas miR-217 was not detected in circulating EVs. We further validated

miR-21-5p levels in plasma EVs from the same subjects by qPCR and confirmed that miR-21-5p levels follow the same age-related inverted U-shaped trend observed for factor 1 (Figure 7(c)).

These data showed that in elderly people circulating EVs are characterised by increased miR-21-5p levels compared with either younger adults and healthy centenarians, suggesting that the EV miR-21-5p content can be a marker of cellular senescence and inflammaging. This finding lends support to our group's earlier report of an inverse U-shaped age-related trend of miR-21-5p purified from total plasma [57].

According to IPA, SIRT1 and miR-21-5p are spokes in a network that includes miRNA loading on factor 1 with a score > 0.60 or < −0.60. *TNF* and *TP53* can be considered as hubs. The association of the miRNAs loaded on factor 1 with the IPA database "diseases and disorders" revealed a significant enrichment of the sub-category "inflammation of organ", confirming the hypothesis that an inverse U-shaped trend reflects high circulating levels of the biomarkers of inflammaging in elderly individuals (Figure 7(d)).

Putative SA loop involving miR-21-5p and miR-217

The main results of the study are reported in Figure 8, which depicts a putative SA loop encompassing miR-21-5p and miR-217. In particular, the miR-21 locus is demethylated in SEN cells, resulting in miR-21-5p over-expression in these cells, which are marked by low levels of DNMT1 and SIRT1. sEVs released from SEN cells are enriched in miR-21-5p and miR-217 and can contribute to reduce DNMT1 and SIRT1 expression in younger recipient cells, promoting demethylation of the locus encoding miR-21 and increasing its transcription. This vicious circle could be critical in the maintenance of the epigenetic "senescence program" that propagates senescence signals from SEN to CON cells through sEVs. The inverse U-shaped age-related trend of miR-21-5p carried by circulating sEVs suggests a potential role for it as a circulating biomarker associated with senescence and inflammaging.

Discussion

Emerging evidence strongly supports the hypothesis that EVs mediate the effects of senescent cells on their micro-environment and that they do so at least partly through their miRNA cargo [23,58–61]. We set out to establish the relative contribution of the miRNAs carried by EVs released from senescent ECs in spreading pro-senescence signals to younger cells. The first relevant finding was that senescent cells

release a significantly greater number of sEVs than control cells, a finding that was corroborated by the detection in senescent cells of a significantly increased number of MVBs, the endocytic organelles that generate sEVs. These data agree with recent studies of a mouse model of oncogene-induced senescence and human lung fibrotic lesions enriched in senescent cells [62], bone marrow stromal cells [63], human prostate cancer cells [24] and chondrocytes [64].

Another major question was whether EVs contained the same miRNA repertoire as the cells that had released them. Global miRNA profiling of SEN and CON cells and their cognate EVs (sEVs and lEVs) showed that cells and their EVs shared about 33% of the miRNAs. Surprisingly, lEVs and sEVs shared only 24%, supporting the hypothesis that different EVs shuttle different cargo [65,66]. Since SEN cells released significantly more sEVs than CON cells, we focused on the miRNAs showing concordant modulation in sEVs and their parental SEN cells. This, we reasoned, would also help reduce the risk of potential contamination from the EVs contained in the FBS serum supplement used in the culture medium [67].

Analysis of SEN sEVs showed that they were enriched in miR-21-5p and miR-217, both of which were over-expressed in SEN cells and were capable of targeting DNMT1 and SIRT1, two key enzymes in methylation pattern maintenance. Our data are in line with previous reports associating miR-21-5p and miR-217 with cellular senescence. MiR-21-5p over-expression has been seen to reduce EC replicative lifespan, whereas its stable knockdown by sponges has been reported to extend it [68,69]. MiR-21-5p over-expression has also been related to the development of cardiac fibrosis [70], T-cell subset alteration [71] and imbalances in platelet function [72], all functions that are affected by ageing. An intriguing mechanism has also been described, where DNMT1 inhibition was induced by miR-21-5p binding the DNMT1 catalytic site rather than its mRNA [54]. As regards miR-217 over-expression, it has been related to a premature senescence-like phenotype both in EC models (through impaired angiogenesis via SIRT1 inhibition [56]) and in fibroblasts (through direct suppression of DNMT1-mediated methylation of p16 and pRb [55]).

Notably, we were able to replicate the same observations in another EC lineage undergoing replicative senescence, and in a model of drug-induced senescence. The expression levels of cellular and sEV miR-21-5p and miR-217 in drug-induced senescence were comparable to those obtained in the replicative senescence models. The variations of the miRNA pool according to the different mechanisms of
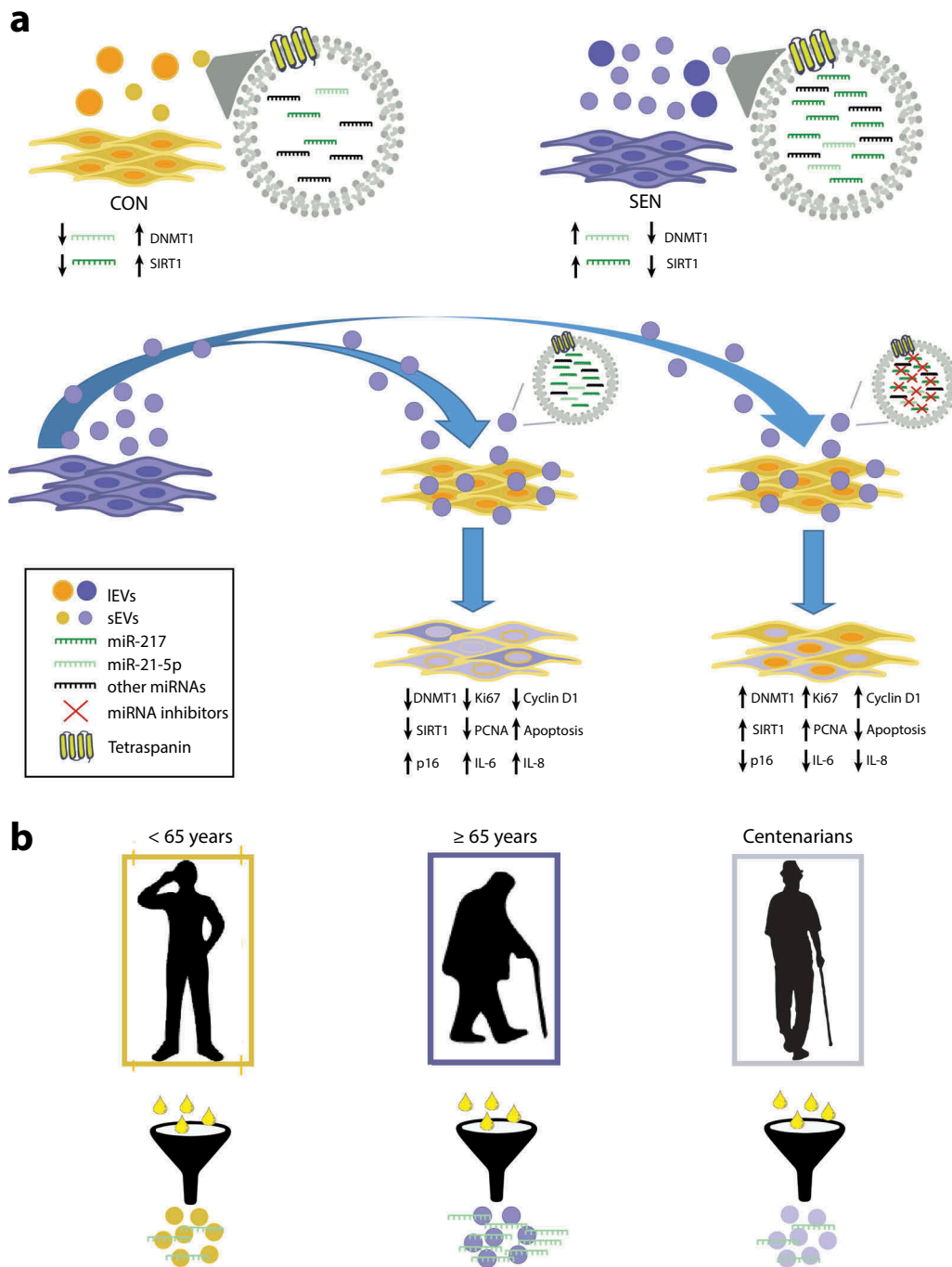
Figure 8. Overview of the SA effects of miR-21-5p and miR-217 carried by SEN sEVs into CON cells. (a) Graphic representation of the SA loop involving miR-21-5p. The miR-21 locus is de-methylated in SEN cells; the resulting miR-21-5p over-expression can contribute to reduce DNMT1/SIRT1 expression in SEN cells. sEVs released from SEN cells are enriched in miR-21-5p; their delivery to CON cells modulates DNMT1/SIRT1 and impairs their replication rate. This vicious cycle may be critical in maintaining the epigenetic "senescence program" through the spread of pro-senescence signals to younger cells through an increased sEV release. (b) MiR-21-5p in sEVs purified from plasma of healthy young, elderly and centenarian individuals showed an inverse U-shaped age-related trend, suggesting that miR-21-5p loaded on sEVs could be a systemic biomarker of senescence and inflammaging.

senescence are under-investigated. In this context, our results support the hypothesis that senescence-associated miRNAs participate in the control of a core set of senescence genes regardless of the pro-senescence stimulus [73].

When we explored the biological effects of SEN sEVs on younger cells, treatment of CON cells with SEN sEVs induced a significant reduction in DNMT1 and SIRT1 expression, which was associated with a reduction in cell replicative rate, with the acquisition

of a senescent phenotype, and with a partial demethylation of the locus encoding for miR-21. The demethylation of the *MIR21* locus was not coupled with the enhanced transcription of the miR-21-5p precursor pri-miR-21 in recipient cells. This suggests that (i) the increased levels of miR-21-5p and miR-217 in CON cells treated with SEN sEVs are related to the intracellular delivery of the sEV cargo, and (ii) a prolonged exposure to SEN sEVs could be required to establish the vicious cycle leading to miR-21-5p transcription in cells treated with CON sEVs. The most striking finding in this context was that miR-21-5p and miR-217 loaded on sEVs played a key role in DNMT1-SIRT1 modulation, with miR-21-5p being the major factor inducing replicative rate reduction in recipient cells. The underexpression of DNMT1 and SIRT1 detected in SEN HUVECs is not induced by changes in the methylation state of their loci, but by fine regulation by miR-21-5p and miR-217. These findings shed new light on the mechanisms promoting the spread of senescence via the bystander effect. Notably, miR-21-5p shuttling through sEVs has been associated with different biological functions depending on donors and recipient cell types [74,75]. While miR-21-5p has been extensively designated as an oncomiR [76], its role on the proliferative rate of non-cancer and replicative senescent cells is still debated. Our findings are in agreement with previous reports showing an anti-proliferative role of miR-21 on endothelial cells [68,77]. We can hypothesise that these effects could be related to the different transcriptional landscape between normal and cancer cells. In the latter, the inhibitory effects of miR-21 on many cell cycle regulators are potentially overwhelmed by gain-of-function somatic mutations.

As a final experiment, we set out to find *in vivo* evidence to compare with our *in vitro* data. Analysis of the miRNome profile of EVs purified from plasma of healthy subjects of different ages demonstrated for the first time that miR-21-5p shuttled by circulating EVs shows an inverse U-shaped trend, and that the trend becomes apparent only when centenarians are included in the analysis. We previously described an inverse U-shaped age-related trend for miR-21-5p during normal ageing and significantly increased miR-21-5p plasma levels in patients with ARDs such as cardiovascular disease and type 2 diabetes [57,61,78].

Notably, non-monotonic age-related trends have first been described for genetic determinants of human longevity; these studies suggested that the effects of mortality trends for different genotypes observed in cross-sectional studies could depend on interactions between genetic and epigenetic factors [79]. Experimental data about such interactions have begun to emerge only in recent years [80].

Our findings strongly support the hypothesis that circulating miR-21-5p may be an archetypal "inflamma-miR" related to cellular senescence and inflammaging, and that its non-monotonic age-related trend may be the result of the complex adaptive/selective remodelling that occurs during ageing. Crucially, therapies targeting miR-21 are already progressing to the clinical trial phase [81,82].

Interestingly, DNMT1 levels in circulating cells from healthy subjects of different ages exhibit a U-shaped pattern that mirrors the expression of miR-21-5p carried by circulating EVs [83].

Altogether, we provide proof of principle that senescent endothelial cells can spread their miRNA signature, thus contributing to the development of a pro-ageing environment, and that these miRNAs can be selectively packaged in and delivered through sEVs. Critically, the results obtained *in vivo* for miR-21-5p lend strong support to the *in vitro* observations and to the notion that cellular senescence is, at least partly, fractal of the ageing process; they also indicate that circulating factors derived from senescent cells can be used as biomarkers to depict and track ageing trajectories [84]. Even though senescence has been described as a terminal process, mounting evidence supports the view that the adverse effects of the senescence program can be attenuated or delayed [85] and that sEVs could play a critical anti-senescence role [86–88].

In conclusion, our findings pave the way for further research, in particular to work out how circulating pro-senescence signals carried by vesicles can become druggable targets that can help modulate the ageing process and delay ARD development. The discovery of several drugs targeting DNMT1 and SIRT1 and the possibility to modulate miRNA expression are making this ambitious goal easier to reach.

Acknowledgments

Disclosure statement

The authors report no conflicts of interest.

Funding

ORCID

Emanuela Mensà http://orcid.org/0000-0002-3284-6161
Michele Guescini http://orcid.org/0000-0001-9372-7038
Angelica Giuliani http://orcid.org/0000-0002-8477-8519
Maria Giulia Bacalini http://orcid.org/0000-0003-1618-2673
Deborah Ramini http://orcid.org/0000-0001-8925-8195
Giacomo Corleone http://orcid.org/0000-0002-6170-9780
Manuela Ferracin http://orcid.org/0000-0002-1595-6887
Gianluca Fulgenzi http://orcid.org/0000-0003-2646-7728
Laura Graciotti http://orcid.org/0000-0002-1874-5217
Francesco Prattichizzo http://orcid.org/0000-0002-2959-2658
Leonardo Sorci http://orcid.org/0000-0002-4356-8873
Michela Battistelli http://orcid.org/0000-0003-4028-0652
Vladia Monsurrò http://orcid.org/0000-0002-9653-8432
Anna Rita Bonfigli http://orcid.org/0000-0002-9619-0181
Maurizio Cardelli http://orcid.org/0000-0002-4480-2473
Rina Recchioni http://orcid.org/0000-0002-7596-3077
Fiorella Marcheselli http://orcid.org/0000-0003-1188-1651
Silvia Latini http://orcid.org/0000-0002-8344-2220
Serena Maggio http://orcid.org/0000-0001-8778-6576
Mirco Fanelli http://orcid.org/0000-0002-9649-8661
Stefano Amatori http://orcid.org/0000-0001-7497-755X
Gianluca Storci http://orcid.org/0000-0001-5145-3091
Antonio Ceriello http://orcid.org/0000-0001-8122-3203
Vilberto Stocchi http://orcid.org/0000-0003-3269-9410
Maria De Luca http://orcid.org/0000-0001-6345-7508
Luca Magnani http://orcid.org/0000-0002-7534-0785
Maria Rita Rippo http://orcid.org/0000-0003-3024-3495
Antonio Domenico Procopio http://orcid.org/0000-0001-9909-2838
Claudia Sala http://orcid.org/0000-0002-4889-1047
Iva Budimir http://orcid.org/0000-0002-5297-8903
Cristian Bassi http://orcid.org/0000-0002-5823-709X
Massimo Negrini http://orcid.org/0000-0002-0007-1920
Paolo Garagnani http://orcid.org/0000-0002-4161-3626
Claudio Franceschi http://orcid.org/0000-0001-9841-6386
Jacopo Sabbatinelli http://orcid.org/0000-0001-9947-6778
Massimiliano Bonafè http://orcid.org/0000-0002-5218-6551
Fabiola Olivieri http://orcid.org/0000-0002-9606-1144

References

[1] Childs BG, Durik M, Baker DJ, et al. Cellular senescence in aging and age-related disease: from mechanisms to therapy. Nat Med. 2015;21(12):1424–1435.

[2] Acosta JC, Banito A, Wuestefeld T, et al. A complex secretory program orchestrated by the inflammasome controls paracrine senescence. Nat Cell Biol. 2013;15(8):978–990.

[3] McHugh D, Gil J. Senescence and aging: causes, consequences, and therapeutic avenues. J Cell Biol. 2018;217(1):65–77.

[4] Franceschi C, Bonafe M, Valensin S, et al. Inflammaging. An evolutionary perspective on immunosenescence. Ann N Y Acad Sci. 2000;908:244–254.

[5] da Silva PFL, Ogrodnik M, Kucheryavenko O, et al. The bystander effect contributes to the accumulation of senescent cells in vivo. Aging Cell. 2019;18(1):e12848.

[6] Fulop T, Witkowski JM, Olivieri F, et al. The integration of inflammaging in age-related diseases. Semin Immunol. 2018;40:17–35.

[7] Baker DJ, Childs BG, Durik M, et al. Naturally occurring p16(Ink4a)-positive cells shorten healthy lifespan. Nature. 2016;530(7589):184–189.

[8] Bussian TJ, Aziz A, Meyer CF, et al. Clearance of senescent glial cells prevents tau-dependent pathology and cognitive decline. Nature. 2018;562(7728):578–582.

[9] Childs BG, Gluscevic M, Baker DJ, et al. Senescent cells: an emerging target for diseases of ageing. Nat Rev Drug Discov. 2017;16(10):718–735.

[10] Prata L, Ovsyannikova IG, Tchkonia T, Kirkland JL. Senescent cell clearance by the immune system: emerging therapeutic opportunities. Semin Immunol. 2018;40:101275.

[11] Watroba M, Dudek I, Skoda M, et al. Sirtuins, epigenetics and longevity. Ageing Res Rev. 2017;40:11–19.

[12] Munk R, Panda AC, Grammatikakis I, et al. Senescence-associated microRNAs. Int Rev Cell Mol Biol. 2017;334:177–205.

[13] Hekmatimoghaddam S, Dehghani Firoozabadi A, Zare-Khormizi MR, et al. Sirt1 and Parp1 as epigenome safeguards and microRNAs as SASP-associated signals, in cellular senescence and aging. Ageing Res Rev. 2017;40:120–141.

[14] Wagner W, Weidner CI, Lin Q. Do age-associated DNA methylation changes increase the risk of malignant transformation? Bioessays. 2015;37(1):20–24.

[15] Lee SH, Lee JH, Lee HY, et al. Sirtuin signaling in cellular senescence and aging. BMB Rep. 2019;52(1):24–34.

[16] Wakeling LA, Ions LJ, Escolme SM, et al. SIRT1 affects DNA methylation of polycomb group protein target genes, a hotspot of the epigenetic shift observed in ageing. Hum Genomics. 2015;9:14.

[17] Zwergel C, Romanelli A, Stazi G, et al. Application of small epigenetic modulators in pediatric medulloblastoma. Front Pediatr. 2018;6:370.

[18] Williams J, Smith F, Kumar S, et al. Are microRNAs true sensors of ageing and cellular senescence? Ageing Res Rev. 2017;35:350–363.

[19] Chanda D, Otoupalova E, Hough KP, et al. Fibronectin on the surface of extracellular vesicles mediates fibroblast invasion. Am J Respir Cell Mol Biol. 2019;60(3):279–288.

[20] de Jong OG, Verhaar MC, Chen Y, et al. Cellular stress conditions are reflected in the protein and RNA content of endothelial cell-derived exosomes. J Extracell Vesicles. 2012;1(1):18396.

[21] Alexander M, Hu R, Runtsch MC, et al. Exosome-delivered microRNAs modulate the inflammatory response to endotoxin. Nat Commun. 2015;6:7321.

[22] Zhang Y, Kim MS, Jia B, et al. Hypothalamic stem cells control ageing speed partly through exosomal miRNAs. Nature. 2017;548(7665):52–57.

[23] Terlecki-Zaniewicz L, Pils V, Bobbili MR, et al. Extracellular vesicles in human skin: cross-talk from senescent fibroblasts to keratinocytes by miRNAs. J Invest Dermatol. 2019;139:2425–2436.e5.

[24] Lehmann BD, Paine MS, Brooks AM, et al. Senescence-associated exosome release from human prostate cancer cells. Cancer Res. 2008;68(19):7864–7871.

[25] Takahashi A, Okada R, Nagao K, et al. Exosomes maintain cellular homeostasis by excreting harmful DNA from cells. Nat Commun. 2017;8:15287.

[26] Takasugi M, Okada R, Takahashi A, et al. Small extracellular vesicles secreted from senescent cells promote cancer cell proliferation through EphA2. Nat Commun. 2017;8:15729.

[27] Eitan E, Green J, Bodogai M, et al. Age-related changes in plasma extracellular vesicle characteristics and internalization by leukocytes. Sci Rep. 2017;7(1):1342.

[28] Takasugi M. Emerging roles of extracellular vesicles in cellular senescence and aging. Aging Cell. 2018;17:2.

[29] Alique M, Ruiz-Torres MP, Bodega G, et al. Microvesicles from the plasma of elderly subjects and from senescent endothelial cells promote vascular calcification. Aging (Albany NY). 2017;9(3):778–789.

[30] Weilner S, Schraml E, Wieser M, et al. Secreted microvesicular miR-31 inhibits osteogenic differentiation of mesenchymal stem cells. Aging Cell. 2016;15(4):744–754.

[31] Hosseinkhani B, Kuypers S, van den Akker NMS, et al. Extracellular vesicles work as a functional inflammatory mediator between vascular endothelial cells and immune cells. Front Immunol. 2018;9:1789.

[32] Liu JY, Souroullas GP, Diekman BO, et al. Cells exhibiting strong p16 (INK4a) promoter activation in vivo display features of senescence. Proc Natl Acad Sci U S A. 2019;116(7):2603–2611.

[33] Regina C, Panatta E, Candi E, et al. Vascular ageing and endothelial cell senescence: molecular mechanisms of physiology and diseases. Mech Ageing Dev. 2016;159:14–21.

[34] Olivieri F, Lazzarini R, Recchioni R, et al. MiR-146a as marker of senescence-associated pro-inflammatory status in cells involved in vascular remodelling. Age (Dordr). 2013;35(4):1157–1172.

[35] Cawthon RM. Telomere measurement by quantitative PCR. Nucleic Acids Res. 2002;30(10):e47.

[36] Rueden CT, Schindelin J, Hiner MC, et al. ImageJ2: imageJ for the next generation of scientific image data. BMC Bioinformatics. 2017;18(1):529.

[37] Riboli E, Hunt KJ, Slimani N, et al. European prospective Investigation into cancer and nutrition (EPIC): study populations and data collection. Public Health Nutr. 2002;5(6B):1113–1124.

[38] Aryee MJ, Jaffe AE, Corrada-Bravo H, et al. Minfi: a flexible and comprehensive Bioconductor package for the analysis of Infinium DNA methylation microarrays. Bioinformatics. 2014;30(10):1363–1369.

[39] Huber W, Carey VJ, Gentleman R, et al. Orchestrating high-throughput genomic analysis with bioconductor. Nat Methods. 2015;12(2):115–121.

[40] Triche TJ Jr., Weisenberger DJ, Van Den Berg D, et al. Low-level processing of illumina infinium DNA methylation bead arrays. Nucleic Acids Res. 2013;41(7):e90.

[41] Fortin JP, Labbe A, Lemire M, et al. Functional normalization of 450k methylation array data improves replication in large cancer studies. Genome Biol. 2014;15 (12):503.

[42] Guescini M, Maggio S, Ceccaroli P, et al. Extracellular vesicles released by oxidatively injured or intact C2C12 myotubes promote distinct responses converging toward myogenesis. Int J Mol Sci. 2017;18:11.

[43] Thery C, Witwer KW, Aikawa E, et al. Minimal information for studies of extracellular vesicles 2018 (MISEV2018): a position statement of the International Society for Extracellular Vesicles and update of the MISEV2014 guidelines. J Extracell Vesicles. 2018;7(1):1535750.

[44] Consortium E-T, Van Deun J, Mestdagh P, et al. EV-TRACK: transparent reporting and centralizing knowledge in extracellular vesicle research. Nat Methods. 2017;14(3):228–232.

[45] Kozomara A, Birgaoanu M, Griffiths-Jones S. miRBase: from microRNA sequences to function. Nucleic Acids Res. 2019;47(D1):D155–D162.

[46] Giuliani A, Cirilli I, Prattichizzo F, et al. The mitomiR/Bcl-2 axis affects mitochondrial function and autophagic vacuole formation in senescent endothelial cells. Aging (Albany NY). 2018;10(10):2855–2873.

[47] Li JH, S L, Zhou H, et al. starBase v2.0: decoding miRNA-ceRNA, miRNA-ncRNA and protein-RNA interaction networks from large-scale CLIP-Seq data. Nucleic Acids Res. 2014;42(Database issue):D92–97.

[48] McQuin C, Goodman A, Chernyshev V, et al. CellProfiler 3.0: next-generation image processing for biology. PLoS Biol. 2018;16(7):e2005970.

[49] Sharma A, Singh K, Almasan A. Histone H2AX phosphorylation: a marker for DNA damage. Methods Mol Biol. 2012;920:613–626.

[50] Cruickshanks HA, McBryan T, Nelson DM, et al. Senescent cells harbour features of the cancer epigenome. Nat Cell Biol. 2013;15(12):1495–1506.

[51] Lopez-Otin C, Blasco MA, Partridge L, et al. The hallmarks of aging. Cell. 2013;153(6):1194–1217.

[52] Turchinovich A, Drapkina O, Tonevitsky A. Transcriptome of extracellular vesicles: state-of-the-art. Front Immunol. 2019;10:202.

[53] Pan W, Zhu S, Yuan M, et al. MicroRNA-21 and microRNA-148a contribute to DNA hypomethylation in lupus CD4+ T cells by directly and indirectly targeting DNA methyltransferase 1. J Immunol. 2010;184(12):6773–6781.

[54] Zhang G, Esteve PO, Chin HG, et al. Small RNA-mediated DNA (cytosine-5) methyltransferase 1 inhibition leads to aberrant DNA methylation. Nucleic Acids Res. 2015;43(12):6112–6124.

[55] Wang B, Du R, Xiao X, et al. Microrna-217 modulates human skin fibroblast senescence by directly targeting DNA methyltransferase 1. Oncotarget. 2017;8(20):33475–33486.

[56] Menghini R, Casagrande V, Cardellini M, et al. MicroRNA 217 modulates endothelial cell senescence via silent information regulator 1. Circulation. 2009;120(15):1524–1532.

[57] Olivieri F, Spazzafumo L, Santini G, et al. Age-related differences in the expression of circulating microRNAs:

miR-21 as a new circulating marker of inflammaging. Mech Ageing Dev. 2012;133(11–12):675–685.

[58] Urbanelli L, Buratta S, Sagini K, et al. Extracellular vesicles as new players in cellular senescence. Int J Mol Sci. 2016;17:9.

[59] Xu D, Tahara H. The role of exosomes and microRNAs in senescence and aging. Adv Drug Deliv Rev. 2013;65 (3):368–375.

[60] Kim KM, Abdelmohsen K, Mustapic M, et al. RNA in extracellular vesicles. Wiley Interdiscip Rev RNA. 2017;8:4.

[61] Dluzen DF, Noren Hooten N, Evans MK. Extracellular RNA in aging. Wiley Interdiscip Rev RNA. 2017;8:2.

[62] Borghesan M, Fafian-Labora J, Eleftheriadou O, et al. Small extracellular vesicles are key regulators of non-cell autonomous intercellular communication in senescence via the interferon protein IFITM3. Cell Rep. 2019;27 (13):3956–3971 e3956.

[63] Umezu T, Imanishi S, Azuma K, et al. Replenishing exosomes from older bone marrow stromal cells with miR-340 inhibits myeloma-related angiogenesis. Blood Adv. 2017;1(13):812–823.

[64] Jeon OH, Wilson DR, Clement CC, et al. Senescence cell-associated extracellular vesicles serve as osteoarthritis disease and therapeutic markers. JCI Insight. 2019;4:7.

[65] Villarroya-Beltri C, Gutierrez-Vazquez C, Sanchez-Cabo F, et al. Sumoylated hnRNPA2B1 controls the sorting of miRNAs into exosomes through binding to specific motifs. Nat Commun. 2013;4:2980.

[66] Murillo OD, Thistlethwaite W, Rozowsky J. exRNA atlas analysis reveals distinct extracellular RNA cargo types and their carriers present across human biofluids. Cell. 2019;177(2):463–477 e415.

[67] Lehrich BM, Liang Y, Khosravi P, et al. Fetal bovine serum-derived extracellular vesicles persist within vesicle-depleted culture media. Int J Mol Sci. 2018;19:11.

[68] Dellago H, Preschitz-Kammerhofer B, Terlecki-Zaniewicz L, et al. High levels of oncomiR-21 contribute to the senescence-induced growth arrest in normal human cells and its knock-down increases the replicative lifespan. Aging Cell. 2013;12(3):446–458.

[69] Zhu S, Deng S, Ma Q, et al. MicroRNA-10A* and microRNA-21 modulate endothelial progenitor cell senescence via suppressing high-mobility group A2. Circ Res. 2013;112(1):152–164.

[70] Thum T, Gross C, Fiedler J, et al. MicroRNA-21 contributes to myocardial disease by stimulating MAP kinase signalling in fibroblasts. Nature. 2008;456 (7224):980–984.

[71] Kim C, Hu B, Jadhav RR, et al. Activation of miR-21-regulated pathways in immune aging selects against signatures characteristic of memory T cells. Cell Rep. 2018;25(8):2148–2162 e2145.

[72] Barwari T, Eminaga S, Mayr U, et al. Inhibition of profibrotic microRNA-21 affects platelets and their releasate. JCI Insight. 2018;3:21.

[73] Lafferty-Whyte K, Cairney CJ, Jamieson NB, et al. Pathway analysis of senescence-associated miRNA targets reveals common processes to different senescence induction mechanisms. Biochim Biophys Acta. 2009;1792(4):341–352.

[74] Hu Y, Rao SS, Wang ZX, et al. Exosomes from human umbilical cord blood accelerate cutaneous wound healing through miR-21-3p-mediated promotion of angiogenesis and fibroblast function. Theranostics. 2018;8(1):169–184.

[75] Mayourian J, Ceholski DK, Gorski PA, et al. Exosomal microRNA-21-5p mediates mesenchymal stem cell paracrine effects on human cardiac tissue contractility. Circ Res. 2018;122(7):933–944.

[76] Ge Y, Zhang L, Nikolova M, et al. Strand-specific in vivo screen of cancer-associated miRNAs unveils a role for miR-21(*) in SCC progression. Nat Cell Biol. 2016;18(1):111–121.

[77] Sabatel C, Malvaux L, Bovy N, et al. MicroRNA-21 exhibits antiangiogenic function by targeting RhoB expression in endothelial cells. PLoS One. 2011;6(2):e16979.

[78] Prattichizzo F, Micolucci L, Cricca M, et al. Exosome-based immunomodulation during aging: A nano-perspective on inflamm-aging. Mech Ageing Dev. 2017;168:44–53.

[79] Yashin AI, De Benedictis G, Vaupel JW, et al. Genes, demography, and life span: the contribution of demographic data in genetic studies on aging and longevity. Am J Hum Genet. 1999;65(4):1178–1193.

[80] Benayoun BA, Pollina EA, Brunet A. Epigenetic regulation of ageing: linking environmental inputs to genomic stability. Nat Rev Mol Cell Biol. 2015;16(10):593–610.

[81] Gomez IG, MacKenna DA, Johnson BG, et al. Anti-microRNA-21 oligonucleotides prevent Alport nephropathy progression by stimulating metabolic pathways. J Clin Invest. 2015;125(1):141–156.

[82] Wang D, Deuse T, Stubbendorff M, et al. Local microRNA modulation using a novel anti-miR-21-eluting stent effectively prevents experimental in-stent restenosis. Arterioscler Thromb Vasc Biol. 2015;35(9):1945–1953.

[83] Ciccarone F, Malavolta M, Calabrese R, et al. Age-dependent expression of DNMT1 and DNMT3B in PBMCs from a large European population enrolled in the MARK-AGE study. Aging Cell. 2016;15(4):755–765.

[84] Olivieri F, Capri M, Bonafe M, et al. Circulating miRNAs and miRNA shuttles as biomarkers: perspective trajectories of healthy and unhealthy aging. Mech Ageing Dev. 2017;165(Pt B):162–170.

[85] Shao Y, Lv C, Wu C, et al. Mir-217 promotes inflammation and fibrosis in high glucose cultured rat glomerular mesangial cells via Sirt1/HIF-1alpha signaling pathway. Diabetes Metab Res Rev. 2016;32(6):534–543.

[86] Yoshida M, Satoh A, Lin JB, et al. Extracellular vesicle-contained eNAMPT delays aging and extends lifespan in mice. Cell Metab. 2019;30(2):329–342 e325.

[87] Hu W, Ru Z, Zhou Y, et al. Lung cancer-derived extracellular vesicles induced myotube atrophy and adipocyte lipolysis via the extracellular IL-6-mediated STAT3 pathway. Biochim Biophys Acta Mol Cell Biol Lipids. 2019;1864(8):1091–1102.

[88] Prattichizzo F, Giuliani A, Sabbatinelli J, et al. Extracellular vesicles circulating in young organisms promote healthy longevity. J Extracell Vesicles. 2019;8 (1):1656044.
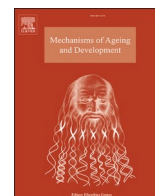
Decreased serum levels of the inflammaging marker miR-146a are associated with clinical non-response to tocilizumab in COVID-19 patients

Jacopo Sabbatinelli [a], Angelica Giuliani [a], Giulia Matacchione [a], Silvia Latini [a],
Noemi Laprovitera [b], Giovanni Pomponio [c], Alessia Ferrarini [c], Silvia Svegliati Baroni [a],
Marianna Pavani [a], Marco Moretti [d], Armando Gabrielli [a,c], Antonio Domenico Procopio [a,e],
Manuela Ferracin [e,**], Massimiliano Bonafè [b,**], Fabiola Olivieri [a,e,*]

[a] *Department of Clinical and Molecular Sciences, Università Politecnica delle Marche, Ancona, Italy*
[b] *Department of Experimental, Diagnostic, and Specialty Medicine (DIMES), University of Bologna, Bologna, Italy*
[c] *Clinica Medica, Department of Internal Medicine, Ospedali Riuniti, Ancona, Italy*
[d] *Laboratory Medicine, Ospedali Riuniti, Ancona, Italy*
[e] *Center of Clinical Pathology and Innovative Therapy, IRCCS INRCA, Ancona, Italy*

ARTICLE INFO

ABSTRACT

Current COVID-19 pandemic poses an unprecedented threat to global health and healthcare systems. The most amount of the death toll is accounted by old people affected by age-related diseases that develop a hyper-inflammatory syndrome. In this regard, we hypothesized that COVID-19 severity may be linked to inflammaging. Here, we examined 30 serum samples from patients enrolled in the clinical trial NCT04315480 assessing the clinical response to a single-dose intravenous infusion of the anti-IL-6 receptor drug Tocilizumab (TCZ) in COVID-19 patients with multifocal interstitial pneumonia.

In these serum samples, as well as in 29 age- and gender-matched healthy control subjects, we assessed a set of microRNAs that regulate inflammaging, i.e. miR-146a-5p, miR-21-5p, and miR-126-3p, which were quantified by RT-PCR and Droplet Digital PCR.

We showed that COVID-19 patients who did not respond to TCZ have lower serum levels of miR-146a-5p after the treatment (p = 0.007). Among non-responders, those with the lowest serum levels of miR-146a-5p experienced the most adverse outcome (p = 0.008). Our data show that a blood-based biomarker, such as miR-146a-5p, can provide clues about the molecular link between inflammaging and COVID-19 clinical course, thus allowing to better understand the use of biologic drug armory against this worldwide health threat.

1. Introduction

The COVID-19 pandemic caused by the SARS-CoV-2 coronavirus is characterized by a striking age-dependent morbidity and mortality, irrespective of ethnicity (Remuzzi and Remuzzi, 2020; Ruan et al., 2020). In Italy, about 1.1 % of COVID-19 patient deaths are attributable to people younger than 50 years, while the death toll of COVID-19 is mainly accounted by people with a median age of 82 years (IQR 74–88). Notably, most of such patients (59.7 %) are affected by at least three age-related diseases (Istituto Superiore di Sanità, 2020). Nowadays, whilst the pandemic is still spreading, COVID-19 is emerging as a transmissible age-related lethal disease, at least in western countries.

A substantial proportion of hospitalized COVID-19 patients show a systemic dysregulation of pro-inflammatory cytokines, a condition known as cytokine storm (Zhou et al., 2020). Such hyper-inflammatory response in COVID-19 patients is associated with extensive lung and endothelial cell damage, microvascular dysfunction, and micro-angiopathy that eventually lead to lung and multiorgan failure (Varga et al., 2020). It is therefore unsurprising that a number of clinical trials have been started to evaluate the effectiveness of anti-cytokine/cytokine receptor antibodies as a treatment for hospitalized COVID-19 patients. Tocilizumab (TCZ), the monoclonal antibody against the interleukin-6 (IL-6) receptor is one of these host-directed therapies (Crisafulli et al., 2020; Liu et al., 2020a; Luo et al., 2020; Xu et al., 2020). Nevertheless,

---

substantial variability in the clinical response of COVID-19 patients to TCZ treatment has been reported, probably due to the contribution of other factors, including age-related biological mechanisms, gender, genetic makeup, disease severity, timing of treatment, and immune activation (Khiali et al., 2020; Wilk et al., 2020). With regard to the latter issue, we have recently proposed that an age-dependent pro-inflammatory status, currently referred to as inflammaging, may facilitate the onset of uncontrolled COVID-19 related hyper-inflammation, particularly in aged people (Bonafè et al., 2020; Storci et al., 2020). Blood-based biomarkers, conceivably linked to the systemic inflammatory state and/or inflammaging, and able to predict the response to TCZ treatment are urgently needed in order to redirect this precious armory to those patients who are likely to benefit at its most. Under this perspective, the assessment of serum/plasma microRNAs (miRNAs) has been emerging as a reliable tool to assess pharmacological interventions in a variety of human diseases, including age-related and infectious diseases (Kong et al., 2012).

In this regard, a set of miRNAs capable of regulating inflammation (also known as inflamma-miRs) such as miR-146a, miR-21-5p, and miR-126-3p, has reported to show age-dependent changes in their blood levels and to be markers of a pro-inflammatory state (i.e. inflammaging) in healthy and non-healthy individuals (Mensà et al., 2019; Olivieri et al., 2013b, 2012). These three miRNAs are all able to target molecules belonging to the nuclear factor κB (NF-κB) pathway, a central mediator of inflammation (Mussbacher et al., 2019). Hyper-inflammatory response is associated with poor outcome in COVID-19 patients and shows multiple connections with the thrombotic phenomena that occur in patients affected by severe COVID-19 (Sriram and Insel, 2020). MiR-146a-5p is of particular interest, given its ability to induce a negative feedback loop that restrains the activation of the NF-κB pathway by targeting TNF receptor associated factor 6 (TRAF6) and Interleukin-1 receptor-associated kinase 1 (IRAK1). The pivotal role of miR-146a-5p has been reported in a number of cell types that orchestrate the inflammatory response, including endothelial cells (Mensà et al., 2019; Olivieri et al., 2013a), microglial cells (Liu et al., 2020b), monocytes and macrophages, (Li et al., 2015; Zhou et al., 2019), and adipocytes (Roos et al., 2016). Recently, a reduced expression of miR-146a-5p was observed in a subgroup of patients affected by acute myeloid leukemia with inflammaging and poor outcome (Grants et al., 2020). Therefore, on the basis of the current literature, a decline in miR-146a-5p levels would be expected to unleash the release of inflammatory cytokines, e.g. IL-6.

Other inflammatory miRNAs, including miR-21-5p, take part to the scenario. This microRNA was previously identified as a cell-free and/or exosome-loaded circulating marker of inflammaging and endothelial senescence (Mensà et al., 2020; Olivieri et al., 2012). Even miR-126-3p, a key regulator of endothelial inflammation and angiogenic processes, has been regarded as a mediator of systemic inflammation (reviewed in Zhong et al., 2018).

The aim of this report is to evaluate the levels of circulating inflamma-miR-146a, -21-5p, and -126-3p in COVID-19 patients treated with TCZ and age-matched healthy control subjects, in order to assess whether such biomarkers of inflammaging may be of help in such a dramatic clinical setting.

2. Materials and methods

Thirty serum samples from COVID-19 patients enrolled in a Phase 2, open-label, single-arm clinical trial (Clinicaltrials.gov, NCT04315480) were available for miRNA assay. The clinical trial was conducted at Università Politecnica delle Marche, Italy and enrolled 46 patients presenting with virologically confirmed COVID-19, characterized by multifocal interstitial pneumonia confirmed by CT-scan and requiring oxygen therapy. Eligible patients presented with worsening respiratory function, defined as either decline of oxygen saturation (SO_2) > 3% or a > 50 % decline in PaO_2/FiO_2 (P/F) ratio in the previous 24 h; need to

increase FiO_2 in order to maintain a stable SO_2 or new-onset need of mechanical ventilation; increase in number or extension of areas of pulmonary consolidation. Assessment of radiological pattern and definition of the extent of lung involvement were performed and scored as previously described (Li et al., 2020). Patients with severe heart failure, bacterial infection, hematological neoplasm, severe neutropenia or thrombocytopenia, and serum alanine aminotransferase > 5x UNL were excluded. All enrolled subjects provided written informed consent. The study was approved by the Regional Institutional Review Board (Comitato Etico Regione Marche) and was conducted in accordance with the Declaration of Helsinki. A Simon's optimal two-stage design was adopted. TCZ was administered as a single-dose intravenous infusion of 8 mg/kg over a 90-minute time span after premedication with 40 mg methylprednisolone. Patients were classified as responders (R) if fulfilling one of the following criteria: i) improvement of oxygen saturation by more than 3% points and/or increase in P/F by 50 % and/or P/F increase above 150 mmHg 72 h after tocilizumab AND persistence of this improvement at day 7, OR ii) no evidence of worsening of respiratory function as defined above. Dead and intubated patients were classified as Non-responders (NR). Samples of serum were collected at baseline (T0) and after 72 h (T1) from TCZ infusion. Twenty-nine age- and gender-matched healthy control subjects (CTR), without SARS-CoV-2 infection or any other acute or chronic illness, were enrolled. Mean age of CTR was 64.1 ± 8.6 years. Serum miRNAs were quantified by RT-PCR and Droplet Digital PCR (ddPCR) in two independent laboratories as previously described (Ferracin et al., 2015; Mensà et al., 2019). To achieve normal distribution, results were expressed as $\log_2$(relative expression) and $\log_2$(copies/µl), respectively. Results were presented as Z-scores to allow proper comparison between relative and absolute quantification.

Data were tested for normality using the Shapiro-Wilk test. Student's *t* test for independent samples and two-way mixed ANOVA with Tukey post hoc tests were used to compare the levels of investigated miRNAs between COVID-19 patients and CTR and between time points in COVID-19 patients, respectively. The agreement between RT-PCR and ddPCR was assessed using Pearson's correlation and Bland-Altman analysis. Pearson's coefficient was used for the estimation of the correlations between miRNAs expression levels and clinical parameters. Exploratory factor analysis was performed as previously described (Spazzafumo et al., 2013) to identify underlying factors in the study population. Two-tailed p value < 0.05 was considered significant. Statistical analysis was performed using SPSS version 26 (IBM, USA).

3. Results

The final study case set was composed of 29 serum samples from patients enrolled in the clinical trial NCT04315480, as one serum sample was excluded due to hemolysis. Demographic and clinical characteristics of the samples are reported in Table 1. None of the patients were smokers. The median time between onset of symptoms and TCZ infusion was 9 days (IQR 4–14 days). At the end of the study, 16 patients were classified as responders (R) and 13 patients as non-responders (NR). Given the age-dependent expression of the investigated miRNAs (Mensà et al., 2019; Rusanova et al., 2018), analyses were conducted after controlling for age. A significant interaction between time and responder status was found for miR-146a-5p levels (F[126] = 6.904, p = 0.014, partial η^2 = 0.210). Analysis of simple main effects of time revealed a significant increase in miR-146a-5p levels in R patients 3 days after the administration of TCZ (Z-score difference = 1.25; p < 0.001), while no significant change was shown in NR patients (p = 0.125). No significant differences in baseline miR-146a-5p levels were found between R and NR (p = 0.392), while post-treatment miR-146a-5p levels were higher in R vs. NR (Z-score difference = 0.98; p = 0.007) (Fig. 1A). Notably, droplet digital ddPCR analysis, which allows for the quantification of miRNA copies/µl of serum, confirmed RT-PCR results (F[125] = 5.696, p = 0.025, partial η^2 = 0.186), with a strong Pearson's

Table 1

Baseline clinical and demographic characteristics of 29 COVID-19 patients treated with tocilizumab (TCZ), divided into responders (R) and non-responders (NR). Data are mean (SD). P value from t tests for continuous variables and z tests for categorical variables. LMWH, low-molecular weight heparin.

Variable	Responder (n = 16)	Non-responder (n = 13)	P value
Age (years)	65.9 (10.6)	69.4 (12.8)	0.424
Gender (males, %)	11 (68.8 %)	6 (46.2 %)	0.219
Time between onset of symptoms and TCZ infusion (days)	9.8 (5.9)	9.6 (3.0)	0.925
Concomitant treatments			
Lopinavir-ritonavir or darunavir-cobicistat	13 (81.3 %)	10 (76.9 %)	0.775
Antibiotics	10 (62.5 %)	9 (69.2 %)	0.705
Prophylactic LMWH	10 (62.5 %)	6 (46.2 %)	0.379
IL-6 (pg/mL)	33.1 (40.9)	146.1 (252.4)	0.088
Hemoglobin (g/dL)	12.9 (1.7)	12.6 (1.1)	0.604
Neutrophils (n/mm^3)	5031 (2580)	6382 (3708)	0.258
Lymphocytes (n/mm^3)	673 (262)	650 (227)	0.801
Platelets (n/mm^3)	200063 (83781)	217769 (76300)	0.561
D-dimer (ng/mL)	573.1 (687.4)	1109.4 (1498.4)	0.287
C-reactive protein (ng/mL)	8.3 (5.3)	13.2 (8.5)	0.095
PaO$_2$/FiO$_2$	146.1 (75.4)	162.2 (48.5)	0.570
1-week follow-up (n, %)			
Home discharge	16 (100 %)	7 (53.8 %)	0.002
Intensive care	0	1 (7.7 %)	0.258
Death	0	5 (38.5 %)	0.006

correlation between techniques (Pearson's r = 0.74, p < 0.0001). The Bland-Altman agreement analysis revealed a small +0.32 Z-score unit bias [95 % CI: -1.09 – 1.73] between ddPCR and RT-PCR, confirming a reasonable agreement between the two methods (Fig. 1B). Absolute quantification of miR-146a-5p copies revealed a mean increase from 3.2 ± 1.4–5.3 ± 1.3 copies per μl in R patients and a mean decrease from 3.4 ± 1.7–2.1 ± 1.6 copies per μl in NR patients.

No significant interaction between the responder status and time was showed for miR-21–5p (F[126] = 1.089, p = 0.306, partial η^2 = 0.040). However, the main effect of time showed that circulating miR-21-5p was 0.433 SD higher at T1 compared to T0 (F[126] = 5.048, p = 0.033, partial η^2 = 0.163), regardless of the responder status (Fig. 1A). Notably, the main effect of time was confirmed by ddPCR (p = 0.007). Bland-Altman analysis revealed a strong agreement between methods (ddPCR – RT-PCR Bias= -0.12, 95 % CI: -0.26 – 0.03). TCZ treatment does not modulate angio-miR-126-3p levels (F[126] = 0.621, p = 0.438, partial η^2 = 0.023), and no difference was observed between R and NR (main effect of responder status, p = 0.202), or time points (main effect of time, p = 0.266).

No significant gender-related difference in the pre- and post-treatment levels of miR-146a-5p, miR-21-5p, and miR-126–3p were shown (data not shown).

Multiple comparisons of age-adjusted circulating inflamma-miRs showed significantly lower miR-146a-5p (mean difference = -1.498, p < 0.001), miR-21-5p (mean difference = -0.486, p = 0.025), and miR-126-3p (mean difference = -0.972, p < 0.001) levels in COVID-19 patients compared to CTR subjects (Fig. 1A).

Partial bivariate correlations adjusted for age were computed to analyze the relations between inflamma-miRs and selected variables, including plasma IL-6, hemoglobin, neutrophil, lymphocyte and platelet count, D-dimer, and PaO2/FiO2 ratio in COVID-19 patients at both time points. The results, summarized in the correlation plot in Fig. 1C, show significant positive correlations between the baseline neutrophil count and the three inflamma-miRs. Moreover, negative correlations exist between post-intervention IL-6 levels and both T0 and T1 inflamma-miR levels. The circulating levels of the three miRNAs are negatively related to Ddimer level at T1.

Finally, an exploratory factor analysis (EFA) was conducted on the COVID-19 study population to identify latent variables that could be

associated with clinical outcomes. The analysis returned 5 factors that cumulatively explain 84.7 % of the total variance. The first factor, which included the 3 inflamma-miRs and age, explained most of the total variance (31.3 %) and was the only factor that was significantly associated with mortality at the univariate logistic regression (p = 0.043, OR 0.07 [95 % CI 0.01 – 0.91]). These data confirmed the notion that a latent variable encompassing low levels of circulating inflamma-miRs and increasing age is associated with mortality, to a higher extent than plasma IL-6. Results of the EFA are summarized in Fig. 2A and reported in Supplementary Table 1. Notably, age-adjusted baseline levels of miR-21-5p (p = 0.016), -126-−3p (p = 0.006), and -146a-5p (p = 0.008) were significantly lower in 5 NR COVID-19 patients (2 males and 3 females) who died in the 1-week follow-up period compared to NR survivors (Fig. 2B).

4. Discussion

To our knowledge, this is the first report showing a significant association between serum miR-146a-5p levels and response to TCZ treatment in COVID-19 patients. Two different PCR-based assays, independently performed in two separate laboratories and providing relative and absolute quantifications of serum miR-146a-5p, revealed a significant increase of miR-146a-5p serum levels only in patients classified as "responders" to TCZ treatment. Although miR-146a-5p does not directly target the mRNAs of IL-6 or its receptor, miR-146a$^{-/-}$ mice displayed high serum IL-6 levels, supporting the functional link between miR-146a-5p and IL-6 levels (Boldin et al., 2011). Indeed, miR-146a-5p acts as a negative regulator of NF-κB, which is in turn a widely acknowledged transcription factor of the IL-6 gene (Su et al., 2020). Also, the transcription of miR-146a-5p is under the control of NF-κB, even if the two molecules – IL-6 and miR-146a-5p – play opposite roles in the inflammatory process. A number of studies was focused on the complex regulatory mechanisms of IL-6 transcription, identifying not only NF-κB but also AP-1, sp-1 and NF-IL6-C/EBP as involved in such modulation (Akira et al., 1990; Libermann and Baltimore, 1990; Luo and Zheng, 2016). Therefore, the unbalance of the IL-6/miR-146a-5p axis could depend, at least in part, from IL-6-stimulating nuclear factors other than NF-κB or synergistically acting with NF-κB, thus dramatically exacerbating IL-6 synthesis without a concomitant induction of miR-146a-5p transcription. COVID-19 patients showed increased IL-6 levels and reduced miR-146a-5p levels compared to healthy age-matched subjects, pointing at the imbalance of the IL-6/miR-146a-5p physiological axis in the pathogenesis of SARS-CoV-2 infection. Noteworthy, a similar scenario was reported in the context of sepsis (Benz et al., 2016).

Overall, our data showed that the response to TCZ is associated with a significant reduction of plasma IL-6 and a significant increase of miR-146a levels, thus suggesting that TCZ treatment is able, at least in the set of responder patients, to offset the IL-6/miR-146a-5p axis unbalance. The observation that miR-146a-5p is significantly reduced in the group of non-responder COVID-19 patients with the worst outcome strongly supports this hypothesis. Notably, the inter-individual variability in the response to an anti-inflammatory treatment, i.e. TCZ, can be related to a number of different factors, including the genetic make-up, lifestyle, previous stimulations of immune cells, and the burden of senescent cells – mainly immune and endothelial cells.

Therefore, even though the number of patients is relatively low, our results suggest that low levels of circulating miR-146a-5p in COVID-19 patients may predict poor outcome among those who develop systemic hyper-inflammation. Notably, circulating miR-146a levels significantly decline with age and chronic age-related diseases and conditions, such as type 2 diabetes and frailty (Mensà et al., 2019; Ong et al., 2019). Current literature agrees about its pivotal role in inflammaging and age-related diseases (Grants et al., 2020). We recently suggested that the features of the current pandemic strongly suggest a role of inflammaging in worse COVID-19 outcomes, which mainly affect old people affected
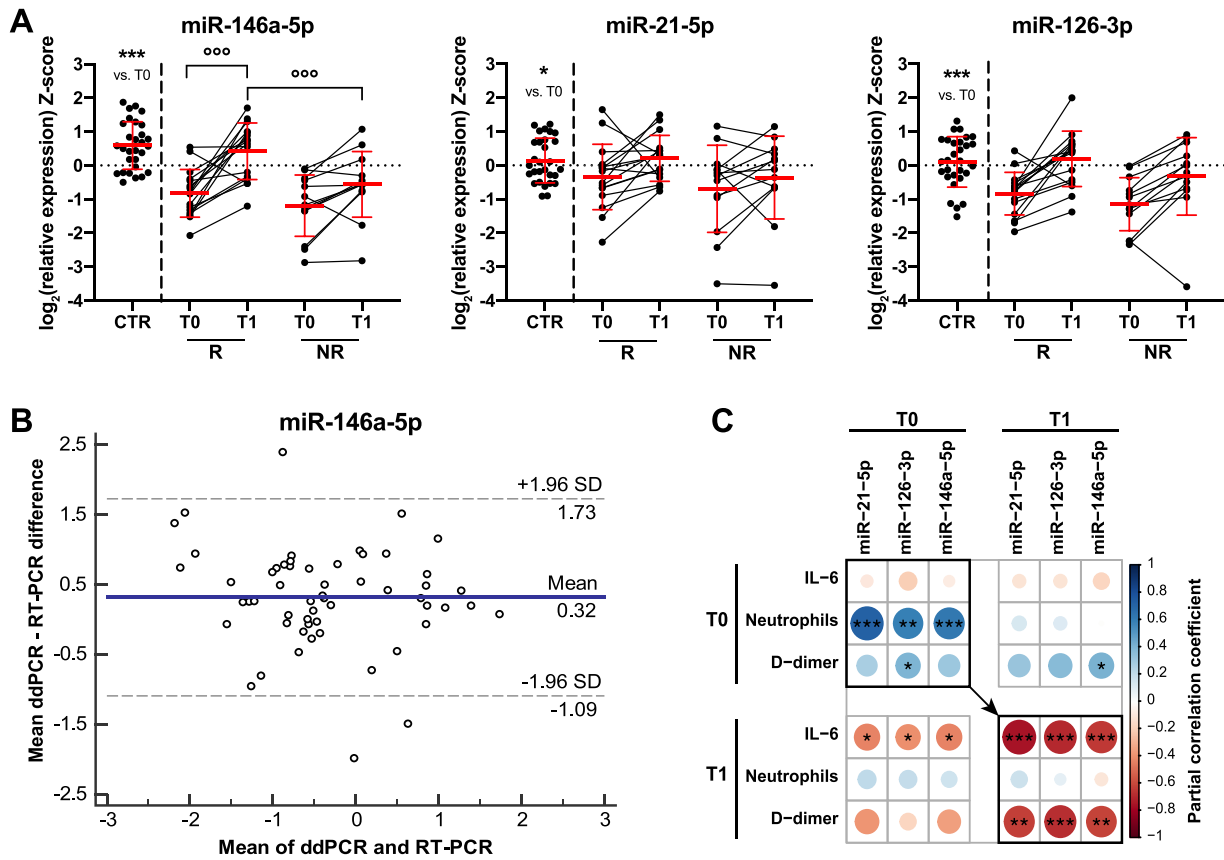
Fig. 1. (A) Serum levels of miR-146a-5p, -21-5p, and -126-3p in 29 COVID-19 patients at baseline (T0) and after 72 h from treatment with tocilizumab (T1), divided into responders (R) and non-responders (NR), and in 29 age-matched healthy control subjects (CTR). Data are expressed as Z-scores of $\log_2$(relative expression) and presented as mean ± SD. *, p < 0.05; ***, p < 0.001 for unpaired *t* test (CTR vs. COVID-19). °°°, p < 0.001 for simple main effects of time (T0 vs. T1) and responder status (R vs. NR). **(B)** Bland-Altman plot for inter-method agreement between Droplet Digital PCR (ddPCR) and RT-PCR in the quantification of circulating miR-146a-5p. The blue line represents the mean bias between the two methods, the dashed lines indicate the limits of agreement. **(C)** Correlation plot showing partial correlations, controlling for age, between inflamma-miR levels and selected variables at both time points. Bold squares indicate correlations between variables assessed at the same time point. The color and the size of the circles depend on the magnitude of the correlation. Blue, positive correlation; red, negative correlation. Significant correlations are marked with * (p < 0.05), ** (p < 0.01), or *** (p < 0.001) (For interpretation of the references to colour in this figure legend, the reader is referred to the web version of this article.).
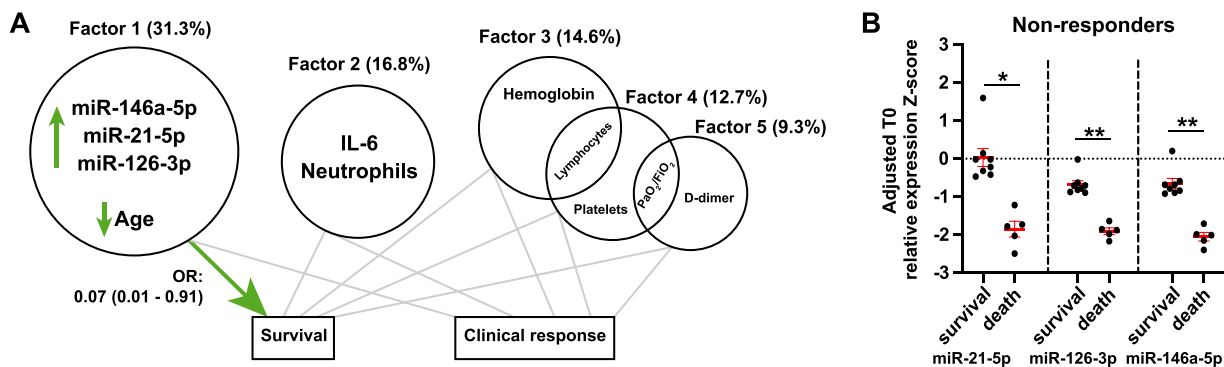
Fig. 2. (A) Summary of exploratory factor analysis and subsequent logistic regressions on COVID-19 patients. Baseline variables are reported into each circle according to the factor loading. The areas of the circles are proportional to the amount of variance (reported in brackets) explained by each factor. Overlapping circles include variables loading onto two factors. The green arrow points out the significant association between factor 1 and survival, while the gray lines indicate non-significant associations. **(B)** Age-adjusted baseline miR-21-5p, -126-3p, and -146-5p levels in dead vs. survivor NR patients. Data are expressed as Z-scores of $\log_2$(relative expression) and presented as estimated marginal mean ± SEM. *, p < 0.05; **, p < 0.01 for one-way ANCOVA (For interpretation of the references to colour in this figure legend, the reader is referred to the web version of this article.).

by age-related diseases (Bonafè et al., 2020; Storci et al., 2020). Interestingly, a randomized controlled trial evaluating the efficacy of a triple antiviral therapy with combined interferon beta-1b, ribavirin, and lopinavir-ritonavir on COVID-19 patients showed that the interferon-induced decline in circulating IL-6 is associated with earlier viral clearance (Hung et al., 2020). Also, glucocorticoids improve severe or critical COVID-19 by activating angiotensin-converting enzyme 2 (ACE2) and by reducing IL-6 levels (Xiang et al., 2020). It has been

recently demonstrated that a strategy including high-dose methylprednisolone, followed by TCZ treatment if needed, may accelerate respiratory recovery, lower hospital mortality and reduce the likelihood of invasive mechanical ventilation in COVID-19-associated cytokine storm syndrome (Ramiro et al., 2020).

The data herein reported support the hypothesis that COVID-19 clinical progression may be accelerated by inflammaging, and/or that COVID-19 may accelerate inflammaging itself. Therefore, our results represent a proof-of-principle for the feasibility of dosing selected inflamma-miRs, specifically miR-146a-5p, as biomarkers of response to anti-inflammatory therapeutic intervention in COVID-19 patients. Moreover, such markers could represent themselves putative druggable targets (Su et al., 2020).

Regarding miR-21-5p and miR-126–3p, even if they were significantly reduced in COVID-19 patients compared to healthy subjects, no significant modulation was observed after TCZ treatment. Functional studies of miR-21 during inflammation are complicated by its numerous molecular targets and by the fact that its expression is regulated by multiple transcription factors (Sheedy, 2015). The existing evidences illustrate the role of miR-126-3p in inflammation, by regulating the NF-κB inhibitor Iκ-Bα (Feng et al., 2012), and endothelial activation (Zhang et al., 2020). However, a clear mechanism linking miR-126-3p and IL-6 levels was not yet described.

Notably, in the factor analysis only a latent variable encompassing all the three selected miRNAs and age showed to be predictive for survival after TCZ treatment.

In conclusion, further larger, multi-center, and possibly prospective clinical trials are necessary to identify the true potential of inflamma-miR assessment as a predictive or prognostic biomarker in tocilizumab administration to COVID-19 patients and therefore validate the clinical relevance of our preliminary observations.

Funding

This study was supported by grants from Università Politecnica delle Marche (RSA grant) and Italian Ministry of Health ("Ricerca corrente"). MF lab is supported by Italian Association for Cancer Research (AIRC), Italy and Pallotti Fund, United States. MB is supported by Pallotti Fund.

Author contribution

JS performed statistical analysis, drafted the paper, and prepared the figure. Angelica Giuliani, GM, SL performed RNA extraction and RT-PCR measurements. NL and MF performed ddPCR quantification. GP and AF provided patient data and clinical advice. SSB, MP, and MM provided sera samples and laboratory data of COVID-19 patients. Armando Gabrielli is the principal investigator of the original trial. ADP critically revised the paper. MF, MB, and FO conceived the idea and wrote the paper. All authors critically revised the paper for important intellectual content and approved of the final version.

Declaration of Competing Interest

The authors report no declarations of interest.

Acknowledgments

The authors want to thank Azienda Ospedaliera Universitaria "Ospedali Riuniti", Ancona, Italy for the support.

Appendix A. Supplementary data

Supplementary material related to this article can be found, in the online version, at doi:https://doi.org/10.1016/j.mad.2020.111413.

References

Akira, S., Isshiki, H., Sugita, T., Tanabe, O., Kinoshita, S., Nishio, Y., Nakajima, T., Hirano, T., Kishimoto, T., 1990. A nuclear factor for IL-6 expression (NF-IL6) is a member of a C/EBP family. EMBO J. 9, 1897–1906.

Benz, F., Roy, S., Trautwein, C., Roderburg, C., Luedde, T., 2016. Circulating MicroRNAs as biomarkers for Sepsis. Int. J. Mol. Sci. 17.

Boldin, M.P., Taganov, K.D., Rao, D.S., Yang, L., Zhao, J.L., Kalwani, M., Garcia-Flores, Y., Luong, M., Devrekanli, A., Xu, J., Sun, G., Tay, J., Linsley, P.S., Baltimore, D., 2011. miR-146a is a significant brake on autoimmunity, myeloproliferation, and cancer in mice. J. Exp. Med. 208, 1189–1201.

Bonafè, M., Prattichizzo, F., Giuliani, A., Storci, G., Sabbatinelli, J., Olivieri, F., 2020. Inflamm-aging: why older men are the most susceptible to SARS-CoV-2 complicated outcomes. Cytokine Growth Factor Rev. 53, 33–37.

Crisafulli, S., Isgro, V., La Corte, L., Atzeni, F., Trifiro, G., 2020. Potential role of anti-interleukin-6 drugs in the treatment of COVID-19: rationale, clinical evidence and risks. BioDrugs. 34, 415–422.

Feng, X., Wang, H., Ye, S., Guan, J., Tan, W., Cheng, S., Wei, G., Wu, W., Wu, F., Zhou, Y., 2012. Up-regulation of microRNA-126 may contribute to pathogenesis of ulcerative colitis via regulating NF-kappaB inhibitor IkappaBalpha. PLoS One 7, e52782.

Ferracin, M., Lupini, L., Salamon, I., Saccenti, E., Zanzi, M.V., Rocchi, A., Da Ros, L., Zagatti, B., Musa, G., Bassi, C., Mangolini, A., Cavallesco, G., Frassoldati, A., Volpato, S., Carcoforo, P., Hollingsworth, A.B., Negrini, M., 2015. Absolute quantification of cell-free microRNAs in cancer patients. Oncotarget 6, 14545–14555.

Grants, J.M., Wegrzyn, J., Hui, T., O'Neill, K., Shadbolt, M., Knapp, D., Parker, J., Deng, Y., Gopal, A., Docking, T.R., Fuller, M., Li, J., Boldin, M., Eaves, C.J., Hirst, M., Karsan, A., 2020. Altered microRNA expression links IL6 and TNF-induced inflammaging with myeloid malignancy in humans and mice. Blood 135, 2235–2251.

Hung, I.F., Lung, K.C., Tso, E.Y., Liu, R., Chung, T.W., Chu, M.Y., Ng, Y.Y., Lo, J., Chan, J., Tam, A.R., Shum, H.P., Chan, V., Wu, A.K., Sin, K.M., Leung, W.S., Law, W. L., Lung, D.C., Sin, S., Yeung, P., Yip, C.C., Zhang, R.R., Fung, A.Y., Yan, E.Y., Leung, K.H., Ip, J.D., Chu, A.W., Chan, W.M., Ng, A.C., Lee, R., Fung, K., Yeung, A., Wu, T.C., Chan, J.W., Yan, W.W., Chan, W.M., Chan, J.F., Lie, A.K., Tsang, O.T., Cheng, V.C., Que, T.L., Lau, C.S., Chan, K.H., To, K.K., Yuen, K.Y., 2020. Triple combination of interferon beta-1b, lopinavir-ritonavir, and ribavirin in the treatment of patients admitted to hospital with COVID-19: an open-label, randomised, phase 2 trial. Lancet 395, 1695–1704.

Istituto Superiore di Sanità, 2020. Characteristics of COVID-19 Patients Dying in Italy.

Khiali, S., Khani, E., Entezari-Maleki, T., 2020. A comprehensive review on tocilizumab in COVID-19 acute respiratory distress syndrome. J. Clin. Pharmacol. 60 (9), 1131–1146.

Kong, Y.W., Ferland-McCollough, D., Jackson, T.J., Bushell, M., 2012. microRNAs in cancer management. Lancet Oncol. 13, e249–e258.

Li, X., Ji, Z., Li, S., Sun, Y.N., Liu, J., Liu, Y., Tian, W., Zhou, Y.T., Shang, X.M., 2015. miR-146a-5p antagonized AGEs- and P.g-LPS-Induced ABCA1 and ABCG1 dysregulation in macrophages via IRAK-1 downregulation. Inflammation 38, 1761–1768.

Li, K., Fang, Y., Li, W., Pan, C., Qin, P., Zhong, Y., Liu, X., Huang, M., Liao, Y., Li, S., 2020. CT image visual quantitative evaluation and clinical classification of coronavirus disease (COVID-19). Eur. Radiol. 30, 4407–4416.

Libermann, T.A., Baltimore, D., 1990. Activation of interleukin-6 gene expression through the NF-kappa B transcription factor. Mol. Cell. Biol. 10, 2327–2334.

Liu, B., Li, M., Zhou, Z., Guan, X., Xiang, Y., 2020a. Can we use interleukin-6 (IL-6) blockade for coronavirus disease 2019 (COVID-19)-induced cytokine release syndrome (CRS)? J. Autoimmun. 111, 102452.

Liu, G.J., Zhang, Q.R., Gao, X., Wang, H., Tao, T., Gao, Y.Y., Zhou, Y., Chen, X.X., Li, W., Hang, C.H., 2020b. MiR-146a ameliorates hemoglobin-induced microglial inflammatory response via TLR4/IRAK1/TRAF6 associated pathways. Front. Neurosci. 14, 311.

Luo, P., Liu, Y., Qiu, L., Liu, X., Liu, D., Li, J., 2020. Tocilizumab treatment in COVID-19: a single center experience. J. Med. Virol. 92, 814–818.

Luo, Y., Zheng, S.G., 2016. Hall of fame among pro-inflammatory cytokines: Interleukin-6 gene and its transcriptional regulation mechanisms. Front. Immunol. 7, 604.

Mensà, E., Giuliani, A., Matacchione, G., Gurău, F., Bonfigli, A.R., Romagnoli, F., De Luca, M., Sabbatinelli, J., Olivieri, F., 2019. Circulating miR146a in healthy aging and type 2 diabetes: age- and gender-specific trajectories. Mech. Ageing Dev. 180, 1–10.

Mensà, E., Guescini, M., Giuliani, A., Bacalini, M.G., Ramini, D., Corleone, G., Ferracin, M., Fulgenzi, G., Graciotti, L., Prattichizzo, F., Sorci, L., Battistelli, M., Monsurrò, V., Bonfigli, A.R., Cardelli, M., Recchioni, R., Marcheselli, F., Latini, S., Maggio, S., Fanelli, M., Amatori, S., Storci, G., Ceriello, A., Stocchi, V., De Luca, M., Magnani, L., Rippo, M.R., Procopio, A.D., Sala, C., Budimir, I., Bassi, C., Negrini, M., Garagnani, P., Franceschi, C., Sabbatinelli, J., Bonafè, M., Olivieri, F., 2020. Small extracellular vesicles deliver miR-21 and miR-217 as pro-senescence effectors to endothelial cells. J. Extracell. Vesicles 9, 1725285.

Mussbacher, M., Salzmann, M., Brostjan, C., Hoesel, B., Schoergenhofer, C., Datler, H., Hohensinner, P., Basilio, J., Petzelbauer, P., Assinger, A., Schmid, J.A., 2019. Cell type-specific roles of NF-kappaB linking inflammation and thrombosis. Front. Immunol. 10, 85.

Olivieri, F., Spazzafumo, L., Santini, G., Lazzarini, R., Albertini, M.C., Rippo, M.R., Galeazzi, R., Abbatecola, A.M., Marcheselli, F., Monti, D., Ostan, R., Cevenini, E., Antonicelli, R., Franceschi, C., Procopio, A.D., 2012. Age-related differences in the expression of circulating microRNAs: miR-21 as a new circulating marker of inflammaging. Mech. Ageing Dev. 133, 675–685.

Olivieri, F., Lazzarini, R., Recchioni, R., Marcheselli, F., Rippo, M.R., Di Nuzzo, S., Albertini, M.C., Graciotti, L., Babini, L., Mariotti, S., Spada, G., Abbatecola, A.M., Antonicelli, R., Franceschi, C., Procopio, A.D., 2013a. MiR-146a as marker of senescence-Associated pro-inflammatory status in cells involved in vascular remodelling. Age 35, 1157–1172.

Olivieri, F., Rippo, M.R., Procopio, A.D., Fazioli, F., 2013b. Circulating inflamma-miRs in aging and age-related diseases. Front. Genet. 4, 121.

Ong, J., Woldhuis, R.R., Boudewijn, I.M., van den Berg, A., Kluiver, J., Kok, K., Terpstra, M.M., Guryev, V., de Vries, M., Vermeulen, C.J., Timens, W., van den Berge, M., Brandsma, C.A., 2019. Age-related gene and miRNA expression changes in airways of healthy individuals. Sci. Rep. 9, 3765.

Ramiro, S., Mostard, R.L.M., Magro-Checa, C., van Dongen, C.M.P., Dormans, T., Buijs, J., Gronenschild, M., de Kruif, M.D., van Haren, E.H.J., van Kraaij, T., Leers, M.P.G., Peeters, R., Wong, D.R., Landewe, R.B.M., 2020. Historically controlled comparison of glucocorticoids with or without tocilizumab versus supportive care only in patients with COVID-19-associated cytokine storm syndrome: results of the CHIC study. Ann. Rheum. Dis. 79, 1143–1151.

Remuzzi, A., Remuzzi, G., 2020. COVID-19 and Italy: what next? Lancet 395, 1225–1228.

Roos, J., Enlund, E., Funcke, J.B., Tews, D., Holzmann, K., Debatin, K.M., Wabitsch, M., Fischer-Posovszky, P., 2016. miR-146a-mediated suppression of the inflammatory response in human adipocytes. Sci. Rep. 6, 38339.

Ruan, Q., Yang, K., Wang, W., Jiang, L., Song, J., 2020. Clinical predictors of mortality due to COVID-19 based on an analysis of data of 150 patients from Wuhan, China. Intensive Care Med. 46, 846–848.

Rusanova, I., Diaz-Casado, M.E., Fernandez-Ortiz, M., Aranda-Martinez, P., Guerra-Librero, A., Garcia-Garcia, F.J., Escames, G., Manas, L., Acuna-Castroviejo, D., 2018. Analysis of plasma MicroRNAs as predictors and biomarkers of aging and frailty in humans. Oxid. Med. Cell. Longev. 2018, 7671850.

Sheedy, F.J., 2015. Turning 21: induction of miR-21 as a key switch in the inflammatory response. Front. Immunol. 6, 19.

Spazzafumo, L., Olivieri, F., Abbatecola, A.M., Castellani, G., Monti, D., Lisa, R., Galeazzi, R., Sirolla, C., Testa, R., Ostan, R., Scurti, M., Caruso, C., Vasto, S., Vescovini, R., Ogliari, G., Mari, D., Lattanzio, F., Franceschi, C., 2013. Remodelling of biological parameters during human ageing: evidence for complex regulation in longevity and in type 2 diabetes. Age Dordr. (Dordr) 35, 419–429.

Sriram, K., Insel, P.A., 2020. Inflammation and thrombosis in COVID-19 pathophysiology: proteinase-activated and purinergic receptors as drivers and candidate therapeutic targets. Physiol. Rev. https://doi.org/10.1152/physrev.00035.2020. In press.

Storci, G., Bonifazi, F., Garagnani, P., Olivieri, F., Bonafe, M., 2020. How studies on inflamm-aging may help to understand and combat COVID-19 pandemic. Preprints, 2020040158.

Su, Y.L., Wang, X., Mann, M., Adamus, T.P., Wang, D., Moreira, D.F., Zhang, Z., Ouyang, C., He, X., Zhang, B., Swiderski, P.M., Forman, S.J., Baltimore, D., Li, L., Marcucci, G., Boldin, M.P., Kortylewski, M., 2020. Myeloid cell-targeted miR-146a mimic inhibits NF-kappaB-driven inflammation and leukemia progression in vivo. Blood 135, 167–180.

Varga, Z., Flammer, A.J., Steiger, P., Haberecker, M., Andermatt, R., Zinkernagel, A.S., Mehra, M.R., Schuepbach, R.A., Ruschitzka, F., Moch, H., 2020. Endothelial cell infection and endotheliitis in COVID-19. Lancet 395, 1417–1418.

Wilk, A.J., Rustagi, A., Zhao, N.Q., Roque, J., Martinez-Colon, G.J., McKechnie, J.L., Ivison, G.T., Ranganath, T., Vergara, R., Hollis, T., Simpson, L.J., Grant, P., Subramanian, A., Rogers, A.J., Blish, C.A., 2020. A single-cell atlas of the peripheral immune response in patients with severe COVID-19. Nat. Med. 26, 1070–1076.

Xiang, Z., Liu, J., Shi, D., Chen, W., Li, J., Yan, R., Bi, Y., Hu, W., Zhu, Z., Yu, Y., Yang, Z., 2020. Glucocorticoids improve severe or critical COVID-19 by activating ACE2 and reducing IL-6 levels. Int. J. Biol. Sci. 16, 2382–2391.

Xu, X., Han, M., Li, T., Sun, W., Wang, D., Fu, B., Zhou, Y., Zheng, X., Yang, Y., Li, X., Zhang, X., Pan, A., Wei, H., 2020. Effective treatment of severe COVID-19 patients with tocilizumab. Proc Natl Acad Sci U S A 117, 10970–10975.

Zhang, X., Wang, X., Fan, M., Tu, F., Yang, K., Ha, T., Liu, L., Kalbfleisch, J., Williams, D., Li, C., 2020. Endothelial HSPA12B exerts protection against sepsis-induced severe cardiomyopathy via suppression of adhesion molecule expression by miR-126. Front. Immunol. 11, 566.

Zhong, L., Simard, M.J., Huot, J., 2018. Endothelial microRNAs regulating the NF-kappaB pathway and cell adhesion molecules during inflammation. FASEB J. 32, 4070–4084.

Zhou, C., Zhao, L., Wang, K., Qi, Q., Wang, M., Yang, L., Sun, P., Mu, H., 2019. MicroRNA-146a inhibits NF-kappaB activation and pro-inflammatory cytokine production by regulating IRAK1 expression in THP-1 cells. Exp. Ther. Med. 18, 3078–3084.

Zhou, F., Yu, T., Du, R., Fan, G., Liu, Y., Liu, Z., Xiang, J., Wang, Y., Song, B., Gu, X., Guan, L., Wei, Y., Li, H., Wu, X., Xu, J., Tu, S., Zhang, Y., Chen, H., Cao, B., 2020. Clinical course and risk factors for mortality of adult inpatients with COVID-19 in Wuhan, China: a retrospective cohort study. Lancet 395 (10229), 1054–1062.